

Documentation of the Lagrangian Particle Model GRAL (Graz Lagrangian Model) V24.11

<https://gral.tugraz.at/>

<https://github.com/GralDispersionModel/GRAL>

Author
Contributing author since version 20.09
Contributions by

Mag. Dr. Dietmar Oettl
Ing. Markus Kuntner
Ing. Dipl.-Ing. Robert Hofstadler

CONTENT

1	Changes to previous versions	9
1.1	Changes to the previous version GRAL 22.09	9
1.2	Changes to the previous version GRAL 22.03	10
1.3	Changes to the previous version GRAL 21.09	10
1.4	Changes to the previous version GRAL 20.09	10
1.5	Changes to the previous version GRAL 20.01	11
1.6	Changes to the previous version GRAL 19.1	12
1.7	Changes to the previous version GRAL 18.1	13
1.8	Changes to the previous version GRAL 17.9	13
1.9	Changes to the previous version GRAL 17.8	13
1.10	Changes to the previous version GRAL 17.1	13
2	Introduction	14
3	General information	15
4	GRAL physics	17
4.1	Turbulence observations in Austria	17
4.2	Wind profile	17
4.3	Vertical dispersion	18
4.4	Horizontal dispersion	23
4.5	Tunnel module	28
4.6	Buoyant plume rise	31
4.7	Odour hour modelling	35
4.8	Dry deposition and sedimentation	38
4.9	Wet deposition	39
4.10	Decay rates	40
5	GRAL methods	41
5.1	Meteorological pre-processor	41
5.2	Time management	43
5.3	Particle management	44
5.4	Coupling with GRAMM (Graz Mesoscale Model)	45
5.5	Flow field in the presence of obstacles	48
5.5.1	Complex terrain (using coarse GRAMM wind fields)	48
5.5.2	Flat terrain (without GRAMM coupling)	54
5.6	Boundary conditions	55
5.7	Computation of concentration statistics	55
5.8	Surface roughness lengths	56
5.9	GRAL Grids	58
5.9.1	Concentration grid	58
5.9.2	Receptor concentrations	58
5.9.3	Flow field grid	58
5.9.4	Buildings and vegetation grid	58
5.9.5	Transient concentration grid	59
6	Compliance with the Austrian Guideline RVS 04.02.12	60
6.1	CALTRANS99	60
6.1.1	Dataset description	60

6.1.2	Characteristics	61
6.1.3	Model set up	61
6.1.4	Results	61
6.2	A2, Biedermannsdorf	63
6.2.1	Dataset description	63
6.2.2	Characteristics	63
6.2.3	Model set up	63
6.2.4	Results	63
6.3	Ehrentalerberg	65
6.3.1	Dataset description	65
6.3.2	Characteristics	65
6.3.3	Model set up	66
6.3.4	Results	66
6.4	Kaisermuehlen	68
6.4.1	Dataset description	68
6.4.2	Characterization	68
6.4.3	Model set up	69
6.4.4	Results	70
6.5	Summary	72
7	Compliance with the German Guideline VDI 3783 - 9	73
7.1	General model evaluation	73
7.2	Scientific model evaluation	74
7.3	Model validation	75
7.3.1	Test case A1-1 (two-dimensionality)	76
7.3.2	Test case A1-2 (scalability)	77
7.3.3	Test case A2 (steady-state)	78
7.3.4	Test cases A3-1 and A3-2 (length of recirculation zone)	79
7.3.5	Test case A4-1 (symmetry)	81
7.3.6	Test case A4-2 (grid size dependency)	82
7.3.7	Test case A5-1 (building orientation)	84
7.3.8	Test case A5-2 (building orientation)	85
7.3.9	Test case B1 – B6 (homogeneity)	86
7.3.10	Test case B7 – B12 (Coriolis force)	88
7.3.11	Test case C1 (wind tunnel data)	88
7.3.12	Test case C2 (wind tunnel data)	89
7.3.13	Test case C3 (wind tunnel data)	91
7.3.14	Test case C4 (wind tunnel data)	93
7.3.15	Test case C5 (wind tunnel data)	95
7.4	Summary	98
8	Compliance with other guidelines from national authorities	99
9	Additional validation cases	99
9.1	Indianapolis	101
9.1.1	Dataset description	101
9.1.2	Characteristics	101
9.1.3	Model set up	101
9.1.4	Results	101
9.2	Kincaid	103
9.2.1	Dataset description	103
9.2.2	Characteristics	103

9.2.3	Model set up	103
9.2.4	Results.....	104
9.3	Lillestroem	106
9.3.1	Dataset description.....	106
9.3.2	Characteristics.....	106
9.3.3	Model set up	106
9.3.4	Results.....	106
9.4	Prairie Grass.....	109
9.4.1	Dataset description.....	109
9.4.2	Characteristics.....	109
9.4.3	Model set up	109
9.4.4	Results.....	109
9.5	Copenhagen	112
9.5.1	Dataset description.....	112
9.5.2	Characteristics.....	112
9.5.3	Model set up	112
9.5.4	Results.....	112
9.6	Idaho.....	114
9.6.1	Dataset description.....	114
9.6.2	Characteristics.....	114
9.6.3	Model set up	114
9.6.4	Results.....	115
9.7	Raaba	117
9.7.1	Dataset description.....	117
9.7.2	Characteristics.....	117
9.7.3	Model set up	117
9.7.4	Results.....	117
9.8	Gratkorn.....	119
9.8.1	Dataset description.....	119
9.8.2	Characterisation	119
9.8.3	Model set up	120
9.8.4	Results.....	121
9.9	Idaho Falls without noise barrier	124
9.9.1	Dataset description (Finn et al., 2010)	124
9.9.2	Characteristics.....	124
9.9.3	Model set up	125
9.9.4	Results.....	125
9.10	Idaho Falls with noise barrier	127
9.10.1	Dataset description (Finn et al., 2010)	127
9.10.2	Model set up	127
9.10.3	Results.....	127
9.11	Elimaeki	129
9.11.1	Dataset description.....	129
9.11.2	Characteristics.....	130
9.11.3	Model set up	130
9.11.4	Results.....	130
9.12	Goettinger Strasse	132
9.12.1	Dataset description.....	132
9.12.2	Characteristics.....	132
9.12.3	Model set up	132
9.12.4	Results.....	132
9.13	Frankfurter Allee, Berlin	135

9.13.1	Dataset description	135
9.13.2	Characteristics	135
9.13.3	Model set up	135
9.13.4	Results	136
9.14	Hornsgatan street canyon, Stockholm	138
9.14.1	Dataset description	138
9.14.2	Characteristics	138
9.14.3	Model set up	138
9.14.4	Results	139
9.15	U-shaped building	141
9.15.1	Dataset description	141
9.15.2	Characteristics	141
9.15.3	Model set up	142
9.15.4	Results	142
9.16	Parking lot Vienna	143
9.16.1	Dataset description	143
9.16.2	Characteristics	143
9.16.3	Model set up	143
9.16.4	Results	144
9.17	Uttenweiler	145
9.17.1	Dataset description	145
9.17.2	Characteristics	145
9.17.3	Model set up	145
9.17.4	Results	145
9.18	Roager	147
9.18.1	Dataset description	147
9.18.2	Characteristics	147
9.18.3	Model set up	148
9.18.4	Results	148
9.19	EOCR	150
9.19.1	Dataset description	150
9.19.2	Characteristics	150
9.19.3	Model set up	150
9.19.4	Results	151
9.20	AGA Experiments	152
9.20.1	Dataset description	152
9.20.2	Characteristics	152
9.20.3	Model set up Texas	152
9.20.4	Model set up Kansas	153
9.20.5	Results	153
9.21	Alaska North Slope Tracer Study	156
9.21.1	Dataset description	156
9.21.2	Characteristics	156
9.21.3	Model set up	156
9.21.4	Results	157
9.22	Ninomiya tunnel	158
9.22.1	Dataset description	158
9.22.2	Characterisation	158
9.22.3	Model set up	158
9.22.4	Results	159
9.23	Hitachi tunnel	160
9.23.1	Dataset description	160

9.23.2	Characterisation	160
9.23.3	Model set up	160
9.23.4	Results.....	161
9.24	Enrei tunnel.....	162
9.24.1	Dataset description.....	162
9.24.2	Characterisation	162
9.24.3	Model set up	162
9.24.4	Results.....	163
9.25	Westvaco Paper Mill	164
9.25.1	Dataset description.....	164
9.25.2	Characterisation	164
9.25.3	Model set up	166
9.25.4	Results.....	166
9.26	2014 Colorado Oil and Gas Drill Rig Field Study.....	168
9.26.1	Dataset description.....	168
9.26.2	Characterisation	168
9.26.3	Model set up	169
9.26.4	Results for the Colorado Oil and Gas Drill Rig Field Study.....	169
10	Dry deposition.....	171
10.1	Test case 1: Mass Conservation	171
10.1.1	Model set up	171
10.1.2	Source configuration	171
10.1.3	Results.....	171
10.2	Deposition velocity - Test Case 2	172
10.2.1	Model set up	172
10.2.2	Source configuration	172
10.2.3	Meteorological input	172
10.2.4	Results.....	173
10.3	Deposition velocity - Test Case 3.....	174
10.3.1	Model set up	174
10.3.2	Source configuration	174
10.3.3	Meteorological input	175
10.3.4	Results.....	175
10.4	Deposition velocity - Test Case 4.....	175
10.4.1	Model set up	175
10.4.2	Source configuration	175
10.4.3	Meteorological input	176
10.4.4	Results.....	176
10.5	Deposition velocity - Test Case 5.....	177
10.5.1	Model set up	177
10.5.2	Source configuration	177
10.5.3	Meteorological input	178
10.5.4	Results.....	178
10.6	Dikopshof.....	178
10.6.1	Dataset description.....	178
10.6.2	Characterisation	179
10.6.3	Model set up	179
10.6.4	Results.....	179
10.7	Deposition velocity - Test Case V21.09.....	180
10.7.1	Model set up	180
10.7.2	Source configuration	180

10.7.3	Meteorological input	181
10.7.4	Results	181
11	Wet deposition	184
11.1	Masenberg	184
11.1.1	Dataset description	184
11.1.2	Characterisation.....	184
11.1.3	Model set up	185
11.1.4	Results.....	186
12	Odour dispersion.....	187
12.1	Concentration variance - Uttenweiler.....	188
12.1.1	Dataset description	188
12.1.2	Characteristics	188
12.1.3	Model set up	188
12.1.4	Results	189
12.2	Odour dispersion from a pig-fattening shed.....	190
12.2.1	Dataset description	190
12.2.2	Characteristics	191
12.2.3	Model set up	191
12.2.4	Results	192
12.3	Odour dispersion within a village	194
12.3.1	Dataset description	194
12.3.2	Characteristics	195
12.3.3	Model set up	196
12.3.4	Results	196
12.4	Odour impact from a farm with multiple sheds.....	198
12.4.1	Dataset description	198
12.4.2	Characteristics	199
12.4.3	Model set up	199
12.4.4	Results	200
13	Vegetation	202
13.1	Test Aspen.....	202
13.1.1	Dataset description	202
13.1.2	Model set up	202
13.1.3	Results	203
15	References.....	204
17	Appendix A.....	219
17.1	Startup parameter	219
17.2	Control files	219
17.2.1	Input files	219
17.2.2	Output files.....	239

1 Changes to previous versions

1.1 Changes to the previous version GRAL 24.04

- Add a new option that allows GRAL to create reproducible results (thanks to [JoshLovesFun](#) for idea, development and testing): see chapter 17.2.1.5
- Fix an error that caused the top line of a *.gff file not to be read

1.2 Changes to the previous version GRAL 23.11

- Fix a bug that has been causing concentrations in the building since version 23.11 for flat terrain and certain building configurations.
- Fix a bug that leads to high wind speeds near the ground when transferring the GRAMM wind profile to the GRAL Grid
- Correct the plume rise calculation, as since version 23.11 the plume rise is too high for very small point sources
- Enable the optional usage of AVX512 processor extension for flow field calculations (see chapter 17.2.1.5)

1.3 Changes to the previous version GRAL 22.09

- Moved to .NET8.0
- The GRAL release is no longer published as an all-in-one file by default

This means that the user must install the .NET8 Runtime and therefore benefits in several ways:

- Smaller published files
- Fewer false warnings from anti-virus programs
- Better performance
- Individual setting options for the Runtime for the respective computer in the *.runtimeconfig.json file
- Same compilation for Windows, Linux and macOS

For Windows users, a published version as a single-file is still available in a separate download

- Revision of the Plume Rise algorithm

The exhaust plume now rises a little more at the source and is released earlier. This fixes small programming flaw and better validation results are achieved.

- The reflection algorithm has been revised

Changes to previous versions

It could happen that individual particles remained in an infinite loop in the reflection algorithm. This effect led to a performance drop in large projects.

- The result files *.grz are written in a separate thread

For very large projects, writing the zipped result files can take several minutes. With this change, writing takes place while the next wind field is being loaded or calculated, which increases overall performance.

- Store original meteopgt.all stabilityclass

The displayed stability class of the original meteorology was incorrect in some cases.

- The used memory is now released at the end of calculation, even if the console window is not closed
- Particles that move very slowly over a longer period of time or are trapped in a cell are sorted out

1.4 Changes to the previous version GRAL 22.03

- Performance improvements when reading large binary files (e.g. GRAL or GRAMM wind files)
- Additional outputs for missing or damaged mandatory input files
- Additional validation datasets (2014 Colorado Oil and Gas Drill Rig Field Study)
- Compiled for .NET6

1.5 Changes to the previous version GRAL 21.09

- An error that occurred when the operating system reported 0 free processor cores, resulting in a division by 0, has been fixed
- An incorrect concentration evaluation above buildings for calculations with flat terrain was fixed
- In the transient calculation mode with flat terrain, building heights were included as terrain in the 3D concentration file

1.6 Changes to the previous version GRAL 20.09

- The arithmetic accuracy of the prognostic flow field calculation has been improved
- The memory consumption for prognostic calculations has been reduced, if not the entire domain area needs to be calculated prognostically
- Output of a file "PrognosticSubDomainAreas.txt" showing the prognostic sub-domains areas – chapter 17.2.2.15

- Optional reduction of prognostic sub-domains depending on the distance to sources (further reduction of memory consumption and faster calculation for large domain areas)
- chapter 17.2.1.5
- Optional deactivation of the online output (reduction of file accesses during the calculation)
- chapter 17.2.1.5
- Optional user defined scaling factor for the deposition velocity within vegetation areas –
chapter 4.8 and chapter 10.7
- A slight overestimation (about 20 %) of the deposition was corrected
- The generation of the vegetation mesh has been fixed
- Several small performance optimizations
- Compiled for .NET5 as single file application for Windows and Linux

1.7 Changes to the previous version GRAL 20.01

- A new option “Adaptive Surface Roughness” (spatially varying surface roughness values) has been implemented
- Ascending or descending line sources are supported
- Additional user information
 - in the transient GRAL mode: average emission modulation, average exit temperature and exit velocity, date and time of the weather situation
 - show the progress when writing the concentration or the flow field files
- Optional building input by using an ESRI ASCII format raster file
- Additional separator characters for exit temperature and exit velocity files
- Creation of additional transient particles in a cell with high pollution concentration
- Better support for steep line sources
- New flow field file format, designed for huge domains with terrain or many buildings
- If artificially generated wind data with very small wind speed differences were used, the current situation of mettimeseries.dat was not assigned correctly in the file meteopgt.all in the transient GRAL mode
- The changed file format for the file GRAL_Meteozeitreihe.dat has been fixed
- A division by zero has been fixed (occurs in rare cases if there is no sub domain but a high surface altitude in cell [1][1])
- The user defined sub domain factor was not applied to buildings
- A warning message appears if the calculation is set to prognostic wind calculation, but no sub-domains have been created (for example if no buildings have been defined)
- The memory consumption and the number of page faults have been reduced

Changes to previous versions

- Erroneous transfer of surface roughness lengths when coupling with GRAMM in the Flow Field module has been fixed

1.8 Changes to the previous version GRAL 19.1

- In rare cases a bound overflow occurred when GRAL was coupled with GRAMM and numerous particles were reflected at the edge towards the GRAMM area. Additional checks avoid this bug.
- Previously, the concentration in the evaluation layer was calculated as a mean value for the entire cell. If the evaluation layer is partially occupied by buildings, the concentration is calculated for the free air volume within the evaluation layer now.
- Previously, the receptor points were placed on the horizontal concentration grid. Now the receptor concentrations are calculated at their real position.
- Exit velocities and temperature differences between tunnel jets, stacks, and ambient air can be prescribed for each dispersion situation individually in the transient GRAL mode.
- A file path for reading and writing microscale flow fields can be defined individually.
- GRAL is available as .NETCore version only. For Windows, a trimmed single file (standalone package *.exe file) is delivered. This file can be started without additional installation of the .NETCore Framework.

For LINUX or advanced windows users, the operating system independent *.dll versions are available. When using these versions, the .NETCore 3.1 Framework must be installed. Installation guides are available at the Microsoft homepage for Windows, Linux and macOS.

- The vertical grid spacing for the microscale flow-field model can be defined more flexible (see 17.2.1.5)
- The size of the prognostic sub-domains around obstacles is made flexible (see 17.2.1.5)
- In complex-terrain simulations, the calculation of the particle trajectories in the lowest grid cells is adopted in order to minimize step-wise concentration patterns due to the step-wise resolution of the terrain in GRAL.
- Decay rates (e.g. bacteria, radioactivity) can be defined for each source group separately (see 17.2.1.27).
- Concentration maps can be saved optionally in ESRI ASCII format (see 17.2.1.5).
- A statistical error of the concentration is estimated at the receptor points, the output appears in the Receptor_Timeseries_Transient.txt file.
- The file Receptor_Timeseries_Transient.txt has a detailed header and in the Transient GRAL Mode, the calculated meteorological data at the receptor point are saved in this file
- A hash code of the application is generated and written to the log file.

1.9 Changes to the previous version GRAL 18.1

- Transient simulation mode has been implemented (see chapt. 5.2)
- Wet deposition can be computed in the transient simulation mode (see chapt. 4.9)
- Vegetation can be taken into account (see chapt. 5.5)
- New particle management to avoid null-particle sources or source parts
- Usage of SIMD functions to improve the performance of the flow field calculation
- Catch and remove trapped particles within the model
- Decay rates have been implemented, which can be used for defining inactivation rates for bacteria for example (see chapt. 4.10)
- A start parameter allows for setting a working directory (see chapt. 17.1)

1.10 Changes to the previous version GRAL 17.9

- A new log-file named "Logfile_GRALCore.txt" is being introduced, in which the main model outputs (e.g. number of sources, source-groups, error messages) are stored.
- Very small line sources < 0.001 m in length are automatically deleted.
- The top model boundary is generally set to 800 m above the lowest domain height, but is at least 300 m above the highest elevation in the domain.
- An inconsistency in the computation of the ambient dissipation rate used for effective plume height calculations has been fixed. Note that with the new version different results will be obtained for point sources with significant plume rise, whenever no microscale prognostic flow field is computed, compared with version 17.9.

1.11 Changes to the previous version GRAL 17.8

- A new warning message has been implemented, whenever the number of particles is too low for resolving all pollutant sources within a model domain. Please visit the new chapter in the GRAL recommendation guide on how to proceed in such cases.

1.12 Changes to the previous version GRAL 17.1

- A bug concerning the computation of the friction velocity when GRAL was coupled with GRAMM has been fixed.
- Whenever GRAMM scl-files (containing stability classes, Obukhov lengths, and friction velocities computed with GRAMM) are available, stability classes are read from this file, otherwise a spatial homogenous stability class taken from the file meteopgt.all is taken.
- Flat roof tops in complex terrain are enabled by using absolute heights of buildings.

2 Introduction

Dispersion modelling in complex terrain and in situations with low wind speeds is a challenging scientific task. Nevertheless, scientists and engineers have to assess air pollution in such environments. It is therefore necessary to develop models and methods, which allow for such assessments with reasonable demands on computational times and with sensible accuracy. This has been the motivation for the development of the Lagrangian dispersion model GRAL at the Graz University of Technology, Institute for Internal Combustion Engines and Thermodynamics ever since 1999.

Since about 2014 the Governments of Tyrol and Styria, Austria, are further developing the model. The ever-growing model and the comprehensive work done on validation has led to the necessity of a detailed model description. Although the main physical assumptions and some validation exercises have been documented in several peer reviewed journals, it is not possible to describe all details of the actual version of GRAL in one single research article. This report aims at describing the physics, the numerical aspects as well as the validation of GRAL, and is therefore part of the overall quality assurance.

3 General information

Current development team:

Physics, Numerics, Programming, Quality Assurance: Dietmar Oettl (Government of Styria, Air Quality Department, Austria)

Programming, Optimization: Markus Kuntner (Government of Tyrol, Emissions-Security-Facilities Department, Austria)

Training and support: Graz University of Technology, Austria

Mail: gral@ivt.tugraz.at

Software requirements:

64 bit Windows, Linux or MacOS system for the .NET8 framework.

Hardware requirements:

Processor with SSE or AVX extension (introduced by Intel in 1999 and supported by AMD)

GRAL is a parallel application; a modern processor with a high number of cores is preferred

Programming language: C# (.NET8 version for Windows, LINUX or macOS)

Availability: Free download from <https://gral.tugraz.at/>

Source Code: <https://github.com/GralDispersionModel/GRAL>

Typical domain sizes: 0.05 km – 100 km

Typical horizontal grid sizes: 2 m – 20 m

Typical vertical grid sizes: 1 m – 5 m; increasing cell heights with elevation by a factor of 1.0 – 1.10 or user-defined grid spacing for four vertical domains

Typical fields of applications:

Simulation of steady-state or transient dispersion of pollutants/odours/bacteria/radioactivity in complex terrain and around/within buildings/obstacles/vegetation for point-, line-, area sources and tunnel portals. The model can simulate the following:

- Dispersion of chemically non-reactive pollutants/odours.
- Computation of so-called odour-hours based on a recently developed concentration-variance model.
- Dry and wet deposition and sedimentation.
- Decay rates for e.g. bacteria/radioactive substances.
- Dispersion from road tunnel portals. GRAL fulfils the requirements of the Technical Guideline RVS 04.02.12 in Austria.

General information

- Dispersion over the full range of wind speeds without any lower threshold, and for all stability conditions.
- Dispersion in built-up areas, including building downwash effects.
- Dispersion influenced by vegetation (e.g. forests).
- Dispersion of stack emissions, taking into account temperature and exit velocity.
- Dispersion in complex terrain, allowing for the effects of both buildings and vegetation.

The effect of buildings and vegetation on dispersion is considered using a micro-scale flow-field model. This is fully integrated into the GRAL code.

Application limits:

GRAL does not handle chemical reactions.

4 GRAL physics

The basic principle of Lagrangian models is the tracing/tracking of a multitude of fictitious particles moving on trajectories within a 3-d windfield. The position of these particles is calculated according to the following basic equation:

$$x_{i,new} = x_{i,old} + (\bar{u}_i + u'_i) \cdot \Delta t$$

Where $x_{i,new}$ denotes the new position in space (with $i = 1,2,3$), and $x_{i,old}$ denotes the previous position, \bar{u}_i the mean velocity component and u' the fluctuating (random, stochastic) part due to turbulence of the particle movement and Δt is a time increment. The frequency of particles passing the counting grid relates the Lagrangian perspective with the Eulerian one.

GRAL as described here is a sophisticated operational model. Latest scientific knowledge was implemented as indicated in the references. However, due to reasons of applicability GRAL is not designed for research purposes but may be used with major modifications for research as well.

4.1 Turbulence observations in Austria

Some of the turbulence parameterizations described hereafter have been derived from own sonic anemometer observations in Graz (sub-urban area with a roughness length ~ 0.6 m) and in an alpine valley near the village of Trebesing, Carinthia (nearby a soccer place with a roughness length ~ 0.15 m). In both cases, measurement heights were 10 m above ground level, and sampling frequency was 1 Hz. Raw data has been rotated in the main wind direction, such that $\bar{u}_2 = \bar{u}_3 = 0$. In addition, data has been detrended before computing turbulence quantities. Measurements in Graz comprise the whole year 1998, while the ones in Trebesing started in Jan. 1998 and ended in May 1998.

4.2 Wind profile

Standard wind profiles in GRAL are kept quite simple and follow nearly proposed ones of the US-EPA (2000):

$$u(z) = u(z_a) \cdot \left(\frac{z}{z_a} \right)^{ex}, \quad (1)$$

$$ex = \text{Max}(0.35 - 0.4 \cdot |L|^{-0.15}, 0.05) \text{ for } L < 0, \text{ and}$$

$$ex = 0.56 \cdot L^{-0.15} \text{ for } L \geq 0$$

L : Obukhov length [m].

GRAL physics

Thus, standard wind profiles change continuously with stratification. In neutral conditions and/or for high roughness lengths (urban conditions), the wind profile exponent is close to 0.20, while for strongly convective conditions it decreases to 0.05, for strongly stable conditions it increases to about 0.40.

When GRAL is coupled with the prognostic mesoscale model GRAMM, 3D flow fields are imported from GRAMM.

4.3 Vertical dispersion

For the vertical wind component fluctuations the model of Franzese et al. (1999) is implemented in GRAL:

$$dw = a(w, z) \cdot dt + [C_0 \cdot \varepsilon(z)]^{0.5} \cdot dW, \quad (2)$$

$$dz(t) = w(t) \cdot dt, \quad (3)$$

where dw is the vertical velocity increment of a particle, C_0 is assumed to be an universal constant set at a value of 4.0 (see e.g. Wilson and Sawford 1996, Degrazia and Anfossi 1998, Anfossi et al. 2000), $\varepsilon(z)$ is the ensemble-average rate of dissipation of turbulent kinetic energy, dW is a random number with zero mean, a variance equal to dt , and a Gaussian probability density function (pdf), and the time-step dt is given by

$$dt(z) = 0.01 \cdot \frac{2 \cdot \sigma_w^2}{C_0 \cdot \varepsilon(z)}. \quad (4)$$

The deterministic acceleration term $a(w, z)$ is assumed to be a function of the vertical velocity:

$$a(w, z) = \alpha(z) \cdot w^2 + \beta(z) \cdot w + \gamma(z), \quad (5)$$

where $\alpha(z)$, $\beta(z)$ and $\gamma(z)$ are unknown parameters, which are determined from the Fokker-Planck equation:

$$w \cdot \frac{\partial P_E(w, z)}{\partial z} = - \frac{\partial [a(w, z) \cdot P_E(w, z)]}{\partial w} + \frac{C_0 \cdot \varepsilon(z)}{2} \cdot \frac{\partial^2 P_E(w, z)}{\partial w^2}, \quad (6)$$

where $P_E(w, z)$ is the Eulerian pdf of the vertical turbulent velocity at a given height z .

By assuming a quadratic functional form for the acceleration, the model of Franzese et al. (1999) does not need any information about the form of $P_E(w, z)$ but only requires the first four Eulerian moments of the vertical velocity. The coefficients in eq. (4) can be expressed as:

$$\alpha(z) = \frac{(1/3) \cdot \partial \overline{w^4} / \partial z - \overline{w^3} / (2 \cdot \overline{w^2}) \cdot \left[\partial \overline{w^3} / \partial z - C_0 \cdot \varepsilon(z) \right] - \overline{w^2} \cdot \partial \overline{w^2} / \partial z}{\overline{w^4} - (\overline{w^3})^2 / \overline{w^2} - (\overline{w^2})^2} \quad (7)$$

$$\beta(z) = \frac{1}{2 \cdot \overline{w^2}} \left[\frac{\partial \overline{w^3}}{\partial z} - 2 \cdot \overline{w^3} \cdot \alpha(z) - C_0 \cdot \varepsilon(z) \right] \quad (8)$$

$$\gamma(z) = \frac{\partial \overline{w^2}}{\partial z} - \overline{w^2} \cdot \alpha(z) \quad (9)$$

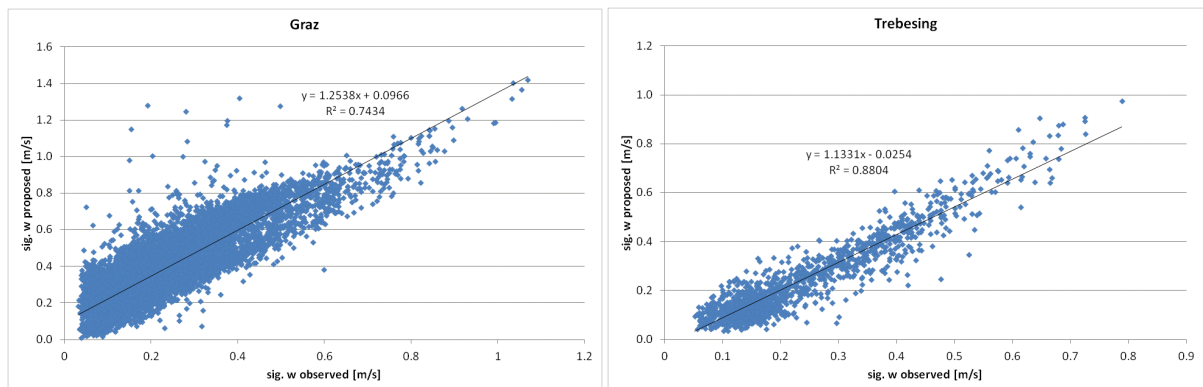
In eq. (7)-(9) $\overline{w^i}$ ($i=1, 2, 3, 4$) denote the highest Eulerian moments of the vertical velocity. The first moment is the mean of the vertical velocity, which is set equal to zero and the second moment - the variance – is calculated in

$$\text{stable and neutral conditions } \overline{w^2} = 1.56 \cdot u_*^2 \quad (10)$$

$$\text{convective conditions } \overline{w^2} = u_*^2 \cdot \left[1.15 + 0.1 \cdot \left(\frac{z_i}{-L} \right)^{0.67} \right]^2. \quad (11)$$

Figure 1 depicts observed versus computed standard deviations of the vertical wind component for all stabilities. For both datasets a slight overestimation of observed values is the case. However coefficients of determination are quite reasonable. Eq. (10) and (11) are independent on height above ground. As reported in Janicke and Janicke (2011), who compared vertical profiles of vertical velocity standard deviations from different measurement campaigns, there is currently no clear picture whether these increase, decrease, or do not vary significantly with height.

Figure 1. Comparison of observed and computed standard deviations of vertical wind fluctuations (all stabilities)



The third moment was taken to be in

GRAL physics

stable and neutral conditions and for the surface layer in general $\overline{w^3} = 0$, (12)

in convective conditions $\overline{w^3} = w_*^3 \cdot 1.1 \cdot \left(\frac{z}{z_i}\right) \cdot \left(1 - \frac{z}{z_i}\right)^2$ (Franzese et al. 1999), (13)

z_i is the PBL height, u_* is the friction velocity, w_* is the convective velocity scale, and h is the height of the stable PBL computed for

$$L \geq 0: h = \text{MIN} \left[0.4 \cdot \left(\frac{u_* \cdot L}{f} \right)^{\frac{1}{2}}, 800 \right] \text{ (Hanna 1982),} \quad (14)$$

$$L < 0: z_i = \text{MIN} \left[0.4 \cdot \left(\frac{u_* \cdot L}{f} \right)^{\frac{1}{2}}, 800 \right] + 300 \cdot e^{0.01L} \quad (15)$$

In eq. (15) – (16) L is the Obukhov length, and $f = 0.0001 \text{ s}^{-1}$ is the Coriolis parameter.

The fourth moment was set in

convective conditions $\overline{w^4} = 3.5 \cdot \overline{w^2(z)}^2$ (Franzese et al. 1999), (16)

in stable and neutral conditions and in the surface layer $\overline{w^4} = 3 \cdot \overline{w^2(z)}^2$, (17)

which is the Gaussian assumption.

The ensemble-average rate of dissipation of turbulent kinetic energy $\varepsilon(z)$ was taken for the entire BL in all conditions in a slightly modified form according to Kaimal and Finnigan (1994)

$$\varepsilon = \frac{u_*^3}{\kappa z} \left[1 + 0.5 \cdot \left| \frac{z}{L} \right|^{0.8} \right]^{1.8} \quad (18)$$

In contrast to the suggested function by Kaimal and Finnigan (1994), eq. (18) in combination with eq. (10)-(11) leads to vertical Lagrangian velocity integral timescales, which do not increase continuously with height, but which asymptotically become constant in stable and convective conditions. In neutral conditions the vertical Lagrangian velocity integral timescale increases continuously with height. This assumption seems to be physically more realistic, especially in stable conditions.

Figure 4 depicts ensemble average rates of turbulent dissipation derived from observations for the Graz dataset and computed ones with eq. (18). The sonic anemometer data (1 Hz) has previously been used for studying turbulence in low wind speed conditions and is described in Anfossi et al. (2004). Dissipation rates have been derived according to the method described in Anfossi et al. (1999). These were pooled and averaged. Thus each point represents an

average value over several hundred single hours. As can be seen, the dissipation rates computed with eq. (18) correspond well with those derived from observations. It should be noted, that also the original function proposed by Kaimal and Finnigan (1994) leads to similar good results.

Figure 2. Comparison of proposed functions for the ensemble average rate of dissipation of turbulent kinetic energy for neutral conditions

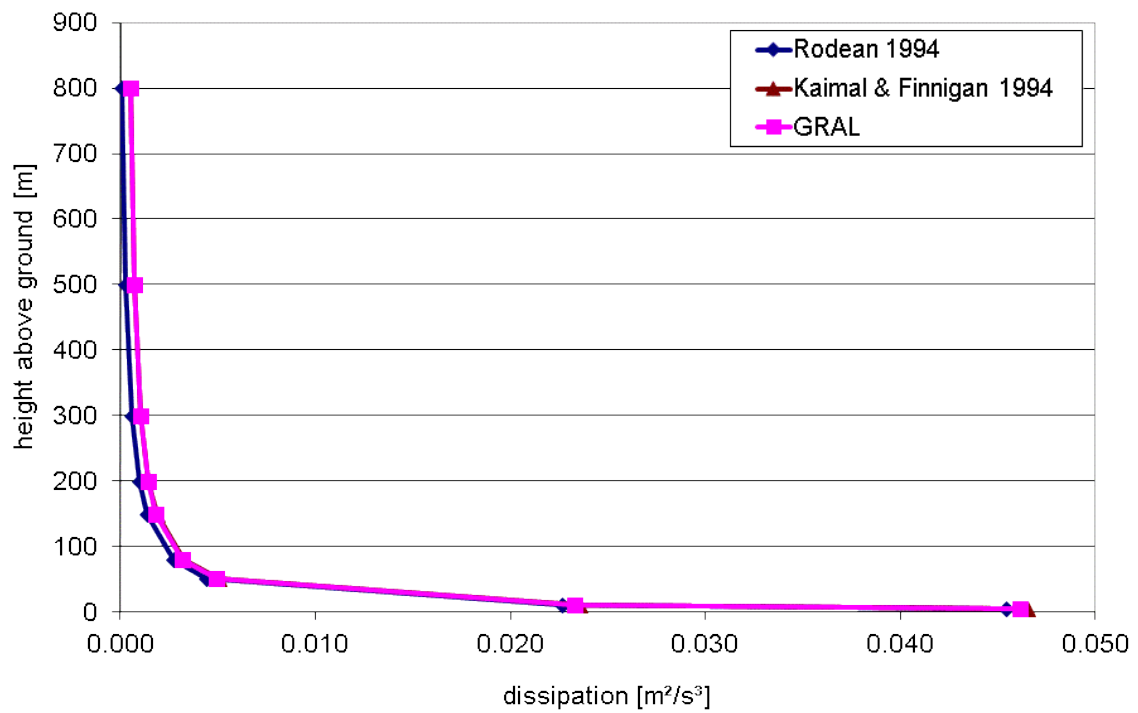


Figure 3. Behaviour of the Lagrangian velocity integral timescale in dependence on the chosen ensemble average rate of turbulent dissipation (eq. 9 is used for the vertical velocity variance) for stable conditions

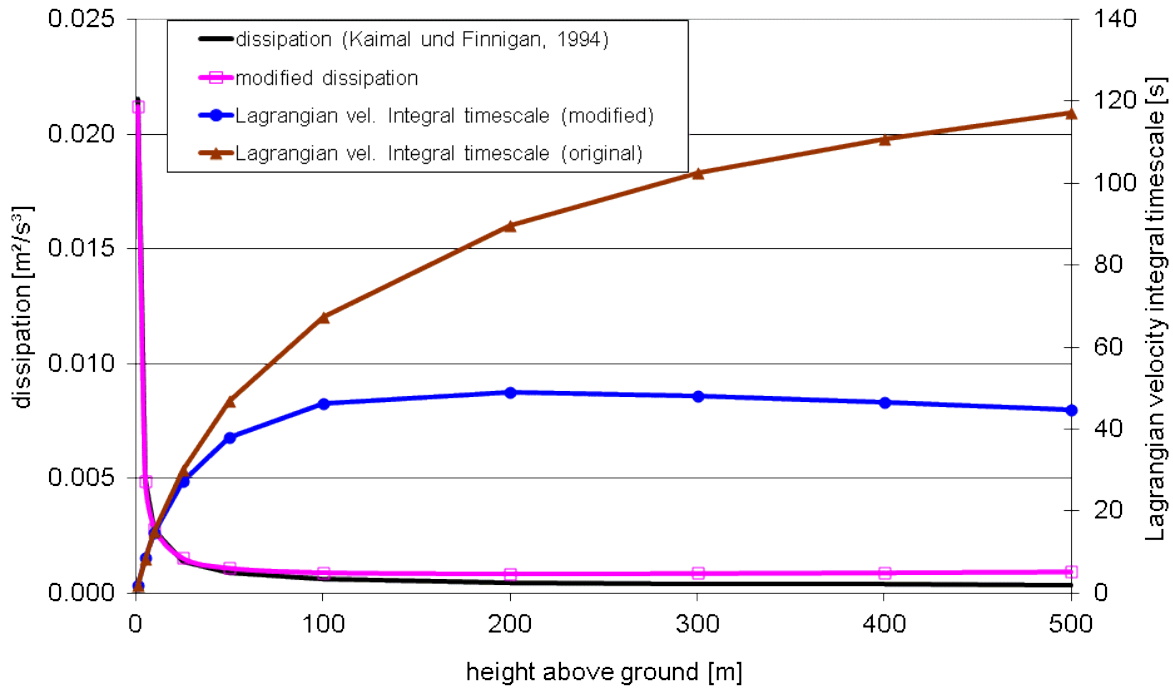
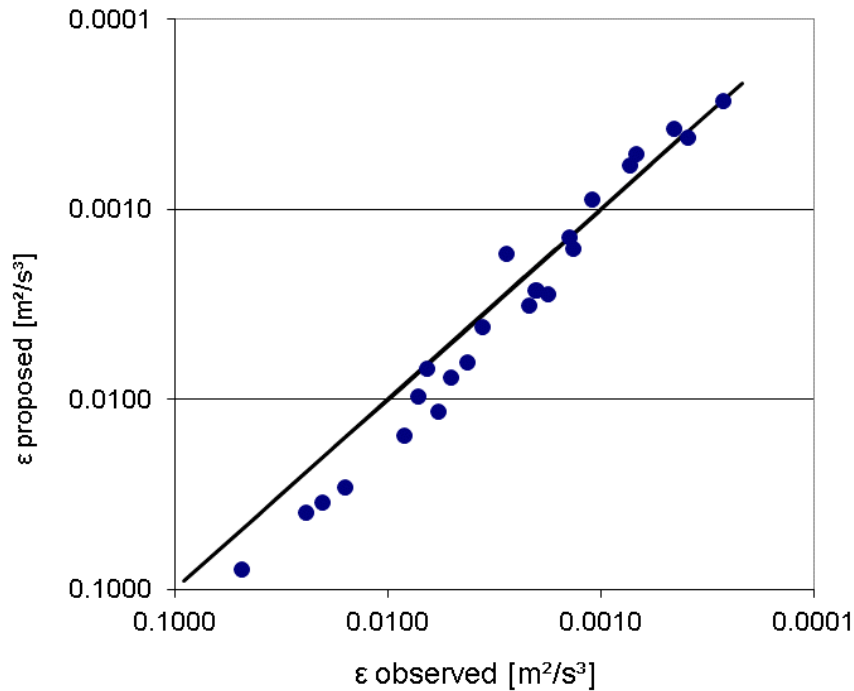


Figure 4. Comparison of ensemble average rates of turbulent dissipation based on observations and computed ones with eq. (18)



4.4 Horizontal dispersion

As discussed in Oettl et al. (2001a) it is important not only to use the cross- and longitudinal-wind standard deviations in a dispersion model, but also to have an idea about the corresponding power spectra. In GRAL observed Eulerian autocorrelation functions¹ (EAF) or parameterized ones can be used. For higher wind speeds an exponential EAF is assumed to approximate EAFs, and for low wind speeds ($<2.0 \text{ m s}^{-1}$) an expression according to Frenkiel (1953) as proposed in Anfossi et al. (2004) is applied:

$$R(\tau) = e^{-p\tau} \cos(q\tau) \quad (19)$$

$R(\tau)$ is the Autocorrelation function, τ is the time lag, p is a parameter that can be associated with the classical integral time scale for fully developed turbulence, and q can be associated with the oscillatory behaviour due to meandering. Parameter q can be obtained by applying a numerical best fit of equation (28) to observed EAFs using least squares or by using the following empirical relationships:

$$m = \frac{8.5}{(\bar{u} + 1)^2} \quad (20)$$

$$T = \frac{m(200m + 350)}{2\pi(m^2 + 1)} \quad (21)$$

$$q = \frac{m}{(m^2 + 1)T} \quad (22)$$

$$p = \frac{C_0 \cdot \varepsilon}{2 \cdot \sigma_u^2} \quad (23)$$

Typical examples of observed and approximated EAFs for the cross-wind component are depicted in Figure 10. While for the low wind speed case ($u=0.5 \text{ m s}^{-1}$) meandering is clearly visible, the cross-wind EAF for the higher wind speed case ($u=1.9 \text{ m s}^{-1}$) is better approximated by an exponential function.

Once parameters p and q were obtained, the following set of Langevin equations (=stochastic differential equation) is taken to model the horizontal dispersion (Anfossi et al., 2010).

¹ The autocorrelation relates the variation of a variable sampled at time t with the same variable at a later time $t + L$, where L is the time lag. In other words, the autocorrelation indicates the persistence of e.g. a wave within a time or space series. If the autocorrelation becomes close to zero, it tells us that there is a random process (e.g. turbulence) occurring with no persistent or regularly-recurring structures. Measurements of autocorrelations can only be carried out in an stationary (Eulerian) framework.

GRAL physics

$$du = \left\{ -p(u - \bar{u}) - q(v - \bar{v}) + \frac{\partial \bar{u}}{\partial x} u + \frac{\partial \bar{u}}{\partial y} v + \sigma_u \frac{\partial \sigma_u}{\partial x} + \frac{(u - \bar{u})}{\sigma_u} \left[\frac{\partial \sigma_u}{\partial x} u + \frac{\partial \sigma_u}{\partial y} v \right] \right\} dt + \sqrt{2 p dt} \sigma_u \xi_u \quad (24)$$

$$dv = \left\{ q(u - \bar{u}) - p(v - \bar{v}) + \frac{\partial \bar{v}}{\partial x} u + \frac{\partial \bar{v}}{\partial y} v + \sigma_v \frac{\partial \sigma_v}{\partial y} + \frac{(v - \bar{v})}{\sigma_v} \left[\frac{\partial \sigma_v}{\partial x} u + \frac{\partial \sigma_v}{\partial y} v \right] \right\} dt + \sqrt{2 p dt} \sigma_v \xi_v \quad (25)$$

du , and dv are the wind fluctuations in x- and y-direction. ξ_u , and ξ_v are increments of a Wiener process² with zero mean, a standard deviation of one and a Gaussian probability density function, and $\sigma_{u,v}$ are the standard deviations of the horizontal wind fluctuations.

The latter ones are calculated by a pure empirical function based on own sonic anemometer observations in Graz and in an Alpine valley (Trebesing):

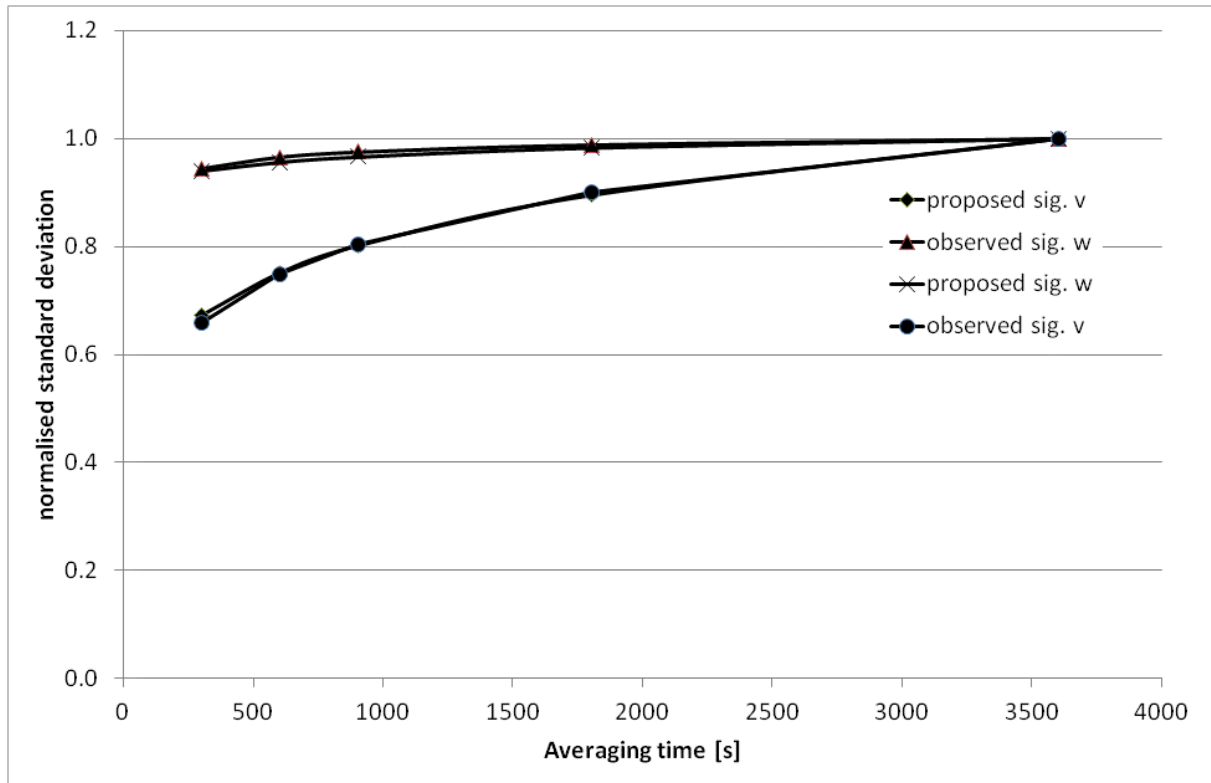
$$\frac{\sigma_{u,v}}{U} = \left(0.2 \cdot \bar{U}^{-0.9} + 0.32 \cdot z_0 + 0.18 \right) * c_{time,uv} \quad (26)$$

In addition, a minimum value of 0.3 m/s is applied for $\sigma_{u,v}$. The empirical factor $c_{time,uv}$ accounts for the influence of the chosen averaging time \bar{T} (usually 3600 s) on $\sigma_{u,v}$. Based on our own sonic anemometer data in Graz the following relationship is used in GRAL:

$$c_{time,uv} = \left(\frac{\bar{T}}{3600} \right)^{0.2} \quad (27)$$

² A Wiener Process is a random process but continuous in time, often termed Brownian motion. Wiener processes are applied in physics to study types of diffusion by Fokker Planck and Langevin equations.

Figure 5. Observed and proposed relationships between the normalised (at 3.600 s) standard deviations of wind component fluctuations and averaging time



Equation (26) is an unusual form to compute $\sigma_{u,v}$. In most cases friction velocity is used as scaling parameter. The following points should be noted about eq. (26):

- From the physical point of view, the proposed relationship is “ugly” as units are not correct. However, similarity theory usually fails in low wind speed conditions making it difficult (impossible?) to find proper scaling parameters.
- The proposed equation is based on the assumption, that horizontal standard deviations of wind speed fluctuations are independent on stability (in contrast to most of proposed formulations in literature), but depend in low wind speed conditions on meandering effects (note that $\sigma_{u,v}/U$ is strongly increasing with decreasing wind speed, thus $\sigma_{u,v}$ does not become zero for wind speeds approaching zero; see Figure 6), and in high wind speed conditions on mechanically induced turbulence that can be expressed as a function of roughness length. Observations near Torino (Italy) indicate that there is almost no dependence on stability, especially with increasing height above ground (Trini-Castelli et al., 2011).
- Observations do not give a clear picture so far on how $\sigma_{u,v}$ is changing with height. Observations near Hamburg (Germany) indicate a moderate increase of $\sigma_{u,v}$ in stable conditions, while in neutral and convective conditions no clear height dependence is visible (Janicke and Janicke, 2011). Eq. (26) results in small vertical changes in

convective and neutral conditions, while in stable conditions $\sigma_{u,v}$ increases significantly with height. In complex terrain vertical profiles may be very site specific, which possibly can better be described with eq. (26), due to the dependency on wind speed, rather than formulations based on friction velocity and Monin-Obukhov length.

- Compared with the new formulations (VDI 3783-8) to be used in German's standard model and with older formulations proposed by Hanna (1982), eq. (26) performs better for the Graz and Trebesing datasets. The comparison of Hanna's and the currently proposed VDI 3783-8 equation with observations Graz and Trebesing is based on computed u_* (according to eq. given in section 5.1) but observed L values and not modeled ones. In practical applications, L is also not available and has to be derived from stability classes, and roughness lengths. Thus, both equations (Hanna, VDI 3783-8) may result in even larger uncertainties as indicated in Figure 8 and Figure 9.

Figure 6. Observed and proposed relationships between $\sigma_{u,v}/\bar{U}$ and the mean wind speed \bar{U} (left: Graz data; right: Trebesing data)

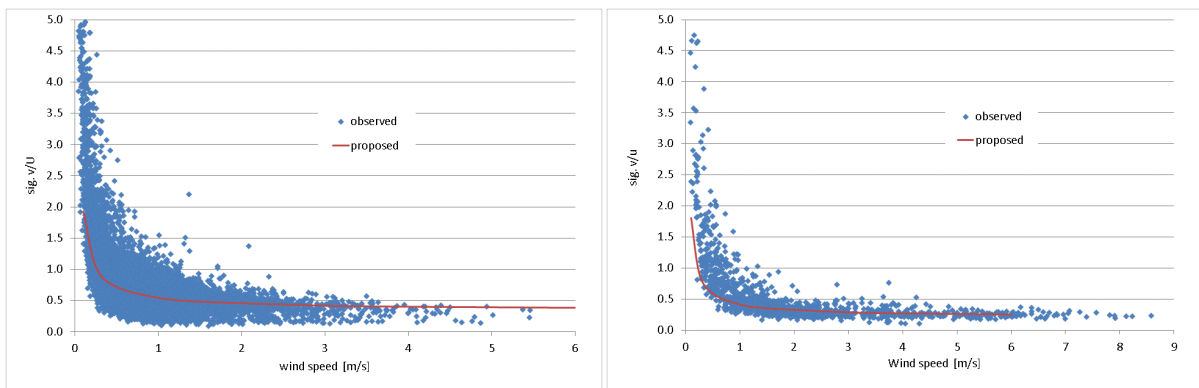


Figure 7. Scatter plot of observed vs. proposed $\sigma_{u,v}$ (Graz: $z_0=0.6m$; Trebesing: $z_0=0.15m$)

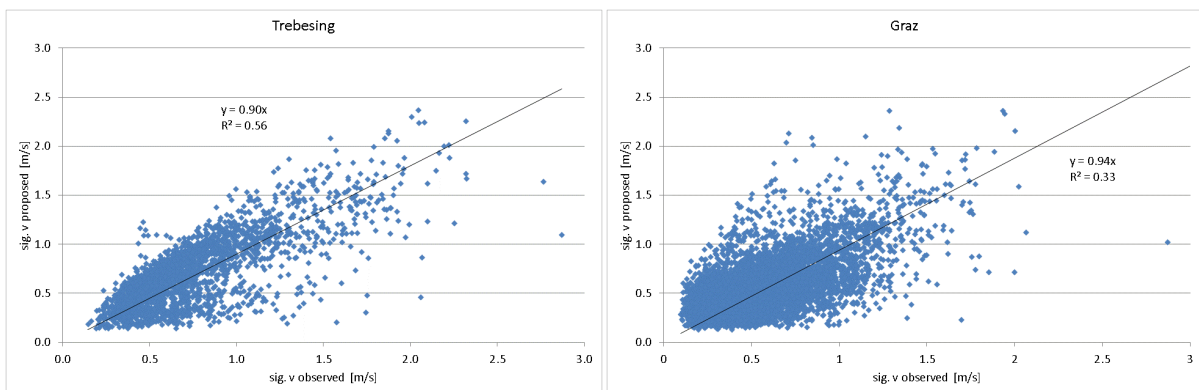


Figure 8. Scatter plot of observed vs. proposed σ_v according to the new VDI 3783-8 standard model

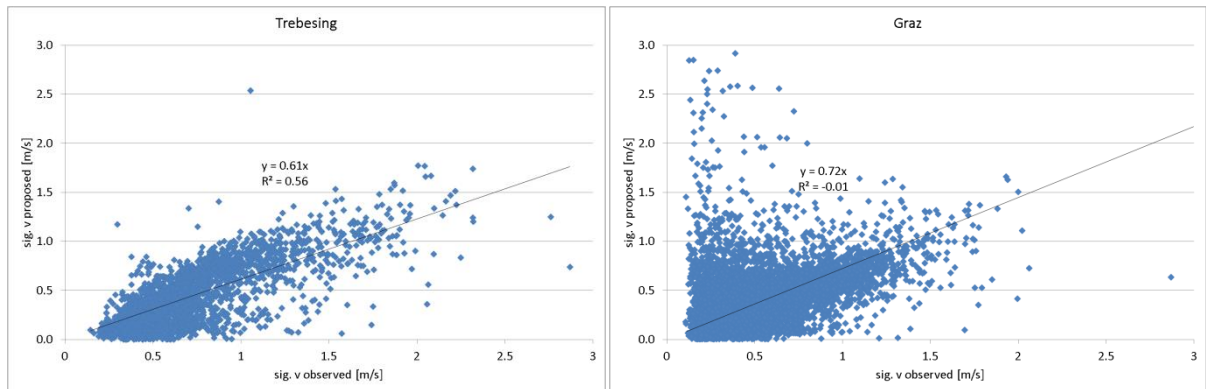


Figure 9. Scatter plot of observed vs. proposed σ_v according to Hanna (1982)

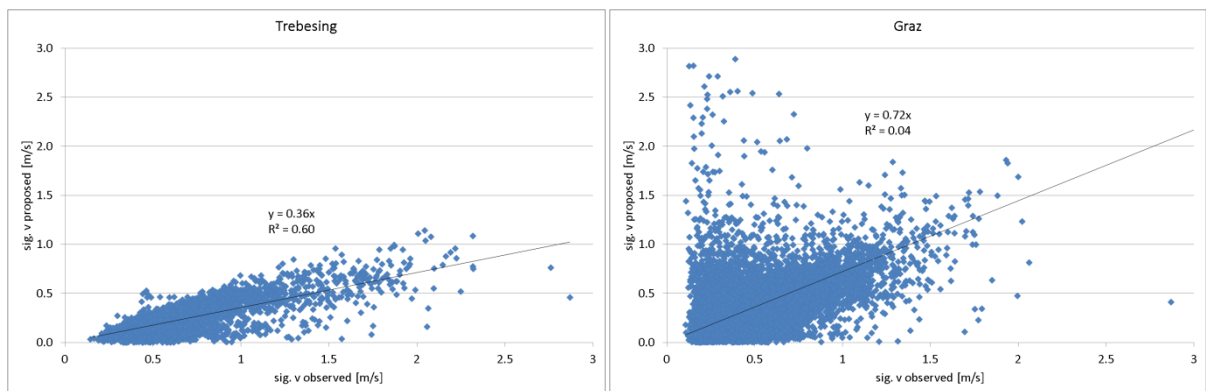
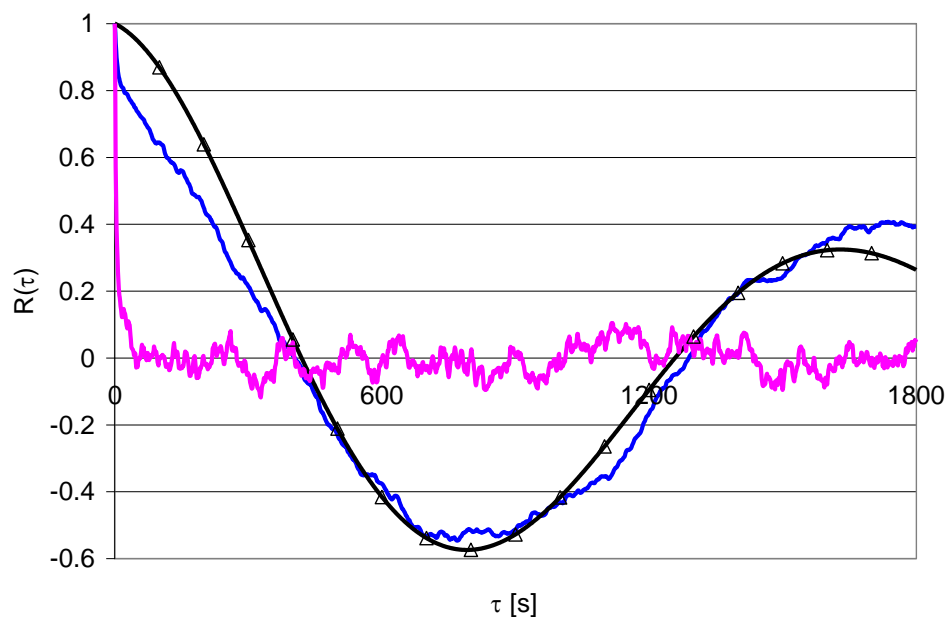


Figure 10. Example of an observed Eulerian autocorrelation function for the cross-wind component (blue), for the vertical wind component (pink) and the modeled cross-wind component with GRAL (black, triangles) in an alpine valley in a low wind speed condition.



4.5 Tunnel module

The development of the tunnel module of GRAL is described in detail in Oetttl et al. (2002). The horizontal position of the tunnel jet is modelled by simulating the along and cross wind component of the jet, which depend on the ambient wind:

$$\frac{dU_p}{dt} = -K \frac{\partial^2 (U_p - U_{pA})}{\partial y^2} \quad (28)$$

$$K = 0.3 \cdot t \quad (29)$$

$$\frac{dU_n}{dt} = \frac{1}{2} \alpha U_{nA}^2 \quad (30)$$

$$\alpha = 5 \cdot e^{-0.005 A_T \cdot U_0} \quad (31)$$

U_p : Along wind component of the tunnel jet [m s^{-1}]

K : Turbulent exchange coefficient [$\text{m}^2 \text{s}^{-1}$]

t : Dispersion time [s]

U_n : Cross wind component of the tunnel jet [m s^{-1}]

U_{pA} : Ambient wind component parallel to the tunnel jet [m s^{-1}]

U_{nA} : Ambient wind component perpendicular to the tunnel jet [m s^{-1}]

U_0 : Exit velocity the tunnel jet [m s^{-1}]

A_T : Cross section of the tunnel [m^2]

The position of the jet stream centre-line is determined largely by the ambient wind. Since the latter fluctuates around a mean value, the position of the jet stream centre-line will also vary. Hence, the dispersion of pollutants from a roadway tunnel portal is enhanced. For the model, as it is described here, it is easy and straightforward to account for ambient wind fluctuations, because the wind direction and –speed can be taken different for each released particle according to observed or parameterized standard deviations of the horizontal wind component fluctuations. A Gaussian distribution is assumed in GRAL for the probability density function of the horizontal wind components.

Note that the stiffness of the tunnel jet is taken dependent on the initial momentum represented by the cross section of the tunnel times the exit velocity.

As soon as the jet stream slows down, the cross-sectional area has to increase in order that the mass balance is kept fulfilled. This is accounted for by increasing the width of the jet stream direct proportional to the decrease of the velocity along the x-axis of the centre-line. The vertical extension of the jet stream is not changed, because the mathematical treatment of the buoyancy (see below) does not allow for an additional vertical velocity to be incorporated in the model formulation. A similar treatment was performed as soon as the jet stream changes its orientation, where particles on the inner arc move slower compared to particles at the edging arc, to keep the mass balance fulfilled.

In order to take buoyancy effects (approximately) of the tunnel jet into account, dissipation rates within the tunnel jet are modified empirically dependent on the temperature difference between tunnel air and ambient air.

$$dW = -\frac{W}{T_W} dt + \varepsilon_W^{0.5} d\omega_W, \quad (32)$$

The dissipation rate is determined according to:

$$\varepsilon_W = 0.06 \cdot \frac{U_p^2}{T_W} \quad (33)$$

$$\varepsilon_W = \text{Max}\left(\frac{\varepsilon_W}{10 \cdot \text{Max}(0.1, \Delta T^2)}, \varepsilon_W \cdot 0.01\right) \text{ for } \Delta T < 0, \text{ and}$$

$$\varepsilon_W = \varepsilon_W \cdot \sqrt{1 + \Delta T \cdot 0.5} \text{ for } \Delta T \geq 0 \quad (34)$$

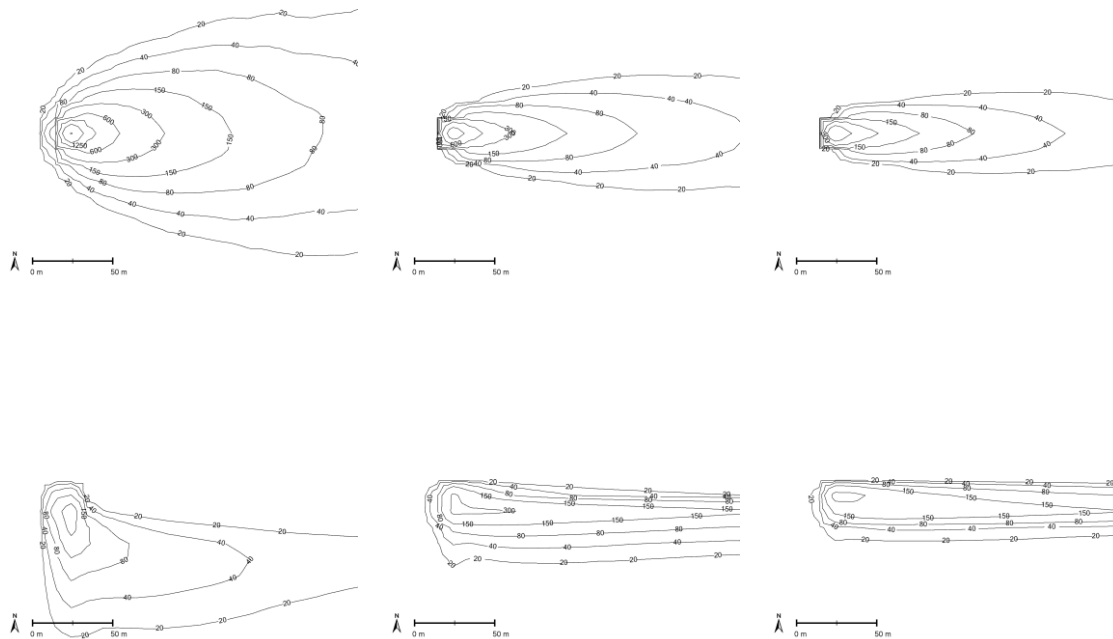
W is the vertical speed of a particle, T_W is the Lagrangian time-scale for the vertical motion, ε_W is the dissipation rate, ω_W are random numbers with zero mean and a variance equal dt , ΔT is the temperature difference between the jet stream at the portal and the ambient temperature. The Lagrangian time-scale for velocity is assumed to increase with time (Hernan and Jimenez, 1982). Note that U_p decreases usually with time:

$$T_W = 2 \cdot \frac{z}{U_p} \quad (35)$$

As soon as the orientation of the tunnel jet is very close to the ambient wind direction, ε_W is set equal to ε_A (eq. 18).

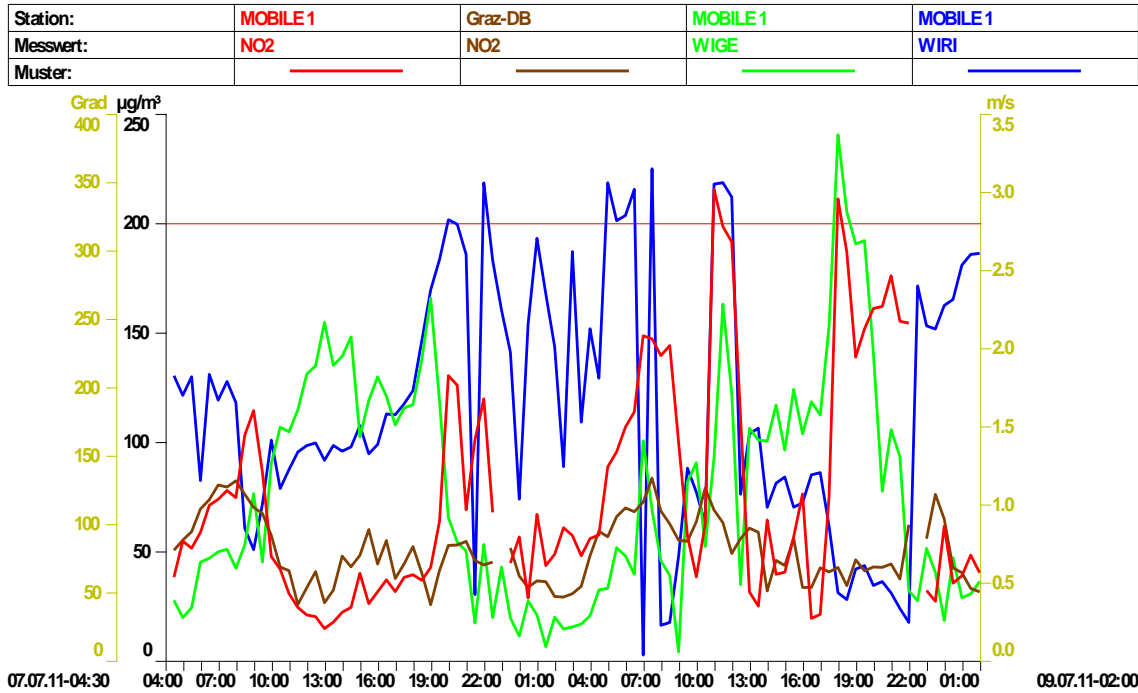
In contrast to the dispersion from e.g. point sources, dispersion from tunnel portals is different as maximum concentrations do not generally increase with decreasing wind speed, but show, according to simulations with GRAL, a maximum for medium range wind speeds.

Figure 11. Comparison of computed concentrations from a point source near ground (top) and a tunnel portal (bottom) for three different wind speeds (left: 1 m/s; middle: 3 m/s; right: 5 m/s)



Observed NO_2 concentration near the southern portal of the Plabutsch tunnel in Graz (~10 km length) show indeed highest concentrations when wind speeds were in the range between 2.5 and 3.5 m/s, while other monitoring stations at curb sites in Graz show decreasing concentrations for such wind speeds.

Figure 12. Observed NO₂ concentrations (red curve) near the Plabutsch tunnel (south portal) and at a curb site in Graz (brown curve); wind speed (green curve) and –direction (blue curve)



4.6 Buoyant plume rise

In GRAL the model of Hurley (2005) is applied in a slightly modified way. The plume grows according to the following plume rise formula:

$$\frac{dG}{dt} = 2R(\alpha v_p^2 + \beta u_a w_p + 0.1 u_p \sqrt{E}) \quad (36)$$

$$\frac{dF}{dt} = -\frac{sM}{u_p} \left(\frac{M}{M_{eff}} u_a + w_p \right) \quad (37)$$

$$\frac{dM}{dt} = F \quad (38)$$

$$G = \frac{T_a}{T_p} u_p R^2 \quad (39)$$

$$F = g u_p R^2 \left(1 - \frac{T_a}{T_p} \right) \quad (40)$$

$$M = \frac{T_a}{T_p} u_p R^2 w_p \quad (41)$$

GRAL physics

$$w_p = \frac{M}{G} \quad (42)$$

$$R = \sqrt{\frac{G + F/g}{u_p}} \quad (43)$$

$$u_p = \sqrt{u_a^2 + w_p^2} \quad (44)$$

G, F, M = plume volume, buoyancy, and momentum flux respectively,

R = plume radius (top-hat cross-section),

E = turbulent kinetic energy,

U, v, w = Cartesian x, y, z components of velocity respectively,

T = temperature,

$$s = \frac{g}{T_a} \cdot \frac{d\theta}{dz} \quad (\text{in GRAL } s \text{ is set to zero for convective and neutral conditions})$$

$$\text{In stable conditions: } \frac{d\theta}{dz} = 0.04 \cdot e^{-0.05L}$$

Subscript a refers to ambient variables, subscript p refers to plume variables,

$\alpha = 0.1, \beta = 0.6$, are vertical plume and bent-over plume entrainment constants respectively.

Anfossi et al. (2003) suggested to take $\beta = 0.7$ to improve results for water tank experiments of Willis and Deardorff (1987). In convective conditions a value of $\beta = 1.0$ has been used in order to improve modelling results for tracer experiments (see chap. 6).

$$\frac{M}{M_{eff}} = \frac{1}{2.25}, \quad g = \text{gravitational constant (9.8 ms}^{-2}\text{)}$$

Initial conditions for these equations are

$$G_0 = \frac{T_a}{T_s} w_s R_s^2, \quad F_0 = N_E g w_s R_s^2 \left(1 - \frac{T_a}{T_s}\right), \quad M_0 = \frac{T_a}{T_s} w_s^2 R_s^2, \quad R_0 = \sqrt{\frac{w_s}{(u_a^2 + w_s^2)^{0.5}}}$$

Plume rise is computed according to

$$dz_p = (w_p + \sigma_p) \cdot dt, \quad (45)$$

where

$$\sigma_p = \frac{\alpha w_p^2 + \beta u_a w_p}{3\sqrt{2}u_p}, \quad \text{and } \sigma_{up} = 2\sigma_{wp}.$$

The horizontal velocity standard deviation is computed by:

$$\sigma_{u,total} = \sqrt{\sigma_{up}^2 + \sigma_{u,ambient}^2} \quad (46)$$

Especially in low wind speed conditions, wind speed and direction usually have large deviations from the average value due to meandering. This leads to enhanced vertical plume spreads as different wind velocities lead to varying effective plume heights. To account for this effect in the vertical direction, the wind speed u_a in GRAL is not taken constant for the averaging period (usually 30 – 60 min), but is taken from a Gaussian pdf with a standard deviation equal to

$$\sigma_{ws} = 0.31 \cdot u_a + 0.25, \quad (47)$$

Dispersion time < 3 s: clamp the wind fluctuation factor between $\text{Max}(1.2, 8 - u_a \cdot 0.3)$ and $\text{Min}(0.8, u_a \cdot 0.06)$

Dispersion time ≥ 3 s: clamp the wind fluctuation factor between 0.1 and 8

which is based on sonic anemometer observations in Graz (for a brief description of this dataset the reader is referred to Anfossi et al., 2004).

Plume rise is terminated when the plume dissipation rate decreases to ambient levels:

$$\varepsilon_p = 1.5 \frac{w_p^3}{(\overline{z_p} - h_s)} < \varepsilon_a(\overline{z_p}) \quad (\text{up to version 18.01 solely in convective conditions}) \quad (48a)$$

Up to version 18.01 in neutral and stable conditions:

$$\varepsilon_p = 0.5 \frac{w_p^3}{(\overline{z_p} - h_s)} < \varepsilon_a(\overline{z_p}) \quad (48b)$$

$\overline{z_p}$ = mean plume height above ground level,

h_s = stack height.

The ambient dissipation rate is determined according to eq. (18). It has to be mentioned that Anfossi et al. (2003) suggested terminating plume rise in stable conditions whenever buoyancy of particles is equal or less than zero. Thus, for non-buoyant plumes with some exit velocity the resulting effective plume height is also zero. To avoid this, only the dissipation rate has been used in stable and neutral conditions for terminating plume rise. But the dissipation rate of the plume has been decreased in order to obtain lower effective plume heights in these conditions.

Within the first 20 s of plume rise, the time step is limited to 0.2 s, and w_p is computed as an average value from the value before and after each time step.

GRAL physics

Our investigations have shown that at high wind speeds, the momentum of the exhaust plume is lost after just a few 1/10 of a second. In some cases, this leads to high concentrations near the stack. In order to reduce this effect, which only occurs in the first time steps (a few 1/10ths of a second), the vertical particle velocity in the first 0.6 seconds after the release is set to at least " $w_p \cdot \text{EXP}(-t/1s)$ with t = time since the start of the release". Since version 24.04, this momentum is limited by formula 18 of VDI guideline 3782 – 2:

$$\Delta \square = 3.0 \cdot w_p \cdot R \cdot u_a^{-1} \quad (48c)$$

4.7 Odour hour modelling

In several countries (e.g. Austria, Germany, Switzerland, Italy) odour assessments are based on so-called odour-hours defined by at least 6 minutes of perceivable odour concentrations. It is well known that dispersion models, such as GRAL, typically provide mean concentrations for averaging times in the range of 30 – 60 minutes. Therefore, modelling odour hours requires an estimate for the 90th percentile of the cumulative frequency distribution. Often the 90th percentile is normalized by the corresponding hourly-mean concentration by defining $R_{90} = \frac{C_{90}}{\bar{C}}$, where \bar{C} is the hourly-mean concentration, and C_{90} the 90th percentile. The model developed for GRAL consists of two steps: (i) computation of the spatial distribution of the concentration variance, and (ii) calculation of R_{90} by applying a slightly modified two-parameter Weibull probability density function (PDF).

The transport equation for the concentration variance $\overline{c'^2}$ of a passive scalar neglecting molecular diffusion can be written as (e.g. Hsieh et al., 2007):

$$\frac{d\overline{c'^2}}{dt} + \overline{U_i} \frac{\partial \overline{c'^2}}{\partial x_i} + \frac{\partial}{\partial x_i} \overline{u'_i c'^2} - 2\overline{u'_i c'^2} \frac{\partial \bar{C}}{\partial x_i} + \varepsilon_c = 0 \quad (49)$$

$\overline{U_i}$ and u'_i are the time-averaged and turbulent wind-velocity components, and ε_c is the dissipation rate of the concentration variance. According to the work of Sykes et al. (1984), Hsieh et al. (2007), and Manor (2014) the turbulent flux of the concentration variance can be computed in analogy to K -theory commonly applied in the advection-diffusion equation for the mean concentration by setting

$$\overline{u'_i c'^2} = -K_i \frac{\partial \overline{c'^2}}{\partial x_i}. \quad (50)$$

K_i are the turbulent exchange components expressed by $K_i = \sigma_{u_i}^2 T_{Li}$. In the latter formulae T_{Li} are the Lagrangian integral time scales and $\sigma_{u_i}^2$ the wind-velocity variances in each direction. Furthermore, Hsieh et al. (2007) suggested

$$\varepsilon_c = \frac{\overline{c'^2}}{t_d}. \quad (51)$$

t_d is a dissipation time scale characteristic for the decay of the concentration variance. The resulting transport equation for the concentration variance is accordingly:

$$\frac{d\overline{c'^2}}{dt} + \overline{U_i} \frac{\partial \overline{c'^2}}{\partial x_i} - \frac{\partial}{\partial x_i} K_i^{(v)} \frac{\partial \overline{c'^2}}{\partial x_i} - 2\sigma_{u_i}^2 T_{Li} \left(\frac{\partial \overline{C}}{\partial x_i} \right)^2 + \frac{\overline{c'^2}}{t_d} = 0 \quad (52)$$

In a next step, eq. (52) is simplified by dropping the transport term $\overline{U_i} \frac{\partial \overline{c'^2}}{\partial x_i}$ and the turbulent diffusion term $\frac{\partial}{\partial x_i} K_i^{(v)} \frac{\partial \overline{c'^2}}{\partial x_i}$, respectively. This step can be justified either when the spatial derivatives of $\overline{c'^2}$ are small, or the dissipation time scale t_d is small. In the latter case the initial concentration variance is diminishing quickly, resulting in little contributions of the advective and turbulent fluxes in eq. (52). Manor (2014), in order to speed up the simulations, abandoned each particle (carrying the concentration variance) already after 2 - 3 dissipation time scales.

As the source term for the concentration variance $2\sigma_{u_i}^2 T_{Li} \left(\frac{\partial \overline{C}}{\partial x_i} \right)^2$ depends strongly on the spatial gradients of the mean-concentration field, significant spatial variations of $\overline{c'^2}$ between two adjacent grid cells will occur solely in regions, where significant changes in mean-concentration gradients can be found. Applying these assumptions to eq. (52) leads to:

$$\frac{d\overline{c'^2}}{dt} = 2\sigma_{u_i}^2 T_{Li} \left(\frac{\partial \overline{C}}{\partial x_i} \right)^2 - \frac{\overline{c'^2}}{t_d} \quad (53)$$

Various functions have been suggested for estimating the dissipation time scale. Manor (2014) suggests a dependency on the Lagrangian integral time scale of the form:

$$t_d = AT_L = A \left| \frac{\partial \overline{U_i}}{\partial x_j} + \frac{\partial \overline{U_j}}{\partial x_i} \right|^{-1} \quad (54)$$

Using the Joint Urban 2003 experimental dataset, Manor (2014) yielded good results by setting $A = 22$. However, Milliez and Carissimo (2008) and Hsieh et al. (2007) chose a value close to unity. Ferrero et al. (2016) suggest a time- and source-dependent function for the time-scale:

$$t_d = T_{L3s} \left[1.3 \left(\frac{t}{t_*} \right) + 1.25 \left(\frac{d_s}{h_s} \right)^{\frac{1}{3}} \right] \quad (55)$$

T_{L3s} is the vertical component of the Lagrangian integral time scale at source height, $t_* = \frac{z_i}{U_0}$

(z_i is the boundary-layer top and U_0 the free stream velocity), d_s and h_s are the source diameter and height. It can be shown that eq. (54) and (55) result in largely different values for t_d in some

cases. Assuming a neutral undisturbed boundary layer ($z_i = 500\text{m}$, $U_0 = 10\text{ m s}^{-1}$, $u_* = 0.54\text{ m s}^{-1}$) and a logarithmic wind profile $u(z) = \frac{u_*}{0.4} \ln\left(\frac{z}{z_0}\right)$ gives 118 s according to eq. (54) using $A = 22$, but a much lower initial value of 0.5 s when applying eq. (9) for $d_s = 0.5\text{ m}$ and $h_s = 10\text{ m}$. Only after one hour has been elapsed, t_d approaches 100 s, which may have little effect in the simulations as $\overline{c'^2}$ will be close to zero already in the first few seconds in this example.

It becomes clear that more research is necessary in the future on this topic. In each of the quoted studies empirical parameters were tuned to get good fits between observed and modelled $\overline{c'^2}$. In the GRAL model the relationship $t_d = 2 T_{L3}$ (unlike T_{L3s} which is evaluated at stack height) has been tested. Apart from being a simple way to estimate t_d , in contrast to eq. (55), there is no dependency on source geometries, which is crucial in applications for regulatory purposes, where overlapping plumes from multiple sources and source configurations have to be taken into account frequently. Eq. (55) is not applicable in such cases. In order to get some idea about the general applicability of setting $t_d = 2 T_{L3}$ the whole methodology has been evaluated on the basis of the Uttenweiler and JU03 data, respectively. Both differ significantly with respect to the prevailing meteorological conditions, the building structures and release conditions.

T_{L3} is obtained using $T_{L3} = \frac{2\sigma_{u_3}^2}{C_0 \varepsilon}$, whereby ε is the dissipation rate of turbulent kinetic energy, and the universal constant C_0 is set equal to 4.0. It should be stressed that resulting dissipation time scales are in most cases of the order of a few seconds, which is in agreement with the assumption of neglecting transport and diffusion in eq. (52). In contrast to the relationships used by Manor (2014), Milliez and Carissimo (2008), and Hsieh et al. (2007), t_d depends on atmospheric stability.

Once the concentration variance has been computed, R_{90} is estimated by utilizing a two-parameter Weibull PDF multiplied by the factor 1.5 to ensure that R_{90} is rather over- than underestimated:

$$R_{90} = \text{Max}\left\{1.5 \frac{(-\ln 0.1)^{1/k}}{\lambda \bar{C}}, 1.5\right\} \quad (56)$$

$$k = \left(\frac{\bar{C}}{\sqrt{\overline{c'^2}}}\right)^{1.086} \quad (57)$$

$$\lambda = \frac{\Gamma\left(1 + \frac{1}{k}\right)}{\bar{C}} \quad (58)$$

$\Gamma(\)$ is the Gamma function in eq. (57).

4.8 Dry deposition and sedimentation

According to the VDI 3945-3 the gravitational settling of aerosols is simply computed by

$$\Delta z = -v_s \Delta t, \quad (59)$$

whereby v_s is the sedimentation velocity. v_s is estimated following VDI 3782-1 in dependency on the so-called „Best-number“ given as

$$w = 4.991E - 5d_p^3 \rho_p \quad (60)$$

In eq. (60) ρ_p is the density [g cm^{-3}], and d_p is the diameter [μm]. For $w < 0.003$ v_s is set to zero, and for $0.003 \leq w < 0.24$ it is computed by

$$v_s = 1,462 \frac{\text{Re}}{d_m} [\text{cm s}^{-1}] \text{ with} \quad (61)$$

$$\text{Re} = \frac{w}{24} \quad (62)$$

For $0.24 \leq w$ the estimation is

$$v_s = 1,462 \frac{\text{Re}}{d_m} [\text{cm s}^{-1}], \text{ with} \quad (63)$$

$$\text{Re} = e^{\sum_{i=0}^6 a_i \ln w^i} \quad (64)$$

Dry deposition is modelled by assuming that a particle hitting a surface deposits a fraction p_d of its mass m :

$$m(t + \Delta t) = (1 - p_d)m(t) \quad (65)$$

Particles are discarded as soon as $m \leq 0$. Assuming that the vertical velocity distribution of the particles near ground level is represented by a Maxwell distribution shifted by the settling velocity v_s with the standard deviation σ_w , the following relationship can be deduced (VDI 3945-3):

$$p_d = \frac{2\sqrt{\pi}v_d}{\sqrt{2}\sigma_w f_s + \sqrt{\pi}v_d} \quad (66)$$

$$f_s = \sqrt{\pi} \kappa_s + \frac{e^{-\kappa_s^2}}{1 + \operatorname{erf}(\kappa_s)} \quad (67)$$

$$\kappa_s = \frac{v_s}{\sqrt{2} \sigma_w} \quad (68)$$

By definition p_d is required to be ≤ 1 . Therefore, the deposition velocity is limited by:

$$v_d \leq v_s + \sqrt{\frac{2}{\pi}} \sigma_w \frac{e^{-\kappa_s^2}}{1 + \operatorname{erf}(\kappa_s)} \quad (69)$$

Dry deposition within vegetation areas

By default, GRAL increases the deposition velocity within vegetation areas by a factor of

$$v_{dep} *= 1.5 * Coverage$$

for gases and particles PM2.5 and PM10 and by a factor of

$$v_{dep} *= 3.0 * Coverage$$

for particles PM30 and larger. Coverage is a value that can be entered for each vegetation area.

It is possible to replace these fixed factors 1.5 and 3 with your own scaling factors starting from GRAL version 21.09. Thus, in connection with the coverage value, a spatial varying deposition velocity can be created.

To use your own scaling factors, you have to create a file named "VegetationDepoFactor.txt" in the Computation folder (see chapter 17.2.1.40).

4.9 Wet deposition

According to the VDI 3945-3 the wet deposition can be computed by

$$\varepsilon_W = r c_W \tau \quad (69a)$$

whereby ε_W is the deposited fraction and τ is the time step. r_W is the washout rate, calculated by the following equation

$$r_W = c_W \left(\frac{F_N}{1 \frac{mm}{h}} \right)^{\alpha_W} \quad (69b)$$

In eq. (69a) c_W and α_W are pollutant specific parameters. F_N is the precipitation rate in mm/h.

4.10 Decay rates

User-defined decay rates λ in s^{-1} reduce the particle mass every time step by applying an exponential function:

$$m_{t+1} = m_t e^{-\lambda t} \quad (69c)$$

Decay rates can be used to simulate inactivation rates of e.g. bacteria, or radioactive decay.

5 GRAL methods

5.1 Meteorological pre-processor

There are several ways for providing meteorological input information:

- 1) Input of wind speed, -direction, u_* , L , $\sigma_{u,v,w}$, m , and T . Such data can for instance be processed from sonic anemometer observations. No vertical gradients are used in this case. Such an input might be appropriate when dealing with simulation of tracer experiments, where detailed data of tracer release, meteorology, and concentrations is available in the surface layer.
- 2) Input of wind speed, -direction, u_* , L , $\sigma_{u,v}$, and h . Wind speed, -direction and $\sigma_{u,v}$ can be provided at various heights. GRAL performs a linear interpolation between the observations.
- 3) Input of wind speed, -direction, and L at various heights. Again a linear interpolation between these observations is performed.
- 4) Input of 3 stability classes (3=stable, 2=neutral, and 1=convective), wind speed, -direction, and frequency.
- 5) Input of 7 stability classes (PGT-classes), wind speed, -direction, and frequency. This is the most common input format for regulatory applications.

Depending on the chosen input options, the corresponding missing turbulence quantities have to be computed by GRAL (meteorological pre-processor).

When stability classes are used as input, the Obukhov length is computed based on the suggestions of the German standard boundary layer model (VDI 3783-8) using the following relationships:

$$L = \text{Min} \left(\left(\frac{1}{(a \cdot [z_0 \cdot 100]^b)} \right)^{-4} \right) \text{ for stability classes A-C,} \quad (70)$$

$$L = \text{Max} \left(\left(\frac{1}{(a \cdot [z_0 \cdot 100]^b)} \right)^4 \right) \text{ for stability classes E-G} \quad (71)$$

$$L = 1000 \text{ for stability class D} \quad (72)$$

a and b are constants, which depend on the stability class, and z_0 is the roughness length.

Table 1. Empirical constants a , and b for the determination of the Obukhov length

	a	b
A	-0.37	-0.55
B	-0.12	-0.50
C	-0.067	-0.56
E	0.01	-0.50
F	0.05	-0.50
G	0.20	-0.55

The friction velocity is then computed according to Venkatram and Du (1997) for

$$\text{stable conditions } \frac{u_a}{u_*} = \frac{1}{k} \cdot \left[\ln \left(\frac{z_a}{z_0} \right) + 5 \cdot \left(\frac{z_a}{L} \right)^2 \right], \quad (73)$$

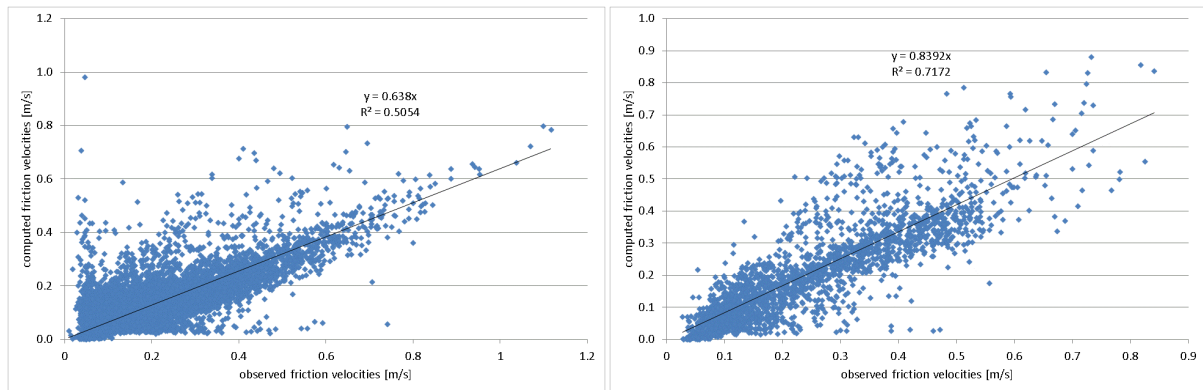
$$\text{and for convective conditions } \frac{u_a}{u_*} = \frac{1}{k} \cdot \left[\ln \left(\frac{z_a}{z_0} \right) - \psi_m \left(\frac{z_a}{L} \right) \right], \quad (74)$$

$$\text{where } \psi_m = \ln \left(\frac{1+x^{-2}}{2} \left[\frac{1+x^{-1}}{2} \right]^2 \right) - 2 \cdot \tan^{-1} x^{-1} + \frac{\pi}{2}, \quad (75)$$

$$\text{and } x = \left(1 - 16 \cdot \frac{z_a}{L} \right)^{0.25}. \quad (76)$$

z_a : is the anemometer height above ground level, and u_a the observed wind speed at that height. The minimum value for u_* is set to 0.02 m/s. From Figure 13 it can be concluded that computed friction velocities are underestimating observed values. This error is partly compensated by the fact, that the expression for the vertical wind standard deviation overestimates observed values (Figure 1). Future work will focus on establishing better estimators for friction velocities.

Figure 13. Comparison of observed vs. computed friction velocities (left: Graz dataset; right: Trebesing dataset)



5.2 Time management

Concentrations are calculated according to:

$$C = \sum_{i=1}^R \frac{m_{p,i}}{dV \cdot T_{ges}} dt, \quad (77)$$

where m_p is the “pollutant mass” of one particle defined by the emission rate per source divided by the assigned number of released particles per time unit and source. R is the total number of integration steps. The total number of released particles (for all sources) is defined by:

$$N = T_{ges} \, dn/dt, \quad (78)$$

where dn/dt are the user-specified released particles per second. dV is the volume of one cell, and T_{ges} is the averaging time for the concentration computation defined by the user (usually 1800 s or 3600 s).

GRAL provides two options for the time series computation:

Steady-state mode (standard):

Computation of steady-state concentration fields: In this case particles are tracked until they leave the model domain regardless the time they need to do so. As the total number of released particles is calculated according to eq. (58), there is no dependence of concentrations on the selected dispersion time. This calculation results in stationary concentration fields for given weather situations.

Transient mode:

Computation of concentrations fields, which are dependent on the averaging time chosen: In this case particles are only tracked until the dispersion time is elapsed. Moreover, the last particle’s position is rendered into a three-dimensional concentration field, which is

stored for the following weather situation. In the following weather situation, each cell of the concentration field is converted back into a particle mass. One single particle is released for each cell of the three-dimensional concentration field. From version 20.09 multiple particles, each with a maximum of 10 times the mass of an average lagrangian particle, are released for one concentration field grid cell. This procedure is used to reduce statistical errors.

The transient concentration grid is based on the Cartesian grid used for the microscale flow-field simulations in the horizontal direction. In vertical direction, it uses the height of the first grid cell of the flow-field grid with an independent vertical stretching algorithm, which is not adjustable by the user (see chapter 5.9.5). The grid itself is terrain following. All these secondary particles share the same properties with regard to mean deposition and sedimentation velocities for each user defined source group.

Emissions can be modulated for each weather situation and source group using the input file "emissions_timeseries.txt" (see Appendix A). Exit velocities and exit temperatures of point and portal sources are also modulateable (per source, see Appendix A).

5.3 Particle management

The total number of released particles (for all sources) is defined by the product of dispersion time and the number of particles released per second specified by the user. Starting from the original GRAL version, the particles are assigned to the sources in proportion to the emission rate. In the GRAL original version, the particle "pollutant mass" was fixed for all particles as a quotient of the total emission rate and the total particle number. Starting by introducing the deposition calculation in GRAL V 17.01, the mass of each particle is calculated from the ratio of the emission rate and the particles assigned to each source.

Due to the nature of Lagrangian particle models, computed pollutant concentrations are prone to a sampling error. This error can be minimized if the number of particles is high enough.

However, it is recommended that the user checks the file 'Logfile_GRALCore.txt', which can be found in the folder directory where GRAL has been launched. In the case of large model domains with a large number of sources, there may not be enough particles defined by the user to adequately represent all sources in the simulation. In these cases, GRAL automatically increases the number of released particles. However, if the total number of particles (as documented in the logfile) is more than about 20 % higher than initially defined

by the user, it is highly recommended to increase the total number of particles in the simulations and to re-run the simulations from the beginning.

The following table lists the minimum number of automatically assigned particles per source, if the total initial number of particles is too low. A source is a point source, a portal source, a line source segment or an area source partial section.

	Minimum Number of Particles per Source			
Number of Sources	Point sources	Tunnel portals	Area sources	Line sources
< 2000	20	20	5	5
2000 up to 30.000	10	10	3	3
>30.000	5	5	1	3

As of GRAL version 20.01 a file “Receptor_Timeseries_Transient.txt” is written at the end of a calculation. This file contains the estimated statistical error for each receptor point in the last line. High error values indicate that too few particles were used in the simulation. A value NA (not available) means that no concentration at this receptor (no particle) has been counted.

At the very beginning of each new dispersion situation, the starting positions of the particles within the source geometry (user defined source volume) are recalculated by a random generator.

5.4 Coupling with GRAMM (Graz Mesoscale Model)

To take the presence of topography into account, GRAL can be linked with the prognostic wind field model GRAMM. GRAMM solves the conservation equations for mass, enthalpy, momentum, and humidity. There exists also a radiation model to take long- and short wave radiation into account. The surface energy balance is calculated in a surface module, where several different land use categories are used to define the surface roughness, the albedo, the emissivity, the soil moisture content, the specific heat capacity of the soil, and the heat transfer coefficient. GRAMM uses a $k-\varepsilon$ Modell for turbulence closure.

GRAMM can only be linked with GRAL, if options 4) or 5) are used as meteorological input (see chap. 5.1). The vertical temperature and humidity gradient as well as the sun azimuth are

GRAL methods

chosen in dependence on the stability class. For instance, in stable conditions a temperature inversion and no solar radiation are defined in GRAMM. This leads to a cooling of the surface and the development of drainage flows.

Complex terrain without buildings:

Here, the wind field and stability classes calculated by GRAMM, and the grid information are used as input to GRAL. As GRAMM uses a terrain-following grid with a rather complex tetrahedral structure (Almbauer, 1995), it was necessary to interpolate the 3D wind fields of GRAMM on a finer Cartesian grid established in GRAL in order to fulfil mass conservation. This is done by forcing the sum of all mass fluxes over the surfaces of each control volume of the Cartesian grid to zero. In GRAL the vertical surface flux (when starting from the bottom: the top surface flux of each cell) is corrected for each cell.

It is easy to show for a Cartesian grid that using this velocity field defined at the surfaces of the control volumes, instead of using the velocities defined in the centres of the corresponding grid cells, is adequate for a Lagrangian dispersion model, provided that the velocities at any location of a particle is computed by linear interpolation.

Table 2. Land use categories used in GRAMM and GRAL

CLC_CODE	LABEL1	LABEL2	LABEL3
111	Artificial surfaces	Urban fabric	Continuous urban fabric
112	Artificial surfaces	Urban fabric	Discontinuous urban fabric
121	Artificial surfaces	Industrial, commercial and transport units	Industrial or commercial units
122	Artificial surfaces	Industrial, commercial and transport units	Road and rail networks and associated land
124	Artificial surfaces	Industrial, commercial and transport units	Airports
131	Artificial surfaces	Mine, dump and construction sites	Mineral extraction sites
141	Artificial surfaces	Artificial, non-agricultural vegetated areas	Green urban areas
211	Agricultural areas	Arable land	Non-irrigated arable land
231	Agricultural areas	Pastures	Pastures
242	Agricultural areas	Heterogeneous agricultural areas	Complex cultivation patterns
243	Agricultural areas	Heterogeneous agricultural areas	Land principally occupied by agriculture, with significant areas of natural vegetation
311	Forest and semi natural areas	Forests	Broad-leaved forest
312	Forest and semi natural areas	Forests	Coniferous forest
313	Forest and semi natural areas	Forests	Mixed forest
321	Forest and semi natural areas	Scrub and/or herbaceous vegetation associations	Natural grasslands
322	Forest and semi natural areas	Scrub and/or herbaceous vegetation associations	Moors and heathland
324	Forest and semi natural areas	Scrub and/or herbaceous vegetation associations	Transitional woodland-shrub
332	Forest and semi natural areas	Open spaces with little or no vegetation	Bare rocks
333	Forest and semi natural areas	Open spaces with little or no vegetation	Sparsely vegetated areas
335	Forest and semi natural areas	Open spaces with little or no vegetation	Glaciers and perpetual snow
411	Wetlands	Inland wetlands	Inland marshes

511	Water bodies	Inland waters	Water courses
512	Water bodies	Inland waters	Water bodies

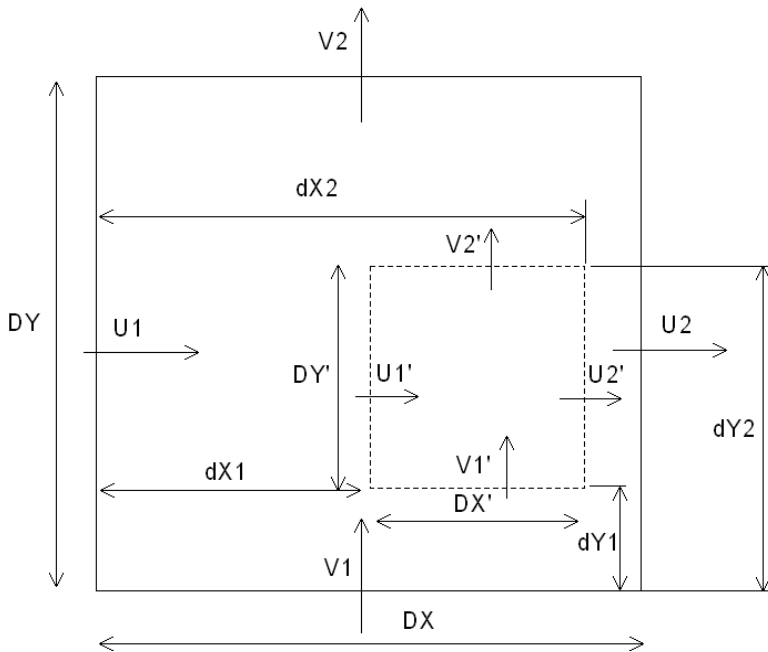
For simplicity the proof is shown for a two-dimensional grid but can easily be extended to three dimensions. Figure 14 shows the nomenclature used afterwards. As the mass fluxes obtained at the surfaces for each control volume from the wind field model comply with mass conservation one can write:

$$U_1 \cdot DY - U_2 \cdot DY + V_1 \cdot DX - V_2 \cdot DX = 0 \quad (79)$$

or

$$\frac{U_1}{DX} - \frac{U_2}{DX} + \frac{V_1}{DY} - \frac{V_2}{DY} = 0 \quad (80)$$

Figure 14. Nomenclature used for proofing, that mass conservation remains fulfilled when using a linear interpolation algorithm to determine the velocity components at each particle location.



For any arbitrary volume (dashed lines in Figure 14) within a hexahedron one can control mass conservation when applying a linear interpolation algorithm in a straight forward manner:

$$U_1' \cdot DY' - U_2' \cdot DY' + V_1' \cdot DX' - V_2' \cdot DX' =$$

$$\left(\frac{U_2 - U_1}{DX} \cdot dX_1 + U_1 \right) \cdot DY' - \left(\frac{U_2 - U_1}{DX} \cdot dX_2 + U_1 \right) \cdot DY' +$$

GRAL methods

$$+\left(\frac{V_2 - V_1}{DY} \cdot dY_1 + V_1\right) \cdot DX' - \left(\frac{V_2 - V_1}{DY} \cdot dY_2 + V_1\right) \cdot DX' \quad (81)$$

And after some simple calculus one obtains:

$$\begin{aligned} U_1' \cdot DY' - U_2' \cdot DY' + V_1' \cdot DX' - V_2' \cdot DX' = \\ DY' \cdot DX' \cdot \left(\frac{U_1}{DX} - \frac{U_2}{DX} + \frac{V_1}{DY} - \frac{V_2}{DY} \right) = 0 \end{aligned} \quad (82)$$

5.5 Flow field in the presence of obstacles

5.5.1 Complex terrain (using coarse GRAMM wind fields)

In case of larger model domains (e.g. urban scale), GRAL provides a simple procedure to take obstacles into account in the dispersion calculations. In GRAL the user can specify a much finer Cartesian grid, than used in GRAMM. For instance, when GRAMM simulations were carried out with a horizontal grid spacing of 300 m, grid sizes of e.g. 5 m in GRAL could be chosen to resolve obstacle structures.

In a first step GRAL interpolates the 3D wind fields of GRAMM on a finer Cartesian grid as described in chap. 5.4. There are two different methods available to take buildings into account:

Diagnostic approach (level 1 - only for very large model domains recommended):

Close to buildings a logarithmic wind profile is introduced. The following function is used:

$$u_{u,v}^* = u_{u,v}^{\text{int}} \cdot \prod_{i=1}^n \frac{\ln\left(\frac{s_i}{z_0}\right)}{\ln\left(\frac{20}{z_0}\right)}, \quad (83)$$

where $u_{u,v}^{\text{int}}$ are the interpolated wind field components from the coarse resolution computations, and s_i are the distances to all nearby buildings within 20 m (Figure 15 and Figure 16). At larger distances no influence of obstacles on the grid point is assumed. A value of 0.1 m (~1/30 of the obstacles dimensions in a street canyon, e.g. parking cars; Zannetti, 1990) is chosen for the roughness length z_0 . Conservation of mass is obtained by solving eq. (64) equation iteratively to get a 3D pressure field which is subsequently used to correct the velocity components:

$$\rho \frac{\partial \bar{u}_i}{\partial x_i} = \frac{\partial^2 \bar{p}}{\partial x_i^2} dt \quad (84)$$

Figure 15. Sketch of the interpolation procedure used to obtain a first guess wind field for the fine Cartesian grid (thin lines), which resolves building structures, from the coarse (thick lines) wind field simulations. Note that the difference between the coarse grid in mesoscale applications and the fine grid is much higher as shown here. Obstacles are marked in grey.

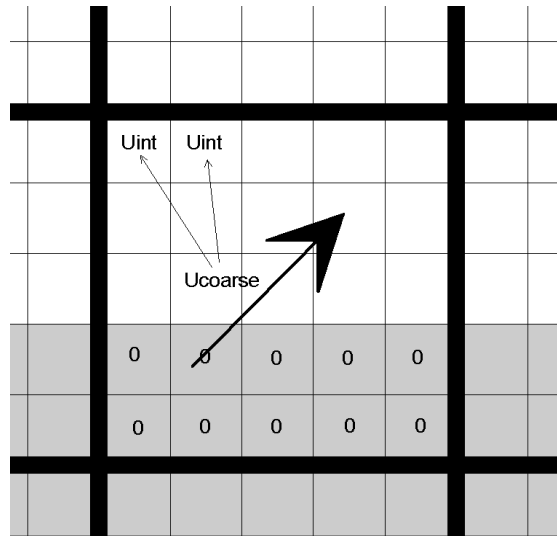
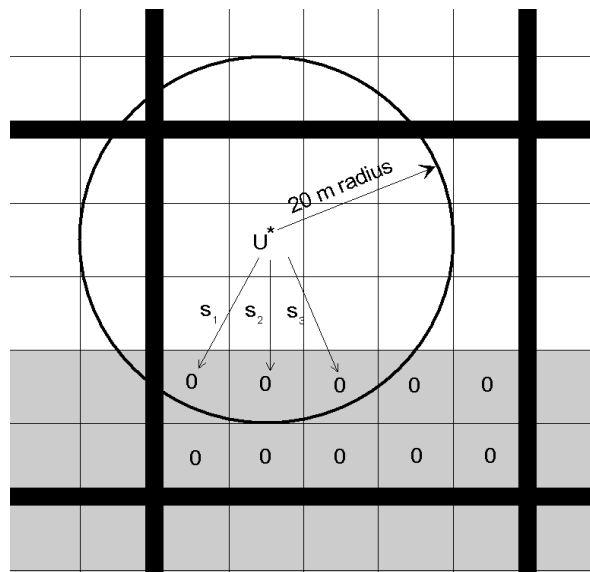


Figure 16. Sketch of the procedure to correct the interpolated wind field of the fine grid by applying a logarithmic wind profile near obstacles. Only obstacles within a distance of 20 m from the cell in consideration are taken into account.



Prognostic approach (level 2 - recommended method):

In this case GRAL simulates the flow around obstacles by solving the well-known Reynolds-averaged Navier-Stokes equations (RANS), neglecting molecular viscosity, Coriolis and buoyancy forces, and utilizing an eddy viscosity turbulence model:

GRAL methods

$$\frac{\partial \bar{u}_i}{\partial t} + \bar{u}_j \frac{\partial \bar{u}_i}{\partial x_j} = -\frac{1}{\rho} \frac{\partial \bar{p}}{\partial x_i} + \frac{\partial}{\partial x_j} \left[K \left(\frac{\partial \bar{u}_i}{\partial x_j} + \frac{\partial \bar{u}_j}{\partial x_i} \right) - \frac{2}{3} \delta_{ij} k \right] \quad (85)$$

\bar{u}_i mean wind speed in horizontal and vertical directions

ρ air density

$\frac{\partial \bar{p}}{\partial x_i}$ mean pressure gradient acceleration

k, ε turbulent kinetic energy, and dissipation rate

K eddy viscosity

Currently three different turbulence models are implemented in the GRAL model :

No-diffusion model :

In this case the turbulent viscosity is set to zero. Although physically unrealistic, this mode facilitates testing the model in the development phase.

Algebraic mixing-length model :

Besides constant turbulent viscosity models, mixing-length models are the most simplest turbulence models. They have first been proposed by Prandtl (1925). The model is based on the assumption that if a turbulent eddy displaces a fluid particle by distance l_m its velocity will differ from its surrounds by an amount $l_m |\partial U / \partial z|$.

$$K = l_m^2 \left| \frac{\partial U}{\partial z} \right| \quad (86)$$

Wilcox (2006) suggests for a mixing layer:

$$l_m = 0.071z \quad (87)$$

Standard $k-\varepsilon$ model:

The standard $k-\varepsilon$ turbulence model (e.g. Rodi, 1980) is defined by:

$$\frac{\partial k}{\partial t} + \bar{u}_j \frac{\partial k}{\partial x_j} = \frac{\partial}{\partial x_j} \left(K \frac{\partial k}{\partial x_j} \right) + P_m + P_b - \varepsilon \quad (88)$$

$$\frac{\partial \varepsilon}{\partial t} + \bar{u}_j \frac{\partial \varepsilon}{\partial x_j} = \frac{\partial}{\partial x_j} \left(K \frac{\partial \varepsilon}{\partial x_j} \right) + \frac{\varepsilon}{k} (1.44 \cdot (P_m + P_b) - 1.92 \cdot \varepsilon) \quad (89)$$

P_m production term for turbulent kinetic energy due to shear stresses

P_b production term for turbulent kinetic energy due to buoyancy

$$P_m = K \cdot \left(\frac{\partial \bar{u}_i}{\partial x_j} + \frac{\partial \bar{u}_j}{\partial x_i} \right) \cdot \frac{\partial \bar{u}_i}{\partial x_j} \quad (90)$$

$$P_b = 1.35 \cdot K \cdot \frac{g}{\theta_0} \frac{\partial \bar{\theta}}{\partial x_3} \quad (91)$$

The temperature gradient $\frac{\partial \bar{\theta}}{\partial x_3}$ is a function of stability class, and is kept constant throughout a simulation. Conservation of mass is obtained by solving the Poisson equation after each time step:

$$\rho \frac{\partial \bar{u}_i}{\partial x_i} = \frac{\partial^2 \bar{p}}{\partial x_i^2} dt, \quad (92)$$

At the lowest grid cell and next to building surfaces the turbulent kinetic energy k and dissipation rate ε are computed diagnostically (Eichhorn, 2011):

$$k = \frac{u_*^2}{\sqrt{c_\mu}} \quad (93)$$

$$\varepsilon = \frac{u_*^3}{\kappa d} \quad (94)$$

c_μ is a constant of the standard $k - \varepsilon$ model (0.09), κ is the von Kármán constant (0.4), u_* is friction velocity, and d is either half of the cell height of the first cell above ground (or buildings), or the distance between cell centres and adjacent vertical building walls.

Typically, eq. (83) is used in CFD-models for computing the turbulent exchange coefficient:

$$K = c_\mu \frac{k}{\varepsilon}, \quad (95)$$

During the model evaluation it became apparent that results depended somehow on the cell sizes when using eq. (94). As a consequence, the required independency of computed flow fields with regard to grid resolution according to the VDI guideline 3783-9 (VDI, 2016) could not be fulfilled. Therefore, a different expression (eq. 95) was tested, which eventually led to compliance with respect to this aspect.

$$K = 0.09 \cdot \sqrt{k} \cdot z \quad (96)$$

GRAL methods

In eq. (96) z is the vertical distance to the surface or the top of obstacles. Note, that although the dissipation rate is not used in eq. (96), the conservation equation for dissipation is still solved to obtain k .

Surface friction:

Regardless of the turbulence model, surface friction is taken into account by adding the following source term in the discretised conservation equations for momentum at the first layer above ground:

$$-\frac{\overline{u_i}}{\overline{v_1}} \cdot \overline{u_*^2} \cdot \Delta x \cdot \Delta y, \quad \text{where} \quad (97)$$

$\overline{v_1}$ is mean wind speed in the first layer

Vegetation:

Currently, vegetation can only be considered when using the (default) mixing-length model. The following source term is added in the momentum equations (e.g. Green, 1992):

$$-c_D n L A D u_i U, \quad (98)$$

where c_D is an empirical drag-coefficient ($0.3n^2$), n is the dimensionless vegetation coverage, LAD the leave-area density [m^2/m^3], u_i the wind-speed component [m/s], and U the total wind speed [m/s].

In addition to this source term in the momentum equations, the mixing length is strongly reduced within the vegetation layer by:

$$l_m = l_m (1 - 0.99n) \quad (99)$$

Numerical solver:

In order to solve the conservation equations numerically, a finite volume method utilizing a staggered grid is applied as drawn in Figure 17 for one dimension. ϕ stands for any conserved quantity, such as turbulent kinetic energy, u -component, or dissipation rate, while u_w is the transport velocity at the western cell face. Non-hydrostatic pressure is also located in the centre of each grid cell (ϕ_p), and transport velocities u_w and u_e are corrected by a non-hydrostatic pressure field (eq. 92) after each time step to match mass conservation.

Conservation equations are solved by a fully implicit time discretization scheme, and the “power-law” method suggested by Patankar (1980). For the west face of a grid cell owing a volume $\Delta x \Delta y \Delta z$ it can be written as (using the notation of Patankar, 1980):

$$a_w = D_w \cdot \max \left[0, \left(1 - \frac{0.1|F_w|}{D_w} \right)^5 \right] + \max[0, F_w] \quad (100)$$

$$D_w = \rho K \frac{\Delta y \Delta z}{\Delta x}, \text{ and } F_w = \rho u_w \Delta y \Delta z \quad (101)$$

The reader is referred to Patankar (1980) for detailed information about all other terms appearing in the fully implicit time discretization equation of any quantity ϕ (here for simplicity written in one dimension):

$$a_p \phi_p = a_e \phi_e + a_w \phi_w + b \quad (102)$$

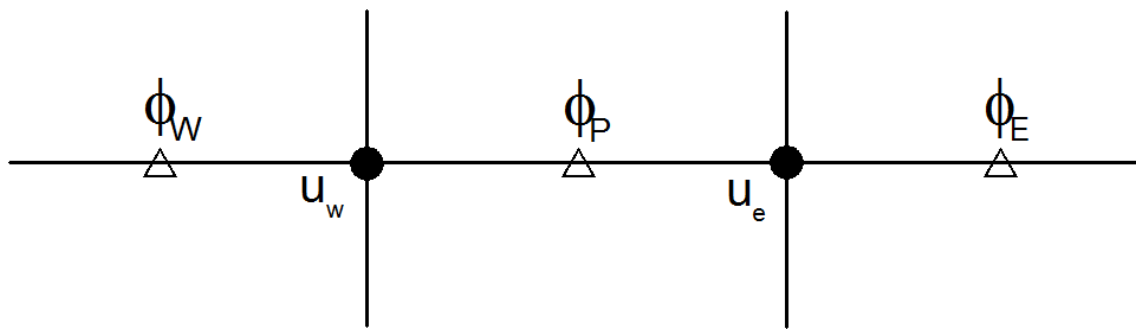


Figure 17. Grid used in GRAL for discretizing conservation quantities

The conservation equations for momentum, turbulent kinetic energy, and dissipation are linearized and iteratively solved using a tri-diagonal-matrix algorithm (TDMA). Finally, the entire algorithm is repeated for each time step using the SIMPLE (Semi-Implicit Method for Pressure Linked Equations) method. In order to ensure numerical stability of the iterative procedure, a relaxation factor of 0.1 was applied during each time step for all velocity components.

Simulations can be performed until an internal convergence criterion is reached. The criterion is formulated by defining a lower limit for the normalised non-hydrostatic pressure correction of 0.012 (summed up over 100 subsequent time steps). Normalisation is done by $\rho \cdot \overline{v_{top}}^2$, where $\overline{v_{top}}$ is the wind speed at the top of the model domain.

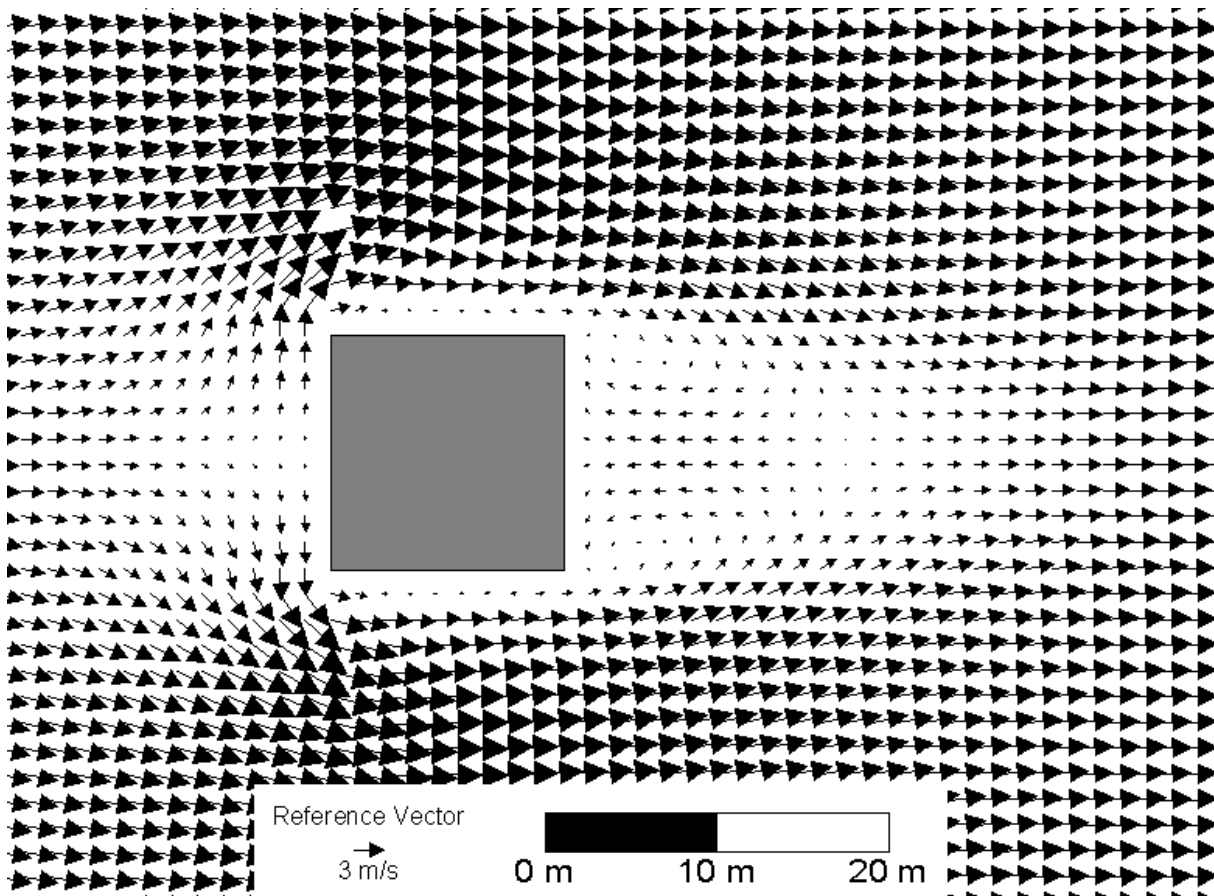
GRAL is mainly used in applications for regulatory purposes. Thus, computation times need to be small enough to enable operation on conventional PCs or Laptops. For larger domains of some hundreds of metres up to a few kilometres, and grid sizes below 5 m, CFD simulations can be quite demanding. In order to make use of multiple CPUs, GRAL has been parallelized. Furthermore, the microscale wind-field model is only applied in regions around buildings up to 15 (this value can be increased by the user) times the building heights. While horizontally only

GRAL methods

constant grid spacing is allowed in the current version, a user may define a stretching factor ≥ 1.0 (or height dependend stretching factors) for the vertical grid to save computation time.

At the inflow boundary of the model, a wind profile was established by using eq. (1), while at the outflow lateral boundaries and at the top of the model domain homogeneous Neumann conditions for the velocity components are imposed to avoid reflexion of waves (Grawe et al., 2013). Whether a lateral side of the modelling domain is classed as an outflow or inflow boundary is determined at the beginning of any simulation by examining the direction of the wind component normal to the specific boundary. Standard profiles for dissipation rate, and standard deviations of wind velocity fluctuations σ_i are calculated (see chap. 4.3 and 4.4) to define lateral boundary conditions and initial values for turbulent kinetic energy and dissipation rate for the microscale flow-field model.

Figure 18. Example of flow computed with GRAL around a cubic like building



5.5.2 Flat terrain (without GRAMM coupling)

The procedure is the same as in chap. 5.5.1, except that instead of the 3D wind fields of GRAMM, vertical profiles of wind speed as computed by eq. (1) are used.

5.6 Boundary conditions

In the vertical direction perfect reflexion of particles is assumed at the bottom of the model domain. As topography is stepwise resolved in GRAL, also in the horizontal directions boundary conditions are necessary. Here reflexion is treated such that particles start at the previous position (before they were found below the surface) and the turbulent velocities are taken negative.

When buildings are present, perfect reflexion in the horizontal would lead to asymmetries in the concentration patterns in low wind speed conditions. This is the case, because eq. (24-25) do not only describe the turbulent fluctuation but also the meandering part. A meandering flow in the vicinity of buildings is not appropriate, because large horizontal motions (=meandering) are suppressed near the walls. While classical turbulent diffusion is stochastic for time scales larger than the Lagrangian integral time, meandering should be stochastic at much larger time scales. Stochastic means that there is no preferred dispersion for each direction (e.g. dispersion towards south has an equal probability as towards north). In case of meandering, perfect reflexion would lead to a preferred direction of dispersion as the negative turbulent velocity after reflexion will be maintained for a long time according to eq. (24-25). To partly overcome this problem, instead of taking the negative value for the turbulent velocity, a random turbulent velocity is taken with an average of zero and a standard deviation equal to $\sigma_{u,v}$ after the reflexion of a particle.

5.7 Computation of concentration statistics

The preferred mode of GRAL is the computation of steady-state concentration fields for classified meteorological conditions (using 3-7 stability classes, 36 wind direction classes, and several wind speed classes). Each of the steady-state concentration fields is stored as separate file. By using a post processing routine (e.g. in the GRAL GUI) pseudo time series of concentration field can be obtained by taking the corresponding time series of classified meteorological situations of a certain period (covering up to several years) and multiplying each concentration field corresponding to certain hours of that period with some emission modulation factors. Usually about 500 – 600 bins of meteorological situations characterise the dispersion conditions, which is considerably less than the computation of e.g. more than more than 8000 hours of one year.

In the GRAL transient mode, all hours of the period (e.g. one year) are calculated and the emission modulation and any possible modulations of the outlet temperature and outlet velocity are calculated inside the GRAL calculation core. Released particles remain in the model area and are further tracked in subsequent weather situations. Each transient concentration field is stored as one separate file.

GRAL methods

GRAL allows the storage of concentration fields in dependence on user specified source groups. Up to 99 source groups can be distinguished (e.g. traffic, domestic heating, industry, re-suspension). In this way, averages, maximum daily means, or maximum concentrations for defined periods can be computed in a rather fast post processing routine.

5.8 Surface roughness lengths

Typically, for flat terrain, the average surface roughness length is defined in line 6 of the file in.dat. When coupled with GRAMM, the spatially GRAMM surface roughness length, if available, using the coarse GRAMM grid will be used by GRAL.

Spatially user defined roughness (from version 20.09)

If the file "RoughnessLengthsGral.dat" is used to define the spatially defined surface roughness, the „Adaptive roughness“ Algorithm value in line 18 of the file in.dat must be greater than 0. In this case, the surface roughness values from the file RoughnessLengthsGral.dat are used for both flat and complex terrain.

Adaptive Roughness algorithm (from version 20.09)

If the upper value of the surface roughness in line 18 of in.dat is greater than 0 and there is no file "RoughnessLengthsGral.dat", the meaning of the surface roughness in line 6 of in.dat changes. In this case, the minimum surface roughness within the GRAL domain area must be specified in line 6.

The local surface roughness is subsequently determined in the "adaptive roughness" algorithm according to the following procedure (pseudo code):

```
Z0Min //(line 6 in in.dat)
```

```
Z0Max //(line 18 in in.dat)
```

- $Z0[x][y] = \text{LowPassFilter}[\text{Log10}(\text{BuildingHeight})]$
- Set the surface roughness to the building wall roughness inside buildings
- $\text{LowPassFilter}[\text{VegetationHeight}]$
- $Z0[x][y] = \text{Max}[\text{Min}[1.5, \text{VegetationHeight}], Z0[x][y]]$
- If topography is available

```
     $Z0[x][y] = \text{Max}[Z0\text{Gramm}[i][j], \text{Min}[Z0\text{Max}, Z0[x][y]]]$ 
```

```
else // Flat Terrain
```

```
     $Z0[x][y] = \text{Max}[Z0\text{Min}, \text{Min}[Z0\text{Max}, Z0[x][y]]]$ 
```

The low pass filter is a two-dimensional gaussian filter whose weighting square is calculated depending on the grid size and the standard deviation.

Based on the experience of the validation data sets, the upper value Z0Max should be in a range between 0.5 m and 1.0 m for most applications.

5.9 GRAL Grids

5.9.1 Concentration grid

The concentration grid is defined in the files in.dat and gral.geb.

The number of horizontal cells, the number of vertical concentration grids (horizontal slices) and the GRAL domain area are defined in the file "gral.geb". The mean height (h_{mean}) and the vertical extension (h_{Delta}) of the horizontal slices are set in the file "in.dat".

The raster concentrations are evaluated at the following relative height above ground level:

$$h_{\text{Conc}} = h_{\text{mean}} \pm h_{\text{Delta}} * 0.5$$

If a concentration cell is partially occupied by buildings, the concentration is calculated for the free air volume within the cell (instead of the entire cell volume) starting from version 20.09.

5.9.2 Receptor concentrations

The concentration at a receptor point is evaluated at the receptor position within a volume defined by the horizontal and vertical concentration grid cell size. If a receptor is above or nearby a building, the raster grid concentration is used instead the real receptor position.

The receptor height is defined above ground level.

5.9.3 Flow field grid

The number of horizontal cells, the cell size in vertical direction and the stretching factors for the flow field grid area are defined in the file "gral.geb".

The horizontal cell size must be an integer part of the grid cell size of the concentrations.

The number of vertical stretching factors is not limited by GRAL.

The flow field grid is a Cartesian grid. When used with terrain, the 1st cell is located at the lowermost terrain cell within the GRAL domain area. The vertical grid height of the flow field grid starts at this lowest point and increases with height, depending on the stretching factors. This grid is therefore not terrain following.

5.9.4 Buildings and vegetation grid

The buildings and vegetation areas are resolved based on the flow field grid in horizontal and vertical direction.

5.9.5 Transient concentration grid

The transient concentration grid is terrain following and used to store the last position and sum up the concentration of particles if a dispersion situation has been finished and to release new “transient” particles at the following dispersion situation.

The horizontal size of the transient grid corresponds to the flow field grid. The vertical size is defined by the vertical grid size of the flow field grid and the following hard coded stretching factors and maximum allowed cell heights:

Up to a height of [m]	Stretching factor	Max. cell height
30	1.0	10
60	1.2	10
100	1.5	10
150	2.0	10
250	10.0	15
400	15.0	20
> 400	20.0	30

6 Compliance with the Austrian Guideline RVS 04.02.12

The accompanying working paper no. 17 of the Austrian Guideline RVS 04.02.12 describes four different datasets for model evaluation. Any dispersion model applied in Austria to assess pollutant dispersion from either road tunnels or/and roads, is required to meet the following quality criteria for these test cases:

Normalized Mean Square Error (NMSE) ≤ 3.0 and | Fraction Bias (FB) | ≤ 0.3

Please visit chapter 9 of this document for the definition of these quality indicators. In the following, GRAL results for the four test cases are described.

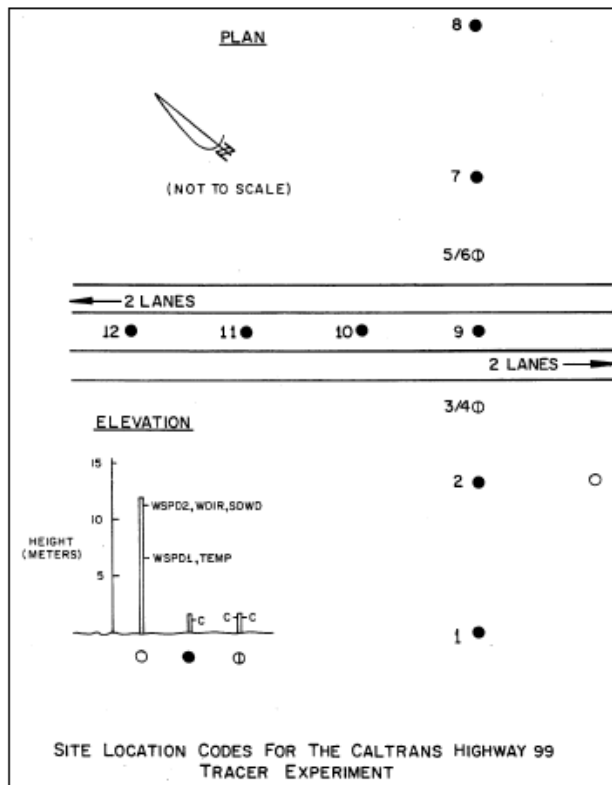
6.1 CALTRANS99

6.1.1 Dataset description

The Caltrans Highway 99 experiment has been used for validating the road dispersion model Caline. The experiment was composed of two parts, the first monitored a tracer gas, SF₆, and the other part monitored CO concentrations. In this work we present results of GRAL using the SF₆ data. The road layout is shown in Figure 19, which is taken from the reference (Benson, 1984).

The road, Highway 99, is composed of two carriageways each 7.3 m wide separated by a 14 m wide central reservation. The area surrounding the Highway 99 is described as open fields and scattered residential developments. The vertical monitors 2 - 7 are uniformly spaced with an interval of 50 m. Monitor 1 is 100 m from monitor 2, similarly for monitors 7 and 8. The four horizontal monitors are uniformly spaced along a 2.5 mile stretch of road. All monitors are at a height of 1 m. The monitors measured SF₆ concentration which was emitted from eight cars driving in a circuit along the highway.

Figure 19. Road layout of the CALTRANS 99 experiment



6.1.2 Characteristics

Wind speeds were rather low during the experiments. For the simulations the wind speed and –direction were used. Instead of taking the provided Turner stability classes, PGT classes were determined based on the method according to US EPA (2000), which gave slightly different but more plausible classes.

6.1.3 Model set up

Model version	GRAL
Topography	Flat Terrain
Obstacles	None
Concentration grid	4 m horizontal, 0.5 m vertical extension, 1 m above ground level
Model domain	4,000 m x 4,000 m
Number of particles	360,000 per $\frac{1}{2}$ hour
Roughness length	0.3 m
Adaptive roughness	0 m

6.1.4 Results

The performance of GRAL is quite good for this experiment, although peak concentrations are overestimated. It is interesting to note that the Austrian standard model OENORM M9440 performs particularly well in this case.

Table 3. Results for the CALTRANS99 experiment

Model	NMSE	FB	References
GRAL V20.01	0.5	0.0	
GRAL V20.09	0.4	0.0	
GRAL V21.09	0.5	0.0	
GRAL V23.11	0.5	0.0	
GRAL V24.04	0.4	0.0	

Figure 20. Observed and modelled mean concentrations as function of the distance to the source

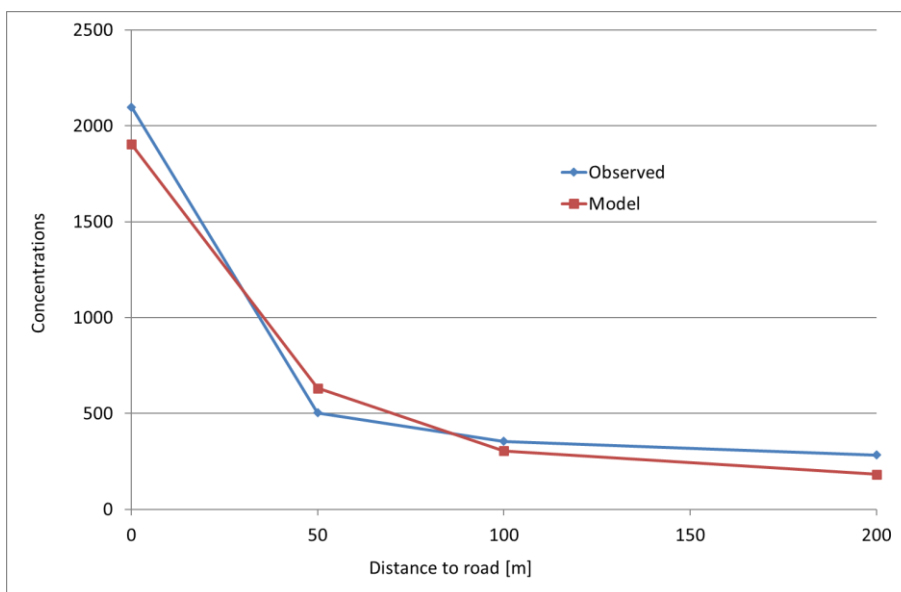
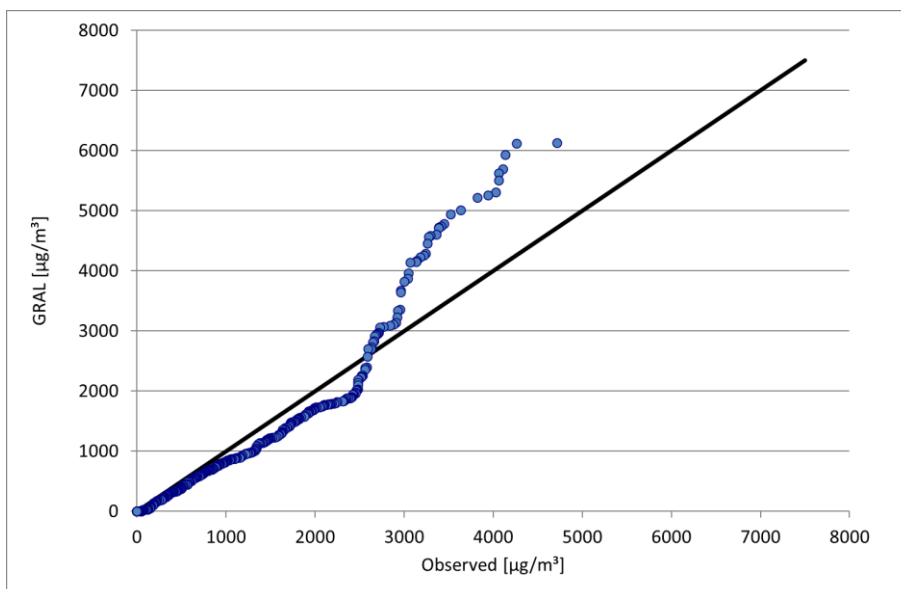


Figure 21. Quantile-quantile plot of observed and modelled concentrations with GRAL V23.11



6.2 A2, Biedermannsdorf

6.2.1 Dataset description

The experiment took place in 1998/98 near the highway A2 south of Vienna in Biedermannsdorf, Austria. Four permanent air quality monitoring stations were set up on both sides of the highway at distances 225 m (west), 66 m (east), 400 m (east), and 900 m (east). Traffic counts were made automatically. About 115.000 veh./d were driving on the A2 at that time. Emissions have been estimated using the Network emission model NEMO (Rexeis, 2005). In this work only NO_x concentrations have been used for comparison purposes. Wind speed and –direction as well as atmospheric stability were provided by the Technical University of Vienna. Wind speeds in this area are relatively high (annual mean wind speed = 3.6 m/s).

6.2.2 Characteristics

Besides the A2 there exists a dam with a noise abatement wall on top of it. All in all, this obstacle is 6 m high. It has been taken into account by using the methodology as described in chapter 5.5.2. Simulations without taking into account this obstacle resulted in overestimations of the concentrations close to the A2. Background concentrations have been determined by means of up- and downwind analysis of observed concentrations.

6.2.3 Model set up

Model version	GRAL
Topography	Flat Terrain
Obstacles	Microscale prognostic model, mixing-length turbulence closure Horizontal resolution: 4 m Vertical resolution: 1.0 m Vertical stretching factor: 1.05
Concentration grid	4 m horizontal, 1 m vertical extension, 4 m above ground level
Model domain	8,440 m x 11,900 m
Number of particles	180,000 per ½ hour
Roughness length	0.25 m

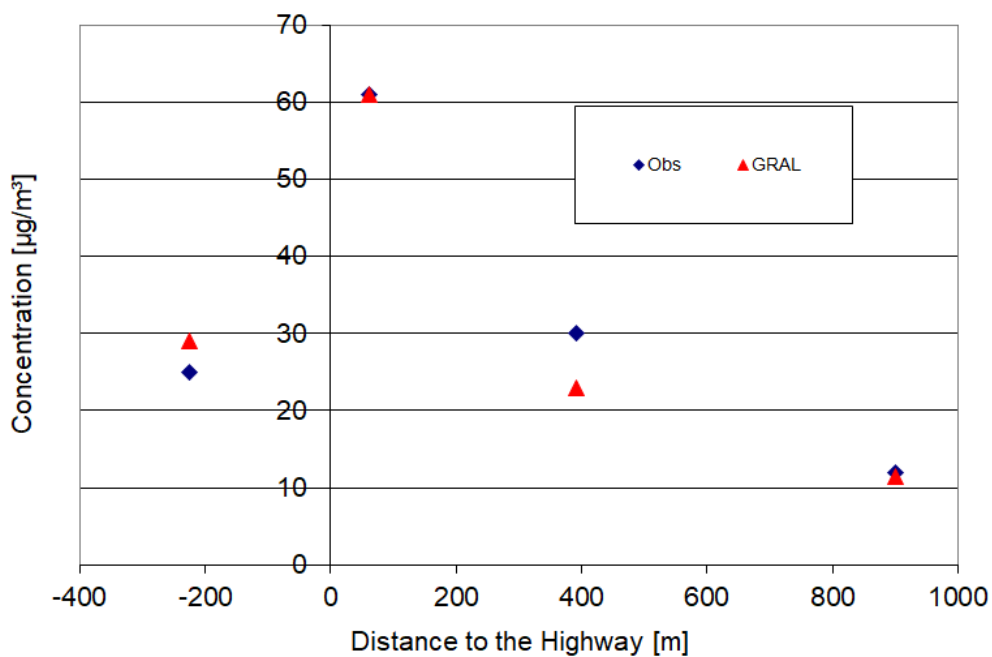
6.2.4 Results

There is some underestimation of the mean NO_x concentration at 400 m east of the A2. Perhaps this is due to local emissions, which have not been considered in the simulations. For the remaining three observational sites excellent agreements are the case.

Table 4. Results for the A2, Biedermannsdorf experiment

Model	NMSE	Mean deviation	References
GRAL (-225m)	-	-0.1	
GRAL (61m)	-	-0.1	
GRAL (391m)	-	0.2	
GRAL (900m)	-	-0.2	
GRAL V20.09 (-225m)	-	-0.2	
GRAL V20.09 (61m)	-	-0.1	
GRAL V20.09 (391m)	-	0.2	
GRAL V20.09 (900m)	-	-0.1	
GRAL V21.09 (-225m)	-	-0.3	
GRAL V21.09 (61m)	-	0.0	
GRAL V21.09 (391m)	-	0.1	
GRAL V21.09 (900m)	-	-0.2	
GRAL V23.11 (-225m)	-	-0.1	
GRAL V23.11 (61m)	-	0.0	
GRAL V23.11 (391m)	-	0.3	
GRAL V23.11 (900m)	-	0.1	

Figure 22. Modelled annual average NO_x concentration for the A2 near Biedermannsdorf, Austria



6.3 Ehrentalerberg

6.3.1 Dataset description

The tunnel has a length of approximately 3 500 m and consists of two bores, one for each direction. SF₆ was released ~1 000 m inside the tunnel in one of the bores 15 minutes before sampling was started. Sampling time was 30 minutes in all eight experiments, and the number of sampling points was around 27 in each run. Immediately after the sampling concentrations were analysed by means of Fourier transformed infrared spectroscopy (FT-IR). Sensitivity analysis with a calibration gas showed an accuracy of measured concentrations to be within $\pm 5 \%$, and a lower detection limit of ~3 ppb. Tracer gas was released at a rate of 7.82 kg h⁻¹. One sampling point was set up inside the tunnel, which allows for the estimation of the exit velocity of the jet stream. Individual pumps with 0.25 l/min each were employed for the grab samplers. 10 l bags allowed for a total measurements time of 30 minutes. The motorway and tunnel portal lie in a cut-section. Meteorological data were observed by means of a sonic anemometer 10 m above ground level.

6.3.2 Characteristics

In all runs mean wind speeds were quite low, which causes the ambient wind to meander. Different wind directions during the experiments allow for a critical testing of a model's capability to simulate the position of the jet stream correctly. In most cases atmospheric stability was unstable, except for run 4, where it was stable.

Since lapse rates were not measured during the experiments, the following approximation was used to estimate the Brunt-Väisälä frequency: In a first step, the stability class was estimated from the Obukhov length and the roughness length according to Golder (1972), and in a second step a typical lapse rate was chosen in dependence on the stability class as they are given in Zannetti (1990).

During the experiments it was found, that a remarkable amount of tracer-gas was advected into the northern bore. In case of run 2, where the wind direction was almost from south the loss of tracer-gas, was found to be more than 50 % of the total release (by means of a sampling point inside the northern bore and flow speed measurements there). Thus, under certain wind directions this effect is not negligible but was not taken into account.

In the simulations with GRAL friction velocity, Monin-Obukhov length, horizontal velocity variance, and wind speed as observed with a sonic anemometer 10 m above ground level has been used. A second simulation with GRAL has also been made using standard meteorological input, namely wind speed at 10 m above ground, and stability class.

6.3.3 Model set up

Model version	GRAL
Topography	None
Obstacles	None
Concentration grid	4 m horizontal, 0.5 m vertical extension, 1 m above ground level
Model domain	332 m x 276 m
Number of particles	720,000 per hour
Roughness length	0.1 m

6.3.4 Results

The dispersion from tunnel portals in low wind speed conditions is perhaps one of the most challenging tasks in licensing procedures. The performance of GRAL is very well regarding the mean concentration as well as the concentration statistics for the case when observed turbulence quantities are used as input.

Table 5. Results for the Ehrentalerberg dataset

Model	NMSE	FB	References
GRAL	0.9	0.1	
GRAL (stability classes)	2.2	0.0	
GRAL V21.09 Sonic	0.9	0.2	
GRAL V23.11 Sonic	1.1	0.2	
GRAL V23.11 (stability classes)	0.9	0.2	
GRAL V24.04 Sonic	0.9	0.2	
GRAL V24.04 (stability classes)	1.1	0.2	

Figure 23. Scatter plot of observed and modelled concentrations (using observed turbulence quantities as input, sonic left, stability classes right, V24.04)

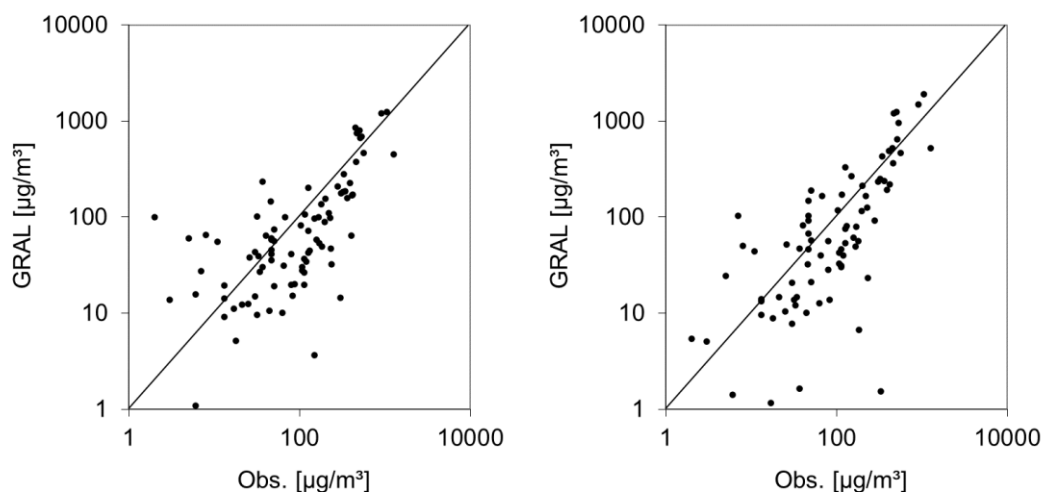
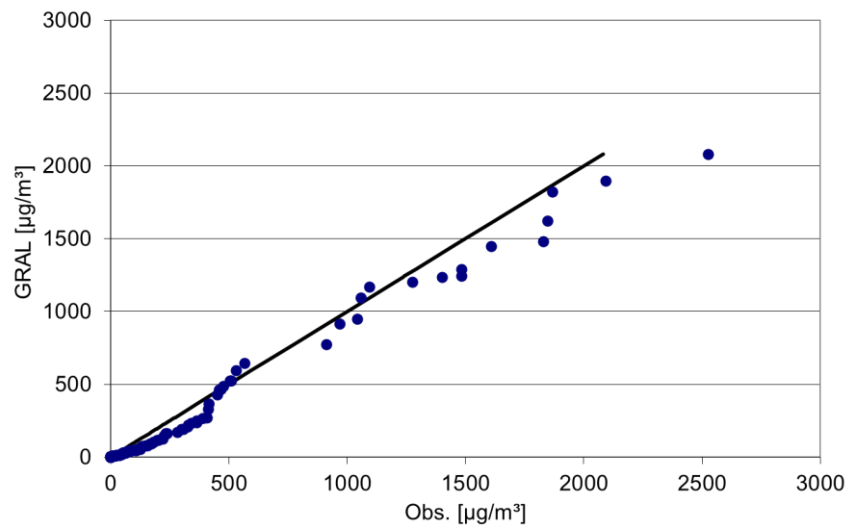


Figure 24. Quantile-quantile plot of observed and modelled concentrations with GRAL V24.04 (using observed turbulence quantities as input)



6.4 Kaisermuehlen

6.4.1 Dataset description

The Kaisermuehlentunnel in Vienna (Austria) has a length of 2150 m and two bores for each direction with six lanes in total. The pollution dispersion was studied (Oetl et al., 2004) at the south-east tunnel portal, where there exist two additional lanes to exit or enter the highway.

Continuous air quality observations were performed at five locations 2.5 m above ground level. Among the various chemical species recorded, NO_x was found to be most related with traffic on the highway and the tunnel jet. Another sampling point was set-up inside the tunnel to determine the emissions from the tunnel portal. The necessary volume flux was derived by recording the flow velocity in the tunnel using a cup anemometer. The method was validated with additional tracer tests by means of N₂O releases inside the tunnel in five cases. Both methods agreed within +/- 10 %. The meteorological data used for modelling is based on wind observations with a cup-anemometer on a 10 m mast at site M1.

The experimental investigation lasted over a period of 10 months, where data was recorded on a half-hourly basis. As considerable background concentrations for NO_x were expected, two distinct meteorological conditions were considered for the model evaluation: First, wind directions between 230 and 275 deg. (979 cases) and second, wind directions between 95 and 125 deg. (826 cases). In the first case the background concentration of NO_x could be determined by use of sampling point M1, and in case of easterly winds, the average of sampling points M2 – M5 was taken as background concentration. Altogether 1805 cases were selected from the data base for the simulations.

6.4.2 Characterization

Average wind speed found during the selected meteorological situations was 3.1 m s⁻¹. Maximum and the minimum wind speeds were 10.2 m s⁻¹ and 0.1 m s⁻¹ respectively. Temperature differences between tunnel and ambient air ranged between -9.1 K and +14.2 K, and exit velocities of the tunnel jet were between 0.9 m s⁻¹ and 6.5 m s⁻¹. Mean NO_x-emission at the portal was 3.9 kg h⁻¹. In order to accurately model NO_x-concentrations, it is necessary to take into account NO_x-emissions resulting from all lanes out and into the tunnel as well as ramps from and to these lanes. For lanes out of the tunnel corresponding NO_x-emissions were determined by the NO_x-emission at the portal divided by the length of the tunnel. As traffic data was not available on an half-hourly basis, NO_x-emissions for lanes into the tunnel were roughly estimated by assuming the same amount of traffic as out of the tunnel. This assumption clearly increases the uncertainty regarding the modelled mean half-hourly concentrations, while one can expect that it is a good estimation for average concentrations over the whole period. Background concentrations for NO_x were 35 µg m³ for easterly wind

directions and $25 \mu\text{g m}^3$ for westerly winds. For the simulations with GRAL, ambient wind speed, -direction, stability class, tunnel exit velocity, and –temperature has been utilized.

The portal itself is situated approximately 5 m below the surroundings. Ramps with lanes into and out of tunnel act as obstacles, such that ambient winds have less influence on the tunnel jet. This is accounted for in the simulations by carrying out GRAMM flow field simulations with a resolution of 25 m. Topographical data has been provided by the courtesy of the city of Vienna (ViennaGIS - www.wien.gv.at/viennagis/). Horizontal resolution of this dataset is 5 m.

As an additional approach, a GRAL V20.09 project was calculated with flat terrain and the terrain was estimated using buildings. The lane ramps (exit and enter the motorway) were digitized using 3D line sources.

Observed wind directions were corrected by 10 deg. in clockwise direction, which improved the simulation results. As the wind vane was orientated manually using a compass, an uncertainty of 10 deg. is within the range of possibility.

6.4.3 Model set up

Model version	GRAL 23.11
Topography GRAMM	3D wind fields simulated with the non-hydrostatic prognostic wind field model GRAMM Horizontal resolution: 25 m Vertical resolution: 5 m Vertical stretching factor: 1,10 Vertical layers: 30 Top level: 827 m Surface energy balance: None Turbulence model: k-ε closure
Topography GRAL	4 m resolution derived from original topographical data; topography adjusted manually (removed artificial terrain peaks due to overlapped road sections)
Obstacles	Microscale prognostic model, mixing-length turbulence closure Horizontal resolution: 4 m Vertical resolution: 1.5 m Vertical stretching factor: 1.0
Concentration grid	4 m horizontal, 0.5 m vertical extension, 2.5 m above ground level
Model domain	500 m x 480 m
Number of particles	90,000 per ½ hour
Surface roughness length	0.2 m
GRAL Mode	Transient, time-depending emission modulation, exit velocity and exit temperature
Line sources	3D line sources
Special hints	The borders of the subsurface route were modelled with walls. This forces GRAL to reflect particles on the side walls.

Model version	GRAL 23.11 optional approach – flat terrain
Obstacles	Microscale prognostic model, mixing-length turbulence closure Horizontal resolution: 4 m Vertical resolution: 1.5 m Vertical stretching factor: 1.0
Concentration grid	4 m horizontal, 0.5 m vertical extension, 2.5 m above ground level
Model domain	500 m x 480 m
Number of particles	90,000 per ½ hour
Surface roughness length	0.35 m
Surface roughness of walls	0,09 m
GRAL Mode	Transient, time-dependent emission modulation, exit velocity and exit temperature
Line sources	3D line sources
Special hints	The terrain has been modelled using buildings

6.4.4 Results

While average concentrations are captured reasonably well by GRAL, peak concentrations at site M5 are underestimated. At site M1 peak concentrations are in better agreement with observations

Table 6. Results for the Kaisermuehlen dataset

Model	NMSE	FB	
GRAL V19.01 M5 (westerly winds)	0.8	0.3	
GRAL V19.01 M4 (westerly winds)	0.8	-0.3	
GRAL V19.01 M3 (westerly winds)	2.4	0.2	
GRAL V19.01 M1 (easterly winds)	0.4	-0.1	
GRAL V20.09 M5	0.9	0.3	
GRAL V20.09 M4	0.9	-0.3	
GRAL V20.09 M3	2.2	0.2	
GRAL V20.09 M1	0.4	-0.1	
GRAL V20.09 M5 optional approach	0.5	0.0	Flat terrain
GRAL V20.09 M4 optional approach	1.0	-0.5	Flat terrain
GRAL V20.09 M3 optional approach	1.8	0.0	Flat terrain
GRAL V20.09 M1 optional approach	0.4	-0.2	Flat terrain
GRAL V23.11 M5	0.9	0.3	
GRAL V23.11 M4	0.9	-0.2	
GRAL V23.11 M3	2.6	0.2	

GRAL V23.11 M1	0.4	0.0	
GRAL V24.04 M5	0.9	0.3	
GRAL V24.04 M4	1.0	-0.24	
GRAL V24.04 M3	2.5	0.2	
GRAL V24.04 M1	0.4	0.0	
GRAL V23.11 M5 optional approach	0.6	0.1	Flat terrain
GRAL V23.11 M4 optional approach	1.0	-0.5	Flat terrain
GRAL V23.11 M3 optional approach	1.7	0	Flat terrain
GRAL V23.11 M1 optional approach	0.4	-0.1	Flat terrain

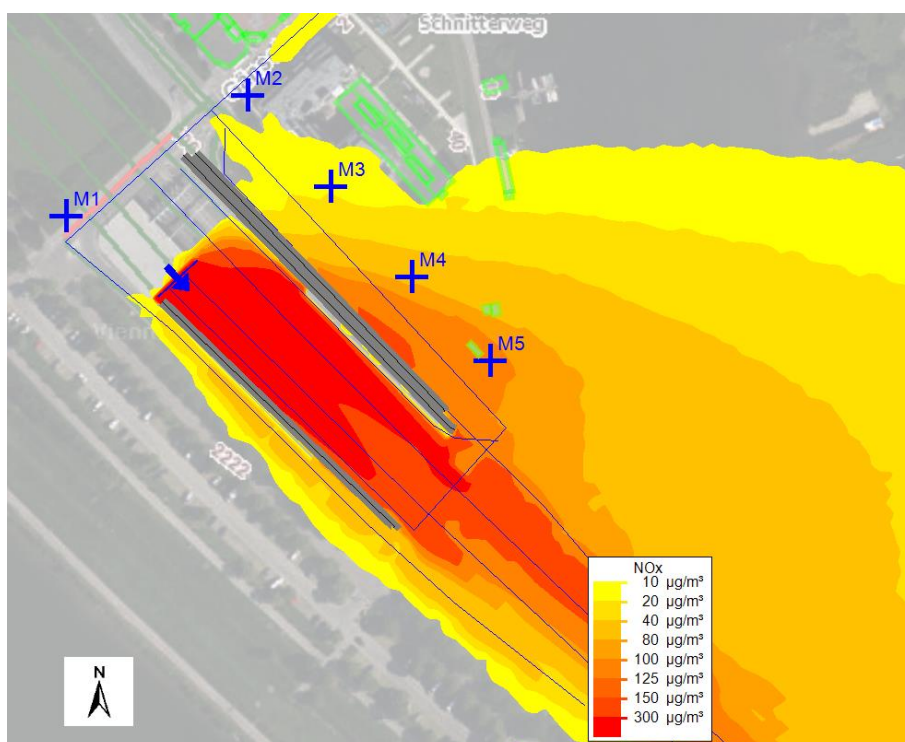
Figure 25. Simulated average NO_x concentrations for westerly winds (V23.11)

Figure 26. Quantile-quantile plot of observed and modelled concentrations for westerly winds at monitoring station M5 (V24.04)

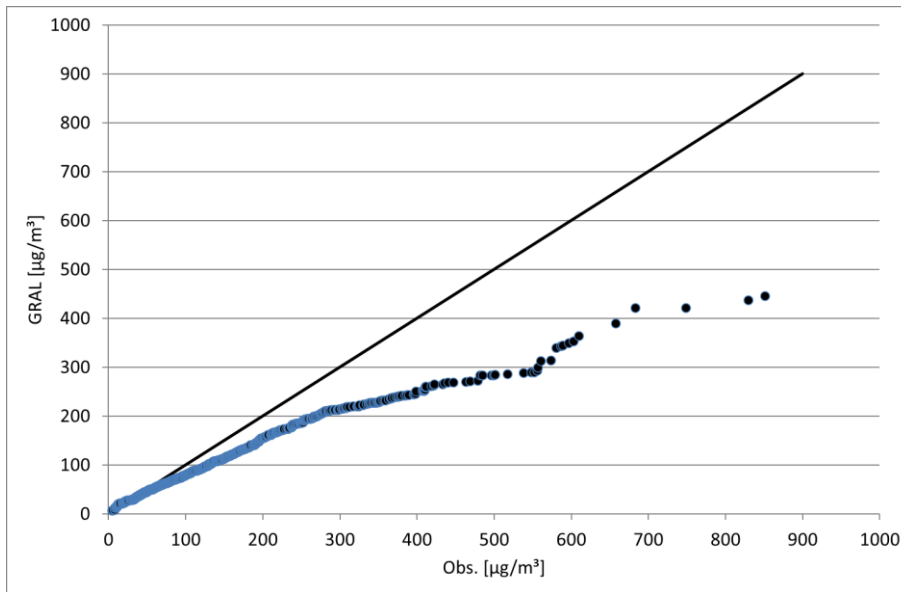
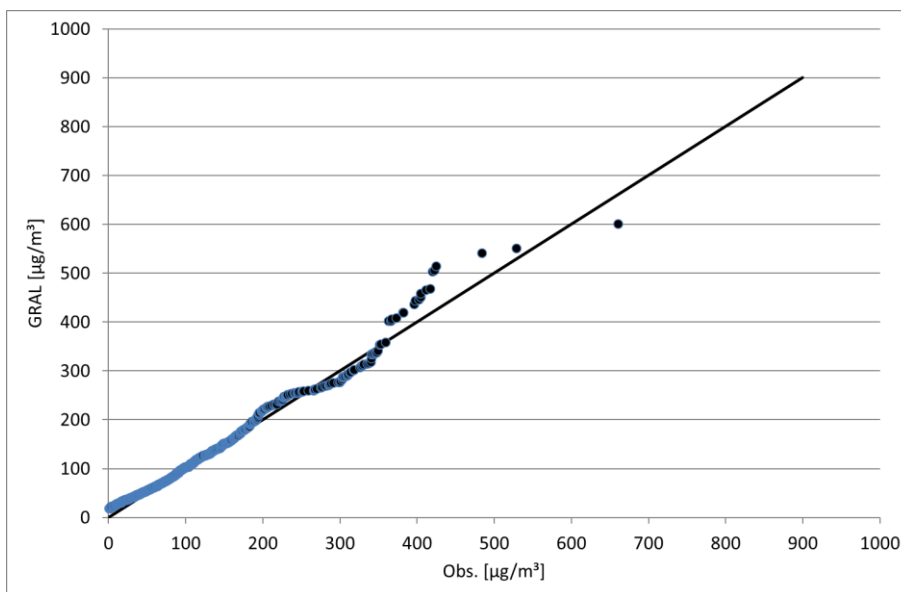


Figure 27. Quantile-quantile plot of observed and modelled concentrations for easterly winds at monitoring station M1 (V24.04)



6.5 Summary

The current version of GRAL satisfies the quality criteria in all cases (except one receptor point in the optional and simplified flat terrain approach for the dataset Kaisermuehlentunnel) and, thus, completely complies with the guideline.

7 Compliance with the German Guideline VDI 3783 - 9

The Association of German Engineers (VDI) issued an evaluation guideline for prognostic microscale wind field models in 2016 (VDI, 2016), which comes with comprehensive wind-tunnel data for testing model performance. The evaluation procedure outlined in the guideline is based on three major steps: (1) The ‘general evaluation’ step, which is about traceability and proper documentation of a model. (2) A ‘scientific evaluation’ step dealing with obligations regarding publications in peer-reviewed scientific journals. (3) The ‘validation’ section, where a model is checked for a number of test cases. These can be classified into three sub-groups: (a) Test cases addressing general model properties, such as the dependency of modelled flows on grid resolution or tests to ensure flow convergence. (b) Test cases without obstacles to check for spatial homogeneity of model results, or the correct treatment of the Coriolis force (if considered in the model), or the formation of correct wind profiles in neutral conditions within the boundary-layer. (c) Test cases using reference data from wind-tunnel observations. In the following all of the requirements of that guideline are listed in detail and compliance or non-compliance with the current GRAL version is outlined.

7.1 General model evaluation

The following documents about the model and the programme (source code) are required:

Brief description: Most of the information required by the guideline for the brief description can be found at the GRAL website (<https://gral.tugraz.at/>).

Detailed description of the model: It shall comprise the basic equations, approximations, parameterizations, and boundary conditions employed. Furthermore, the evaluation of the model according to the VDI guideline 3783-9 shall be explained in detail. It is this report that aims at providing all this information in combination with the report about recommendations when using GRAL.

Manual: The manual is about the installation, user interface, and general operation of the model. All these subject matters are included in the GRAL User Guide, except of an example application, which is also demanded by the guideline.

Technical reference (optional): Shall consist of the programming conventions, the programming language, a list of variables, a data-flow diagram as well as a functional diagram. Such a technical reference is currently not available for the microscale flow model of GRAL.

Furthermore, it is required that a third party is allowed to inspect the source code of the programme. The source code of GRAL can be requested by anyone interested in it.

Finally, there have to be two certified publications on model physics and model results in at least two different professional journals. Currently, three publications in international peer-reviewed professional journals (Oettl 2014, Oettl 2015a, Oettl 2015b) and several peer-reviewed conference proceedings (e.g. Oettl 2015c; Grawe et al., 2014) are available.

7.2 Scientific model evaluation

This section deals with the basic equations and parameterizations used in the model. The guideline requires the following methodological approaches:

Table 7: Scientific evaluation according to VDI 3783-9

	YES	NO
All three wind components prognostic	X	
Continuity equation complete or inelastic approximation	X	
Continuous flux rates as a function of location	X	
Continuous flux rates as a function of stratification	Not applicable	
Direct calculation of near-ground flows or wall functions	X	
Symmetry of the friction tensor	X	
Buildings explicitly resolved	X	
Building roughness taken into account	X	

It can be seen from Table 7 that GRAL meets all criteria. Stratification is not taken directly into account in the flow field simulations, but it affects the initial vertical profiles for turbulent kinetic energy, dissipation, and wind speed.

7.3 Model validation

In the following, model results for 10 different test cases are outlined of which 6 are based on comparisons with wind-tunnel observations. In addition, some automatic consistency checks shall be carried out according to the guideline. Some of these checks can be done when launching the online control functionality of the GRAL graphical user interface. However, not all of the required checks can be undertaken as can be seen from the next table. Conservation of mass is displayed on the screen online during the GRAL simulation every 100 integration steps.

Table 8: Requirements for the model validation according to VDI 3783-9

	YES	NO
Specification of the computational grid	X	
Online control: 2-Δt waves checkpoint	X	
Online control: standard deviations		X
Online control: area mean values		X
Online control: conservation of mass	X	
Online control: plausible values	X	
Online control: 2-Δx, 2-Δy waves	X	
Online control: results independent on grid	X	
Online control: check of results	X	

In every section, results for the test cases are presented in detail. Model results are evaluated by a point-by-point comparison with either wind-tunnel observations or model results. The guideline defines so-called hit rates q in the following way:

$$q = \frac{N}{n} = \frac{1}{n} \sum_{i=1}^n N_i \quad (103)$$

with

$$N_i = \begin{cases} 1 & \text{if } \left| \frac{P_i - O_i}{O_i} \right| \leq D \quad \text{or} \quad |P_i - O_i| \leq W, \\ 0 & \text{else} \end{cases} \quad (104)$$

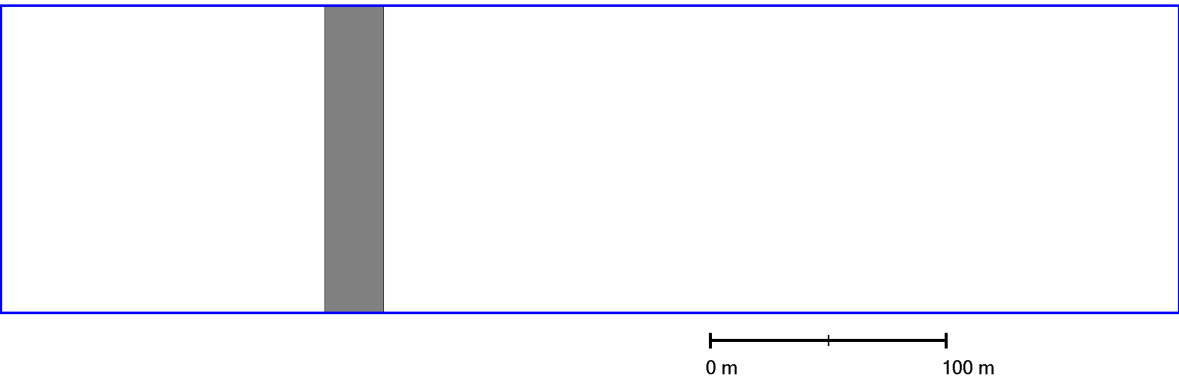
where N is the number of data points counted as hit, n is the total number of data points, and O_i and P_i are observed and modelled wind speed components at location i , respectively. The required maximum relative difference D the maximum absolute difference W differ in all cases.

Simulations have been carried out with the three different options in the GRAL model for treating turbulence. The recommend option is currently the algebraic mixing-length model.

7.3.1 Test case A1-1 (two-dimensionality)

In this test case the so-called two-dimensionality of results is checked, i.e. the results in y -direction shall be homogeneous within the context of the model inaccuracy. The building configuration is consists of a 2D obstacle over the entire width of the model domain.

Figure 28: Building configuration and model domain for test case A1-1



Topography	Flat terrain
Obstacles	Microscale prognostic model Horizontal resolution: 2.5 m Vertical resolution: 2.5 m Vertical stretching factor: 1.0 Relaxation factor velocity: 0.1 Relaxation factor pressure correction: 1.0 Minimum iterations: 100 Maximum iterations: until convergence (10.000) Number of vertical cells: 100
Model domain	X_{\min} : -150m X_{\max} : 350m Y_{\min} : -20m Y_{\max} : 20m Z_{\max} : 252m
Surface roughness length	0.1 m
Wall roughness length	0.01 m

Table 9: Hit rates for test case A1-1 ($W = 0.01$, $D = 0.05$); no-diffusion

	<i>Data points</i>	<i>Hit rates</i>	<i>Required hit rates</i>
q_u	83,800	1,00	0.95
q_w	83,800	1,00	0.95

Table 10: Hit rates for test case A1-1 ($W = 0.01$, $D = 0.05$); mixing-length model

	<i>Data points</i>	<i>Hit rates</i>	<i>Required hit rates</i>
q_u	83,800	1,00	0.95
q_w	83,800	1,00	0.95

Table 11: Hit rates for test case A1-1 ($W = 0.01$, $D = 0.05$); k - ε model

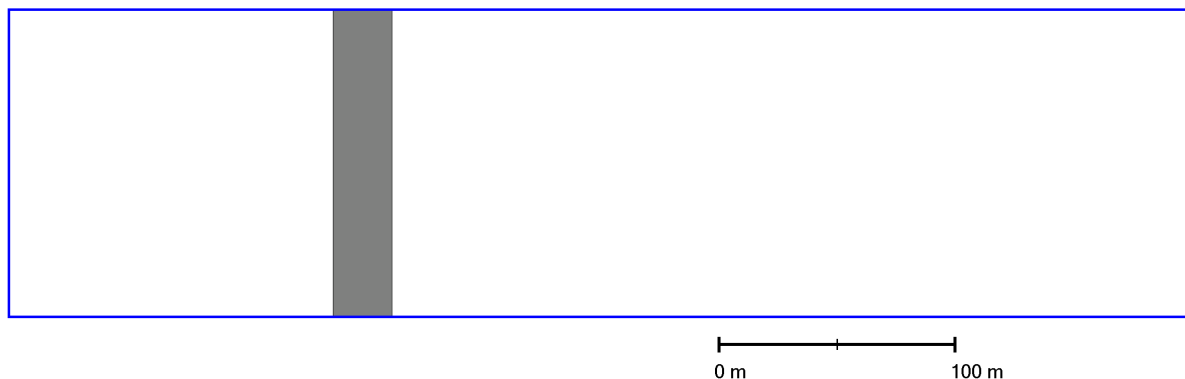
	<i>Data points</i>	<i>Hit rates</i>	<i>Required hit rates</i>
q_u	83,800	1,00	0.95
q_w	83,800	1.00	0.95

7.3.2 Test case A1-2 (scalability)

In this test case the independence of the solution from the chosen velocity of the approach flow is checked. The building configuration is the same as for test case A1-1. The difference is the approaching flow speed, which is 1 m/s at a height of 75 m in contrast to test case A1-1, where it reads 10 m/s.

It should be noted that in GRAL simulations are performed for every dispersion situation separately and are not scaled based on simulations with a certain reference wind speed.

Figure 29: Building configuration and model domain for test case A1-2



Topography	Flat terrain
Obstacles	Microscale prognostic model Horizontal resolution: 2.5 m Vertical resolution: 2.5 m Vertical stretching factor: 1.0 Relaxation factor velocity: 0.12 Relaxation factor pressure correction: 1.0 Minimum iterations: 100 Maximum iterations: until convergence (10.000) Number of vertical cells: 100
Model domain	X_{\min} : -150m

	X_{\max} : 350m Y_{\min} : -20m Y_{\max} : 20m Z_{\max} : 252m
Surface roughness length	0.1 m
Wall roughness length	0.01 m

Table 12: Hit rates for test case A1-2 ($W = 0.01$, $D = 0.05$); no diffusion

	<i>Data points</i>	<i>Hit rates</i>	<i>Required hit rates</i>
q_u	4,080	0.99	0.95
q_w	4,080	1.00	0.95

Table 13: Hit rates for test case A1-2 ($W = 0.01$, $D = 0.05$); mixing-length model

	<i>Data points</i>	<i>Hit rates</i>	<i>Required hit rates</i>
q_u	4,080	0.98	0.95
q_w	4,080	1.00	0.95

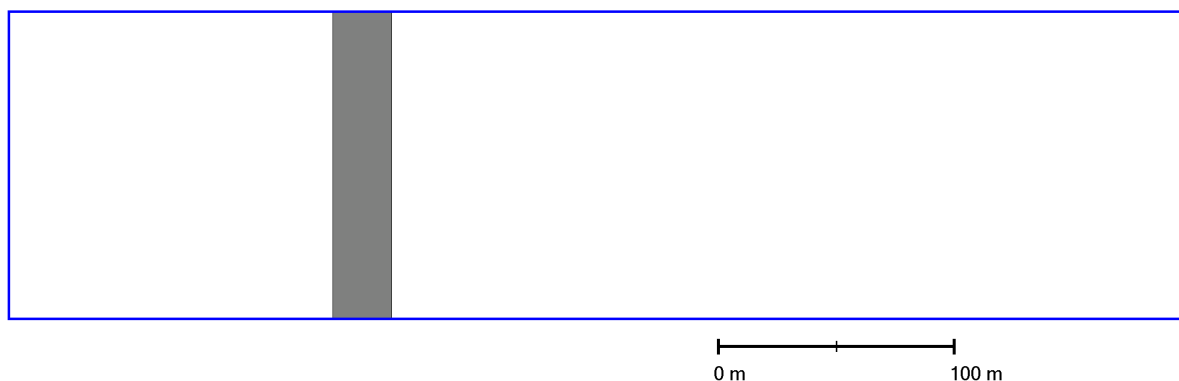
Table 14: Hit rates for test case A1-2 ($W = 0.01$, $D = 0.05$); k - ϵ model

	<i>Data points</i>	<i>Hit rates</i>	<i>Required hit rates</i>
q_u	4,080	0.87	0.95
q_w	4,080	0.50	0.95

7.3.3 Test case A2 (steady-state)

In this test case the independence of the solution from the integration time is checked. The whole model set up is the same as for test case A1-2. Simulations were performed until the convergence criterion (see chapter 5.5) was fulfilled. Subsequently the simulations were being continued until the integration time was doubled.

Figure 30: Building configuration and model domain for test case A2



Topography	Flat terrain
Obstacles	Microscale prognostic model Horizontal resolution: 2.5 m Vertical resolution: 2.5 m Vertical stretching factor: 1.0 Relaxation factor velocity: 0.1 Relaxation factor pressure correction: 1.0 Minimum iterations: 100 Maximum iterations: until convergence, then doubled (20.000) Number of vertical cells: 100
Model domain	X_{\min} : -150m X_{\max} : 350m Y_{\min} : -20m Y_{\max} : 20m Z_{\max} : 252m
Surface roughness length	0.1 m
Wall roughness length	0.01 m

Table 15: Hit rates for test case A2 ($W = 0.01$, $D = 0.05$); no-diffusion

	<i>Data points</i>	<i>Hit rates</i>	<i>Required hit rates</i>
q_u	4,080	1.00	0.95
q_w	4,080	1.00	0.95

Table 16: Hit rates for test case A2 ($W = 0.01$, $D = 0.05$); mixing-length model

	<i>Data points</i>	<i>Hit rates</i>	<i>Required hit rates</i>
q_u	4,080	1.00	0.95
q_w	4,080	1.00	0.95

Table 17: Hit rates for test case A2 ($W = 0.01$, $D = 0.05$); k - ε model

	<i>Data points</i>	<i>Hit rates</i>	<i>Required hit rates</i>
q_u	4,080	1.00	0.95
q_w	4,080	1.00	0.95

7.3.4 Test cases A3-1 and A3-2 (length of recirculation zone)

These test cases are essentially the same as A1-1, except that the surface roughness is varied between 0.1 and 0.03 m. It is required that the length of the recirculation zone is between $4H$ and $5H$ in case of A3-1 (surface roughness 0.1 m), and that the recirculation zone increases when the surface roughness is reduced to 0.03 m.

The purpose of this test case is to demonstrate that the length of the recirculation zone depends on the turbulence state of the approaching flow. It should be noted that the wind speed at 75 m above ground level is kept equal to 1 m s^{-1} for both cases. In neutral conditions the initial wind profile is independent on the surface roughness (see eq. 1). This implies that the horizontal standard deviations, which are the main source for turbulent kinetic energy in the GRAL model in low-wind-speed conditions, remain almost unchanged (it decreases by about 3 % according to eq. 26). Therefore, it cannot be expected that recirculation zones differ much. However, it can be demonstrated that lower turbulence levels lead to a significant increase in the length of the recirculation zone by using the file inputzr.dat as input (see chap. 17.2.1.3). In this file not only the vertical wind profile but also the horizontal standard deviations for the wind fluctuations can be defined by the user. While the wind speed at 75 m was set equal to 1 m s^{-1} in both cases, the horizontal standard deviations in case of 0.03 m roughness length have been taken half the values of those for the case with 0.1 m. In the latter case, the standard deviations have been computed according to eq. 26. Further, the Obukhov length was taken to be -500 m and -250 m in case of a roughness length of 0.1 m and 0.03 m, respectively. This leads to slightly different vertical wind profiles according to eq. (1). More precisely, the vertical wind-speed gradient decreases below 75 m for lower roughness lengths. In case of the mixing-length turbulence model, this leads to lower turbulent exchange coefficients and, thus, should lead to larger recirculation zones.

It can be seen that in all cases the model responds correctly and suggests increasing recirculation lengths with decreasing turbulence levels. When the diffusion coefficients are set to zero, the only effect on the wake region is due to effects in the first grid layer above the surface.

Topography	Flat terrain
Obstacles	Microscale prognostic model Horizontal resolution: 2.5 m Vertical resolution: 2.5 m Vertical stretching factor: 1.0 Relaxation factor velocity: 0.1 Relaxation factor pressure correction: 1.0 Minimum iterations: 100 Maximum iterations: until convergence (10.000) Number of vertical cells: 100
Model domain	X_{\min} : -150m X_{\max} : 350m Y_{\min} : -20m Y_{\max} : 20m Z_{\max} : 252m
Surface roughness length	0.1 m and 0.03 m
Wall roughness length	0.01 m

Table 18: Length of the recirculation zones; no-diffusion

<i>Surface roughness</i>	<i>Recirculation length</i>	<i>Required recirculation length</i>
0.1 m	114 m	100 – 125 m
0.03 m	121 m	Larger than for 0.1 m surface roughness

Table 19: Length of the recirculation zones; mixing-length model

<i>Surface roughness</i>	<i>Recirculation length</i>	<i>Required recirculation length</i>
0.1 m	116 m	100 – 125 m
0.03 m	122 m	Larger than for 0.1 m surface roughness

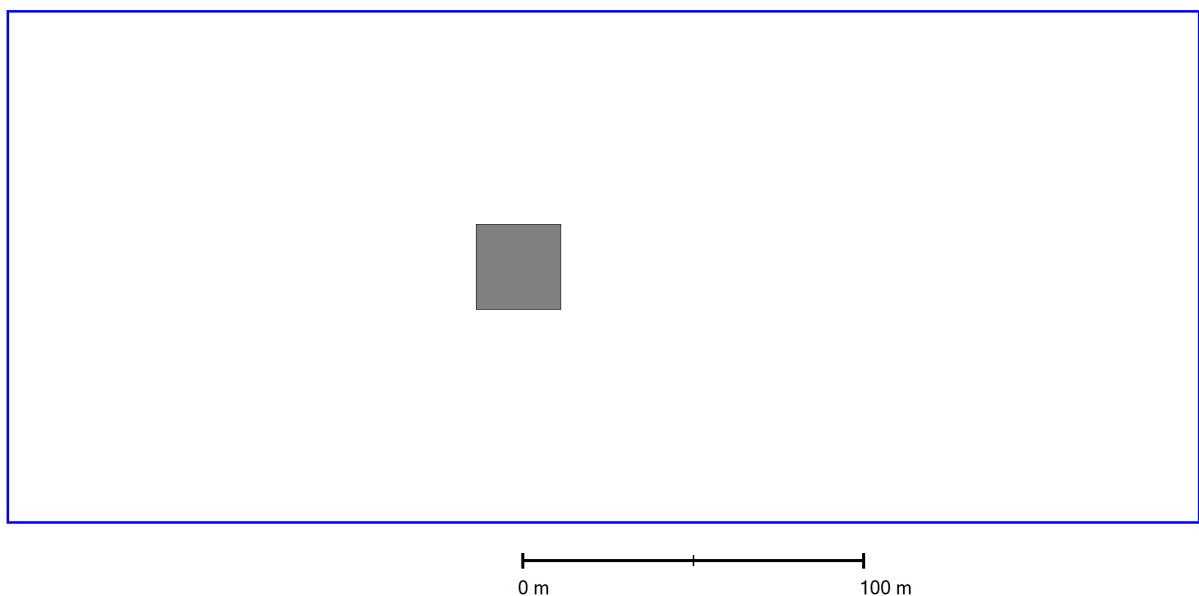
Table 20: Length of the recirculation zones; k - ϵ model

<i>Surface roughness</i>	<i>Recirculation length</i>	<i>Required recirculation length</i>
0.1 m	109 m	100 – 125 m
0.03 m	119 m	Larger than for 0.1 m surface roughness

7.3.5 Test case A4-1 (symmetry)

Given the chosen obstacle configuration, the results shall be symmetrical around the axis $y=0$. The configuration consists of a single cubic building with dimensions $W=B=H=25\text{m}$.

Figure 31: Building configuration and model domain for test case A4-1



Topography

Flat terrain

Obstacles	Microscale prognostic model Horizontal resolution: 2.5 m Vertical resolution: 2.5 m Vertical stretching factor: 1.0 Relaxation factor velocity: 0.1 Relaxation factor pressure correction: 1.0 Minimum iterations: 100 Maximum iterations: until convergence (1100) Number of vertical cells: 40
Model domain	X_{\min} : -150m X_{\max} : 200m Y_{\min} : -75m Y_{\max} : 75m Z_{\max} : 101m
Surface roughness length	0.1 m
Wall roughness length	0.01 m

Table 21: Hit rates for test case A4-1 ($W = 0.01$, $D = 0.05$); no-diffusion

	<i>Data points</i>	<i>Hit rates</i>	<i>Required hit rates</i>
q_u	87,199	1.00	0.95
q_v	87,199	0.99	0.95
q_w	87,199	1.00	0.95

Table 22: Hit rates for test case A4-1 ($W = 0.01$, $D = 0.05$); mixing-length model

	<i>Data points</i>	<i>Hit rates</i>	<i>Required hit rates</i>
q_u	87,199	1.00	0.95
q_v	87,199	0.99	0.95
q_w	87,199	1.00	0.95

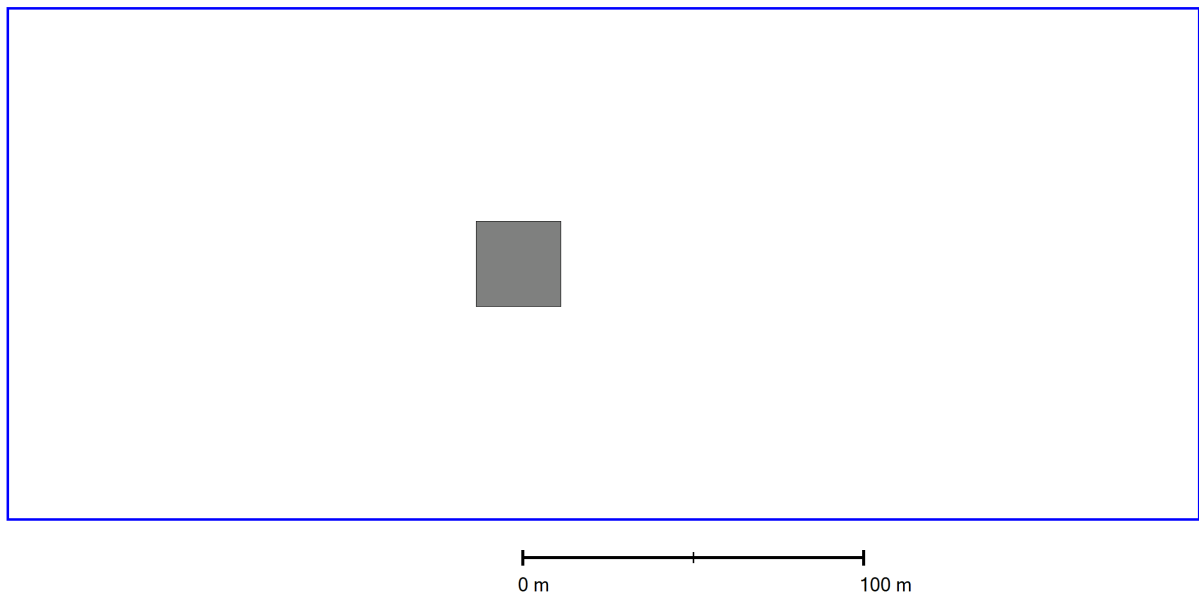
Table 23: Hit rates for test case A4-1 ($W = 0.01$, $D = 0.05$); k - ϵ model

	<i>Data points</i>	<i>Hit rates</i>	<i>Required hit rates</i>
q_u	87,199	1.00	0.95
q_v	87,199	0.99	0.95
q_w	87,199	1.00	0.95

7.3.6 Test case A4-2 (grid size dependency)

The dependence of model results on grid width is tested. The configuration is the same as for test case A4-1.

Figure 32: Building configuration and model domain for test case A4-2



Topography	Flat terrain
Obstacles	Microscale prognostic model Horizontal resolution: 2.5m / 1.25 m Vertical resolution: 2.5m / 1.25 m Vertical stretching factor: 1.0 Relaxation factor velocity: 0.1 Relaxation factor pressure correction: 1.0 Minimum iterations: 100 Maximum iterations: until convergence (700 / 2300) Number of vertical cells: 40
Model domain	X _{min} : -150m X _{max} : 200m Y _{min} : -75m Y _{max} : 75m Z _{max} : 102m
Surface roughness length	0.1 m
Wall roughness length	0.01 m

Table 24: Hit rates for test case A4-2 ($W = 0.01$, $D = 0.05$); no diffusion

	<i>Data points</i>	<i>Hit rates</i>	<i>Required hit rates</i>
q_u	9,512	0.96	0.95
q_v	9,512	0.99	0.95
q_w	9,512	0.99	0.95

Table 25: Hit rates for test case A4-2 ($W = 0.01$, $D = 0.05$); mixing-length model

	<i>Data points</i>	<i>Hit rates</i>	<i>Required hit rates</i>
q_u	9,512	0.95	0.95
q_v	9,512	0.99	0.95
q_w	9,512	1.00	0.95

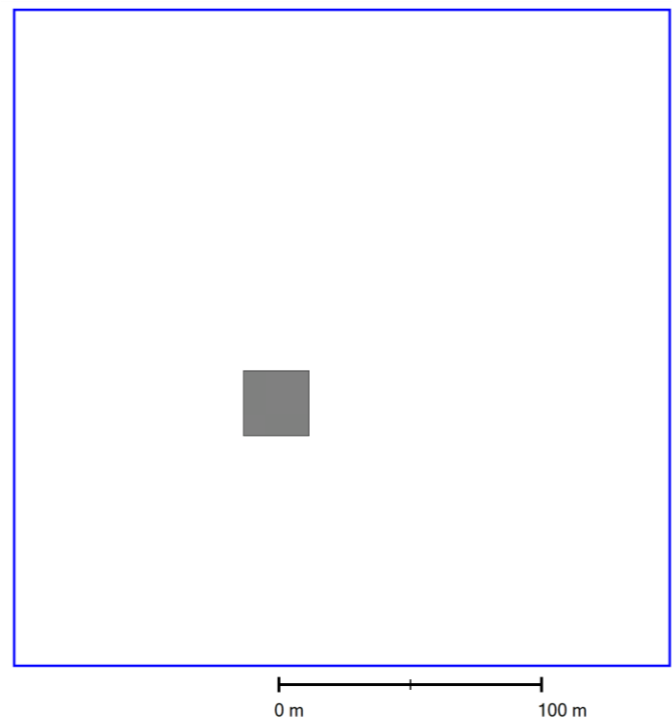
Table 26: Hit rates for test case A4-2 ($W = 0.01$, $D = 0.05$); k - ϵ model

	<i>Data points</i>	<i>Hit rates</i>	<i>Required hit rates</i>
q_u	9,512	0.97	0.95
q_v	9,512	1.00	0.95
q_w	9,512	1.00	0.95

7.3.7 Test case A5-1 (building orientation)

The dependence of model results on the orientation of the walls of the building with respect to the coordinate axes is tested. Test case A5-1 forms the base case, while test case A5-2 is used for comparison purposes. The configuration is the same as for test case A4-1.

Figure 33: Building configuration and model domain for test case A5-1



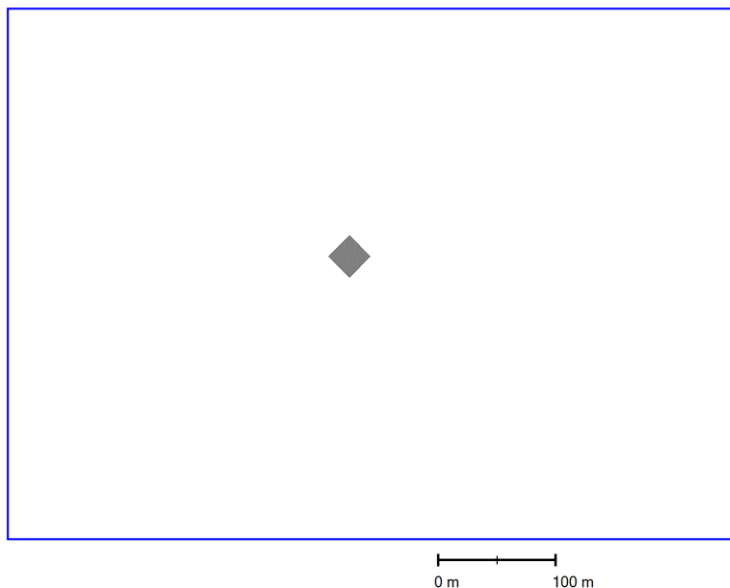
Topography	Flat terrain
Obstacles	Microscale prognostic model Horizontal resolution: 2.5 m Vertical resolution: 2.5 m Vertical stretching factor: 1.0

	Relaxation factor velocity: 0.1 Relaxation factor pressure correction: 1.0 Minimum iterations: 100 Maximum iterations: until convergence (1700) Number of vertical cells: 40
Model domain	X_{\min} : -100m X_{\max} : 150m Y_{\min} : -100m Y_{\max} : 150m Z_{\max} : 102m
Surface roughness length	0.1 m
Wall roughness length	0.01 m

7.3.8 Test case A5-2 (building orientation)

The dependence of model results on the orientation of the walls of the building with respect to the coordinate axes is tested. Test case A5-1 forms the base case, while test case A5-2 is used for comparison purposes. The configuration is the same as for test case A5-1.

Figure 34: Building configuration and model domain for test case A5-2



Topography	Flat terrain
Obstacles	Microscale prognostic model Horizontal resolution: 2.5 m Vertical resolution: 2.5 m Vertical stretching factor: 1.0 Relaxation factor velocity: 0.1 Relaxation factor pressure correction: 1.0 Minimum iterations: 100 Maximum iterations: until convergence (1100) Number of vertical cells: 40
Model domain	X_{\min} : -290m

	X_{\max} : 332m Y_{\min} : -240m Y_{\max} : 210m Z_{\max} : 102m
Surface roughness length	0.1 m
Wall roughness length	0.01 m

Table 27: Hit rates for test case A5-2 ($W = 0.06$, $D = 0.25$); no diffusion

	<i>Data points</i>	<i>Hit rates</i>	<i>Required hit rates</i>
q_u	-	0.96	0.66
q_v	-	0.96	0.66
q_w	-	0.98	0.66

Table 28: Hit rates for test case A5-2 ($W = 0.06$, $D = 0.25$); mixing-length model

	<i>Data points</i>	<i>Hit rates</i>	<i>Required hit rates</i>
q_u	-	0.96	0.66
q_v	-	0.96	0.66
q_w	-	0.99	0.66

Table 29: Hit rates for test case A5-2 ($W = 0.06$, $D = 0.25$); $k-\epsilon$ model

	<i>Data points</i>	<i>Hit rates</i>	<i>Required hit rates</i>
q_u	-	0.97	0.66
q_v	-	0.97	0.66
q_w	-	0.99	0.66

7.3.9 Test case B1 – B6 (homogeneity)

The independency of model results from the direction of the approach flow as well as the calculation accuracy of the programme is tested. These tests are performed without buildings. Flow directions are from 0, 32.3, 45, 90 180, and 270 degrees.

Topography	Flat terrain
Obstacles	Microscale prognostic model Horizontal resolution: 2.0 m Vertical resolution: 2.0 m Vertical stretching factor: 1.0 Relaxation factor velocity: 0.1 Relaxation factor pressure correction: 1.0 Minimum iterations: 100

	Maximum iterations: until convergence (1000) Number of vertical cells: 40
Model domain	X_{\min} : -10m X_{\max} : 10m Y_{\min} : -10m Y_{\max} : 10m Z_{\max} : 82m
Surface roughness length	0.1 m
Wall roughness length	0.01 m

Table 30: Hit rates for test case B1 ($W = 0.01$, $D = 0.05$); all models same results

	<i>Data points</i>	<i>Hit rates</i>	<i>Required hit rates</i>
q_u		1.00	0.95
q_v		1.00	0.95
q_w		1.00	0.95

Table 31: Hit rates for test case B2 ($W = 0.01$, $D = 0.05$) ; all models same results

	<i>Data points</i>	<i>Hit rates</i>	<i>Required hit rates</i>
q_u		1.00	0.95
q_v		1.00	0.95
q_w		1.00	0.95

Table 32: Hit rates for test case B3 ($W = 0.01$, $D = 0.05$) ; all models same results

	<i>Data points</i>	<i>Hit rates</i>	<i>Required hit rates</i>
q_u		1.00	0.95
q_v		1.00	0.95
q_w		1.00	0.95

Table 33: Hit rates for test case B4 ($W = 0.01$, $D = 0.05$) ; all models same results

	<i>Data points</i>	<i>Hit rates</i>	<i>Required hit rates</i>
q_u		1.00	0.95
q_v		1.00	0.95
q_w		1.00	0.95

Table 34: Hit rates for test case B5 ($W = 0.01$, $D = 0.05$) ; all models same results

	<i>Data points</i>	<i>Hit rates</i>	<i>Required hit rates</i>
q_u		1.00	0.95
q_v		1.00	0.95
q_w		1.00	0.95

Table 35: Hit rates for test case B6 ($W = 0.01$, $D = 0.05$) ; all models same results

	<i>Data points</i>	<i>Hit rates</i>	<i>Required hit rates</i>
q_u		1.00	0.95
q_v		1.00	0.95
q_w		1.00	0.95

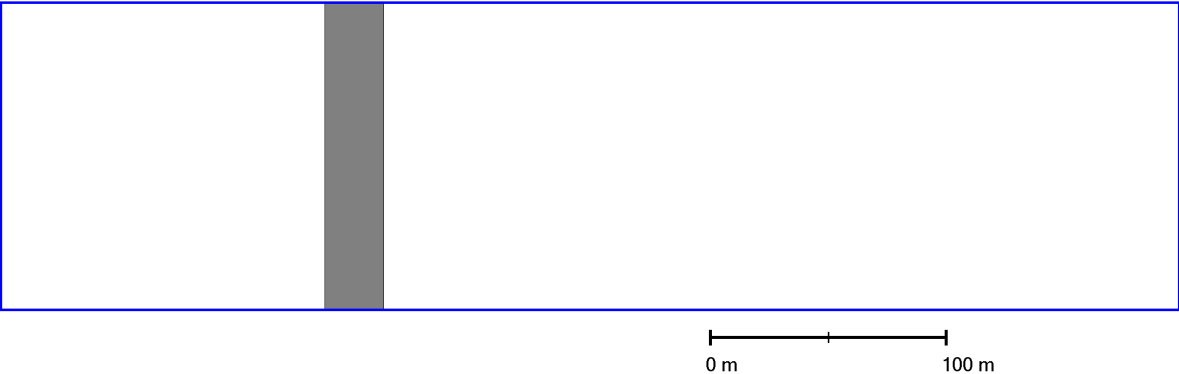
7.3.10 Test case B7 – B12 (Coriolis force)

The independency of model results from the direction of the approach flow as well as the effect of the Coriolis force is tested. As the Coriolis force is not taken into account in GRAL microscale flow field simulations, these tests are not performed.

7.3.11 Test case C1 (wind tunnel data)

This is the first test case out of 6, where model results are compared with wind tunnel observations. The building configuration consists of a 2D obstacle over the entire width of the model domain (same as for test case A1-1). Apart from the comparison with wind-tunnel data, it is also required that the length of the recirculation zone is between $4H$ and $5H$, and that this length increases when the surface roughness is reduced to 0.03 m.

Figure 35: Building configuration and model domain for test case C1



Topography	Flat terrain
Obstacles	Microscale prognostic model Horizontal resolution: 2.5 m Vertical resolution: 2.5 m Vertical stretching factor: 1.0 Relaxation factor velocity: 0.1 Relaxation factor pressure correction: 1.0 Minimum iterations: 100 Maximum iterations: until convergence (10.000) Number of vertical cells: 100
Model domain	X_{min} : -150m X_{max} : 350m Y_{min} : -65m Y_{max} : 65m

	Z_{\max} : 252m
Surface roughness length	0.1 m
Wall roughness length	0.01 m

Table 36: Hit rates for test case C1 ($W = 0.07$, $D = 0.25$); numbers in brackets denote hit rates in the near field; no-diffusion

	<i>Data points</i>	<i>Hit rates</i>	<i>Required hit rates</i>
q_u	651 (293)	0.73 (0.44)	0.66
q_w	651 (293)	0.78 (0.88)	0.66

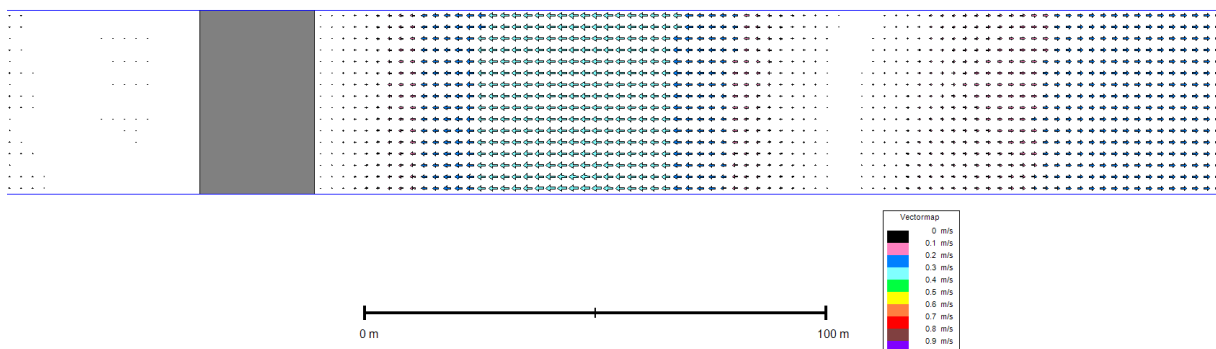
Table 37: Hit rates for test case C1 ($W = 0.07$, $D = 0.25$); numbers in brackets denote hit rates in the near field; mixing-length model

	<i>Data points</i>	<i>Hit rates</i>	<i>Required hit rates</i>
q_u	651 (293)	0.74 (0.46)	0.66
q_w	651 (293)	0.80 (0.89)	0.66

Table 38: Hit rates for test case C1 ($W = 0.07$, $D = 0.25$); numbers in brackets denote hit rates in the near field; k - ϵ model

	<i>Data points</i>	<i>Hit rates</i>	<i>Required hit rates</i>
q_u	651 (293)	0.72 (0.41)	0.66
q_w	651 (293)	0.73 (0.92)	0.66

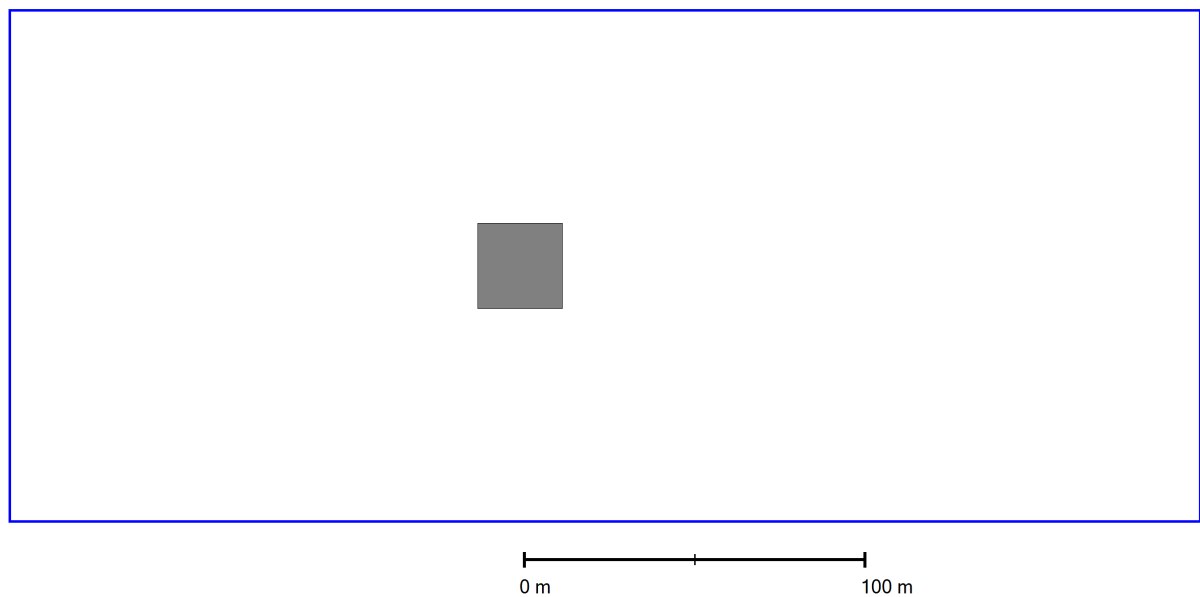
Figure 36: Simulated flow pattern for test case C1 near the ground; no-diffusion



7.3.12 Test case C2 (wind tunnel data)

The building configuration consists of a cubic obstacle with $W=H=L=25$ m (same as for test case A3-1).

Figure 37: Building configuration and model domain for test case C2



Topography	Flat terrain
Obstacles	Microscale prognostic model Horizontal resolution: 2.5 m Vertical resolution: 2.5 m Vertical stretching factor: 1.0 Relaxation factor velocity: 0.1 Relaxation factor pressure correction: 1.0 Minimum iterations: 100 Maximum iterations: until convergence (1100) Number of vertical cells: 40
Model domain	X_{\min} : -150m X_{\max} : 200m Y_{\min} : -75m Y_{\max} : 75m Z_{\max} : 101m
Surface roughness length	0.1 m
Wall roughness length	0.01 m

Table 39: Hit rates for test case C2 ($W = 0.06$, $D = 0.25$); numbers in brackets denote hit rates in the near field; no-diffusion

	<i>Data points</i>	<i>Hit rates</i>	<i>Required hit rates</i>
q_u	870 (482)	0.94 (0.90)	0.66
q_v	362 (197)	0.97 (0.94)	0.66
q_w	870 (482)	0.89 (0.81)	0.66

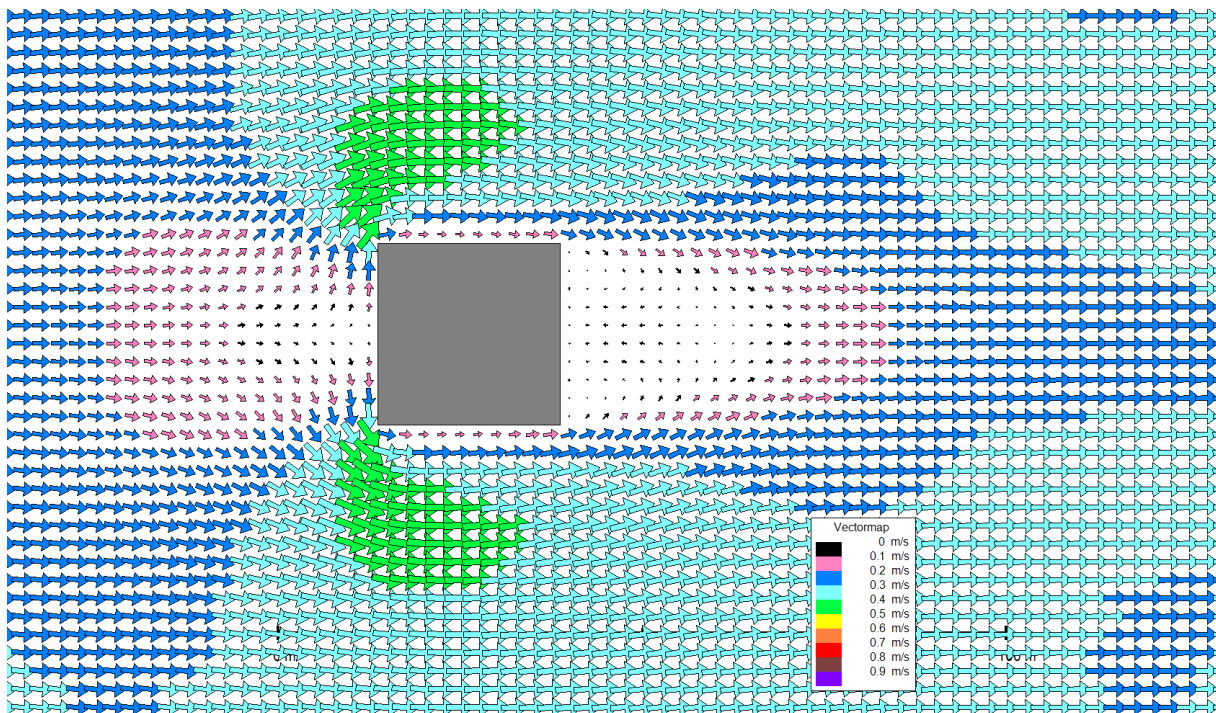
Table 40: Hit rates for test case C2 ($W = 0.06$, $D = 0.25$); numbers in brackets denote hit rates in the near field; mixing-length model

	<i>Data points</i>	<i>Hit rates</i>	<i>Required hit rates</i>
q_u	870 (482)	0.94 (0.89)	0.66
q_v	362 (197)	0.97 (0.94)	0.66
q_w	870 (482)	0.90 (0.82)	0.66

Table 41: Hit rates for test case C2 ($W = 0.06$, $D = 0.25$); numbers in brackets denote hit rates in the near field; k - ϵ model

	<i>Data points</i>	<i>Hit rates</i>	<i>Required hit rates</i>
q_u	870 (482)	0.87 (0.77)	0.66
q_v	362 (197)	0.96 (0.93)	0.66
q_w	870 (482)	0.89 (0.80)	0.66

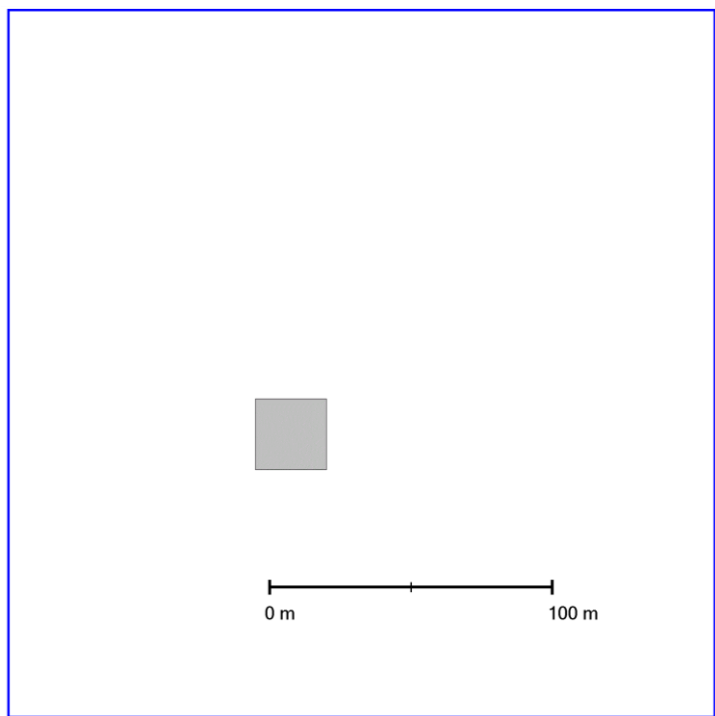
Figure 38: Simulated flow pattern for test case C2 near the ground



7.3.13 Test case C3 (wind tunnel data)

The building configuration consists of a cubic obstacle with $W=H=L=25$ m (same as for test case A4-1), but the approaching flow is from 225 deg. Eichhorn and Kniffka (2010) found that the approaching flow in the wind-tunnel was not exactly from 225 deg., but was 223 deg., simulations were performed with the latter value.

Figure 39: Building configuration and model domain for test case C3



Topography	Flat terrain
Obstacles	Microscale prognostic model Horizontal resolution: 2.5 m Vertical resolution: 2.5 m Vertical stretching factor: 1.0 Relaxation factor velocity: 0.1 Relaxation factor pressure correction: 1.0 Minimum iterations: 100 Maximum iterations: until convergence (1200) Number of vertical cells: 40
Model domain	X_{\min} : -100m X_{\max} : 150m Y_{\min} : -100m Y_{\max} : 150m Z_{\max} : 101m
Surface roughness length	0.1 m
Wall roughness length	0.01 m

Table 42: Hit rates for test case C3 ($W = 0.06$, $D = 0.25$); numbers in brackets denote hit rates in the near field; no diffusion

	Data points	Hit rates	Required hit rates
q_u	706 (415)	0.85 (0.75)	0.66
q_v	706 (415)	0.79 (0.66)	0.66
q_w	789 (383)	0.72 (0.56)	0.66

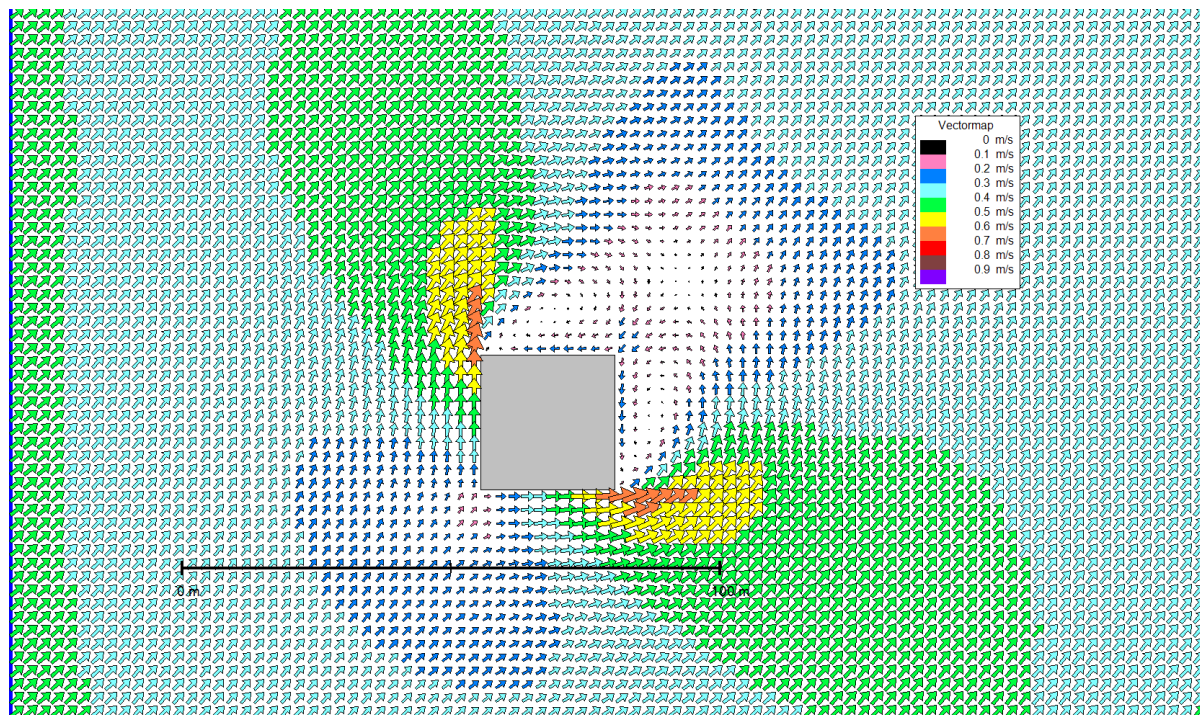
Table 43: Hit rates for test case C3 ($W = 0.06$, $D = 0.25$); numbers in brackets denote hit rates in the near field; mixing-length model

	<i>Data points</i>	<i>Hit rates</i>	<i>Required hit rates</i>
q_u	706 (415)	0.85 (0.75)	0.66
q_v	706 (415)	0.79 (0.66)	0.66
q_w	789 (383)	0.74 (0.59)	0.66

Table 44: Hit rates for test case C3 ($W = 0.06$, $D = 0.25$); numbers in brackets denote hit rates in the near field; k - ϵ model

	<i>Data points</i>	<i>Hit rates</i>	<i>Required hit rates</i>
q_u	706 (415)	0.84 (0.73)	0.66
q_v	706 (415)	0.77 (0.61)	0.66
q_w	789 (383)	0.72 (0.55)	0.66

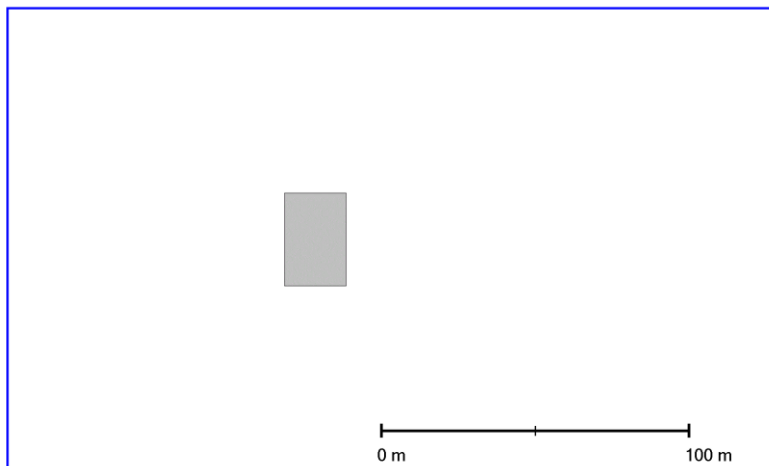
Figure 40: Simulated flow pattern for test case C3 near the ground



7.3.14 Test case C4 (wind tunnel data)

The building configuration consists of an obstacle with extensions $L=20\text{m}$, $H=25\text{m}$, and $W=30\text{ m}$.

Figure 41: Building configuration and model domain for test case C4



Topography	Flat terrain
Obstacles	Microscale prognostic model Horizontal resolution: 2.5 m Vertical resolution: 2.5 m Vertical stretching factor: 1.0 Relaxation factor velocity: 0.1 Relaxation factor pressure correction: 1.0 Minimum iterations: 100 Maximum iterations: until convergence (1500) Number of vertical cells: 40
Model domain	X_{\min} : -100m X_{\max} : 150m Y_{\min} : -75m Y_{\max} : 75m Z_{\max} : 102m
Surface roughness length	0.1 m
Wall roughness length	0.01 m

Table 45: Hit rates for test case C5 ($W = 0.07$, $D = 0.25$); numbers in brackets denote hit rates in the near field; no diffusion

	<i>Data points</i>	<i>Hit rates</i>	<i>Required hit rates</i>
q_u	1134 (641)	0.89 (0.82)	0.66
q_v	616 (327)	0.89 (0.81)	0.66
q_w	518 (314)	0.92 (0.87)	0.66

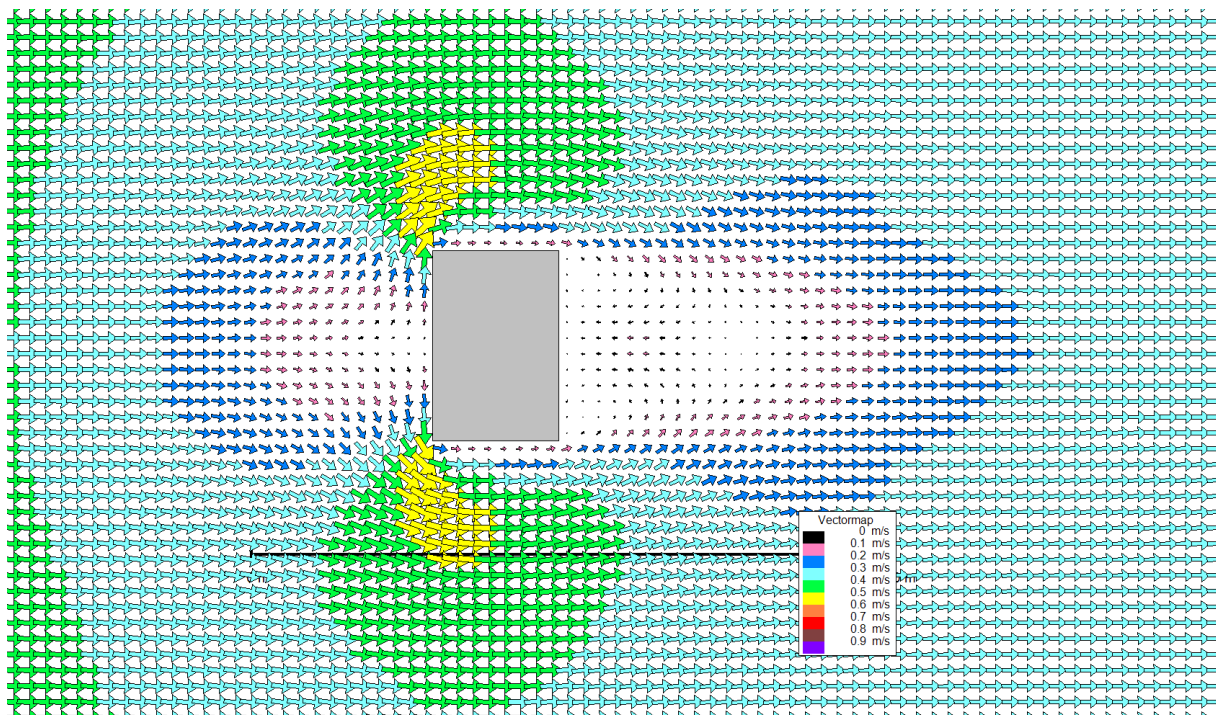
Table 46: Hit rates for test case C5 ($W = 0.07$, $D = 0.25$); numbers in brackets denote hit rates in the near field; mixing-length model

	<i>Data points</i>	<i>Hit rates</i>	<i>Required hit rates</i>
q_u	1134 (641)	0.89 (0.81)	0.66
q_v	616 (327)	0.89 (0.82)	0.66
q_w	518 (314)	0.91 (0.85)	0.66

Table 47: Hit rates for test case C5 ($W = 0.07$, $D = 0.25$); numbers in brackets denote hit rates in the near field; k - ϵ model

	<i>Data points</i>	<i>Hit rates</i>	<i>Required hit rates</i>
q_u	1134 (641)	0.85 (0.75)	0.66
q_v	616 (327)	0.89 (0.80)	0.66
q_w	518 (314)	0.91 (0.86)	0.66

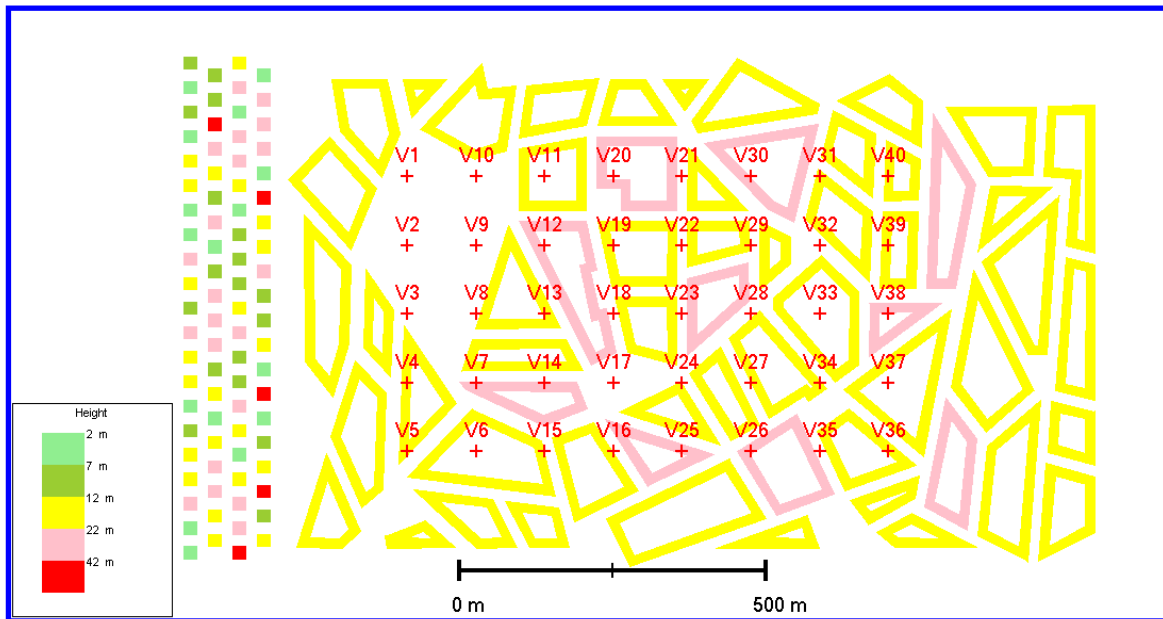
Figure 42: Simulated flow pattern for test case C5 near the ground



7.3.15 Test case C5 (wind tunnel data)

The building configuration consists of a complex arrangement of obstacles typical for European style cities. The test case requires different surface roughness lengths: within the built-up areas 0.034 m and outside 0.1 m. GRAL just supports one homogenous roughness length. As the observations were carried out entirely between the buildings, the roughness length was set to 0.034 m for the entire model domain.

Figure 43: Building configuration and model domain for test case C5, crosses indicate the location of profile observations in the wind tunnel



Topography	Flat terrain
Obstacles	Microscale prognostic model Horizontal resolution: 2.0 m Vertical resolution: 0.6 m Vertical stretching factor: 1.0 Relaxation factor velocity: 0.10 Relaxation factor pressure correction: 1.00 Minimum iterations: 100 Maximum iterations: until convergence (7500) Number of vertical cells: 40
Model domain	X_{\min} : -1100m X_{\max} : 800m Y_{\min} : -500m Y_{\max} : 500m Z_{\max} : 1068m
Surface roughness length	0.034 m
Wall roughness length	0.001 m

Table 48: Hit rates for test case C5 ($W = 0.08$, $D = 0.25$); no diffusion

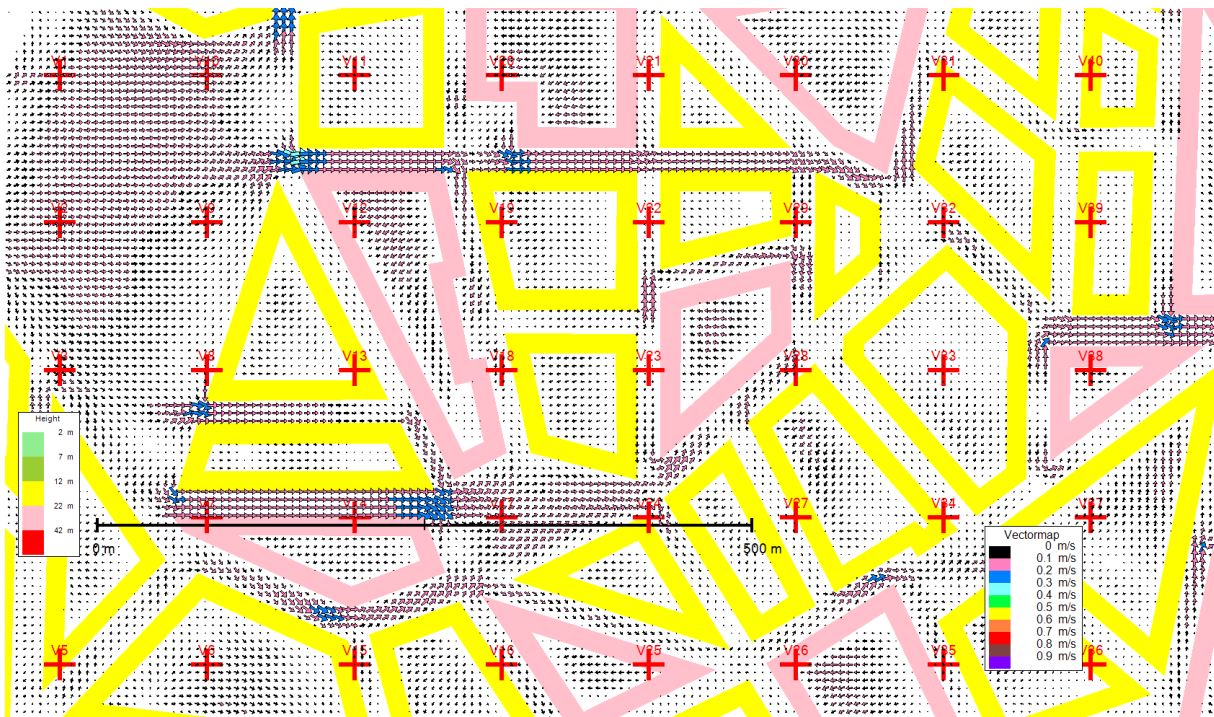
	<i>Data points</i>	<i>Hit rates</i>	<i>Required hit rates</i>
q_u	1838	0.66	0.66
q_v	1838	0.78	0.66
$q_{u,v}$	1838	0.55	0.50

Table 49: Hit rates for test case C5 ($W = 0.08$, $D = 0.25$); mixing-length model

	Data points	Hit rates	Required hit rates
q_u	1838	0.67	0.66
q_v	1838	0.79	0.66
$q_{u,v}$	1838	0.56	0.50

Table 50: Hit rates for test case C5 ($W = 0.08$, $D = 0.25$); $k-\varepsilon$ model

	Data points	Hit rates	Required hit rates
q_u	1838	0.68	0.66
q_v	1838	0.79	0.66
$q_{u,v}$	1838	0.57	0.50

Figure 44: Simulated flow pattern for test case C5 near the ground (every 3th vector is shown)

7.4 Summary

GRAL does not comply with guideline VDI 3783-9 with regard to the following requirements:

- There is no online control of the standard deviations of wind-components for each layer.
- There is no online control whether the domain-averaged wind components are monotonically in- or decreasing or if they oscillate with a period of $2 \Delta t$.

Non-compliance is due to formal criteria only, while the performance criteria of the test cases are met when using either the non-diffusion or the mixing-length approaches. The more sophisticated standard k - ϵ model performs worse than the simple models in many situations. Only for the most complex test case C5 it gives slightly better results. It is not possible to provide a conclusive answer for this behaviour. One aspect might be that the implicit algorithm to solve the RANS equations is fast, but probably introduces some false diffusion, especially in wake regions. It might also be the case that programming errors are the cause for this odd result.

Nevertheless, the mixing-length model not only fulfils the criteria set up in the VDI guideline, but also offers two advantages, namely (i) that it is much faster than the standard k - ϵ model and (ii) it does not generate artificial turbulence in applications where complex terrain is step-wise resolved by the GRAL grid. Hence, the mixing-length model is recommended as standard model.

8 Compliance with other guidelines from national authorities

GRAL is recommended by the National Health and Medical Research Council, Australian Government, as dispersion model for regulatory purposes for road tunnel portal emissions (NHMRC, 2008).

9 Additional validation cases

Model validation is crucial not only for the determination of expected accuracy but also for model development. It is important to know that all datasets used for model validation have their own peculiarities, which makes it often difficult to determine whether differences between observations and model results are due to shortcomings of the model or observational issues. Hence, it is recommended using as much datasets as possible to evaluate model performance for a certain type of application, especially if turbulence parameterisations are to be tested. There are many statistical measures discussed in literature, which can serve as indicator for model performance. Many of them fit well for scientific purposes. For instance, the normalised mean square error (NMSE) is often used, because it allows for a dataset independent comparison of model results (ASTM, 2000).

$$NMSE = \frac{\overline{(C_0 - C_p)^2}}{\overline{C_0 C_p}} \quad (105)$$

The disadvantage of the NMSE is that it has no indication of over- or underestimation, which is crucial in applications for regulatory purposes. Thus, in the following also the fractional bias is utilized.

$$FB = \frac{C_p - C_o}{0.5 \cdot (C_0 + C_p)} \quad (106)$$

Chang und Hanna (2004) suggested using an upper bound for the NMSE < 4, and a max. fractional bias of +/-0.3 as criteria to define acceptable model performance. GRAL fulfils these criteria in 28 out of 29 experiments. In previous versions of the manual (up to 20.01) comparisons with other dispersion models were also included. These comparisons showed, that AUSTAL2000 meets the criteria in 5 experiments out of 12, and ADMS in 5 out of 15 experiments (see GRAL Documentation V20.01 and earlier).

Depending on the experimental set, other models may also perform better than GRAL. The results may vary even for different GRAL versions, different GRAL options or small changes

Additional validation cases

in the GRAL setting. For this reason, the Model Set Up is specified for each test data set and the results of other models are no longer mentioned from manual version 20.09 onwards.

The following abbreviations are used:

GRAL/level2: GRAL computes flow and turbulence fields around buildings itself, based on the Navier-Stokes equations and the mixing-length turbulence model.

GRAL/level1: GRAL computes only a simple mass conservative flow field around buildings.

GRAL: no buildings have been considered.

9.1 Indianapolis

9.1.1 Dataset description

The Indianapolis experiment was performed by EPRI (Electric Power Research Institute) during September and October in 1985 at the Perry K power plant (e.g. Olesen, 2005). The site was on the south-west edge of Indianapolis in a mixed industrial/commercial urban area. The SF₆ tracers were released from an 83.8-m stack (diameter of 4.72 m). The individual surrounding buildings had no influence on the plume dispersion due to buoyant plume rise up to 100 m or more occurring most of the time. 142 out of 170 releases with measurements of near surface concentrations and meteorology covering a wide range of stability classes and wind speeds at daytime and nighttime were taken for model evaluation. Measurements were taken on an hourly basis. The mixing heights were determined from the site mini sodar profiles. There were ten arcs ranging from 0.25 km to 12 km from the release at which concentrations were observed.

9.1.2 Characteristics

The stack dimensions are typical for such facilities. Among the various meteorological parameters only the stability classes (PGT) and the wind speed in 11 m above ground level has been used. Although the exit velocity (5.8 – 14.4 m/s) and the exit temperature (484 K – 508 K) varied during the experiments, only mean values have been used in GRAL for simplicity. This might leave to somewhat worse results. In GRAL the maximum concentrations in each distance have been taken, while observations are based on maximum concentrations at certain receptor points at several distances. This may lead to some inaccuracies in the comparison. Due to the high roughness length of 1 m, observed concentrations did not vary much with stability.

9.1.3 Model set up

Topography	Flat Terrain
Obstacles	None
Concentration grid	100 m horizontal, 2 m vertical extension, 3 m above ground level
Model domain	7,100 m x 7,500 m
Number of particles	720,000 per hour
Roughness length	1.5 m

9.1.4 Results

GRAL performs significantly better than the Austrian standard model OENORM M9440, although concentrations are underestimated. The average concentration distribution corresponds still in a satisfying way with observations. Peak concentrations are underestimated by about a factor of two.

Additional validation cases

Table 51. Results for the Indianapolis experiment

Model	NMSE	FB	References
GRAL V20.01	0.9	-0.1	
GRAL V20.09	0.8	-0.1	
GRAL V21.09	0.8	-0.1	
GRAL V23.11	0.8	-0.1	
GRAL V24.04	0.8	-0.1	

Figure 45. Observed and modelled mean normalised concentrations as function of the distance to the stack with GRAL V24.04

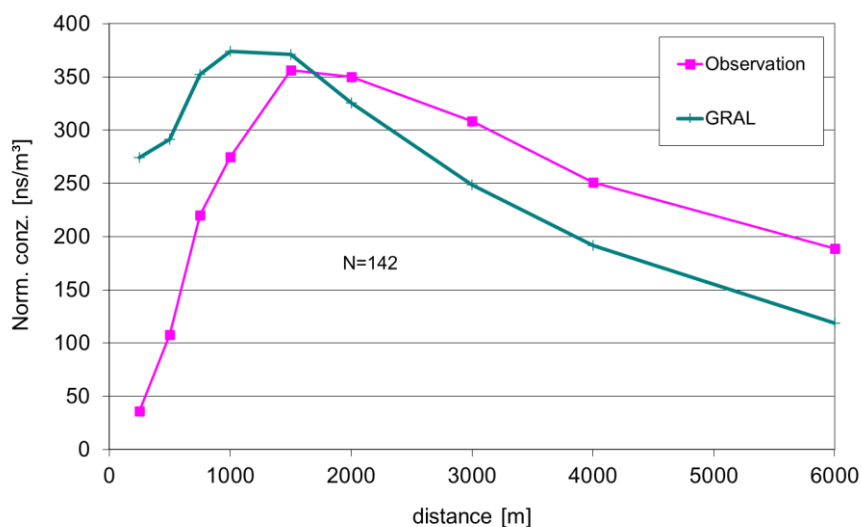
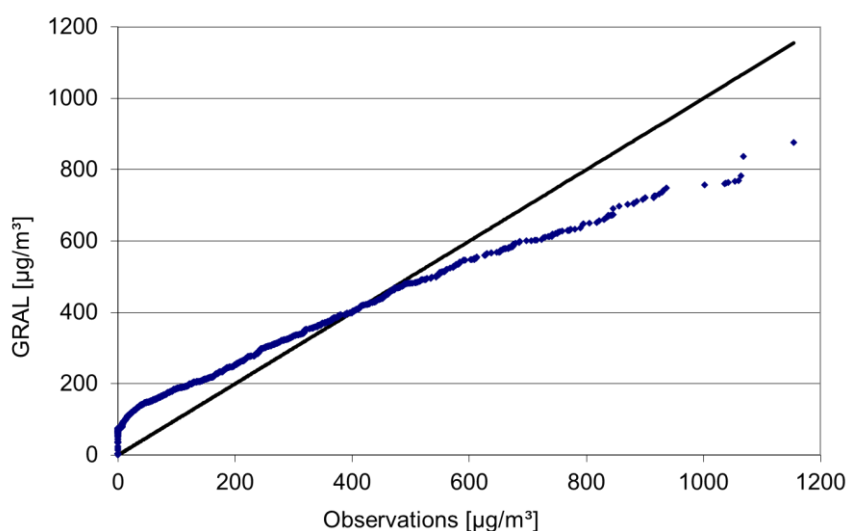


Figure 46 Quantile-quantile plot of observed and modelled normalised concentrations (V24.04)



9.2 Kincaid

9.2.1 Dataset description

The Kincaid field experiment was performed as part of the EPRI Plume Model Validation and Development Project. A very comprehensive experimental campaign was conducted in 1980 and 1981 (Olesen, 2005). The Kincaid power plant is situated in Illinois, USA and is surrounded by flat farmland with some lakes. The power plant has a 187 m stack with a diameter of 9 m. During the experiment, SF₆ was released from the stack. The tracer releases started some hours before the sampling. There is a nearby building with a height of approximately 75 meter. It is rectangular – 25 m by 95 m – with the long side oriented east – west. The stack is 152 m south of the centre of the southern edge of the building, and 182 m south of the tallest part of the building, which has a maximum significant elevation of 74.4 m.

9.2.2 Characteristics

At least for Austrian conditions, the stack of 187 m is exceptional high and not typical for most power plant facilities. The tracer experiments covered almost only neutral and convective conditions with relatively high wind speeds (average > 4 m/s). Although the exit velocity (4.2 – 39.3 m/s) and the exit temperature (369 K – 457 K) varied during the experiments, only their mean values have been used in the GRAL simulations. This might leave to somewhat worse results. In GRAL the maximum concentrations in each distance have been taken, while the observations are based on maximum concentrations at certain receptor points at several distances. This may lead to some inaccuracies in the comparison. Among the various meteorological parameters only the stability classes (PGT) and the wind speed in 10 m above ground level has been used.

9.2.3 Model set up

Topography	Flat Terrain
Obstacles	Microscale prognostic model, mixing-length turbulence closure Horizontal resolution: 10 m Vertical resolution: 5 m Vertical stretching factor: 1.0
Concentration grid	10 m horizontal, 4 m vertical extension, 3.5 m above ground level
Model domain	13,200 m x 6,000 m
Number of particles	720,000 per hour
Roughness length	0.025 m
Adaptive Roughness	0 m

Additional validation cases

9.2.4 Results

By taking the influence of the nearby building into account, GRAL is able to reproduce observed concentrations reasonably, although peak concentrations are underestimated by about a factor of two.

Table 52. Results for the Kincaid experiment

Model	NMSE	FB	References
GRAL/level 2	1.6	0.2	
GRAL V20.09	1.6	0.3	
GRAL V21.09	1.6	0.28	
GRAL V23.11	2.3	-0.2	
GRAL V24.04	2.2	-0.0	

Figure 47. Observed and modelled mean normalised concentrations as function of the distance to the stack with GRAL V24.04

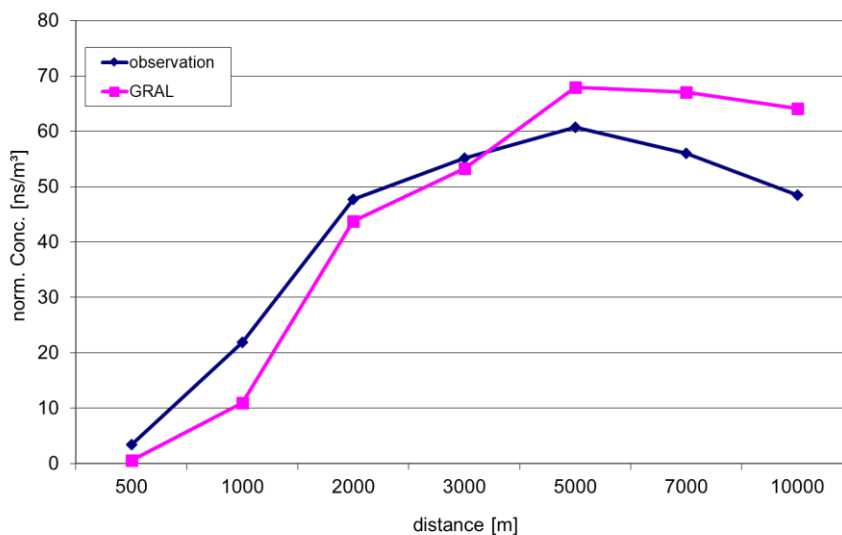
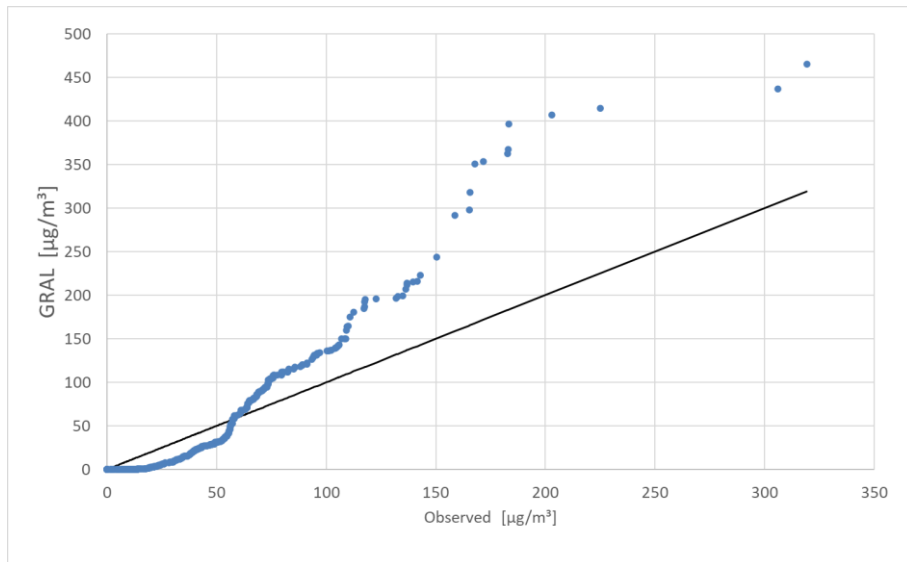


Figure 48. Quantile-quantile plot of observed and modelled normalised concentrations with GRAL V24.04



9.3 Lillestroem

9.3.1 Dataset description

The tracer experiments took place in Norway, near Oslo, in 1987 (Olesen, 2005). They were performed by the Norwegian Institute of Air Research (NILU). The experiments were carried out in a flat residential area with 6-10 m high buildings and trees. A tracer system was used in which SF₆ was released from a mast 36 m above the ground. Each experiment consisted of two sequential 15-min periods. Meteorological measurements were carried out along the 36 m high mast. The temperature during the tracer experiments was low (-20° C), and the ground was snow covered. The sun was above the horizon, but at a very low angle.

9.3.2 Characteristics

There were almost only low wind speed conditions. Only 22 concentration observations from all together 8 experiments were available for comparison purposes. Hence, from a statistical point of view the dataset is almost too small for model evaluation. The tracer release took place without any buoyancy or exit velocity. In the simulations with GRAL friction velocity, Obukhov length, horizontal velocity variance, and wind speed as observed with a sonic anemometer 10 m above ground level has been used. A second simulation with GRAL has also been made using standard meteorological input, namely wind speed at 10 m above ground, and stability class.

9.3.3 Model set up

Topography	Flat Terrain
Obstacles	None
Concentration grid	25 m horizontal, 3 m vertical extension, 3 m above ground level
Model domain	1,350 m x 700 m
Number of particles	450,000 per 900 seconds
Roughness length	0.5 m

9.3.4 Results

GRAL shows good agreement with observed concentrations in contrast to other models. Results are strongly improved when using observed turbulence quantities rather than using standard meteorological input (stability classes) in this case. It should be noted that due to the low number of observations, a sound statistical evaluation of model results is questionable.

Table 53. Results for the Lillestroem experiment

Model	NMSE	FB	References
GRAL V20.09	0.4	-0.1	
GRAL V20.09 (stability classes)	2.4	0.7	
GRAL V21.09	0.4	-0.1	
GRAL V21.09 (stability classes)	2.4	0.7	
GRAL V23.11	0.4	-0.1	
GRAL V23.11 (stability classes)	2.3	0.7	
GRAL V24.04	0.4	-0.1	
GRAL V24.04 (stability classes)	2.2	0.6	

Figure 49 Observed and modelled mean normalised concentrations as function of the distance to the source with GRAL V24.04

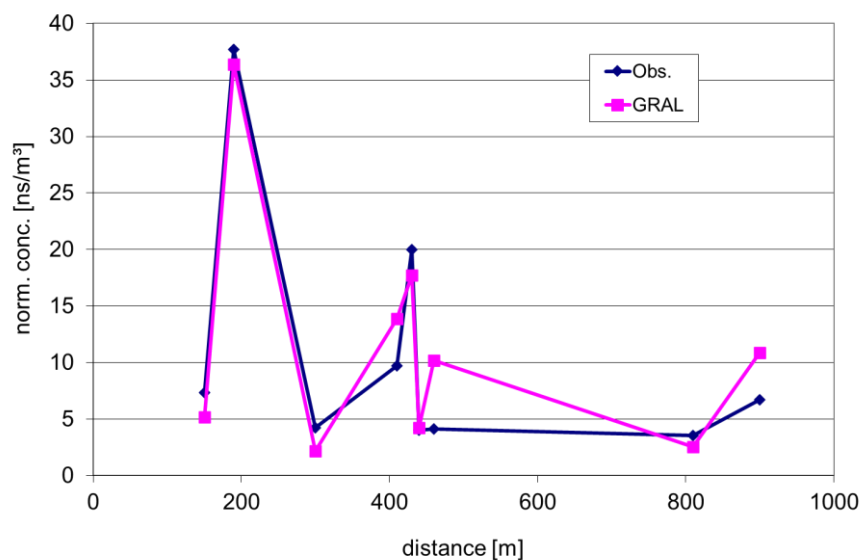
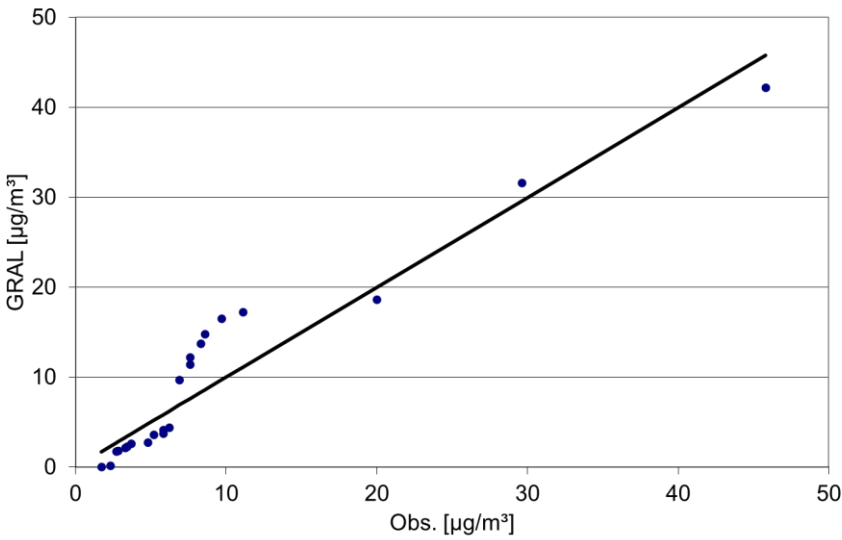


Figure 50. Quantile-quantile plot of observed and modelled normalised concentrations with GRAL V24.04

Additional validation cases



9.4 Prairie Grass

9.4.1 Dataset description

The Prairie Grass field experiment was carried out, by the Air Force Cambridge Research Centre, in north central Nebraska during July and August 1956 (Barad, 1958). It has become a standard database used for evaluation of models for continuous plume release near the ground over flat terrain. The site is surrounded by an agricultural field, where the grass had been cut and was short dry stubble at the time of the experiments. The 20-minute releases of SO₂ were conducted from a point source at a height of 0.46 m. There were 44 tests over a variety of atmospheric stability conditions with an average wind speed of 5 m/s. The sampling was done for a 10-minute period starting in the middle of the 20-minute release at a height of 1.5 m along five arcs downwind distances (50, 100, 200, 400, and 800 m).

Since the experiment was performed with relatively high sampling time resolution (10 minutely), maximum concentrations of the SO₂ plume might not be precisely captured at the sampling arcs far away from the release.

9.4.2 Characteristics

The major problem with this dataset is the small averaging time of 10 minutes, which is much smaller than the usual averaging time in air quality observations. Especially in low wind speed conditions this leads to substantial lower standard deviations of wind velocity in the horizontal directions, as meandering occurs at much larger time intervals. In GRAL, meandering has been “switched off” (the classical Lagrangian autocorrelation function is used) to simulate this experiment. In addition, the provided values for the friction velocity, the Monin-Obukhov length, and the standard deviation of the wind direction are used together with the wind speed near the ground. A second simulation with GRAL has also been made using standard meteorological input, namely wind speed at 10 m above ground, and stability class.

9.4.3 Model set up

Topography	Flat Terrain
Obstacles	None
Concentration grid	4 m horizontal, 0.5 m vertical extension, 1.5 m above ground level
Model domain	1,600 m x 2,000 m
Number of particles	240,000 per 600 seconds
Roughness length	0.006 m

9.4.4 Results

GRAL performs quite well for this dataset, especially when observed turbulence quantities are used. Utilizing standard meteorological input (stability classes), gives worse results.

Additional validation cases

Table 54. Results for the Prairie Grass experiment

Model	NMSE	FB	References
GRAL V20.09	0.9	-0.1	
GRAL V20.09 (stability classes)	1.0	0.2	
GRAL V21.09	0.9	-0.1	
GRAL V23.11	0.8	0.0	
GRAL V23.11 (stability classes)	1.0	0.2	
GRAL V24.04			
GRAL V24.04 (stability classes)			

Figure 51. Observed and modelled mean normalised concentrations as function of the distance to the source with GRAL V23.11

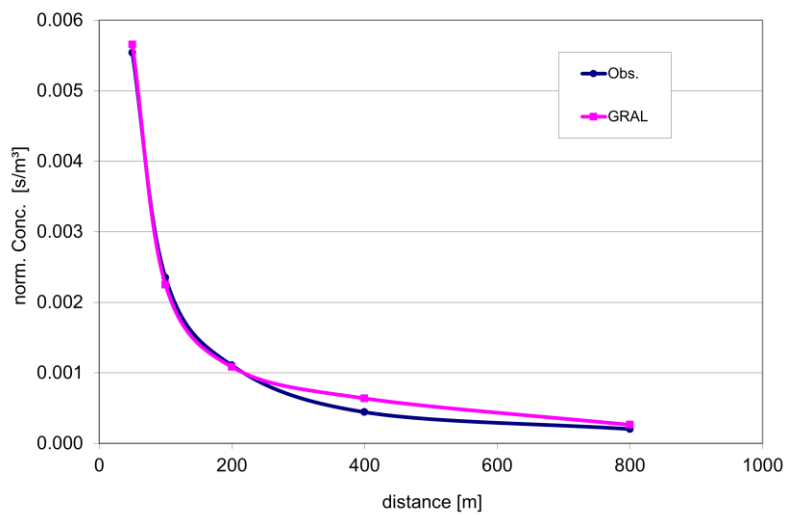
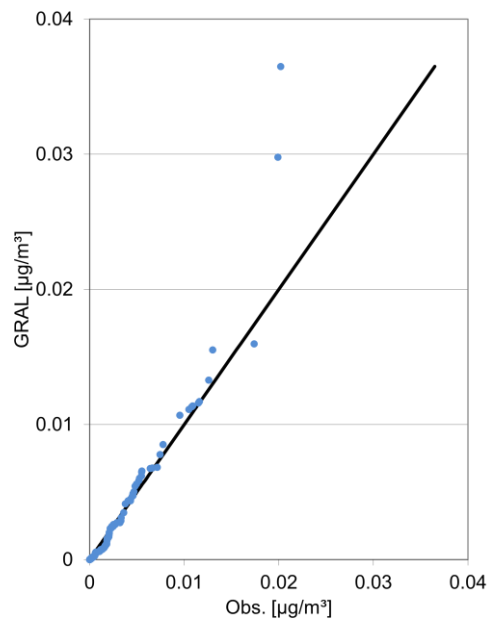


Figure 52. Quantile-quantile plot of observed and modelled normalised concentrations with GRAL V23.11



9.5 Copenhagen

9.5.1 Dataset description

The experiments took place in the Northern part of Copenhagen in 1978-79 (Olesen, 2005). They were carried out under neutral and unstable conditions. The tracer SF₆ was released without buoyancy from a tower at a height of 115 m, and collected at ground-level positions in up to three crosswind series of tracer sampling units, positioned 2-6 km from the point of release. The site was mainly residential. The tracer sampling units were mounted at lampposts at a height of 2-3 meters above the ground. The meteorological measurements performed during the experiments included three-dimensional wind velocity fluctuations at the height of release. The temperature and wind speed profile along the mast was taken from routine measurements. The mixing height was determined from daily radio sounding at Copenhagen, which was carried out around the time of tracer sampling.

9.5.2 Characteristics

Like the Lillestroem dataset, a release without buoyancy at a height of over 100 m above ground level is rarely found in real world conditions. For statistical analysis only few observations are available, which brings forward some uncertainty when judging model performance. For the simulations the provided wind speed at 10 m above ground, and stability class was used.

9.5.3 Model set up

Topography	Flat Terrain
Obstacles	None
Concentration grid	4 m horizontal, 3 m vertical extension, 3 m above ground level
Model domain	6,500 m x 2,000 m
Number of particles	1,440,000 per hour
Roughness length	0.5 m

9.5.4 Results

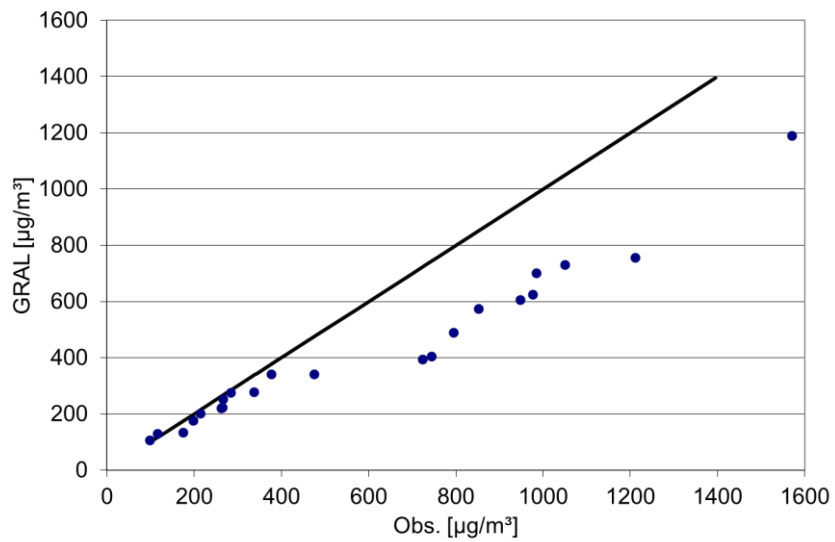
GRAL performs satisfactory compared to other available model results. It must be said that model results may depend strongly on the type of input parameters used, as has been demonstrated by Janicke (2005).

Table 55. Results for the Copenhagen experiment

Model	NMSE	FB	References
GRAL V20.09	0.4	0.3	
GRAL V23.11	0.9	-0.7	
GRAL V23.11 (stability classes)	0.5	0.3	

GRAL V24.04	0.8	-0.6	
GRAL V24.04 (stability classes)	0.5	0.3	

Figure 53. Quantile-quantile plot of observed and modelled normalised concentrations with GRAL V24.04



9.6 Idaho

9.6.1 Dataset description

The tracer experiments were performed at the Idaho National Engineering Laboratory (INEL) in south-eastern Idaho, USA (Sagendorf and Dickson, 1974). The INEL is located in a broad, relatively flat plain at an elevation of about 1500 m. The climate is dry and of semidesert type. Ten experiments in low winds were conducted: Nine in stable conditions and one in near neutral conditions. The tracer (SF_6) was released 1.5 m above ground level. Each experiment lasted one hour, except experiment 10 that lasted 49 minutes. Ground level concentrations were measured at 0.76 m by sixty samplers (separated by 6 degrees) on three arcs with radii 100, 200 and 400 m (for a total of 180 samplers). Besides these ground level samplers, eight towers located on the second arc in a sector included between N-E and S, recorded the tracer concentration at 2 m, 4.5 m, 6 m and 9 m during the last five experiments. Finally meteorological information (wind speed \overline{U} , direction ϑ , and standard deviation of wind direction σ_ϑ) was recorded at sixth levels (2 m, 4 m, 8 m, 16 m, 32 m and 61 m) on a meteorological tower located on the second arc, at about 238 degrees. The temperature gradient, between 32 and 8 m, and plume spread, defined as the sector width in degrees over which the tracer was detected, at the 200 m arc were also measured.

9.6.2 Characteristics

There is some uncertainty about the effective source height as indicated by visual observations of contemporarily released oil fog plumes. Brusasca et al. (1992) assumed 3 m as effective release height, which is also used here. Standard deviations of wind directions, mean wind speed and –direction have been used for the simulations. Monin-Obukhov length and friction velocity have been taken from Oetl et al. (2001a). A second simulation with GRAL has also been made using standard meteorological input, namely wind speed at 8 m above ground, and stability class. Wind speeds were rather low in all experiments. Only arcwise maximum concentrations have been compared with simulated concentrations. Thus only 30 data pairs were available for statistical analysis, which is very low for a meaningful interpretation.

9.6.3 Model set up

Topography	Flat Terrain
Obstacles	None
Concentration grid	10 m horizontal, 0.3 m vertical extension, 0.76 m above ground level
Model domain	1,000 m x 1,000 m
Number of particles	180,000 per hour
Roughness length	0.03 m

9.6.4 Results

As other models developed for low wind speed conditions, GRAL performs very well, too, regardless the meteorological input data used.

Table 56. Results for the Idaho experiment

Model	NMSE	FB
GRAL	0.3	0.1
GRAL (stability classes)	0.3	0.0
GRAL V23.11	0.3	0.1
GRAL V23.11 (stability classes)	0.3	0.0
GRAL V24.04	0.3	0.0
GRAL V24.04 (stability classes)	0.3	0.0

Figure 54. Observed and modelled mean peak concentrations as function of the distance to the source

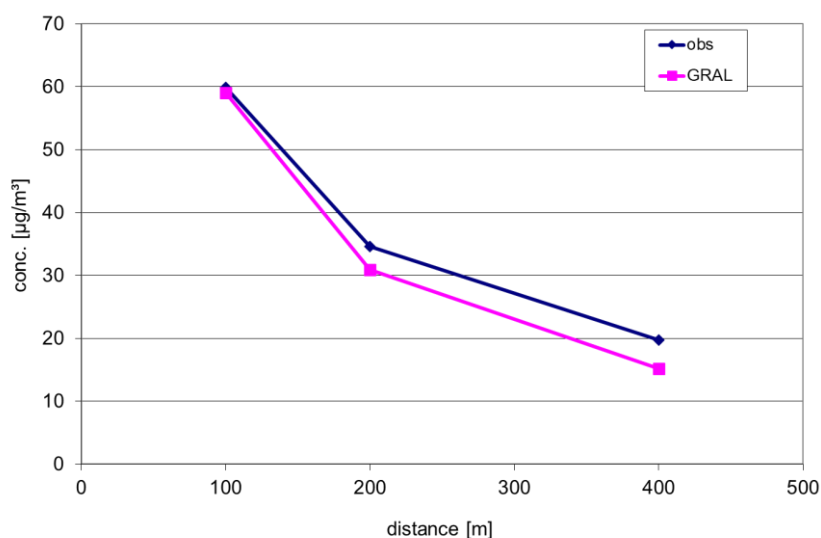
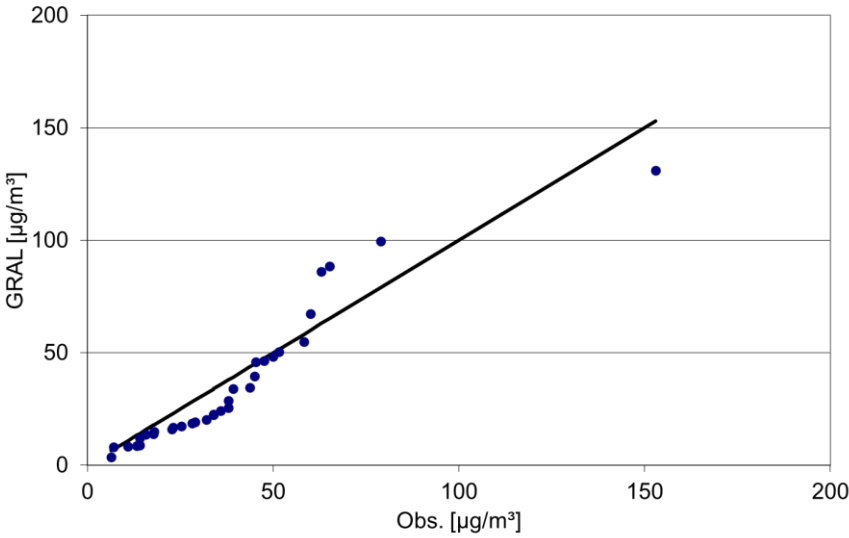


Figure 55 Quantile-quantile plot of observed and modelled peak concentrations with V24.04

Additional validation cases



9.7 Raaba

9.7.1 Dataset description

The Graz University of Technology, Institute of Internal Combustion Engines and Thermodynamics, made 6 tracer experiments in relatively flat terrain in the surroundings of the city of Graz in May 2003 to study near surface dispersion in extremely low wind conditions (Anfossi et al., 2006). The surroundings can be characterised as inhomogeneous with one larger building about 10 m height and some smaller trees and bushes within about 100 m distance to the tracer release. The tracer release and sampling took place on a meadow about 0.3 m height. SF₆ was used as tracer and was sampled (30 samplers equally distributed) on an arc at 50 m distance to the point of release at 1.4 m a.g.l., which was in the centre of the arc and at 1.6 m a.g.l. Each experiment lasted 30 minutes. The samples were taken in aluminium coated plastic bags, which were analysed by means of an FTIR (Fourier Transformed Infrared Spectroscopy) device immediately after each experiment. Wind data was recorded by two sonic anemometers (Type METEK USA-1) with 1 Hz frequency at 1.5 m and 6.0 m a.g.l.

9.7.2 Characteristics

Observed concentrations have been compared with modelled ones paired in space and time, which in general leads to worse results as if only arcwise maximum concentrations would have been taken for comparison. Wind speeds were extremely low, partly even below 0.1 m/s!

9.7.3 Model set up

Topography	Flat Terrain
Obstacles	None
Concentration grid	5 m horizontal, 0.5 m vertical extension, 1.4 m above ground level
Model domain	200 m x 200 m
Number of particles	720,000 per ½ hour
Roughness length	0.01 m
Adaptive roughness	0 m

9.7.4 Results

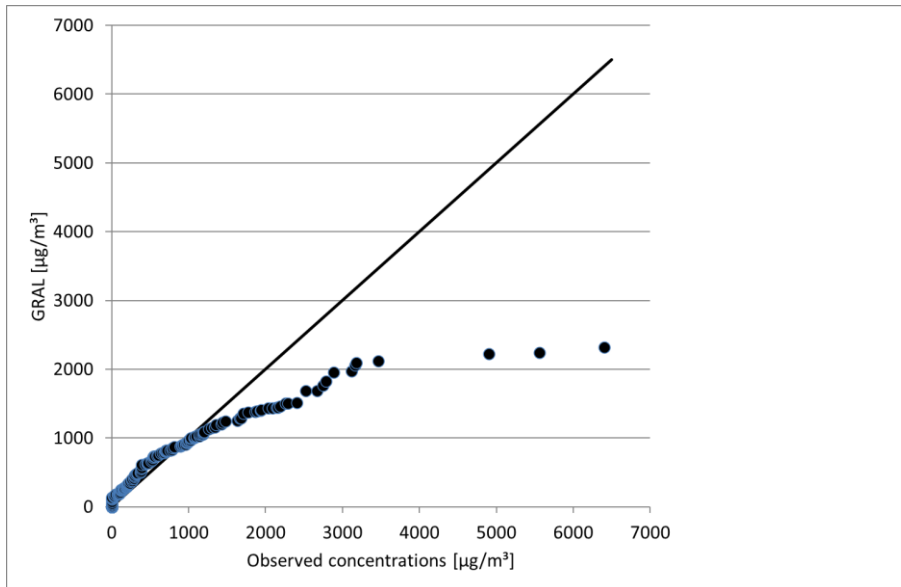
In comparison with results from other models, GRAL performs well for these extreme low wind speed experiments. It must be noted that peak concentrations are substantially underestimated by GRAL.

Additional validation cases

Table 57. Results for the Raaba experiment

Model	NMSE	FB	References
GRAL V20.01	1.4	0.0	
GRAL V20.01 (stability classes)	1.3	-0.2	
GRAL V20.09	1.5	0.1	
GRAL V20.09 (stability classes)	1.4	-0.1	
GRAL V21.09	1.5	0.1	
GRAL V21.09 (stability classes)	1.4	-0.1	
GRAL V23.11	1.6	0.2	
GRAL V23.11 (stability classes)	1.4	-0.1	
GRAL V24.04	1.6	0.2	
GRAL V24.04 (stability classes)	1.4	-0.1	

Figure 56. Quantile-quantile plot of observed and modelled concentrations V24.04



9.8 Gratkorn

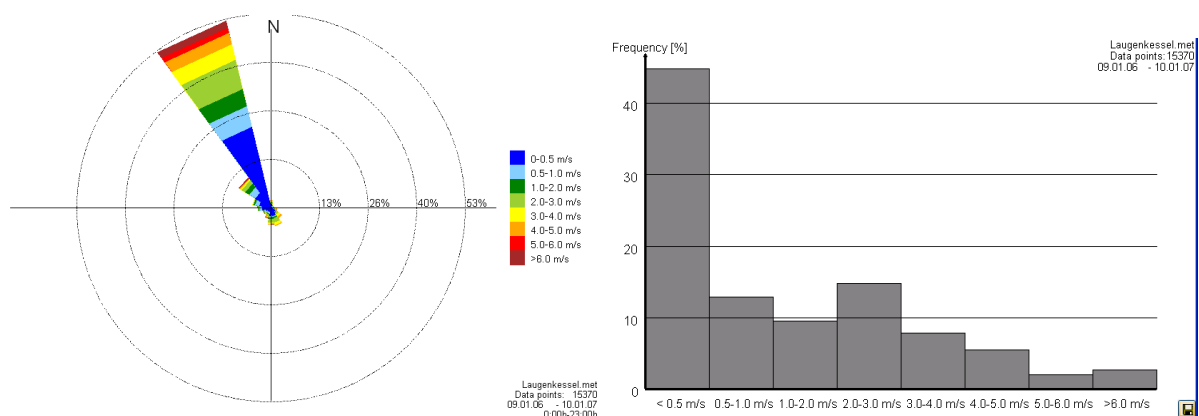
9.8.1 Dataset description

The air quality department of Styria/Austria operates three permanent air quality monitoring station near a paper-mill in very complex terrain. In addition, one mobile monitoring station has been operated for a couple of weeks in the surroundings. Stack emissions are measured continuously together with wind speed and –direction at a height of 45 m above ground level. The paper-mill is situated in a small basin north of Graz, and stack emissions impinge at the area of the monitoring station. Surrounding hills reach maximum heights of about 1.000 m, while the valley floor is at a height of about 350 m. Background concentrations have been estimated from observed average concentrations in dependence on wind direction. There are no major other sources in the surroundings. The hills are mostly covered with forests, while the basin floor is densely populated. The stack is 65 m high and has a diameter of 3 m. Exhausts are emitted with an average exit velocity of 7 m/s, and a mean temperature of 342 K. There are nearby buildings with heights up to 45 m.

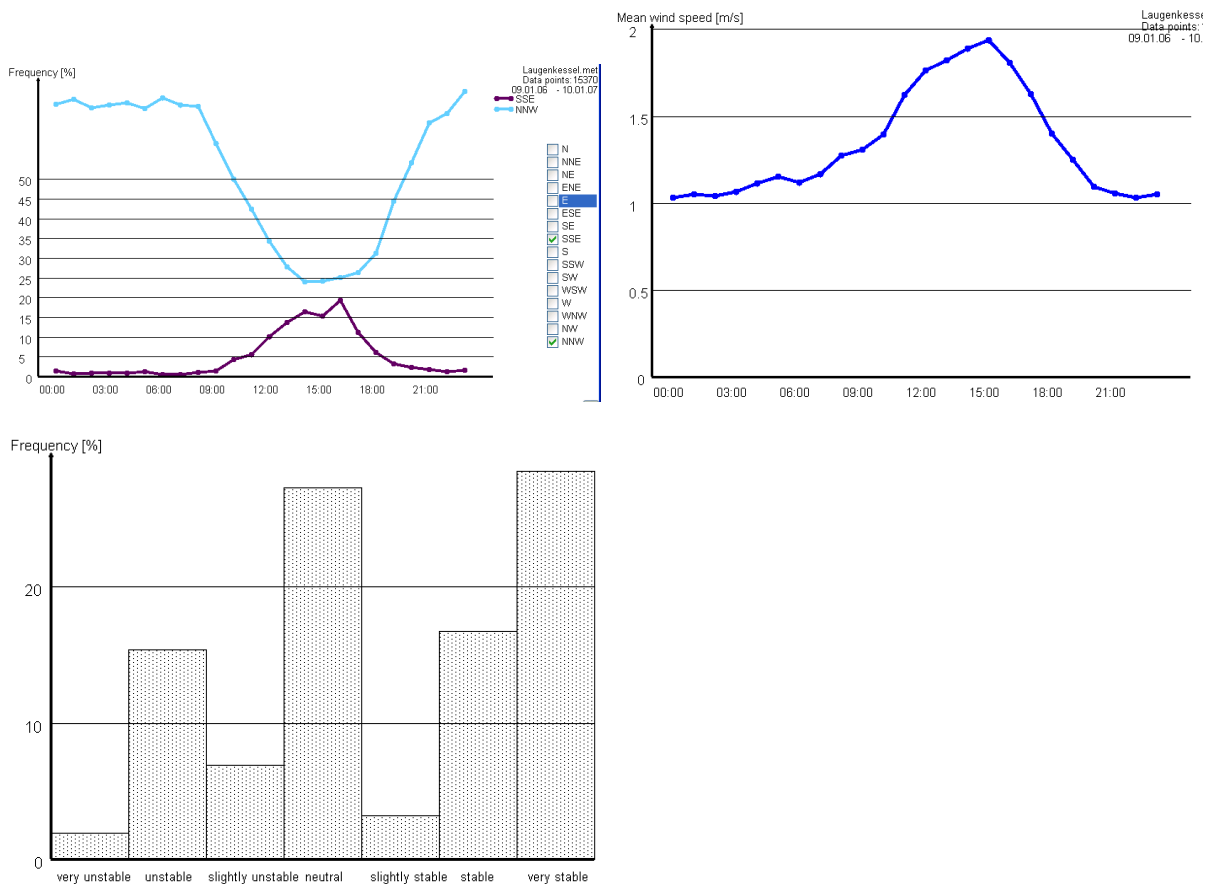
9.8.2 Characterisation

Wind speeds are rather low (annual mean wind speed at 45 m above ground level: 1.3 m/s). Low wind speed conditions ($u < 1.0$ m/s) occur in about 60 % of the time. A mountain/valley wind system prevails most of the time with southerly winds during the day and northerly winds during the night. At the floor of the basin, southerly winds dominate in the second half of night up to a height of about 50 m (Oettl, 1996). Stable dispersion conditions occur in about 50 % of the time. This dataset is very similar to modelling applications in licensing procedures, where few input data is available and allows thus for an uncertainty estimation of the model in practical applications. Note, that the monitoring station Straßengel-Kirche is situated on an isolated hill approximately 70 m above the basin floor. This hill is not resolved entirely by the wind field simulation.

Figure 57. Dispersion characteristics



Additional validation cases



9.8.3 Model set up

Topography GRAMM	3D wind fields simulated with the non-hydrostatic prognostic wind field model GRAMM Horizontal resolution: 100 m Vertical resolution: 10 m Vertical stretching factor: 1,33 Vertical layers: 17 Top level: 3,843 m Surface energy balance: CORINE landuse data Turbulence model: k-ε closure
Topography GRAL	25 m resolution derived from original topographical data
Obstacles	Microscale prognostic model, mixing-length turbulence closure Horizontal resolution: 10 m Vertical resolution: 5 m Vertical stretching factor: 1.00 Minimum iterations: 100 Maximum iterations: until 500 Number of vertical cells: 40
Concentration grid	50 m horizontal, 3 m vertical extension, 3.5 above ground level
Model domain	8,000 m x 7,100 m
Number of particles	360,000 per ½ hour
Roughness length	CORINE landuse data
Adaptive roughness	0 m

9.8.4 Results

GRAL has been operated in both steady-state and transient mode. While in steady-state mode GRAL underestimates concentrations at two receptors, in transient mode good agreement is found at all observational points.

The mobile air quality monitoring station was operated for a couple of weeks only, thus the estimated yearly average concentration at that site, based on comparison with the other sites running the whole year, is associated with some uncertainty. The estimation of background concentrations is rather difficult and therefore the determination of the additional concentration is not reliable, especially for low measured (and additional) concentrations, such as at the monitoring station Gratwein.

Table 58. Results for the Gratkorn dataset GRAL V 20.01

Model	NMSE	FB	References
GRAL V 20.01 steady-state, Straßengel-Kirche	-	0.0	
GRAL V 20.01 steady-state, Judendorf	-	0.6	
GRAL V 20.01 steady-state, Mobile	-	0.5	
GRAL V 20.01 steady-state, Gratwein	-	0.1	
GRAL V 20.01 transient, Straßengel-Kirche	-	0.1	
GRAL V 20.01 transient, Judendorf	-	0.2	
GRAL V 20.01 transient, Mobile	-	-0.1	
GRAL V 20.01 transient, Gratwein	-	-0.1	

Table 59. Results for the Gratkorn dataset GRAL V 20.09

Model	NMSE	FB	References
GRAL V 20.09 steady-state, Straßengel-Kirche	-	0.1	
GRAL V 20.09 steady-state, Judendorf	-	0.5	
GRAL V 20.09 steady-state, Mobile	-	0.5	
GRAL V 20.09 steady-state, Gratwein	-	0.1	

Table 60. Results for the Gratkorn dataset GRAL V 20.09 “Adaptive Roughness”

Model	NMSE	FB	References
GRAL V 20.09 steady-state, Straßengel-Kirche	-	0.0	
GRAL V 20.09 steady-state, Judendorf	-	0.0	
GRAL V 20.09 steady-state, Mobile	-	0.3	
GRAL V 20.09 steady-state, Gratwein	-	-0.9	

Additional validation cases

Table 61 Results for the Gratkorn dataset GRAL V 23.11

Model	NMSE	FB	References
GRAL V 23.11 steady-state, Straßengel-Kirche	-	-0.1	
GRAL V 23.11 steady-state, Judendorf	-	0.1	
GRAL V 23.11 steady-state, Mobile	-	-0.3	
GRAL V 23.11 steady-state, Gratwein	-	-0.2	

Table 62 Results for the Gratkorn dataset GRAL V 23.11 “Adaptive Roughness”

Model	NMSE	FB	References
GRAL V 20.09 steady-state, Straßengel-Kirche	-	-0.3	
GRAL V 20.09 steady-state, Judendorf	-	0.1	
GRAL V 20.09 steady-state, Mobile	-	-0.2	
GRAL V 20.09 steady-state, Gratwein	-	-0.2	

Table 63 Results for the Gratkorn dataset GRAL V 24.04

Model	NMSE	FB	References
GRAL V 24.04 steady-state, Straßengel-Kirche	-	-0.27	
GRAL V 24.04 steady-state, Judendorf	-	-0.25	
GRAL V 24.04 steady-state, Mobile	-	0.15	
GRAL V 24.04 steady-state, Gratwein	-	-0.2	

Figure 58. Comparison of observed and modeled annual mean SO_2 concentration GRAL V24.04

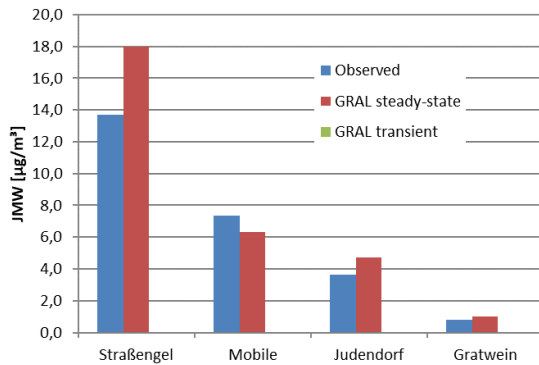
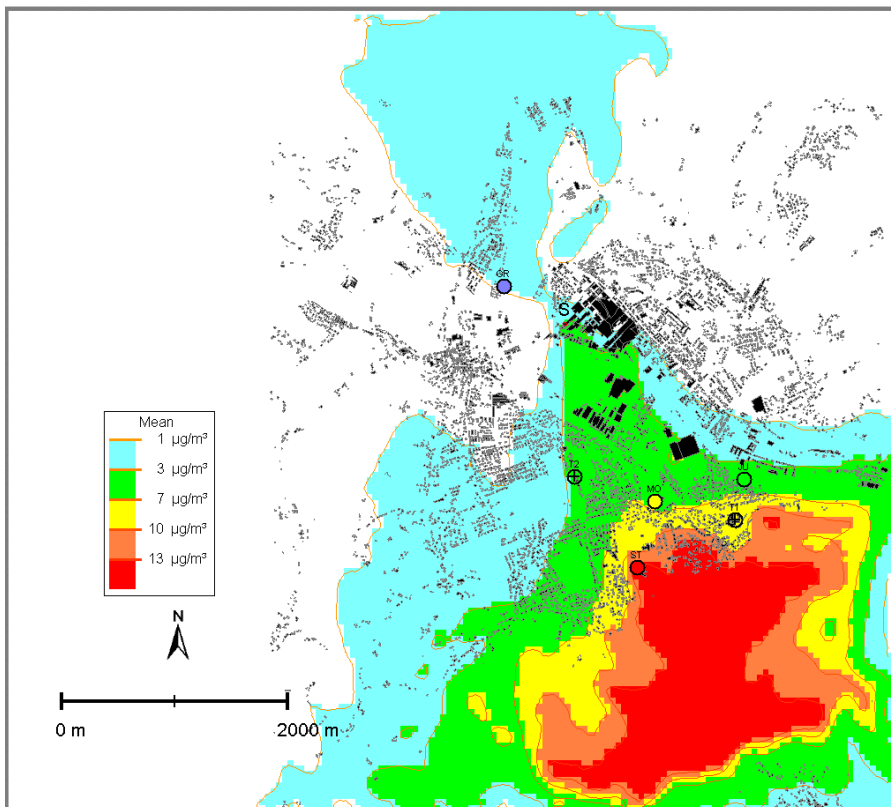


Figure 59. Modelled annual average concentrations [$\mu\text{g}/\text{m}^3$] for the Gratkorn dataset 3.5 m (bottom) above ground level; crosses indicate monitoring stations, the circle indicates the stack. Results are for steady mode GRAL V24.04

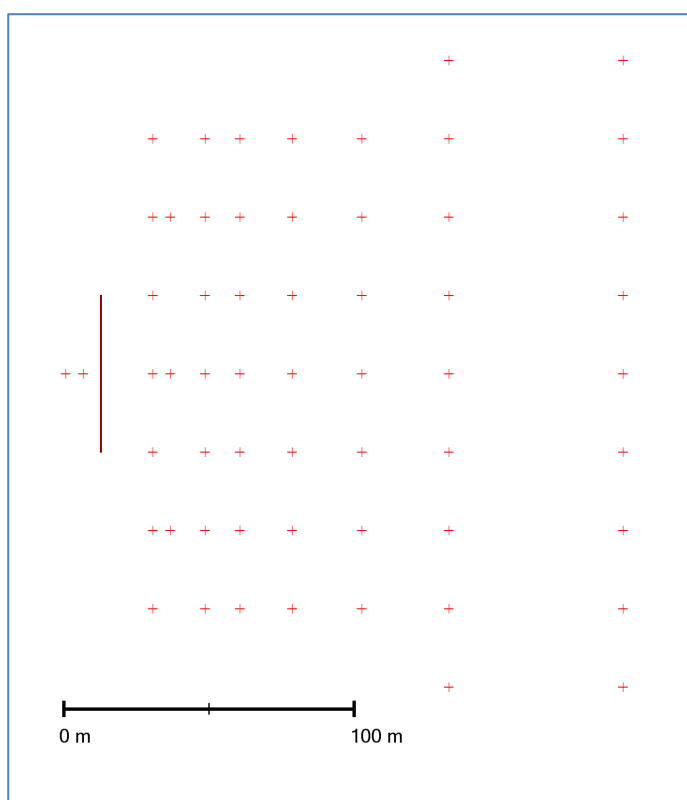


9.9 Idaho Falls without noise barrier

9.9.1 Dataset description (Finn et al., 2010)

In this experiment a 54 m long line source 1 m above ground level was used as source, from which SF₆ tracer gas was released. A grid of 58 receptor points was set up 1.5 m above ground level to sample tracer gas over 15 minute intervals. A total of 60 sampling intervals were carried out. Experimental data were collected on four separate days in October 2008 at the NOAA Tracer Test Facility on the U.S. DOE's Idaho National Laboratory, during which a range of meteorological conditions were observed (ranging from convective to very stable). Several meteorological measurements were used, though, only the data from the sonic located upwind of the source 3 m above ground level has been used here. Apart from the mean wind speed and wind direction, observed friction velocity, standard deviations of horizontal and vertical wind velocities, and Obukhov lengths have been used. The experimental site was characterized by low lying scrubs at heights in the range of 10 – 30 cm.

Figure 60. Experimental layout of the Idaho Falls experiment (crosses = sampling points, line = line source)

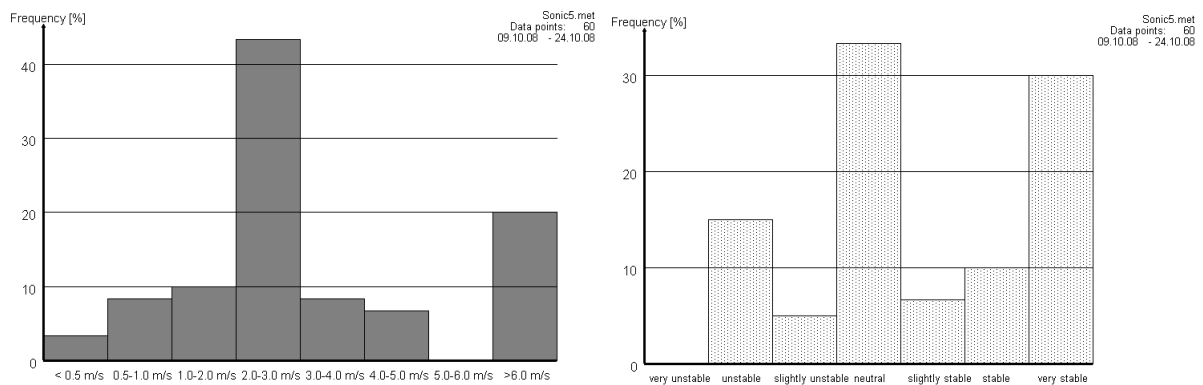


9.9.2 Characteristics

Wind speeds were mostly in the range between 2.0 and 4.0 m/s, and wind directions were in most cases perpendicular to the line source. Highest concentrations were naturally found during stable conditions, making model evaluation statistics (see Table 64) very sensitive to

model performance in these particular conditions. Especially during stable conditions very low vertical velocity standard deviations were recorded, even lower than observed friction velocities (typically standard deviations of vertical velocities are a bit higher than the friction velocity – see chapter 4.3). The line source has been simulated in GRAL as an area source with a width of 0.4 m and a vertical extension of 0.5 m.

Figure 61. Observed frequencies of wind speeds and stabilities



9.9.3 Model set up

Topography	Flat Terrain
Obstacles	None
Concentration grid	5 m horizontal, 0.5 m vertical extension, 1.5 m above ground level
Model domain	360 m x 350 m
Number of particles	450,000 per hour
Roughness length	0.03 m

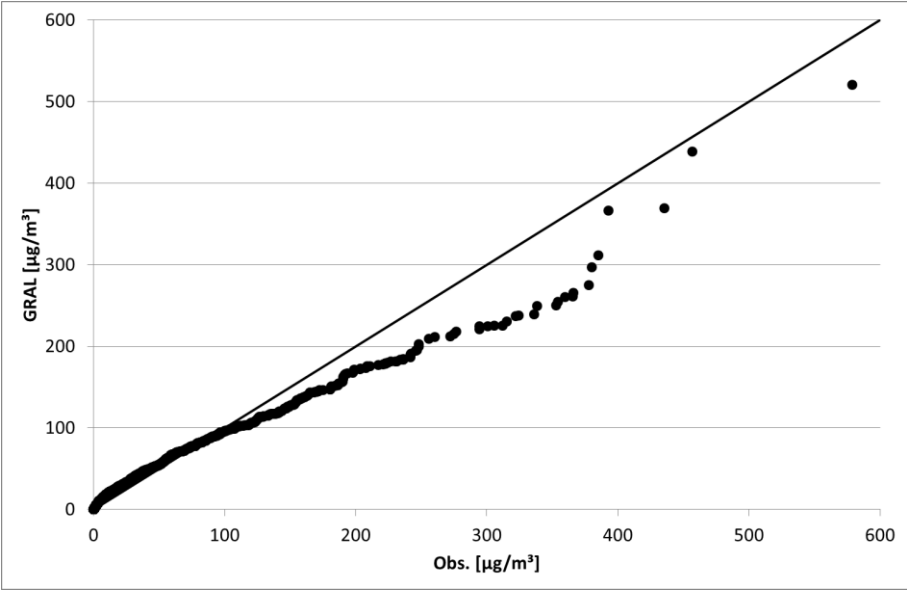
9.9.4 Results

Table 64. Results for the Idaho Falls experiment without noise barrier

Model	NMSE	FB	References
GRAL	2.5	0.0	

Additional validation cases

Figure 62. Quantile-quantile plot of observed and modelled concentrations

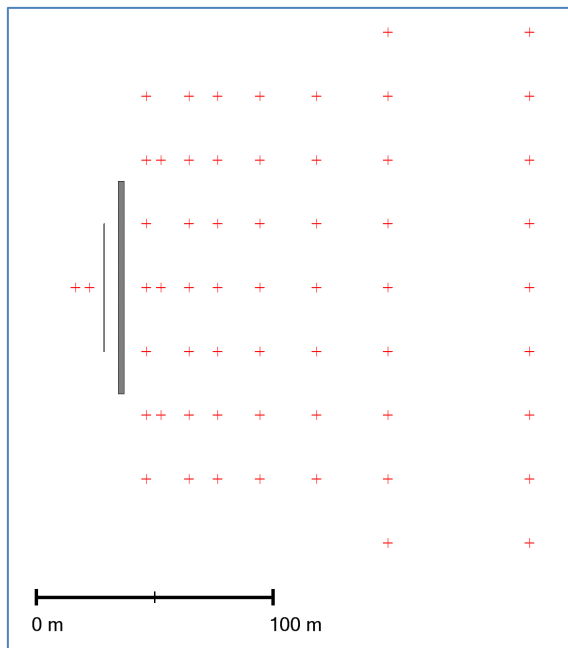


9.10 Idaho Falls with noise barrier

9.10.1 Dataset description (Finn et al., 2010)

A description of the site and the experiment is given in section 9.9. The difference is in this case a noise barrier made of straw bales with a height of 6 m and a length of 90 m close to the line source. See also Oettl (2014) for more details about the experimental layout and previous GRAL simulations.

Figure 63. Experimental layout of the Idaho Falls experiment with noise barrier (crosses = sampling points, grey line = straw bales, black line = line source)



9.10.2 Model set up

Topography	Flat terrain
Obstacles	Microscale prognostic model, mixing-length turbulence closure Horizontal resolution: 2 m Vertical resolution: 0.5 m Vertical stretching factor: 1.0 Minimum iterations: 100 Maximum iterations: 500 Number of vertical cells: 40
Concentration grid	2 m horizontal, 0.5 m vertical extension, 1.5 m above ground level
Model domain	360 m x 350 m
Number of particles	450,000 per hour
Roughness length	0.03 m

9.10.3 Results

In order to be able to provide meaningful statistics of model performance for the effect of the noise barrier, it was necessary to omit the two receptor points upwind of the line source. Note

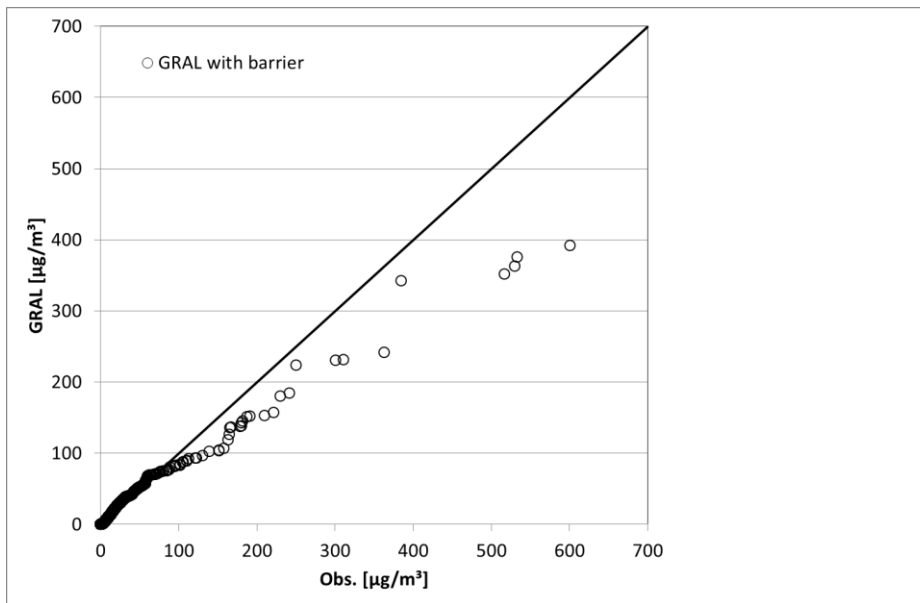
Additional validation cases

that on average, observed concentrations at these two sites were about 20 times higher than for the downwind receptor points.

Table 65. Results for the Idaho Falls experiment without noise barrier

Model	NMSE	FB	References
GRAL	3.3	0.0	

Figure 64. Quantile-quantile plot of observed and modelled concentrations

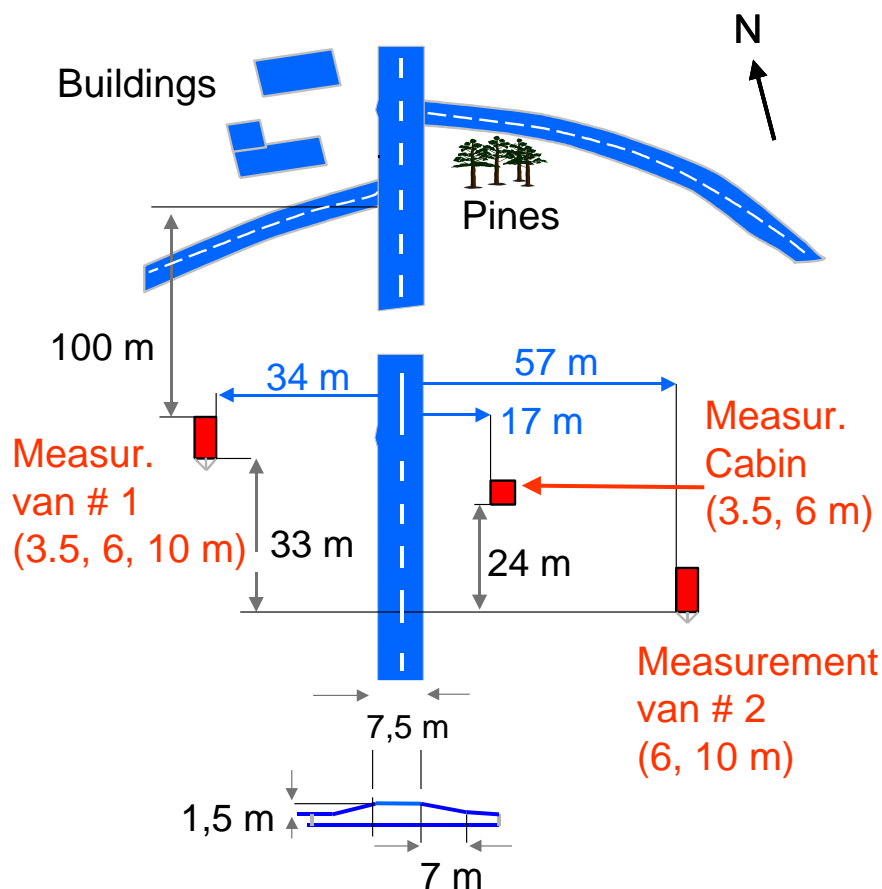


9.11 Elimaeki

9.11.1 Dataset description

The locations of the measurement devices with respect to the road segment in question are shown in Figure 65. The road itself is a straight line for a distance of more than a kilometre in both directions from the measurement site and its orientation is 30° east of north. Flat terrain, homogenous land-use and very few obstacles characterize the surroundings. The dataset comprises electronically-performed traffic counts, measured and pre-processed meteorological data and the concentrations for NO_x, NO₂ and O₃ at three locations and at various heights (see Figure 65). As the monitoring stations were located on both sides of the road, background concentrations could be determined for all wind directions. Traffic volumes were automatically classified as heavy-duty and light-duty traffic, for both driving directions. Traffic flow on the road was fairly low, on the average approximately 7200 vehicles/day. The average speed of the vehicles was approximately the same as the speed limit, 100 km/h, with a very moderate variation. Only the NO_x concentrations were considered in this work, in order to avoid the additional uncertainties related to the chemical transformation of NO into NO₂.

Figure 65. Road layout of the Elimaeki experiment



Additional validation cases

9.11.2 Characteristics

Use was made of emission factors of NO_x that are functions of the vehicle driving speed, and correspond to a vehicle speed of 100 km/h; these values are 2.23 and 12.3 g/km for light- and heavy-duty vehicles, respectively. The above mentioned emission factor values have been obtained as weighted average values, based on the classification of vehicles to various categories and the vehicle frequency distributions. Light-duty vehicles were classified to gasoline-powered passenger cars (with and without a catalytic converter), diesel-powered passenger cars, and vans; heavy-duty vehicles were classified to trucks (with a without a trailer) and buses. Due to the lack of field measurements of emissions, it is not possible to provide an error estimation for these emission rates.

For the simulations, wind speed at 10 m, and the estimated stability classes (mostly neutral) been used. Only results at 3.5 m height at a distance of 34 m are presented.

9.11.3 Model set up

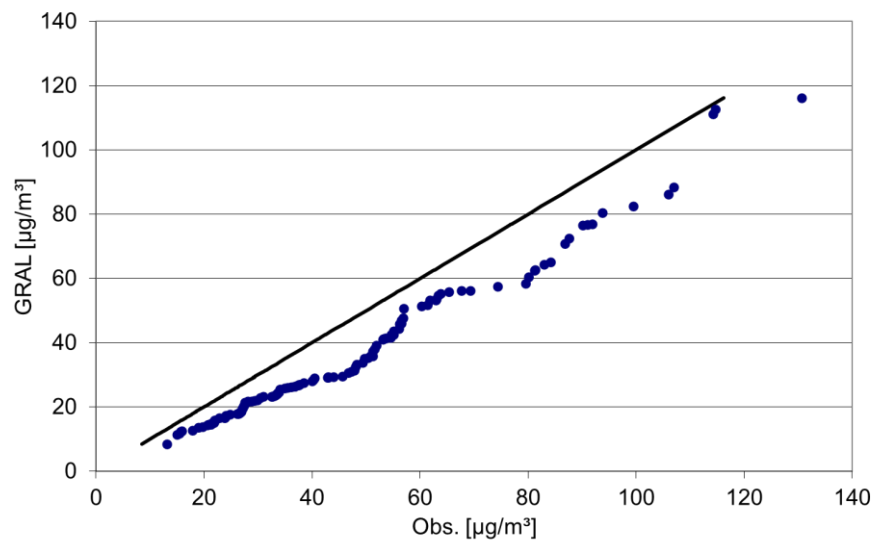
Topography	Flat Terrain
Obstacles	None
Concentration grid	5 m horizontal, 0.5 m vertical extension, 3 m above ground level
Model domain	500 m x 600 m
Number of particles	108,000 per hour
Roughness length	0.1 m

9.11.4 Results

Table 66. Results for the Elimaeki experiment

Model	NMSE	FB	References
GRAL V20.09	0.1	0.2	
GRAL V21.09	0.1	0.2	
GRAL V23.11	0.2	0.3	
GRAL V24.04	0.1	0.2	

Figure 66. Quantile-quantile plot of observed and modelled concentrations with GRAL V24.04



9.12 Goettinger Strasse

9.12.1 Dataset description

The Goettinger Strasse is a street canyon in Hannover, Germany. In this work one permanent air quality monitoring station was available for comparison purposes. The road has four lanes, two in each direction. Traffic flow is around 30.000 veh./d. The width of the street canyon is about 25 m and buildings are approximately 20 m high. In this work, the year 1994 has been taken for comparison purposes.

9.12.2 Characteristics

Wind speeds in this area are relatively high (annual mean = 3.9 m/s) compared to typical Austrian conditions south of the Alps. Thus only neutral atmospheric stability was assumed in the simulations.

9.12.3 Model set up

Topography	Flat terrain
Obstacles	Microscale prognostic model, mixing-length turbulence closure Horizontal resolution: 2 m Vertical resolution: 2 m Vertical stretching factor: 1.0 Minimum iterations: 100 Maximum iterations: 500 Number of vertical cells: 40
Concentration grid	2 m horizontal, 0.5 m vertical extension, 1.5 m above ground level
Model domain	300 m x 500 m
Number of particles	360,000 per hour
Roughness length	0.2 m
Prognostic radius around sources	50 m

9.12.4 Results

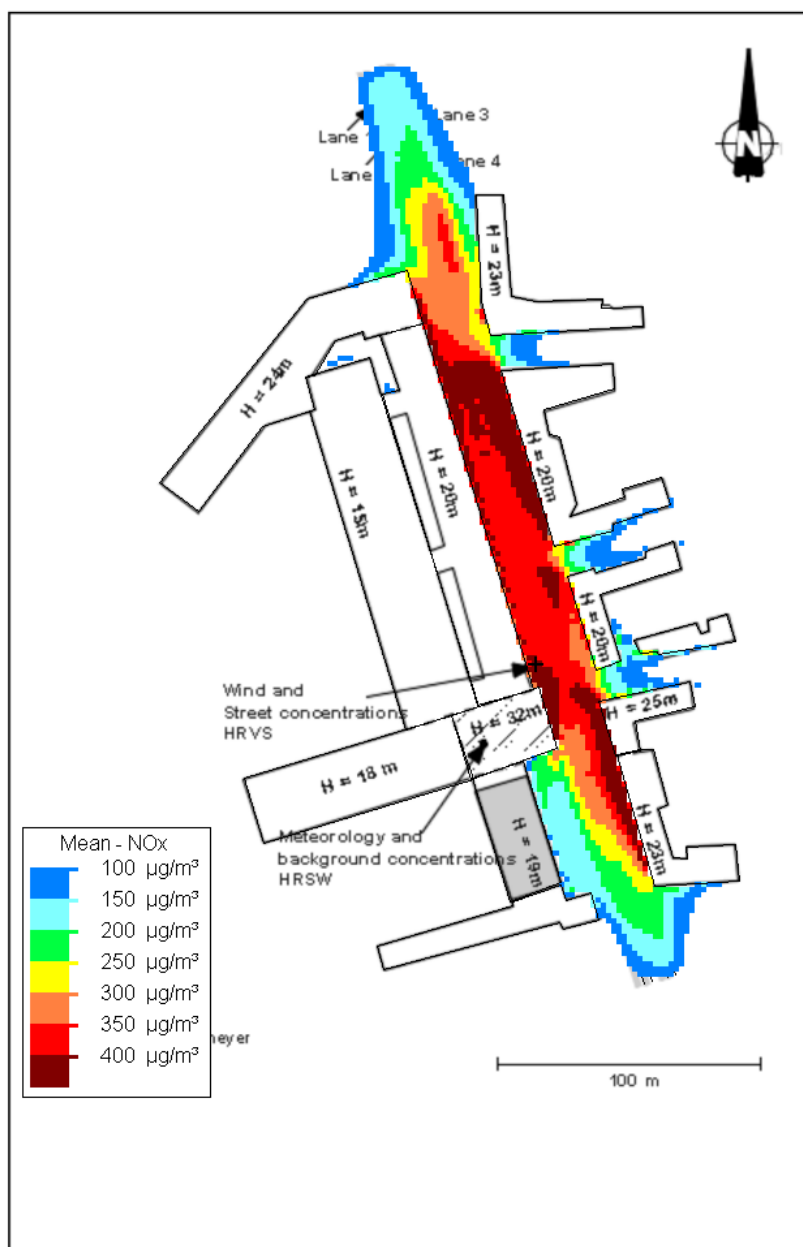
The average NO_x concentration is captured well with GRAL/level2. Peak concentrations are overestimated. GRAL/level1 and GRAL without taking buildings into account underestimates the average concentration significantly.

Table 67. Results for the Goettinger Strasse experiment

Model	NMSE	FB	References
GRAL	3.7	1.0	
GRAL/level 1	2.4	0.7	
GRAL/level 2	0.8	-0.3	
GRAL V20.09 "Adaptive roughness"	0.8	-0.2	

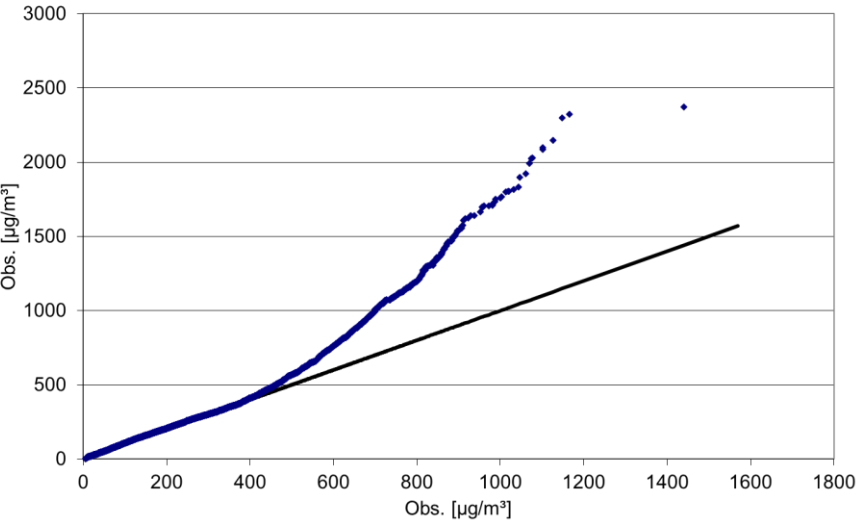
GRAL V21.09 "Adaptive roughness"	0.7	-0.2	
GRAL V23.11 "Adaptive roughness"	0.8	-0.2	
GRAL V24.04	0.7	-0.1	

Figure 67. Modelled annual average NO_x concentration for the Goettinger Strasse (grey=buildings, cross=monitoring station) with GRAL/level2



Additional validation cases

Figure 68 Quantile-quantile plot of observed and modelled concentration with GRAL V24.04



9.13 Frankfurter Allee, Berlin

9.13.1 Dataset description

Local authorities are operating one permanent air quality monitoring station within the street canyon of the Frankfurter Allee in Berlin (Germany). Data was provided within the frame of the street emissions ceiling (SEC, Moussiopoulos et al., 2004) project aiming at a comparison of different dispersion models for such type of applications led by the Aristotle University of Athens, Greece. Width of the street canyon is about 42 m and buildings height is approximately 21 m. The street consists of three lanes in each direction. Traffic counts have been performed automatically (approx. 55.000 veh./d) and emissions were computed by the model COPERT 3. In this work only observed NO_x concentrations have been used for comparison purposes. Wind speed, –direction, and background concentrations were available from roof top measurements near the Frankfurter Allee. Only hours have been considered with background concentrations equal or smaller than the street level concentrations. Stability classes have been computed according to the US-EPA (2000) SRDT method.

9.13.2 Characteristics

As is it almost always the case when observing concentrations in street canyons, there exists large spatial concentration gradients, which makes it difficult to compare observations with modelling results. Often, the actual observed concentration can be found within a few meters of the defined receptor point in the modelled concentration distribution. Only average diurnal modulations of emissions were available, which brings forward some uncertainty regarding modelled peak concentrations.

9.13.3 Model set up

Topography	Flat terrain
Obstacles	Microscale prognostic model, mixing-length turbulence closure Horizontal resolution: 2 m Vertical resolution: 2 m Vertical stretching factor: 1.0 Minimum iterations: 100 Maximum iterations: 500 Number of vertical cells: 40
Concentration grid	2 m horizontal, 0.5 m vertical extension, 3.8 m above ground level
Model domain	600 m x 600 m
Number of particles	360,000 per hour
Roughness length	1.5 m

9.13.4 Results

The annual mean NO_x concentration has been simulated well with GRAL/level2, while GRAL/level1 shows some underestimation. When buildings are not taken into account, GRAL underestimates concentrations significantly. Peak concentrations with GRAL/level2 are overestimated by about 75 %.

Table 68. Results for the Frankfurter Allee experiment

Model	NMSE	FB	References
GRAL	3.9	1.0	
GRAL/level 1	2.3	0.5	
GRAL/level 2	1.4	-0.1	
GRAL V20.09 "Adaptive roughness"	1.3	-0.2	
GRAL V21.09	1.4	-0.1	
GRAL V23.11	1.4	0.0	
GRAL V23.11 "Adaptive roughness"	1.4	0.0	
GRAL V24.04	1.4	0.0	

Figure 69. Modelled annual average NO_x concentration for the Frankfurter Allee (grey=buildings, cross=monitoring station) with GRAL V23.11

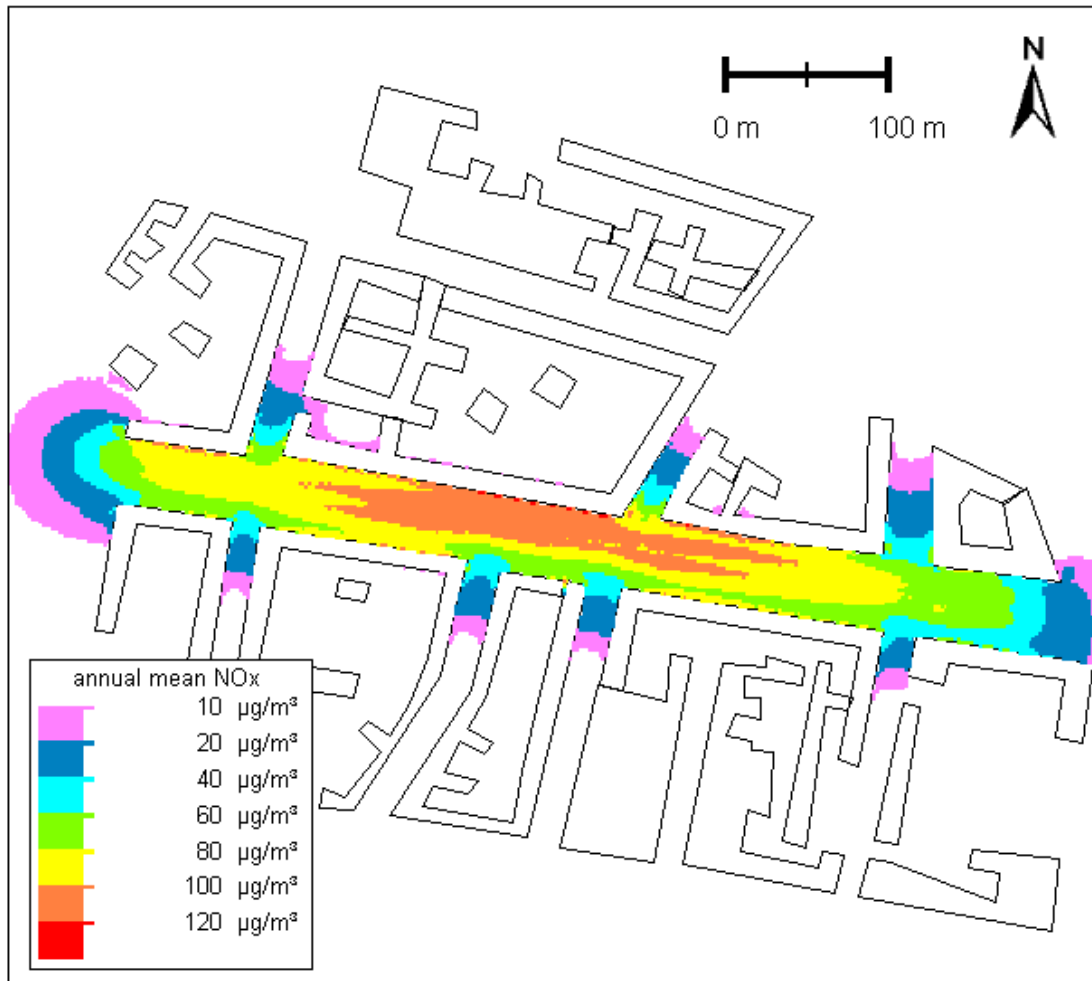
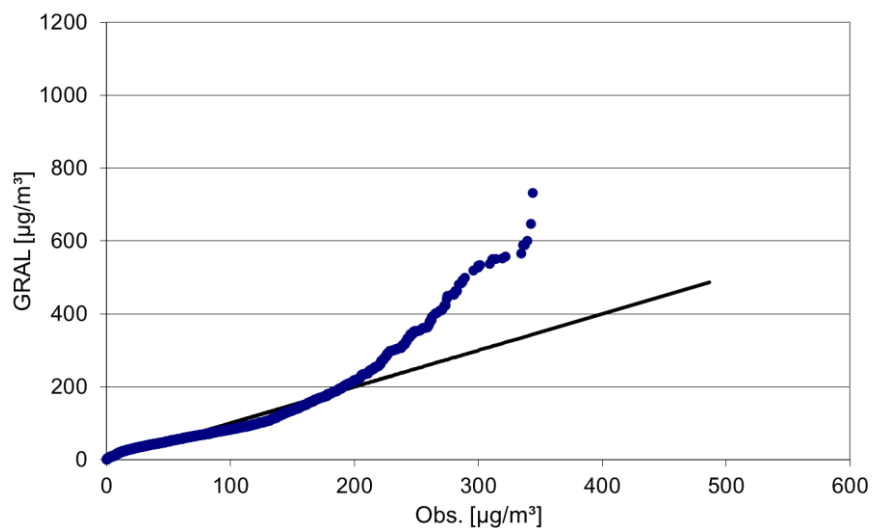


Figure 70 Quantile-quantile plot of observed and modelled concentrations with GRAL V24.04



9.14 Hornsgatan street canyon, Stockholm

9.14.1 Dataset description

Local authorities are operating one permanent air quality monitoring station within the street canyon Hornsgatan (Sweden). Data was provided within the frame of the street emissions ceiling (SEC, Moussiopoulos et al., 2004) project aiming at a comparison of different dispersion models for such type of applications led by the Aristotle University of Athens, Greece. Width of the street canyon is about 24 m and buildings height is approximately 24 m. The street consists of two lanes in each direction. Traffic counts have been performed automatically (approx. 35.000 veh./d) and emissions were computed by the model COPERT 3. In this work only observed NO_x concentrations have been used for comparison purposes. Wind speed, – direction, and background concentrations were available from roof top measurements near Hornsgatan. Only hours have been considered with background concentrations equal or smaller than the street level concentrations. Neutral atmospheric stability have been assumed, because of the presence of buildings and the high wind speeds in that area (annual average wind speed = 3.4 m/s).

9.14.2 Characteristics

As is it almost always the case when observing concentrations in street canyons, there exists large spatial concentration gradients, which makes it difficult to compare observations with modelling results. Often, the actual observed concentration can be found within a few meters of the defined receptor point in the modelled concentration distribution. Only average diurnal modulations of emissions were available, which brings forward some uncertainty regarding modelled peak concentrations.

9.14.3 Model set up

Topography	Flat terrain
Obstacles	Microscale prognostic model, mixing-length turbulence closure Horizontal resolution: 2 m Vertical resolution: 2 m Vertical stretching factor: 1.0 Minimum iterations: 100 Maximum iterations: 500 Number of vertical cells: 40
Concentration grid	2 m horizontal, 0.25 m vertical extension, 3.8 m above ground level
Model domain	220 m x 210 m
Number of particles	540,000 per hour
Roughness length	1.0 m

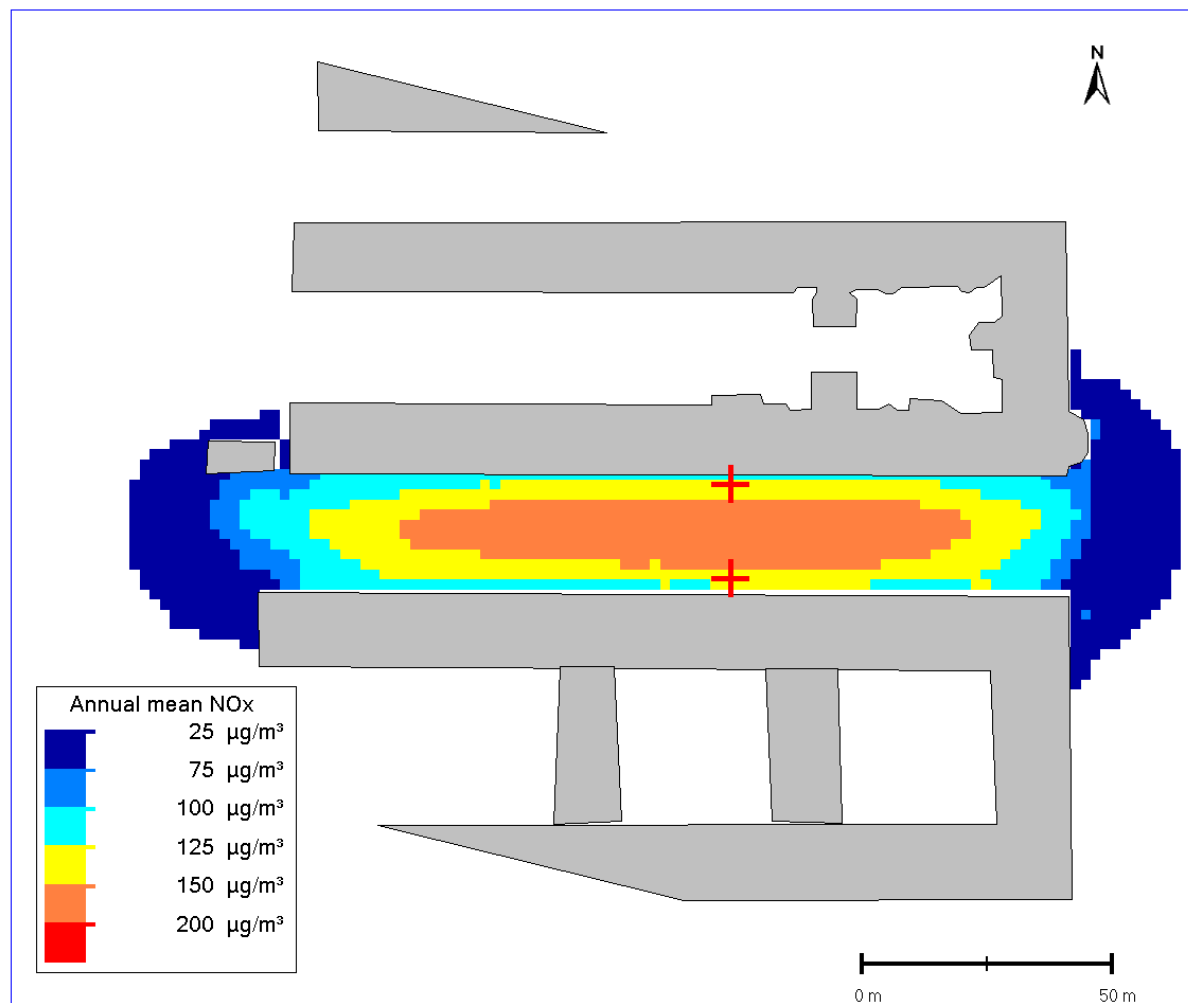
9.14.4 Results

The annual mean NO_x concentration and also peak concentrations have been simulated well with GRAL/level2. When buildings are not taken into account, GRAL underestimates concentrations significantly.

Table 69. Results for the Hornsgatan street canyon experiment

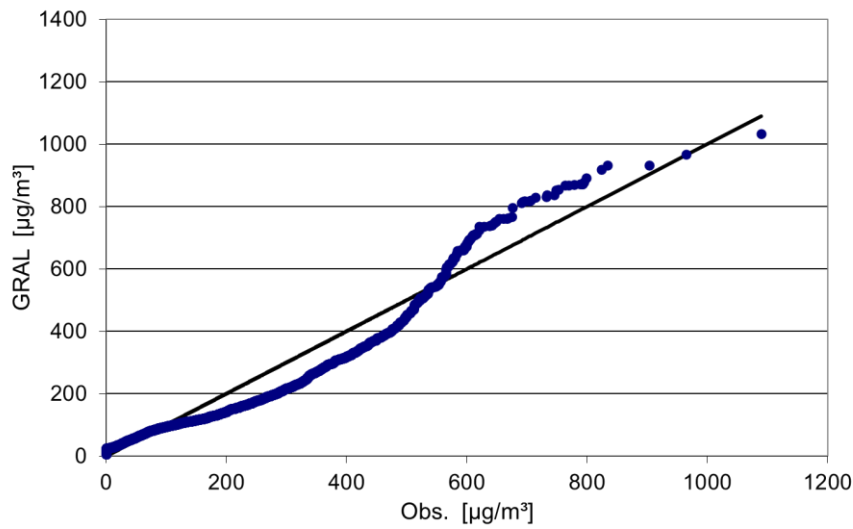
Model	NMSE	FB	References
GRAL	4.6	1.1	
GRAL/level 1	1.6	0.4	
GRAL/level 2	0.8	0.1	
GRAL V20.09 „Adaptive roughness“	0.8	0.1	
GRAL V23.11	0.9	0.2	
GRAL V23.11 „Adaptive roughness“	0.8	0.1	
GRAL V24.04	0.9	0.1	

Figure 71. Modelled annual average NO_x concentration for the Hornsgatan street canyon (grey=buildings, crosses=monitoring stations) with GRAL V23.11



Additional validation cases

Figure 72 Quantile-quantile plot of observed and modelled concentrations with GRAL V24.04

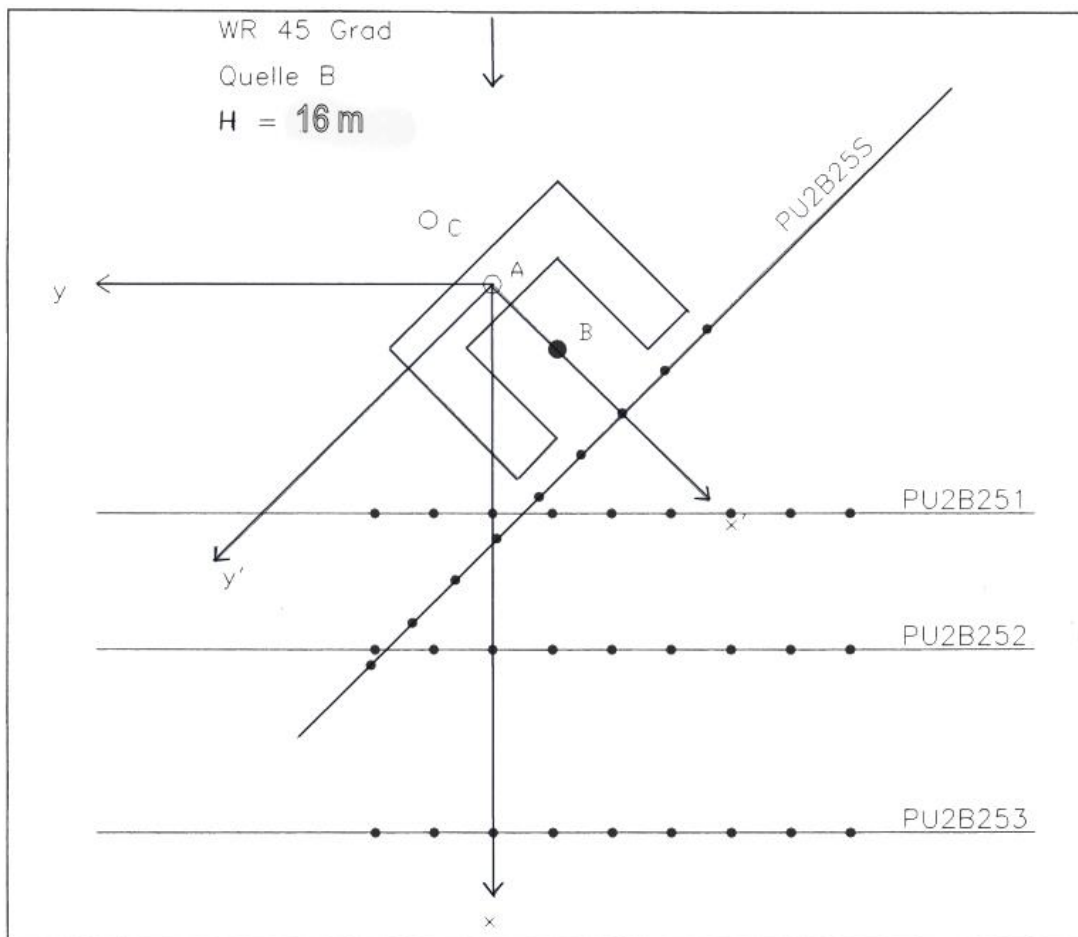


9.15 U-shaped building

9.15.1 Dataset description

Flassak and Blessing (2007) used wind tunnel data of Klein et al. (1994) to evaluate the microscale prognostic model MISKAM and the Lagrangian particle model AUSTAL2000. Three different positions for point sources relative to the U-shaped building have been investigated (on top, windward- and leeward side at the bottom). The building in the wind tunnel corresponds with a real world height of 16 m, and has a width of 52 m, and a length of 40 m. Concentrations have been scaled by the wind speed at reference height and the emission rate. Observations took place along lines perpendicular to the mean wind direction at distances of 25 m, 50 m, and 80 m.

Figure 73. Experimental layout of the wind tunnel tests performed by Klein et al. (1994)



9.15.2 Characteristics

In this work the experiments with 45 deg. wind direction relative to the buildings orientation was used. Comparisons were made only at receptor points 50 m from the source. Experiments have been performed for a point source without buoyancy and with zero vertical exit velocity. Atmospheric stability was neutral in all cases. It is assumed that concentrations can be scaled

Additional validation cases

by the mean wind speed at reference height. Performance statistics for the modes MISKAM and AUSTAL2000 have been obtained by visual inspection of the provided graphs in Flassak and Blessing (2007). There is some uncertainty about how turbulence profiles of the wind tunnel correspond with real atmosphere conditions.

9.15.3 Model set up

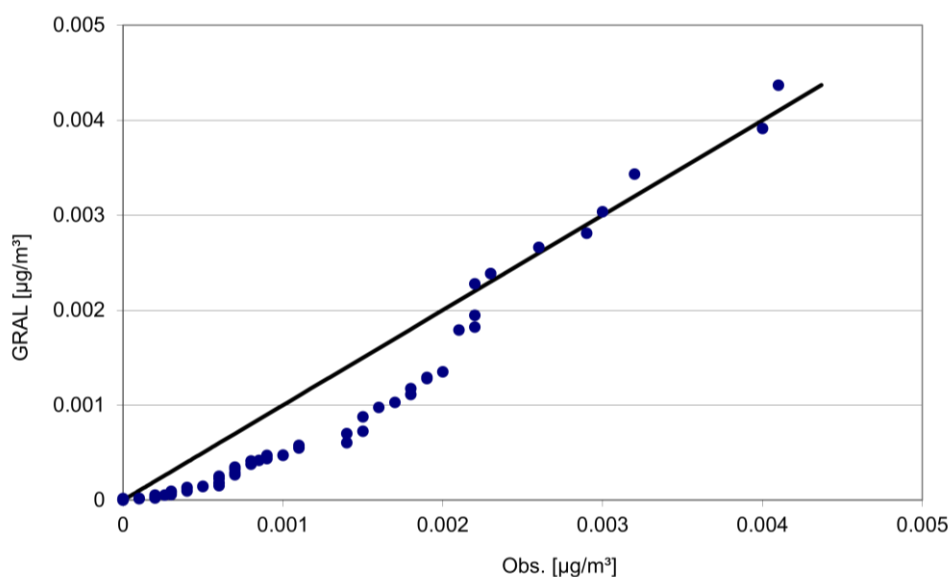
Topography	Flat terrain
Obstacles	Microscale prognostic model, mixing-length turbulence closure Horizontal resolution: 2 m Vertical resolution: 1 m Vertical stretching factor: 1.0 Minimum iterations: 100 Maximum iterations: 500 Number of vertical cells: 40
Concentration grid	2 m horizontal, 0.5 m vertical extension, 0 m, 8 m, 16 m above ground level
Model domain	266 m x 204 m
Number of particles	1,080,000 per hour
Roughness length	1.0 m

9.15.4 Results

Table 70. Results for the U-shaped building dataset

Model	NMSE	FB	References
GRAL V20.09 „Adaptive roughness“	1.6	0.3	
GRAL/level 2	1.8	0.2	
GRAL V23.11 „Adaptive roughness“	1.6	0.3	
GRAL V 24.04			

Figure 74. Quantile-quantile plot of observed and modelled concentrations V 23.11 „Adaptive roughness“

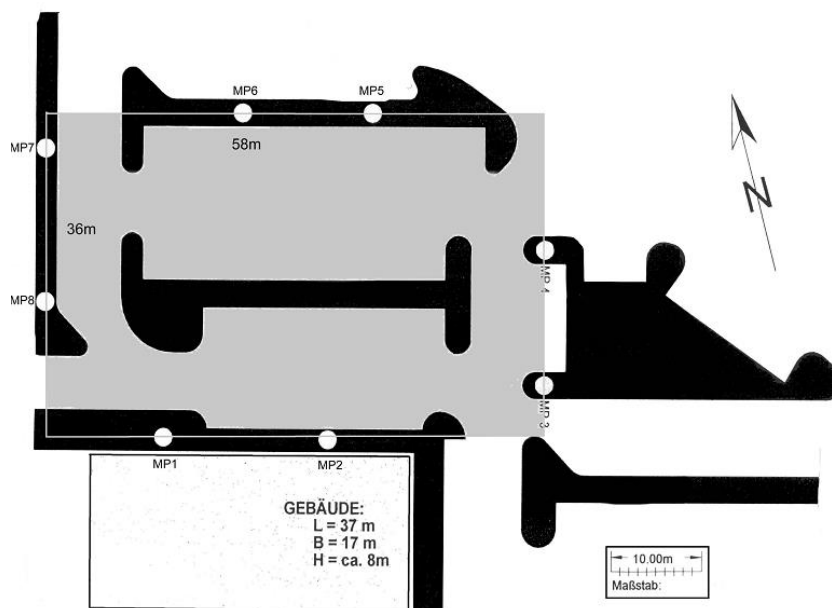


9.16 Parking lot Vienna

9.16.1 Dataset description

The experiment was conducted at a small parking lot in Vienna in 1999 by the Graz University of Technology. At the edge of the parking area, 8 sampling points for SF_6 have been located. Sampling took place over a period of 30 minutes. All in all 6 experiments were available for comparison purposes. Wind speeds ranged between 1.3 and 2.8 m/s, atmospheric stability was assumed to be neutral. There was a nearby building with extensions of 37 m x 17 m x 8 m.

Figure 75. Experimental layout of the parking lot in Vienna



9.16.2 Characteristics

Wind speeds ranged between 1.3 m/s and 2.8 m/s and only neutral atmospheric stabilities were encountered. The parking lot has been simulated as area source.

9.16.3 Model set up

Topography	Flat terrain
Obstacles	Microscale prognostic model, mixing-length turbulence closure Horizontal resolution: 2 m Vertical resolution: 1 m Vertical stretching factor: 1.0 Minimum iterations: 100 Maximum iterations: 500 Number of vertical cells: 40
Concentration grid	2 m horizontal, 1 m vertical extension, 1 m above ground level

Additional validation cases

Model domain	120 m x 90 m
Number of particles	360,000 per ½ hour
Roughness length	0.2 m

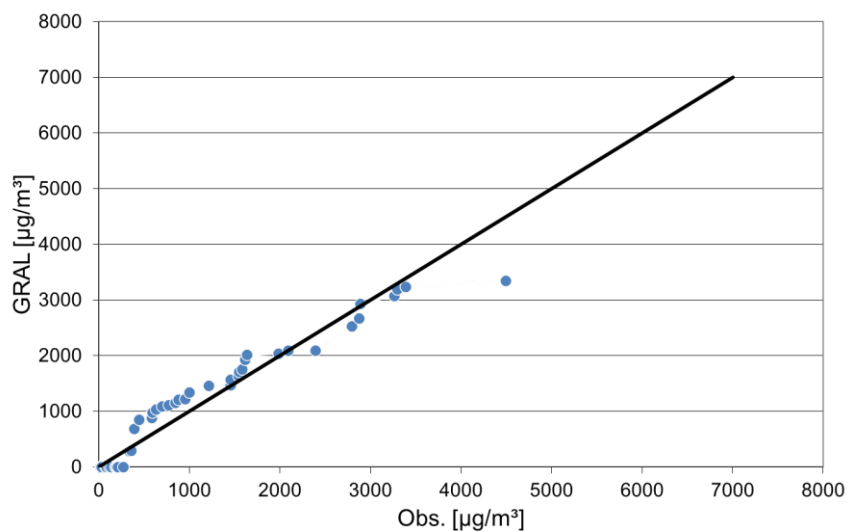
9.16.4 Results

There is a good agreement between simulated and observed concentrations for the GRAL/level2 simulations. Also the peak concentrations were simulated very well.

Table 71. Results for the Vienna parking lot experiment

Model	NMSE	FB	References
GRAL	2.4	0.4	
GRAL/level 1	2.3	0.3	
GRAL/level 2	1.3	-0.1	
GRAL V 20.09 „Adaptive roughness“	1.3	0.0	
GRAL V 21.09 „Adaptive roughness“	1.2	0.1	
GRAL V 23.11 „Adaptive roughness“	1.3	0.1	
GRAL V 24.04	1.2	0.0	

Figure 76 Quantile-quantile plot of observed and modelled concentrations with GRAL V24.04



9.17 Uttenweiler

9.17.1 Dataset description

The experiment was conducted at a single located pig stable near Uttenweiler in Germany (Bächlin et al., 2002). The stable has a base of 30x50m², the height of the ridge is about 8 m and a single forced ventilation released in a height of 8.5 m. 15 single experiments odour measurements accompanied by simultaneous SF₆ tracer gas measurements were performed at two cross sections downwind the farm with 11 and 12 measuring points. From these measurements both mean concentrations as well as the characteristics of concentration fluctuations can be deduced. Wind speed and –direction were observed by means of one sonic anemometer and a cup anemometer within 10 m above ground level.

9.17.2 Characteristics

The averaging interval was 10 minutes, which is not usual in practice. Thus some caution has to be taken, when judging model results as models are usually designed to provide average concentrations for 30 – 60 minutes. Wind speeds were almost relatively high and only neutral atmospheric stability was encountered. Concentrations are compared paired in time and space.

9.17.3 Model set up

Topography	Flat terrain
Obstacles	Microscale prognostic model, mixing-length turbulence closure Horizontal resolution: 2 m Vertical resolution: 1 m Vertical stretching factor: 1.0 Minimum iterations: 100 Maximum iterations: 500 Number of vertical cells: 40
Concentration grid	2 m horizontal, 0.2 m vertical extension, 1.5 m above ground level
Model domain	500 m x 470 m
Number of particles	1,200,000 per 600 seconds
Roughness length	0.01 m

9.17.4 Results

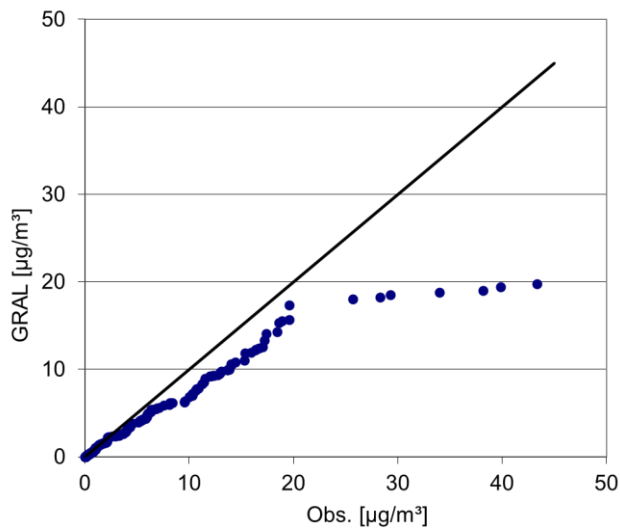
There is good agreement between simulated and observed mean concentrations.

Additional validation cases

Table 72. Results for the Uttenweiler experiment

Model	NMSE	Mean deviation	References
GRAL	2.3	0.6	
GRAL/level1	1.6	-0.1	
GRAL/level2	1.3	0.1	
GRAL V20.09 „Adaptive roughness“ and vegetation	1.5	0.3	
GRAL V21.09 „Adaptive roughness“ and vegetation	1.4	0.3	
GRAL V23.11 „Adaptive roughness“ and vegetation	1.4	0.3	
GRAL V24.04	1.3	0.3	

Figure 77 Quantile-quantile plot of observed and modelled concentrations V23.11 “Adaptive roughness” and vegetation



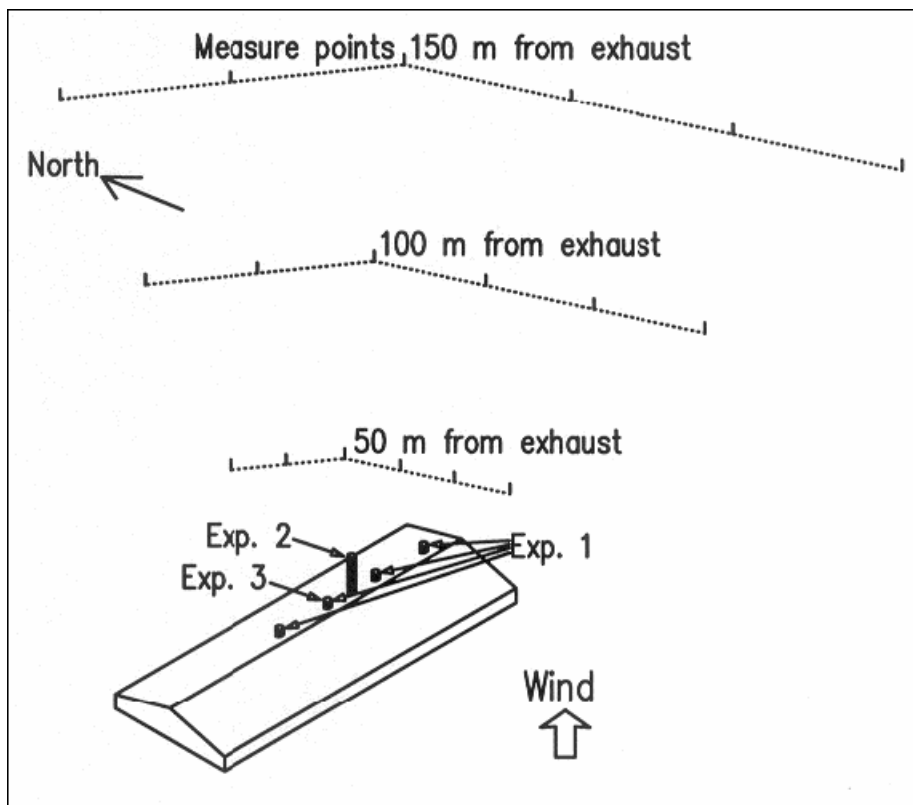
9.18 Roager

9.18.1 Dataset description

The experiment was conducted at a single located pig stable near Roager in Denmark (Ellerman and Løfstrøm, 2002). The stable has a base of 61x23m², the height of the ridge is 5.7 m. The existing exhausts were 0.65 m above the ridge. In addition to tracer experiments using four of the existing exhausts, dispersion from a single stack 6 m above the roof ridge, and from four artificial exhausts 3 m above roof ridge have been investigated. The diameter of the four existing heights was 0.95 m and the exit velocity was 5.1 m/s. In case of the artificial exhausts, diameters were 0.125 m.

21 experiments have been taken for model comparison. Only observed peak concentrations at distances 50 m, 100 m, and 150 m have been used. Averaging time for sampling was 30 minutes. Wind speed and –direction were observed by means of one sonic anemometer 7 m above ground level. Wheat fields surrounded the pig stable during the experiments.

Figure 78. Experimental layout of the Roager pig stable



9.18.2 Characteristics

Wind speeds ranged between moderate and high, atmospheric stabilities have been derived from given Monin-Obukhov lengths. Concentrations have been compared paired in space and time.

Additional validation cases

9.18.3 Model set up

Topography	Flat terrain
Obstacles	Microscale prognostic model, mixing-length turbulence closure Horizontal resolution: 2 m Vertical resolution: 0.5 m Vertical stretching factor: 1.0 Minimum iterations: 100 Maximum iterations: 500 Number of vertical cells: 40
Concentration grid	2 m horizontal, 0.4 m vertical extension, 1.8 m above ground level
Model domain	300 m x 300 m
Number of particles	360,000 per ½ hour
Roughness length	0.05 m
Prognostic radius around sources	150 m

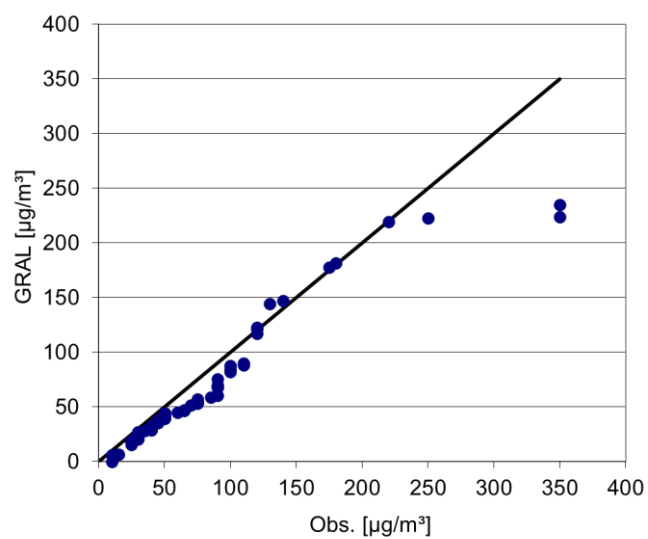
9.18.4 Results

There is a good agreement between simulated and observed concentrations, although peak concentrations are a bit underestimated by GRAL/level2 simulations.

Table 73. Results for the Roager experiment

Model	NMSE	FB	References
GRAL	2.1	0.8	
GRAL/level 1	0.7	-0.2	
GRAL/level 2	0.6	0.2	
GRAL V 20.09 „Adaptive roughness“	0.7	0.1	
GRAL V 21.09 „Adaptive roughness“	0.7	0.1	
GRAL V 23.11 „Adaptive roughness“	0.8	0.3	
GRAL V 24.04	0.7	0.2	

Figure 79 Quantile-quantile plot of observed and modelled concentrations V24.04

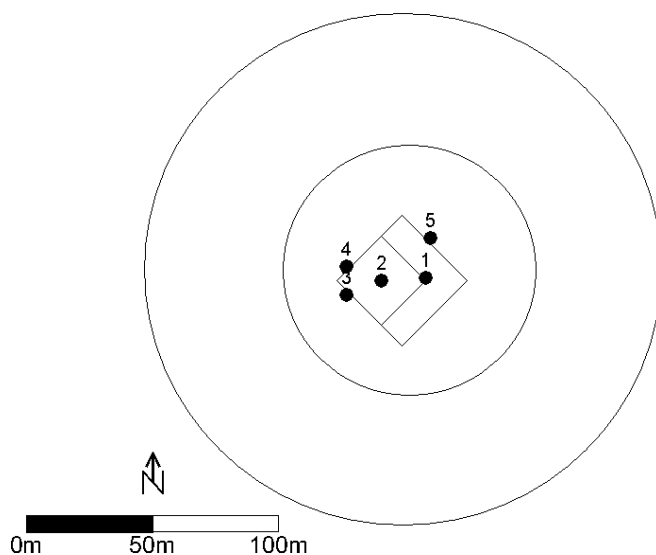


9.19EOCR

9.19.1 Dataset description

The Experimental Organically Cooled Reactor (EOCR) study (Start et al., 1981) involved a simultaneous release of three tracer gases at three levels (1 m, 25 m and 30 m) around the EOCR test reactor building at the Idaho National Engineering Laboratory. The terrain was flat with low-lying shrubs. The main building was 25 m high. There was also an adjacent building with a height of 7 m to the northeast and southeast of the main building. The tracer releases typically occurred simultaneously and were conducted during 22 separate time periods. Tracer sampler coverage was provided at eight concentric rings at distances of about 50, 100, 200, 400, 800, 1200, and 1600 m from the release points. Most of the meteorological data were measured on site and conditions were mainly unstable.

Figure 80. Experimental layout



9.19.2 Characteristics

Buildings have not been orientated along the mean wind field. Maximum arcwise concentrations have been compared with modelled ones.

9.19.3 Model set up

Topography	Flat terrain
Obstacles	Microscale prognostic model, mixing-length turbulence closure Horizontal resolution: 2 m Vertical resolution: 2 m Vertical stretching factor: 1.0 Minimum iterations: 100 Maximum iterations: 500 Number of vertical cells: 40
Concentration grid	2 m horizontal, 1 m vertical extension, 1 m above ground level

Model domain	400 m x 400 m
Number of particles	1,440,000 per hour
Roughness length	0.15 m

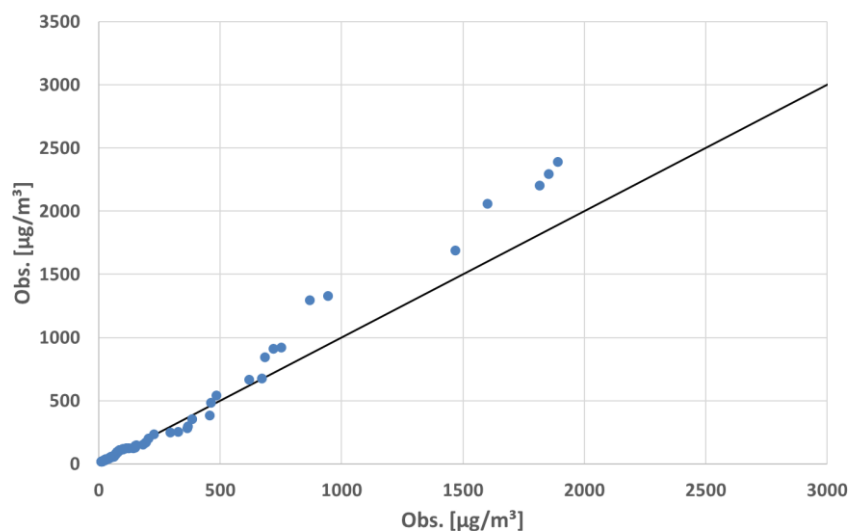
9.19.4 Results

GRAL/level2 performs well. Peak concentrations could be captured as well as average concentrations.

Table 74. Results for the EOGR experiment

Model	NMSE	FB	References
GRAL	2.2	-0.4	
GRAL/level 1	2.7	-0.5	
GRAL/level 2	0.7	-0.1	
GRAL V 21.09 „Adaptive roughness“	1.2	0.2	
GRAL V 20.09 „Adaptive roughness“	1.2	0.2	
GRAL V 23.11 „Adaptive roughness“	1.4	0.2	
GRAL V 24.04	0.9	0.0	

Figure 81 Quantile-quantile plot of observed and modelled concentrations for GRAL V24.04



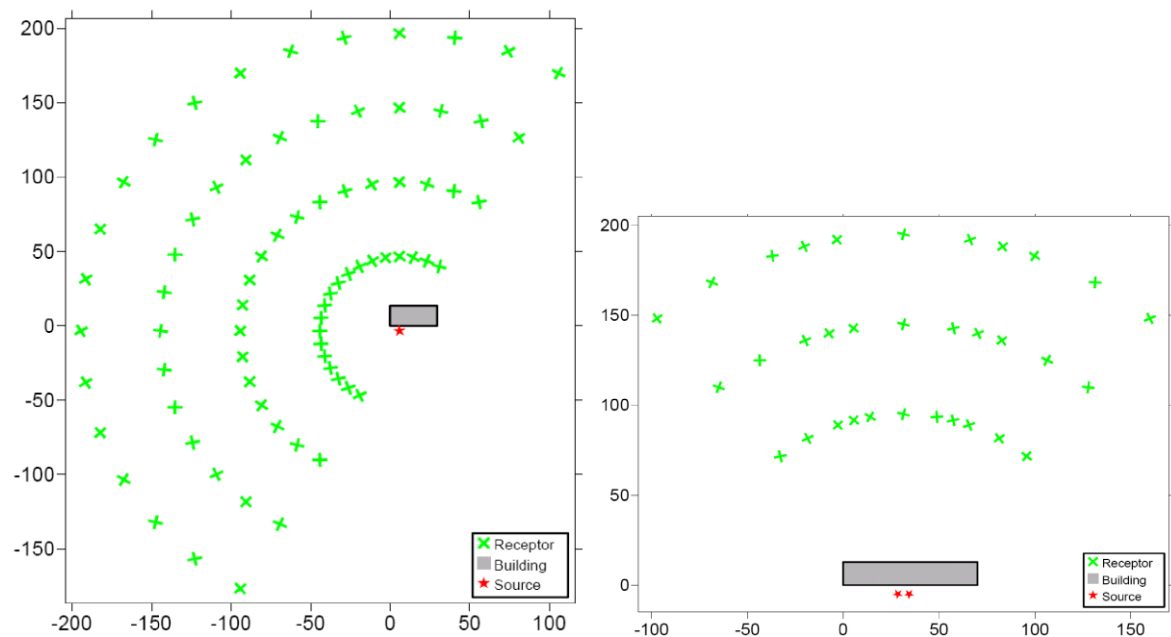
9.20AGA Experiments

9.20.1 Dataset description

The American Gas Association (AGA) experiments occurred during spring and summer 1980 at gas compressor stations in Texas and Kansas. At each test facility, one of the gas compressor stacks was retrofitted to accommodate SF₆ tracer gas emissions. In addition, stack height extensions were provided for some of the experiments (with the normal stack height close to 10 m). Stack height to building height ratios for the tests ranged from 0.95 to 2.52. The tracer samplers were located between 50 and 200 m away from the release point.

Exit temperatures were very high and varied between 616 and 644 K, exit velocities were between 8.1 and 15.2 m/s. Meteorological conditions were mainly unstable. Wind speeds ranged between 2 and 11 m/s.

Figure 82. Experimental layouts (left Texas; right Kansas; sketches taken from CERC; 2007)



9.20.2 Characteristics

Buildings have not been orientated along the mean wind field. Maximum arcwise concentrations have been used for comparison purposes.

9.20.3 Model set up Texas

Topography	Flat terrain
Obstacles	Microscale prognostic model, mixing-length turbulence closure Horizontal resolution: 2 m Vertical resolution: 1 m Vertical stretching factor: 1.0 Minimum iterations: 100 Maximum iterations: 500

	Number of vertical cells: 40
Concentration grid	2 m horizontal, 1 m vertical extension, 1 m above ground level
Model domain	380 m x 400 m
Number of particles	1.440.000 per hour
Roughness length	0.1 m
Prognostic radius around sources	150 m

9.20.4 Model set up Kansas

Topography	Flat terrain
Obstacles	Microscale prognostic model, mixing-length turbulence closure Horizontal resolution: 2 m Vertical resolution: 1 m Vertical stretching factor: 1.0 Minimum iterations: 100 Maximum iterations: 500 Number of vertical cells: 40
Concentration grid	4 m horizontal, 0.5 m vertical extension, 1 m above ground level
Model domain	364 m x 410 m
Number of particles	1.440.000 per hour
Roughness length	0.4 m
Prognostic radius around sources	150 m

9.20.5 Results

GRAL/level2 underestimates peak concentrations. It is amazing that the observed mean concentration in case of the Kansas experiments is very similar for the 10 m stack and the 24 m high stack. Furthermore observed concentrations during the Kansas experiments for the 9.75 m high stack are 4 times the observed concentrations for the 9.75 high stack during the Texas experiments on average. All in all both experiments have extreme variations in observed concentrations making it impossible for dispersion models to perform well in both cases.

GRAL/level 2 overestimates – as most other models – in case of Kansas concentrations significantly. The overestimation is mainly a result from the simulations for the 9.75 m stack (the one lower than the adjacent building). It is important to know that GRAL results are extremely sensitive to certain input parameters in this case, such as stack height or stack diameter.

Additional validation cases

Table 75. Results for the AGA-Texas experiments

Model	NMSE	FB	References
GRAL	1.0	0.4	
GRAL/level 1	0.7	-0.3	
GRAL/level 2 V20.01	1.0	-0.35	
GRAL V20.09 „Adaptive roughness“	1.0	-0.2	
GRAL V21.09 „Adaptive roughness“	1.0	-0.2	
GRAL V23.11 „Adaptive roughness“	0.8	0.1	
GRAL V24.04	0.7	0.0	

Figure 83 Quntile-quantile plot of observed and modelled concentrations for the Texas experiments GRAL V23.11 „Adaptive roughness“

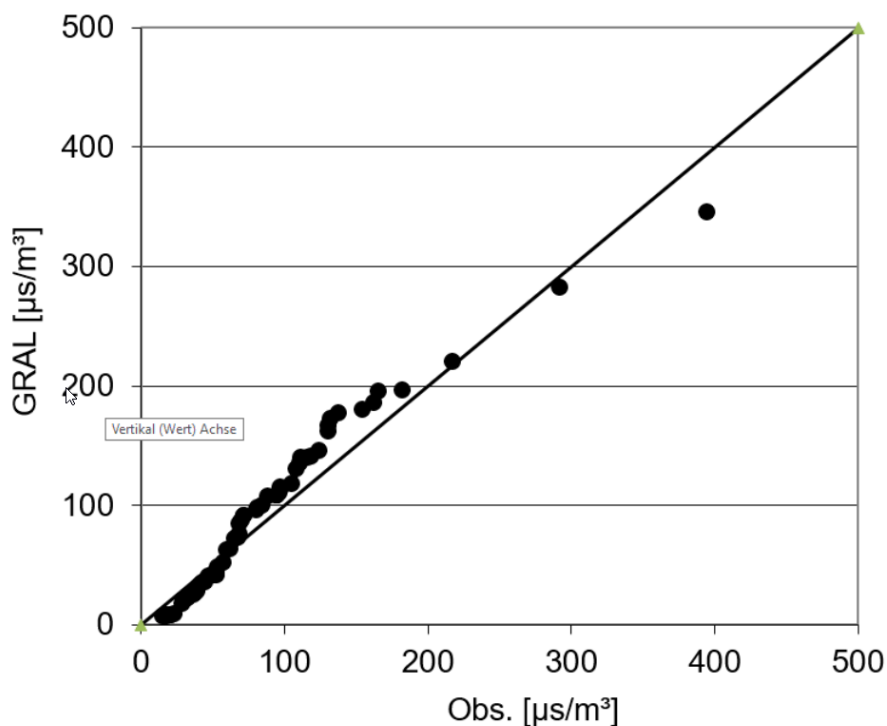
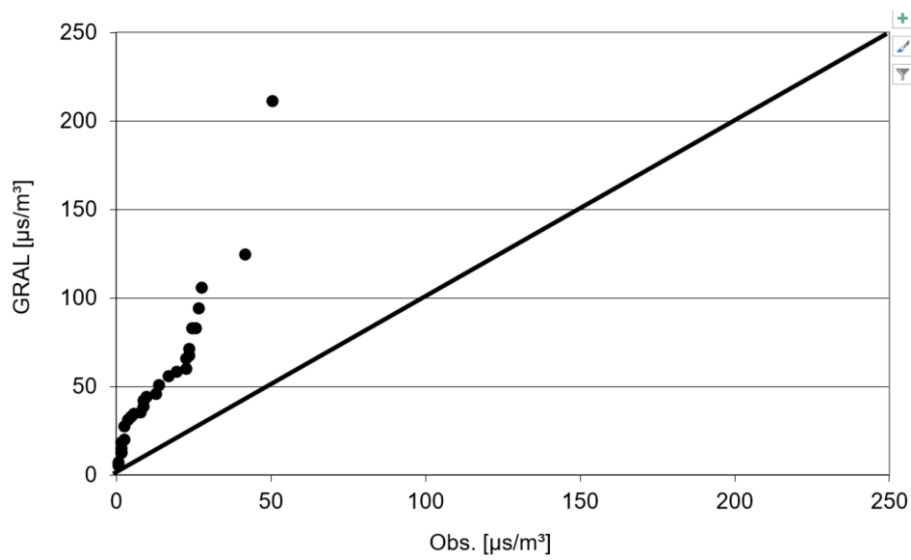


Table 76. Results for the AGA-Kansas experiments

Model	NMSE	FB	References
GRAL	2.8	-0.9	
GRAL/level 1	3.5	-1.0	
GRAL/level 2	5.4	-1.1	
GRAL V 20.09 „Adaptive roughness“	4.3	-1.0	
GRAL V 21.09 „Adaptive roughness“	4.2	-1.0	
GRAL V 23.11 „Adaptive roughness“	4.2	-1.0	
GRAL V 24.04	5.1	-1.1	

Figure 84 Quantile-quantile plot of observed and modelled concentrations for the Kansas experiments V24.04

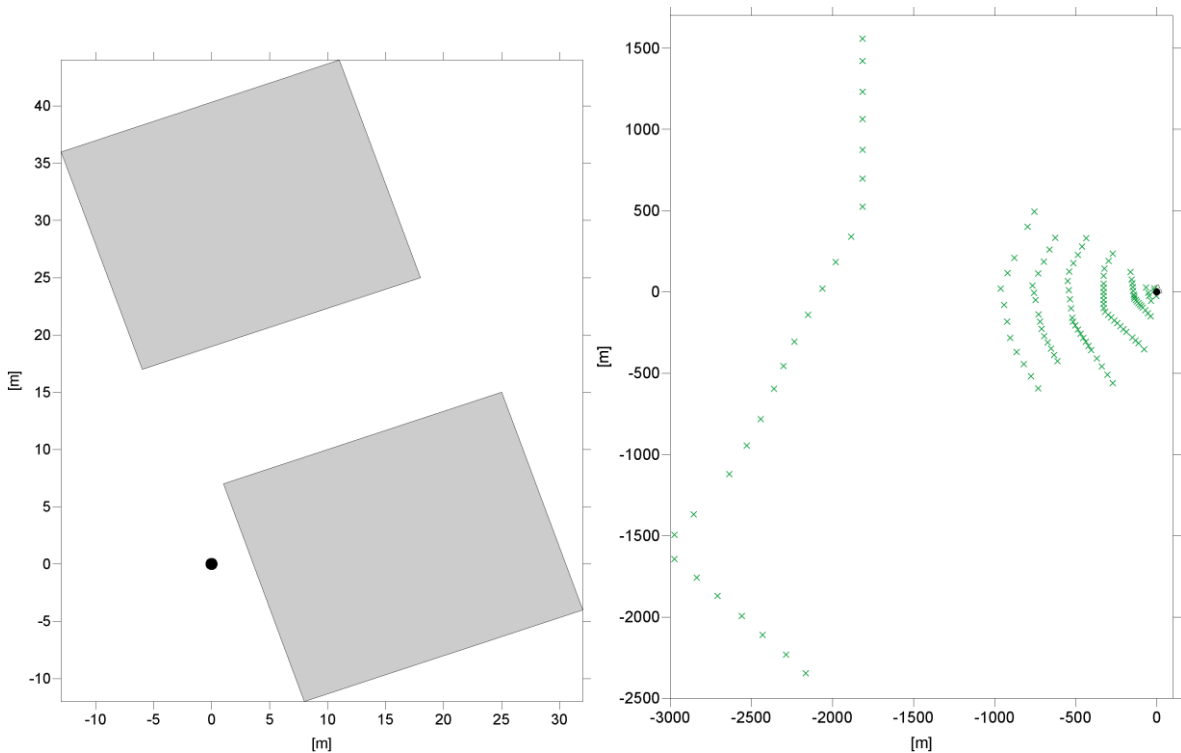


9.21 Alaska North Slope Tracer Study

9.21.1 Dataset description

All in all 38 tracer experiments were available for model evaluation. SF_6 was released from a 39 m high turbine stack situated close to two 34 m high buildings. Exit temperature was 850 K and exit velocity was 18 m/s. Sampling took place along 8 arcs between 50 and 3000 m downwind of the source. Meteorological data, including wind speed, -direction were available from an on-site tower 33 m above ground level. Wind speeds ranged between 3.0 and 18.4 m/s. Most of the experiments were taken during neutral atmospheric conditions, in only six cases stability was stable. All data was downloaded from US-EPA (2003).

Figure 85. Experimental layout (left: buildings and stack locations; right: receptor locations)



9.21.2 Characteristics

Buildings have not been orientated along the mean wind field. Arcwise maximum concentrations have been used for comparison purposes.

9.21.3 Model set up

Topography	Flat terrain
Obstacles	Microscale prognostic model, mixing-length turbulence closure Horizontal resolution: 6 m Vertical resolution: 2 m Vertical stretching factor: 1.01 Minimum iterations: 100 Maximum iterations: 500

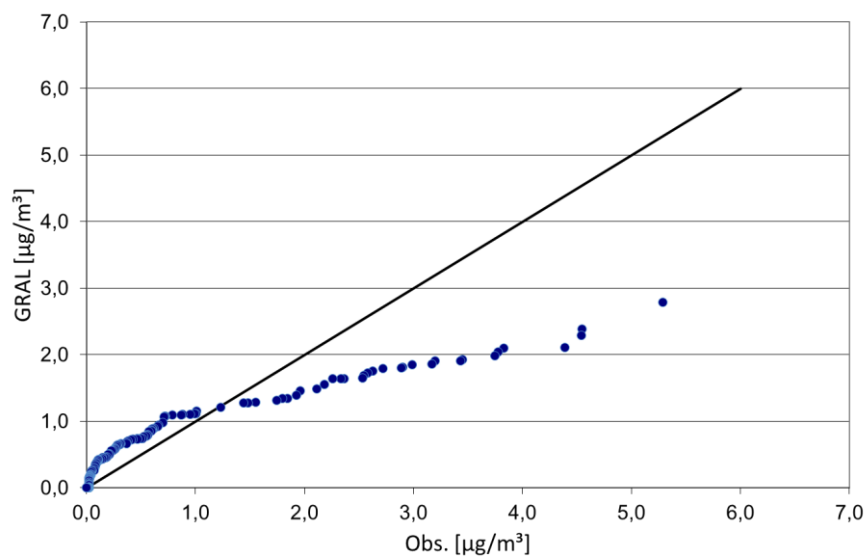
	Number of vertical cells: 40
Concentration grid	6 m horizontal, 1 m vertical extension, 1 m above ground level
Model domain	3,900 m x 4,500 m
Number of particles	540,000 per hour
Roughness length	0.025 m

9.21.4 Results

Table 77. Results for the Alaska experiments

Model	NMSE	Mean deviation	References
GRAL/level 2	3.7	0.3	
GRAL V20.09 „Adaptive roughness“	2.0	-0.4	
GRAL V21.09 „Adaptive roughness“	1.8	-0.4	
GRAL V23.11	2.9	0.2	
GRAL V24.04	2.5	0.1	

Figure 86 Quantile-quantile plot of observed and modelled concentrations for the Alaska experiments V24.04



9.22 Ninomiya tunnel

9.22.1 Dataset description

The tracer experiment was performed by the Japanese Highway Public Corporation in the year 1994. Table 78 lists some relevant information regarding the tunnel and the tracer experiments. The portal lies in rather steep topography. About 10 meteorological monitoring stations were placed in the surroundings of the portal, to provide an input for the wind field models.

Table 78. Some information concerning the tracer experiment at the Ninomya tunnel in Japan.

	Ninomiya tunnel
Length and ventilation system	445 m (-)
Highway	Odawara-Atsugi road
Traffic volume	30,000 veh./day
Experiment date	20.Jan-1.Feb 94
No. of sampling sites: SF ₆	64
No. of runs	21
Tracer release period [h]	144

9.22.2 Characterisation

The varying meteorological conditions (wind speed, -direction, and stability) during the SF₆ tracer tests allows for a critical evaluation of models. SF₆ was released inside the tunnel. It is assumed, that the tracer gas was immediately mixed with ambient air in the tunnel as a consequence of high turbulence introduced by moving vehicles. Temperature differences were assumed to be zero, due to the small length of the tunnel.

It should be kept in mind that statistical measures for model evaluation depend strongly on model results for those samplers closest to the portal. For instance, concentrations varied by a factor of 4 within 8 m distance between two samplers near the portal.

9.22.3 Model set up

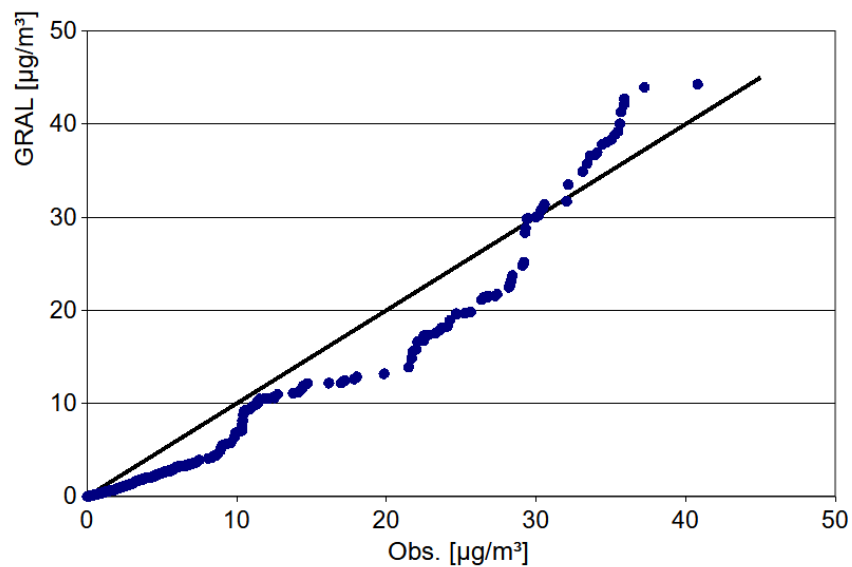
Topography GRAMM	3D wind fields simulated with the non-hydrostatic prognostic wind field model GRAMM Horizontal resolution: 20 m Vertical resolution: 10 m Vertical stretching factor: 1,1 Vertical layers: 20 Top level: 583 m Turbulence model: k-ε closure
Topography GRAL	5 m resolution derived from original topographical data
Obstacles	None
Concentration grid	3 m horizontal, 1 m vertical extension, 1.5 m above ground level
Model domain	590 m x 690 m
Number of particles	180,000 per hour
Roughness length	0.2 m

9.22.4 Results

Table 79. Results for the Ninomiya dataset

Model	NMSE	FB	References
GRAL V20.01	0.7	0.3	
GRAL V20.09 „Adaptive roughness“	2.0	0.1	
GRAL V21.09 „Adaptive roughness“	2.0	0.1	
GRAL V23.11 „Adaptive roughness“	2.1	0.1	
GRAL V24.04	1.1	0.29	

Figure 87 Quantile-quantile plot of observed and modelled concentrations V24.04



9.23 Hitachi tunnel

9.23.1 Dataset description

The tracer experiment was performed by the Japanese Highway Public Corporation in the year 1995. Table 80 lists some relevant information regarding the tunnel and the tracer experiments. The portal lies in rather steep topography. About 10 meteorological monitoring stations were placed in the surroundings of the portal, to provide an input for the wind field models.

Table 80. Some information concerning the tracer experiment at the Hitachi tunnel in Japan.

	Hitachi tunnel
Length and ventilation system	2439 m (jet fan)
Highway	Joban expressway
Traffic volume	24,000 veh./day
Experiment date	3.-9.Feb 95
No. of sampling sites: SF ₆	85
No. of runs	18
Tracer release period [h]	159

9.23.2 Characterisation

Varying meteorological conditions (wind speed, wind direction, and stability) during the SF₆ tracer tests allows for a critical evaluation of models. SF₆ was released inside the tunnel. It is assumed, that tracer gas was immediately mixed with ambient air in the tunnel as a consequence of high turbulence introduced by the moving vehicles. Measured temperature differences between ambient air and air inside the tunnels were not available for the simulations.

It should be kept in mind that statistical measures for model evaluation depend strongly on model results for those samplers closest to the portal. For instance, concentrations varied by a factor of 4 within 8 m distance between two samplers near the portal.

9.23.3 Model set up

Topography GRAMM	3D wind fields simulated with the non-hydrostatic prognostic wind field model GRAMM Horizontal resolution: 16 m Vertical resolution: 5 m Vertical stretching factor: 1,17 Vertical layers: 20 Top level: 655 m Turbulence model: k-ε closure
Topography GRAL	5 m resolution derived from original topographical data
Obstacles	None
Concentration grid	4 m horizontal, 0.3 m vertical extension, 1.5 m above ground level
Model domain	520 m x 515 m
Number of particles	180,000 per hour

Roughness length	0.2 m
------------------	-------

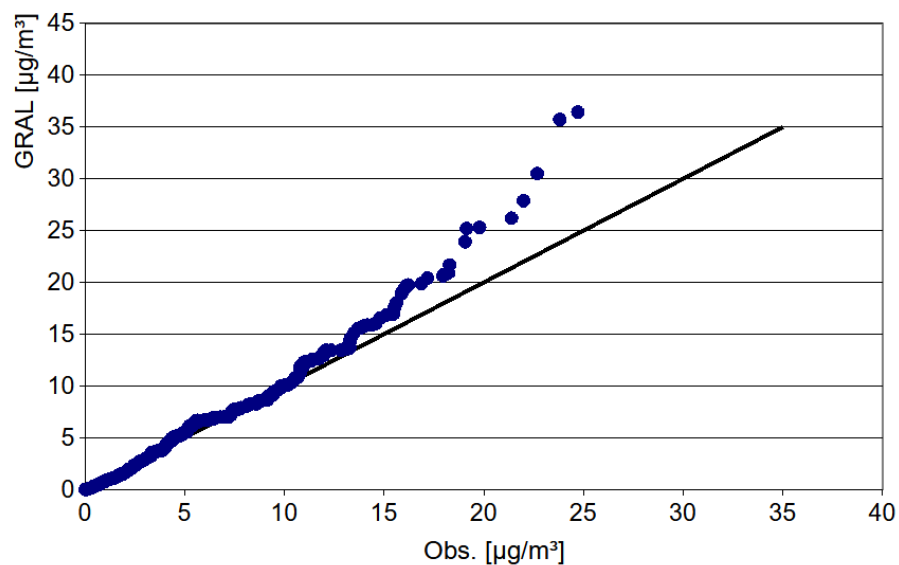
9.23.4 Results

GRAL slightly overestimates average and peak concentrations.

Table 81. Results for the Hitachi dataset

Model	NMSE	FB	References
GRAL	2.8	-0.2	
GRAL V20.09	2.3	-0.2	
GRAL V21.09	2.3	-0.2	
GRAL V23.11 "adaptive roughness"	2.3	-0.3	
GRAL V24.04	2.1	-0.02	

Figure 88 Quantile-quantile plot of observed and modelled concentrations V24.04



9.24 Enrei tunnel

9.24.1 Dataset description

The tracer experiment was performed by the Japanese Highway Public Corporation in the year 1995. Table 82 lists some relevant information regarding the tunnel and the tracer experiments. The portal lies in rather steep topography. About 10 meteorological monitoring stations were placed in the surroundings of the portal, to provide an input for the wind field models.

Table 82. Some information concerning the tracer experiment at the Enrei tunnel in Japan.

	Enrei tunnel
Length and ventilation system	1800 m (jet fan)
Highway	Chuo expressway
Traffic volume	32,000 veh./day
Experiment date	23.-29.Nov 95
No. of sampling sites: SF ₆	86
No. of runs	17
Tracer release period [h]	168

9.24.2 Characterisation

Varying meteorological conditions (wind speed, wind direction, and stability) during the SF₆ tracer tests allows for a critical evaluation of models. SF₆ was released inside the tunnel. It is assumed, that tracer gas was immediately mixed with ambient air in the tunnel as a consequence of the high turbulence introduced by moving vehicles. Measured temperature differences between ambient air and air inside the tunnels were not available for the simulations.

It should be kept in mind that statistical measures for model evaluation depend strongly on model results for those samplers closest to the portal. For instance, concentrations varied by a factor of 4 within 8 m distance between two samplers near the portal.

9.24.3 Model set up

Topography GRAMM	3D wind fields simulated with the non-hydrostatic prognostic wind field model GRAMM Horizontal resolution: 16 m Vertical resolution: 5 m Vertical stretching factor: 1,13 Vertical layers: 20 Top level: 410 m Turbulence model: k-ε closure
Topography GRAL	5 m resolution derived from original topographical data
Obstacles	None
Concentration grid	4 m horizontal, 0.3 m vertical extension, 1.5 m above ground level
Model domain	549 m x 456 m
Number of particles	180,000 per hour

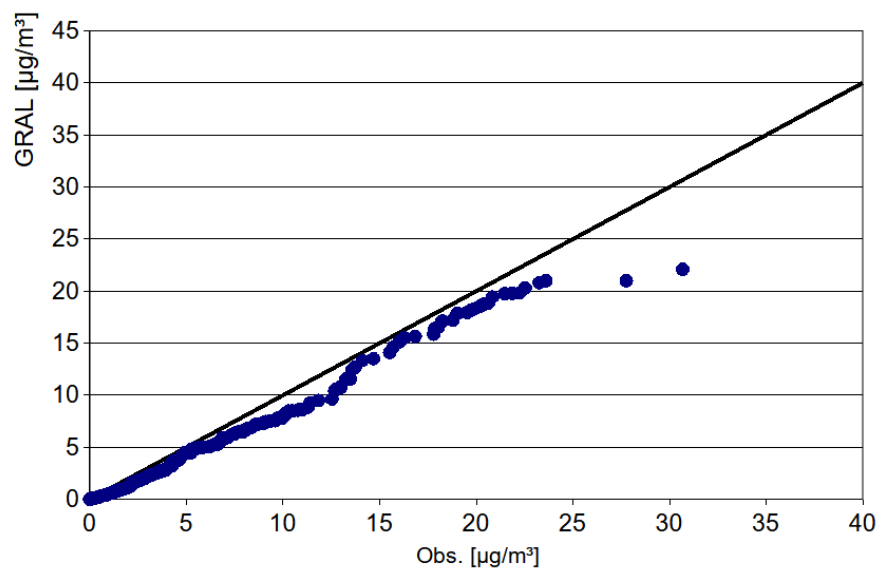
Roughness length	0.2 m
------------------	-------

9.24.4 Results

Table 83. Results for the Enrei dataset

Model	NMSE	FB	References
GRAL	3.0	0.1	
GRAL V20.09	3.0	-0.2	
GRAL V21.09	3.0	-0.2	
GRAL V23.11	3.0	-0.2	
GRAL V24.04	3.0	0.2	

Figure 89 Quantile-quantile-plot of observed and modelled concentrations V23.11



9.25 Westvaco Paper Mill

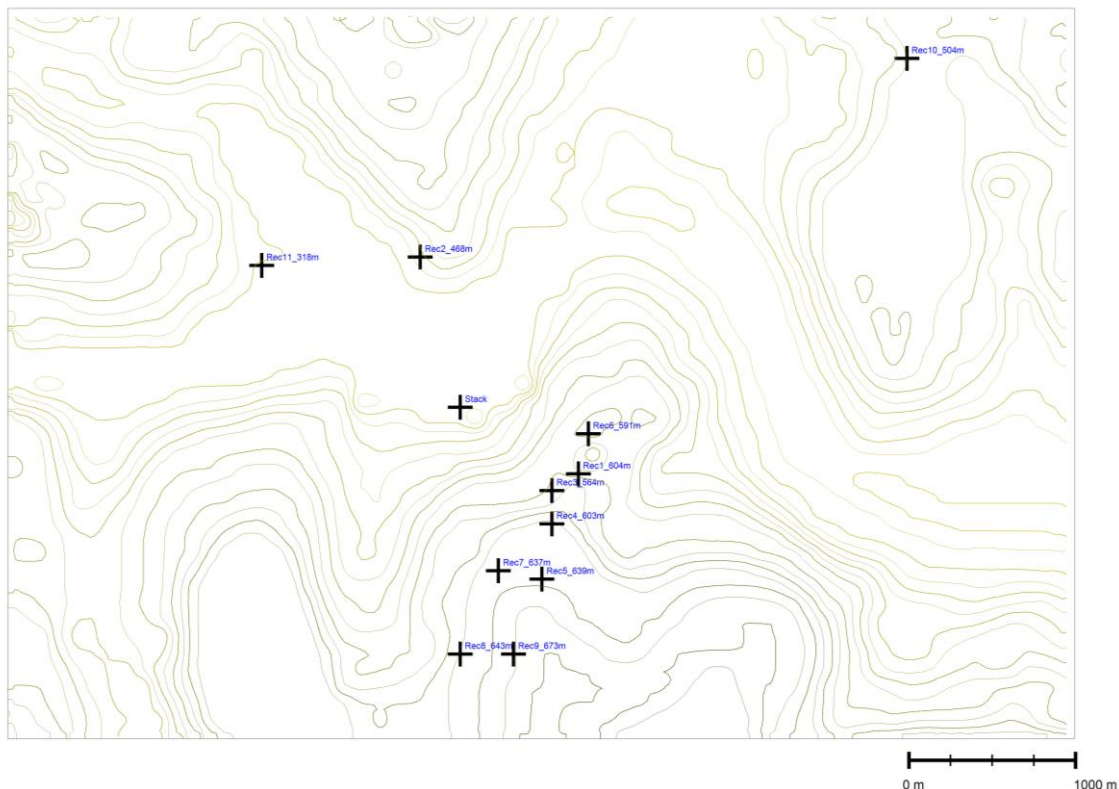
9.25.1 Dataset description

The Westvaco monitoring program was carried out during a 2-year period from December 1979 through November 1981.

The Westvaco Paper Mill was located in a complex terrain in the Potomac River valley. A 190 m stack source released SO₂, the source data were registered continuously. Concentration measurements were taken on an hourly basis at eleven SO₂ monitors surrounding the Paper Mill and two Meteorological Towers. Eight SO₂ monitor towers were located on a ridge southeast of the main stack. The hills are mostly covered with forests.

The input data for the GRAL model were taken from the US EPA website for the AERMOD model validation. The topographical data were not known exactly, they were transferred manually from topographical maps.

Figure 90. GRAL model domain showing the stack source, terrain and receptors



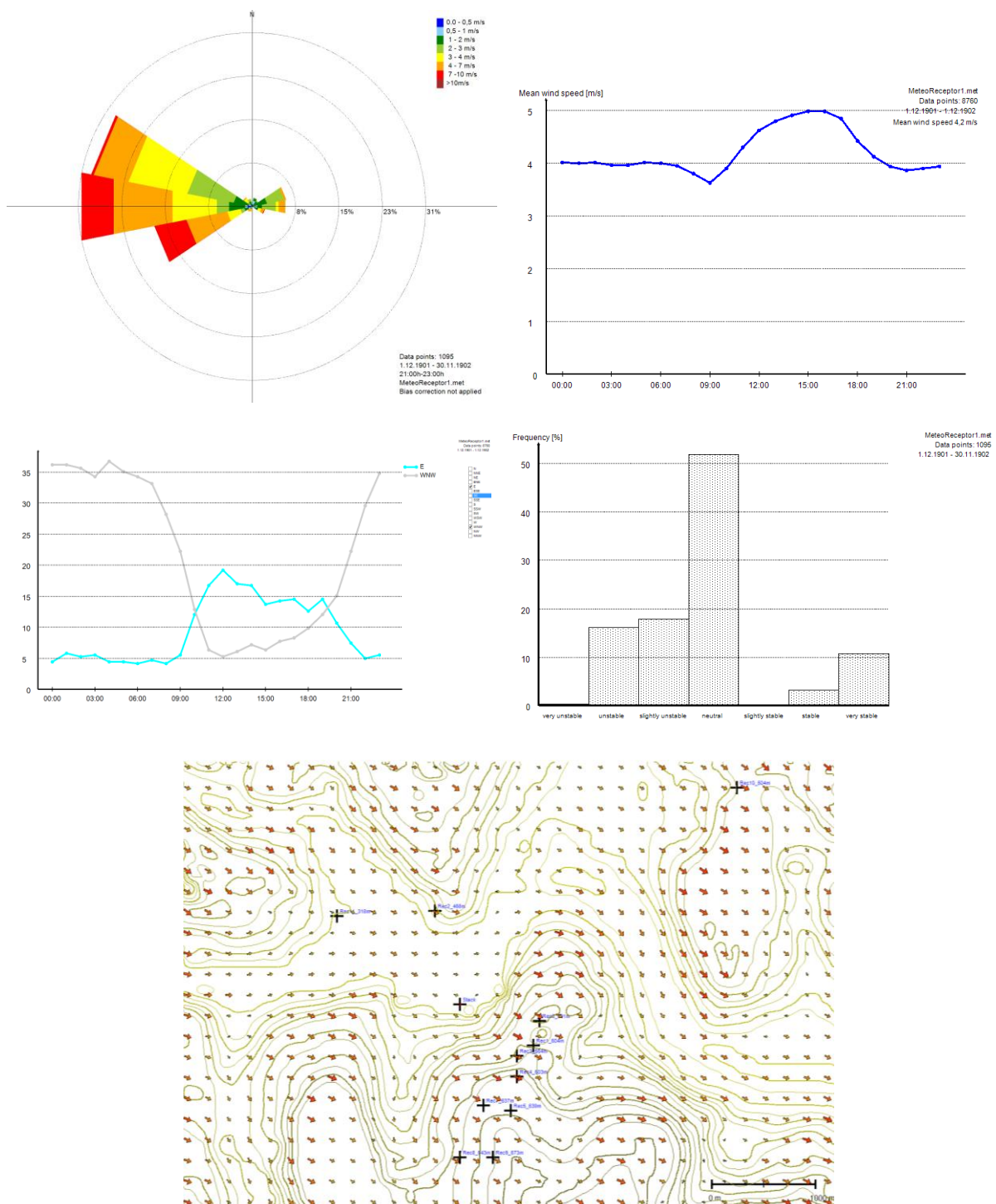
9.25.2 Characterisation

The wind speeds are rather high; the measured annual mean wind speed at 30 m above ground level was at 3.8 m/s. The wind system prevails most of the time with westerly winds during the night and westerly or easterly winds during the daytime.

The stability classes for the GRAL model were calculated using the Sigma-A method based on the US-EPA report “Meteorological Monitoring Guidance for Regulatory Modeling Applications” (EPA-454/R-99-005).

The GRAMM calculation is based on the meteorological measured data and the topography. The calculated meteorological data in a height of 30 m above terrain and a wind vector map at a height of 10 m above ground are shown in Figure 91.

Figure 91. GRAMM meteo data for Receptor 1 at 30 m above terrain and vector map at 10 m above terrain for one significant meteorological situation



Additional validation cases

9.25.3 Model set up

Topography GRAMM	3D wind fields simulated with the non-hydrostatic prognostic wind field model GRAMM 20.09 Horizontal resolution: 100 m Vertical resolution: 10 m Vertical stretching factor: 1,33 Vertical layers: 17 Surface energy balance: manually defined landuse data, roughness length 1 m
Topography GRAL	25 m resolution
Obstacles	Microscale prognostic model, mixing-length turbulence closure Horizontal resolution: 25 m Vertical resolution: 2 m Vertical stretching factor: 1.01 Minimum iterations: 100 Maximum iterations: until 500 Number of vertical cells: 40
Concentration grid	25 m horizontal, 2 m vertical extension, 4 m above ground level
Model domain	6400 m x 4400 m
Number of particles	360,000 per hour
Roughness length	manually defined landuse data, roughness length 0.5 m
GRAL Mode	Transient GRAL mode, time series for the emission rate, exit temperature and exit velocity of the buoyant source

9.25.4 Results

GRAL has been operated in transient mode using time series on an hourly basis for the emission rate, exit temperature and exit velocity of the buoyant source. Compared to AERMOD, GRAL V20.09 performs much better for the annual mean values, marginally worse for the maximum 24 h mean values and worse for the maximum one-hour average values. GRAL version 21.09 gives the same results as version 20.09.

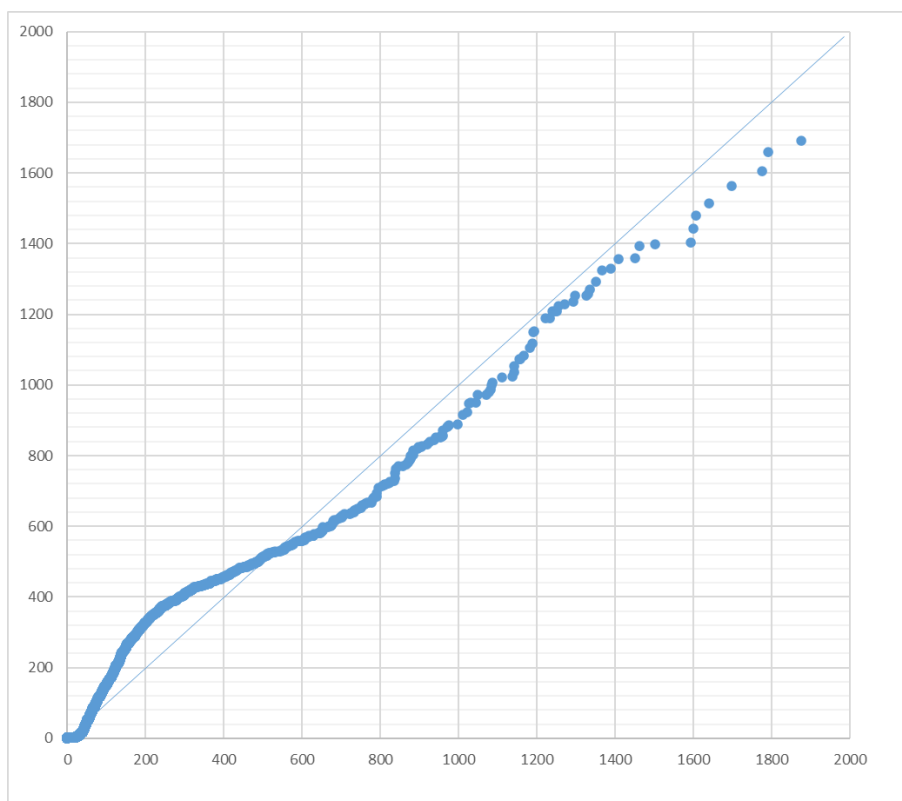
Table 84 Results for the Westvaco dataset V23.11

		SO ₂ concentration in µg/m ³ for receptors										
		R1	R2	R3	R4	R5	R6	R7	R8	R9	R10	R11
Annual average	Observed	49	14	35	30	30	71	30	27	25	16	19
	GRAL	75	12	47	35	22	90	21	17	17	17	6
1 h avg. maximum	Observed	1909	1191	1697	2290	2341	2269	2234	2210	1859	552	533
	GRAL	857	1692	1658	1242	1105	1028	1123	742	1595	223	703
24 h avg. maximum	Observed	436	86	415	370	403	390	689	327	285	114	167
	GRAL	218	85	187	210	123	348	103	66	100	79	59

Table 85 Results for the WestVaco dataset

Model		NMSE	FB
GRAL/level 2 V20.09 transient, all receptors	annual average	0.0	0.0
GRAL/level 2 V20.09 transient, all receptors	1 h maximum	0.4	0.6
GRAL/level 2 V20.09 transient, all receptors	24 h maximum	0.8	0.8
GRAL V23.11 transient, all receptors	annual average	0.0	0.0
GRAL V23.11 transient, all receptors	1 h maximum	0.3	0.6
GRAL V23.11 transient, all receptors	24 h maximum	0.8	0.8
GRAL V24.04 transient	annual average	0.0	0.0
GRAL V24.04 transient	1 h maximum	0.2	0.46
GRAL V24.04 transient	24 h maximum	0.8	0.8

Figure 92 Quantile-quantile plot of observed and modelled concentrations using GRAL V24.04



9.26 2014 Colorado Oil and Gas Drill Rig Field Study

9.26.1 Dataset description

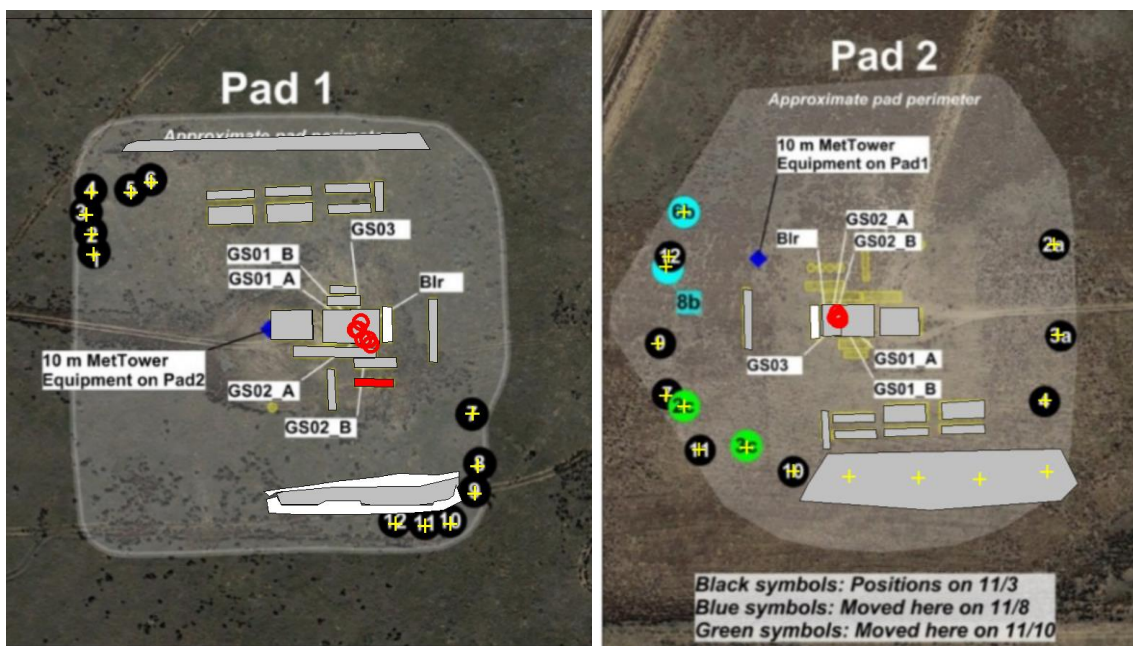
This data set includes extensive meteorological measurements and measurements of NO_x, NO₂, and ozone, as well as emission data for two drill rig sites.

The measurements covered a period between October 10 and November 16 in 2014. Data were collected at 5-minute and hourly intervals.

The rigs were powered by diesel-powered generators. The exhaust gases were released into the open air at a low height above the roof of the generator containers. The terrain is largely flat, except for a few ridges of earth.

The measurement campaign included two separate areas, Pad 1 and Pad 2.

Figure 93. GRAL model domain showing the sources, buildings and receptors for Pad 1 and Pad 2



9.26.2 Characterisation

The wind speeds were rather high; the measured mean wind speed at 10 m above ground level was at 3.5 m/s for Pad 1 and 3.7 m/s for Pad2.

The stability classes for the GRAL model were calculated using the cloud method based on the US-EPA report "Meteorological Monitoring Guidance for Regulatory Modeling Applications" (EPA-454/R-99-005).

9.26.3 Model set up

Obstacles	Microscale prognostic model, mixing-length turbulence closure Horizontal resolution: 2 m Vertical resolution: 1 m Vertical stretching factor: 1.0 Minimum iterations: 100 Maximum iterations: until 500 Number of vertical cells: 40
Concentration grid	4 m horizontal, 2 m vertical extension, 3 m above ground level
Model domain	200 m x 200 m
Number of particles	1080000 per hour
Roughness length	0.01 m
GRAL Mode	Transient GRAL mode, time series for the emission rate, exit temperature and exit velocity of all sourcea

9.26.4 Results for the Colorado Oil and Gas Drill Rig Field Study

GRAL has been operated in transient mode using time series on an hourly basis for the emission rate, exit temperature and exit velocity of the buoyant source.

GRAL/level 2 overestimates concentrations significantly for both Pads. The overestimation is related to the high wind speeds and the low stack heights, so that the plume rise is underestimated. It is important to know that GRAL results are extremely sensitive to certain input parameters in this case, such as stack height or stack diameter. The diameter, along with the exhaust gas velocity, determines the exhaust gas volume and thus the exhaust gas heat flow. The higher the exhaust gas volume, the higher the plume rise, even at high wind speeds.

Table 86. Results for the Denver Julesburg dataset Pad 1

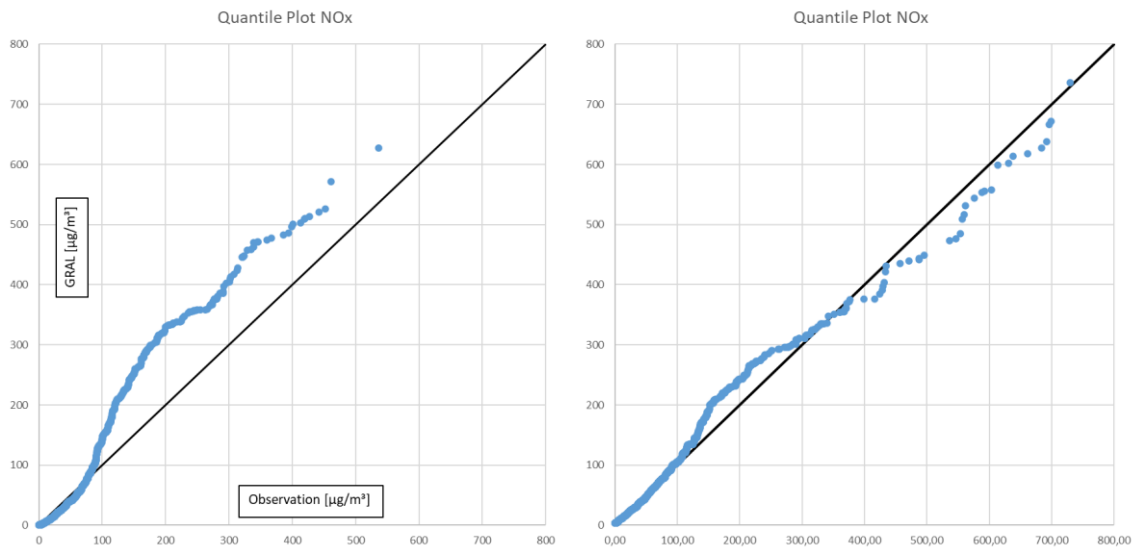
Model		NMSE	FB
GRAL/level 2 V22.09 transient, all receptors	Campaign average	4.4	0.2
GRAL V23.11 transient, all receptors		2.6	-0.2
GRAL V24.04 transient, all receptors		2.5	-0.1

Table 87. Results for the Denver Julesburg dataset Pad 2

Model		NMSE	FB
GRAL/level 2 V22.09 transient, all receptors	Campaign average	2.6	0.2
GRAL V23.11 transient, all receptors		1.9	-0.1
GRAL V24.04 transient, all receptors		1.6	0.0

Additional validation cases

Figure 94 Quantile-quantile plot of observed and modelled concentrations using GRAL V 24.04 for Pad 1 (left) and Pad 2 (right)



10 Dry deposition

The test cases documented hereafter will comprise in particular the conservation of mass and the ability to resemble the prescribed deposition velocity for a certain range of values.

The deposition velocity can be calculated as the ratio between the flux density of the passive scalar and its mean concentration at a reference level near the ground.

In the test cases the concentration near the ground is evaluated in the layer between 0.5 and 1.5 m. The concentration obtained in this way, though, is dependent on the roughness length. Therefore, the calculation of the deposition velocity is prone to some uncertainty.

The test cases cover situations with deposition velocities up to 0.05 m/s. Higher values for the deposition velocity are not validated and may lead to an underestimation of deposition rates.

10.1 Test case 1: Mass Conservation

10.1.1 Model set up

Topography	Flat Terrain
Obstacles	None
Concentration grid	10 m horizontal, 1 m vertical extension, 1 m above ground level
Model domain	1000 m x 1000 m
Number of particles	60,000 per hour
Roughness length	0.2 m

10.1.2 Source configuration

Point source, stack height 20m, exit velocity 0.1 m/s, exit temperature 50°C, diameter 1.0 m, particle density 11 g/cm³.

Particle size	Emission rate	Emission rate	V _{Dep}
PM _{2.5}	0.0014 kg/h	0,034 kg/d	0.001 m/s
PM ₁₀	0.0014 kg/h	0,034 kg/d	0.01 m/s
PM ₁₀₀	0.1372 kg/h	3,292 kg/d	0.05 m/s

10.1.3 Results

Due to the high particle density, all PM₁₀₀ particles are deposited in the very vicinity of the source. For this reason, the mass of the deposited particles should correspond with the daily emission rate.

Dry deposition

The sum of the deposition values over all cells is 32941.86 mg/m²/d, which represents an emission rate (for the given cell size of 10x10 m²) of 3294.2 g/d. Having in mind that there is an additional deposition of PM₁₀ and PM_{2.5}, GRAL is able to reproduce the PM₁₀₀ emission rate by the deposited particles, thus, the conservation of mass is fulfilled.

10.2 Deposition velocity - Test Case 2

10.2.1 Model set up

Topography	Flat Terrain
Obstacles	None
Concentration grid	10 m horizontal, 1 m vertical extension, 1 m above ground level
Model domain	2000 m x 2000 m
Number of particles	180,000 per hour
Roughness length	0.2 m

10.2.2 Source configuration

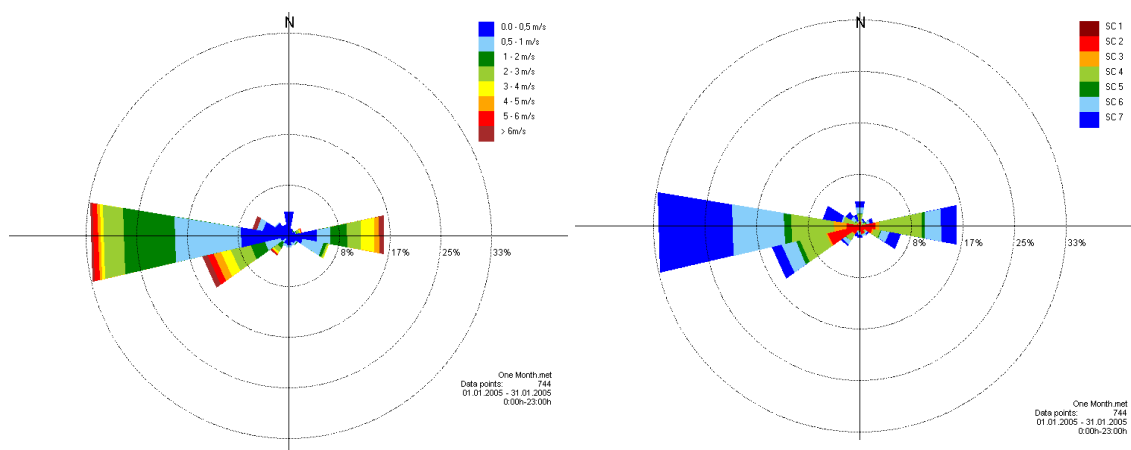
Point source, stack height 20m, exit velocity 0.1 m/s, exit temperature 50°C, diameter 1.0 m, particle density 2 g/cm³

Particle size	Emission rate	Emission rate	V _{Dep}
PM _{2.5}	0 kg/h	0 kg/d	0.00 m/s
PM ₁₀	1 kg/h	24 kg/d	0.01 m/s
PM ₁₀₀	0 kg/h	0 kg/d	0.00 m/s

10.2.3 Meteorological input

To consider several meteorological conditions a set of about 250 situations were calculated.

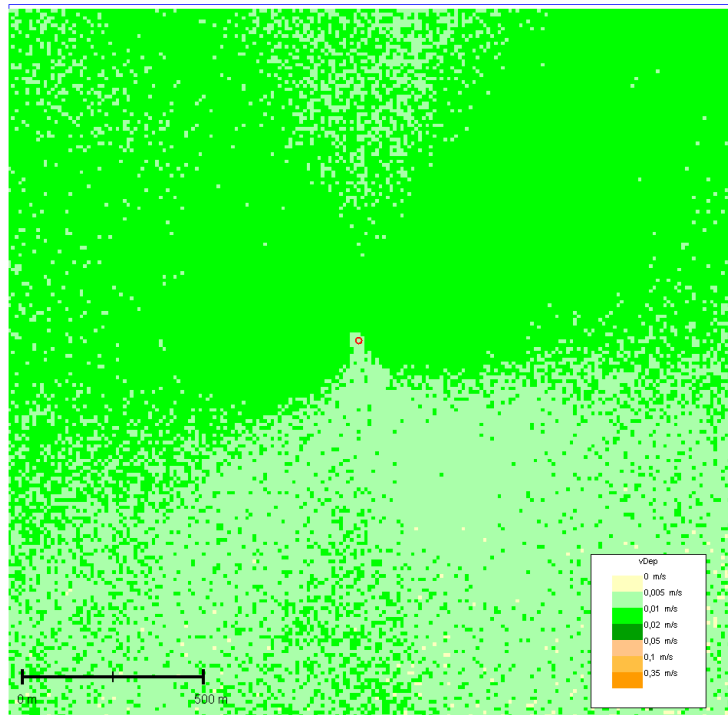
Figure 95. Meteorological input data



10.2.4 Results

GRAL meets the deposition velocity of 0.01 m/s in most areas but underestimates deposition in areas, where wind directions have a low frequency.

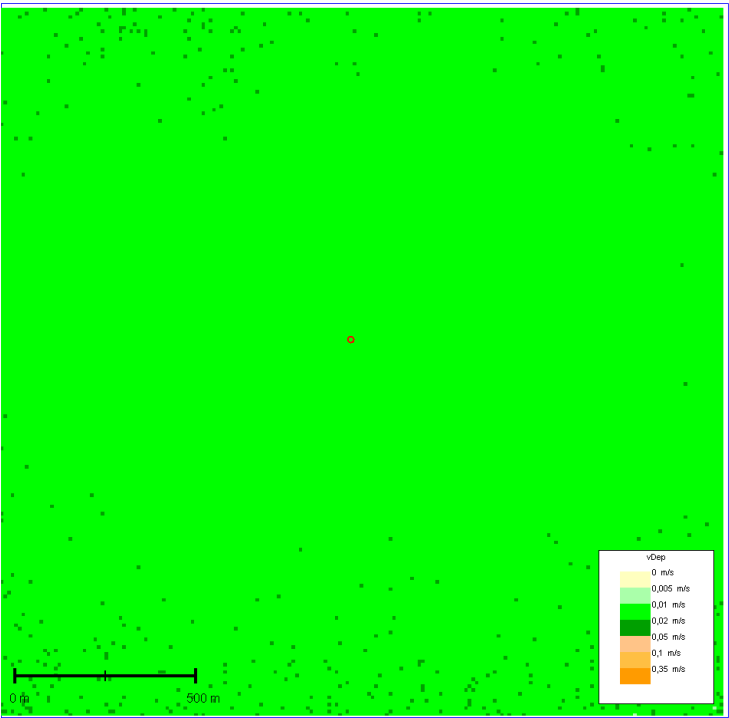
Figure 96. Horizontal plane illustrating computed deposition velocities for a roughness length of $z_0 = 0.2\text{m}$



For an increased roughness length of 1.5 m, GRAL performs better to meet the prescribed deposition value of 0.01 m/s.

Dry deposition

Figure 97. Horizontal plane illustrating computed deposition velocities for a roughness length of $z_0 = 1.5\text{m}$



10.3Deposition velocity - Test Case 3

10.3.1 Model set up

Topography	Flat Terrain
Obstacles	None
Concentration grid	5 m horizontal, 1 m vertical extension, 1 m above ground level
Model domain	1200 m x 1200 m
Number of particles	360,000 per hour
Roughness length	0.2 m

10.3.2 Source configuration

Line source, vertical extension 3 m, width 7 m, particle density 0 g/cm³ - no sedimentation

Particle size	Emission rate	Emission rate	V _{Dep}
PM _{2.5}	0.15 kg/h	3,6 kg/d	0.01 m/s
PM ₁₀	0 kg/h	0 kg/d	0.00 m/s
PM ₁₀₀	0 kg/h	0 kg/d	0.00 m/s

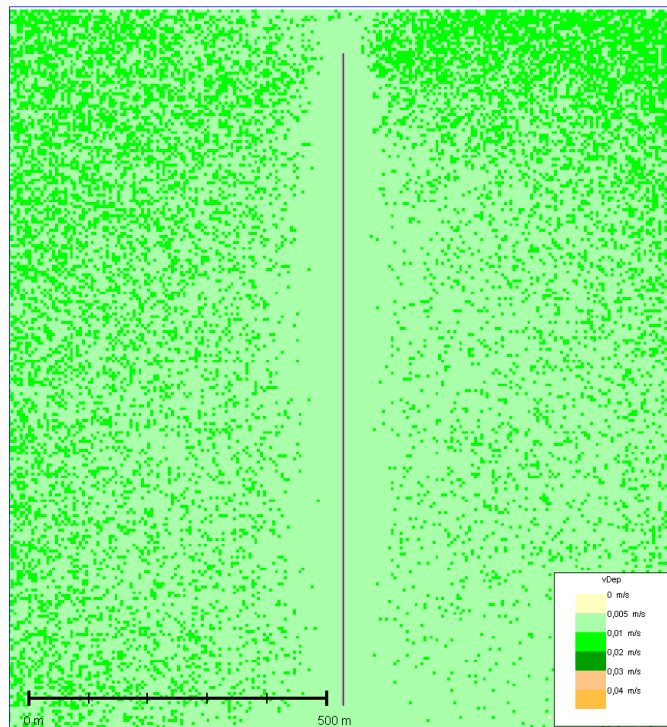
10.3.3 Meteorological input

See test case 2

10.3.4 Results

GRAL meets the deposition velocity of 0.01 m/s in most areas.

Figure 98. Horizontal plane illustrating computed deposition velocities for a roughness length of $z_0 = 0.2\text{m}$



10.4 Deposition velocity - Test Case 4

10.4.1 Model set up

Topography	Flat Terrain
Obstacles	None
Concentration grid	10 m horizontal, 1 m vertical extension, 1 m above ground level
Model domain	2000 m x 2000 m
Number of particles	360,000 per hour
Roughness length	0.5 m

10.4.2 Source configuration

Point source, stack height 20m, exit velocity 0.1 m/s, exit temperature 50°C, diameter 1.0 m, particle density 2 g/cm³

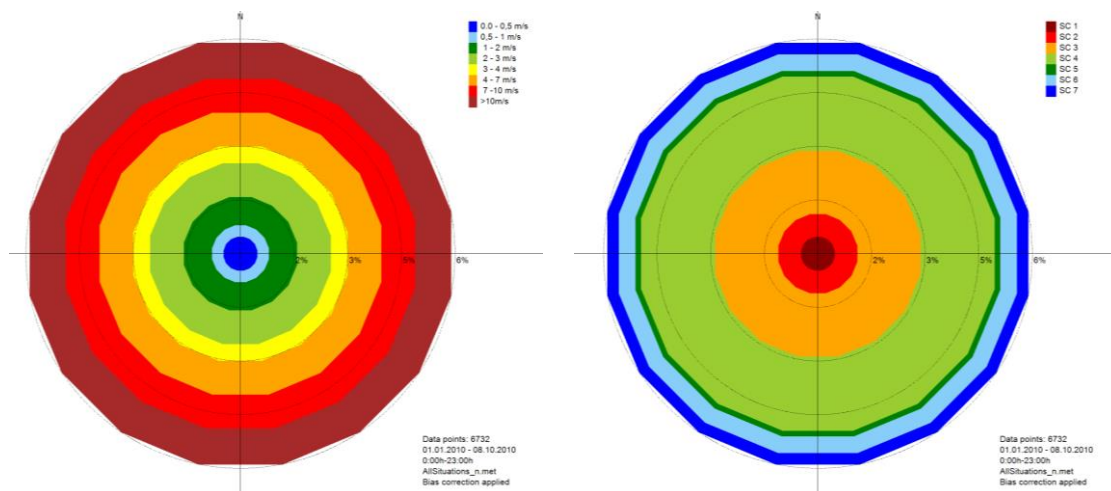
Dry deposition

Particle size	Emission rate	Emission rate	V _{Dep}
PM _{2.5}	0 kg/h	0 kg/d	0.00 m/s
PM ₁₀	1 kg/h	24 kg/d	0.05 m/s
PM ₁₀₀	0 kg/h	0 kg/d	0.00 m/s

10.4.3 Meteorological input

In this case about 1,200 different situations (artificial equally distributed wind directions) have been utilized in the simulations.

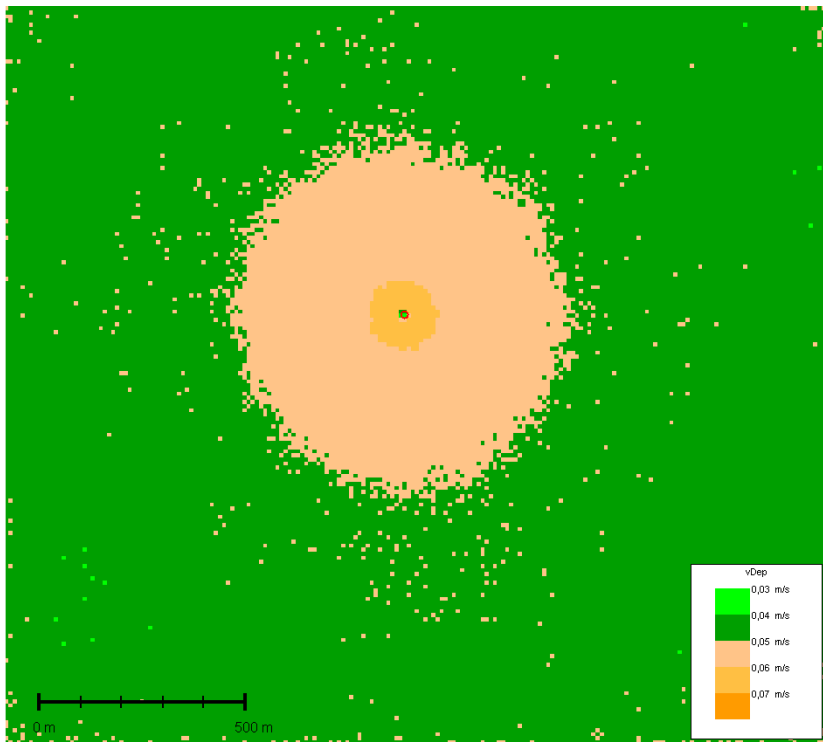
Figure 99. Meteorological input data



10.4.4 Results

GRAL meets the prescribed deposition velocity of 0.05 m/s within a maximum deviation of ± 0.005 m/s.

Figure 100. Horizontal plane illustrating computed deposition velocities for a roughness length of $z_0 = 0.5\text{m}$



10.5 Deposition velocity - Test Case 5

10.5.1 Model set up

Topography	Flat Terrain
Obstacles	None
Concentration grid	10 m horizontal, 1 m vertical extension, 1 m above ground level
Model domain	2000 m x 2000 m
Number of particles	360,000 per hour
Roughness length	0.2 m

10.5.2 Source configuration

Area source, 100x100 m², vertical extension 4 m, particle density 1 g/cm³

Particle size	Emission rate	Emission rate	V _{Dep}
PM _{2.5}	0 kg/h	0 kg/d	0.00 m/s
PM ₁₀	0,2 kg/h	4,8 kg/d	0.01 m/s
PM ₁₀₀	0 kg/h	0 kg/d	0.00 m/s

Dry deposition

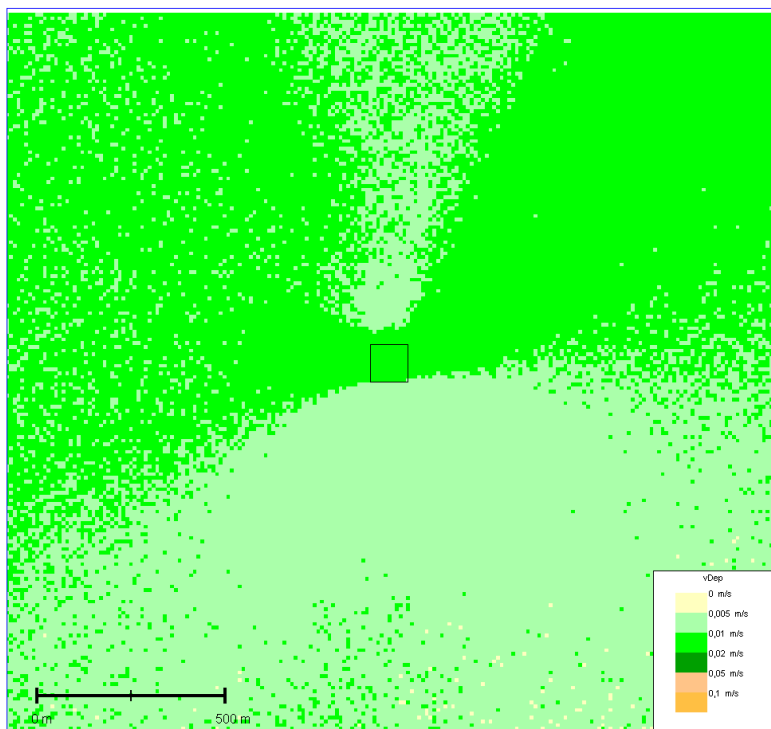
10.5.3 Meteorological input

See test case 2.

10.5.4 Results

GRAL meets the deposition velocity of 0.01 m/s in most areas but slightly underestimates deposition in areas, where wind directions have a low-frequency.

Figure 101. Horizontal plane illustrating computed deposition velocities for a roughness length of $z_0 = 0.2\text{m}$



10.6 Dikopshof

10.6.1 Dataset description

The tracer experiment was performed at the Friedrich-Wilhelms University, Germany, on 18 Februar 2009 (Lodomez, 2010) and consisted of a one hour release of particles, of which 95 % of the total mass was made up by particles in the range $\text{PM}_{2.5} - \text{PM}_{10}$, and 5 % smaller than $\text{PM}_{2.5}$. Two sonic anemometers were used for wind observation at 3 m height above ground level. A total of 12 observational points were placed near a point source, which had a height of 6.5 m above ground level and a diameter of 0.9 m. Exit velocity was constant 10 m s^{-1} . The release rate was 50 g h^{-1} .

Figure 102. Experimental layout



10.6.2 Characterisation

The average observed wind speed 3 m above ground level during the particle release was 3.2 m s^{-1} and the average wind direction was about 165 deg. The corresponding GRAL stability class was neutral (class 4). In GRAL, for particles with an aerodynamic diameter below $\text{PM}_{2.5}$ the standard deposition velocity is 0.001 m s^{-1} , while for particles in the range $\text{PM}_{2.5} - \text{PM}_{10}$ it is 0.01 m s^{-1} . In addition the settling velocity has been calculated in GRAL using a particle density of 2.8 g cm^{-3} .

10.6.3 Model set up

Topography GRAMM	none
Topography GRAL	none
Obstacles	None
Concentration grid	10 m horizontal, 1 m vertical extension
Model domain	480 m x 370 m
Number of particles	360,000 per hour
Roughness length	0.1 m

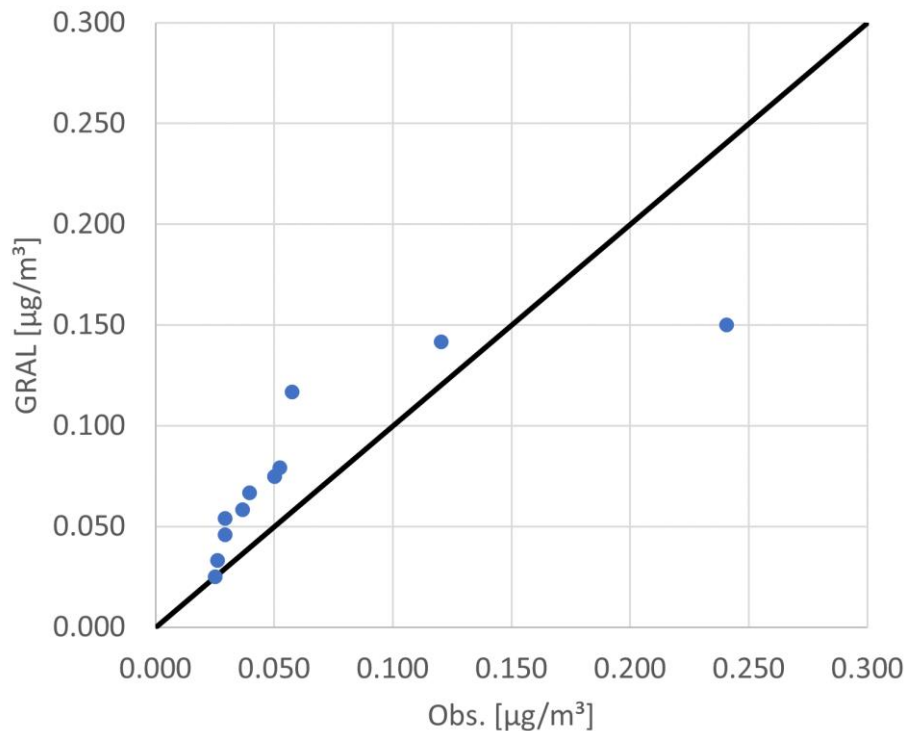
10.6.4 Results

Table 88. Results for the Dikopshof dataset

Model	NMSE	FB	References
GRAL	1.2	0.1	
GRAL V21.09	0.0	-0.2	
GRAL V23.11	0.0	-0.2	

Dry deposition

Figure 103. Quantile-quantile plot of observed and modelled deposition values [mg/m^2] for the Dikopshof experiment GRAL V23.11



10.7 Deposition velocity - Test Case V21.09

10.7.1 Model set up

Topography	Flat Terrain
Obstacles	None
Concentration grid	5 m horizontal, 1 m vertical extension, 1 m above ground level
Model domain	1590 m x 1500 m
Number of particles	360,000 per hour
Roughness length	0.2 m

10.7.2 Source configuration

Line source, 1400 m, vertical extension 4 m, 0.4 m above ground

Particle size	Emission rate	v_{Dep}
PM _{2.5}	0.01 kg/h	0.001 m/s
PM ₁₀	0,99 kg/h/km	0.01 m/s
PM ₁₀₀	0 kg/h	0.00 m/s

10.7.3 Meteorological input

See test case 2 (chapter 10.2).

10.7.4 Results

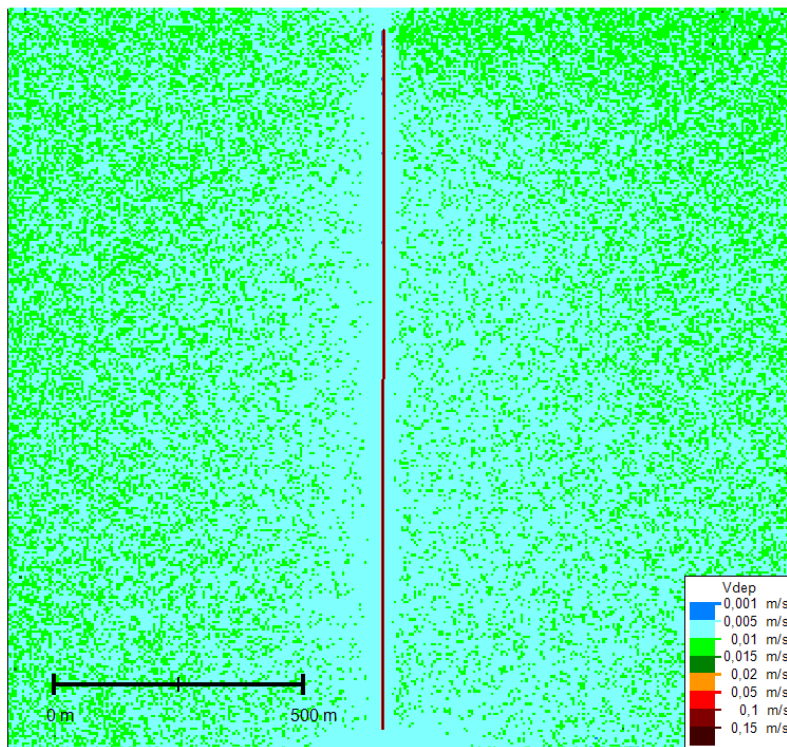
GRAL meets the deposition velocity of $0.01 \text{ m/s} \pm 0.002 \text{ m/s}$ in most areas (see Figure 104).

Using the default scaling factor (see chapter 4.8) one will get significantly higher deposition velocities of $0.01\text{-}0.015 \text{ m/s}$ (see Figure 105) within the vegetation area (green rectangle in the lower right panel, Coverage = 100 %).

With a user defined scaling factor of 5, even higher deposition velocities of up to 0.02 m/s are calculated within the vegetation area (see Figure 106). However, a value of 0.05 m/s is not reached.

Significantly better results can be achieved with the "Adaptive Roughness" option if roughness lengths between 0.2 m and 1.0 m are used. In this case, a deposition velocity of 0.05 m/s is approximately achieved within the vegetation area using a scaling factor of 5 (see Figure 107).

Figure 104. Horizontal plane illustrating computed deposition velocities for a roughness length of $z_0 = 0.2 \text{ m}$



Dry deposition

Figure 105. Horizontal plane illustrating computed deposition velocities for a roughness length of $z_0 = 0.2\text{m}$ within and around a vegetation area using the default scaling factor

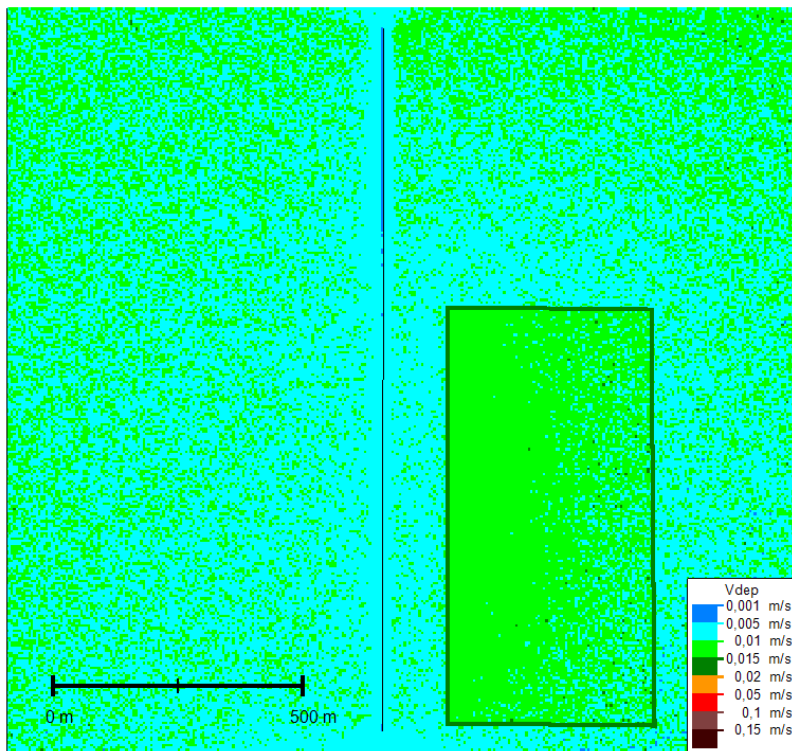


Figure 106. Horizontal plane illustrating computed deposition velocities for a roughness length of $z_0 = 0.2\text{m}$ within and around a vegetation area and a user defined scaling factor of 5

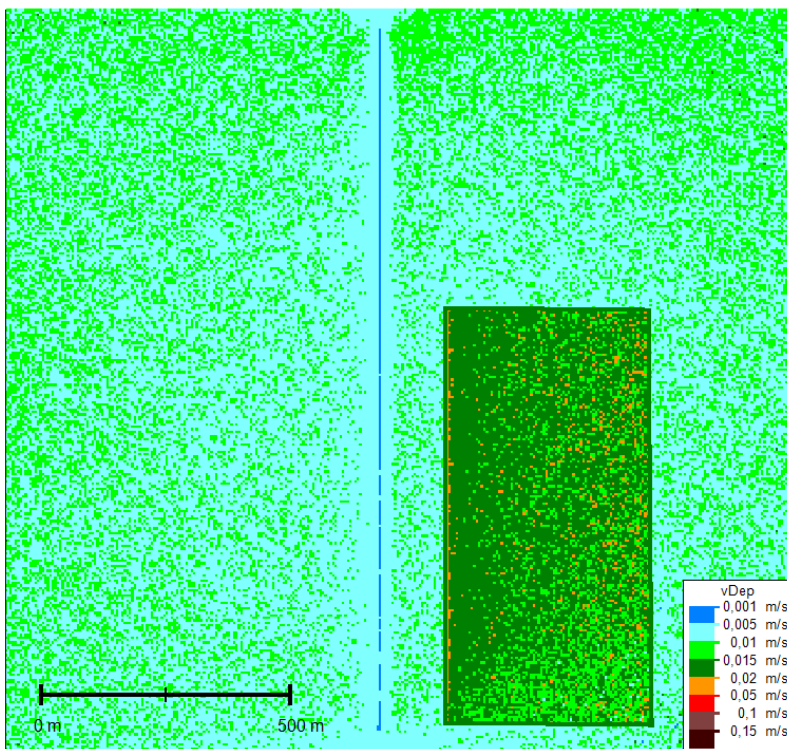
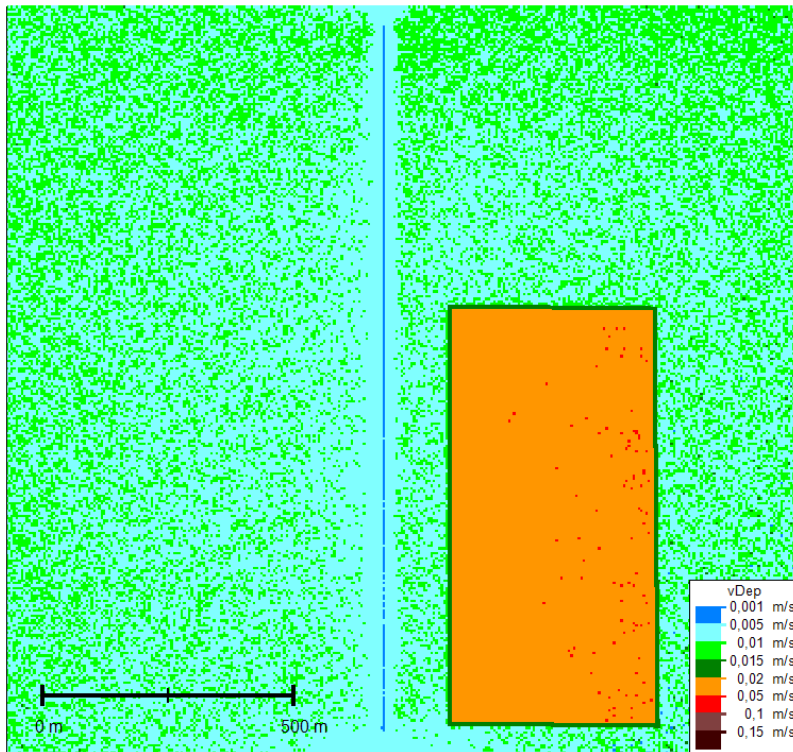


Figure 107. Horizontal plane illustrating computed deposition velocities for a roughness length of $z_0 = 0.2\text{m} - 1.0\text{ m}$ (option “Adaptive roughness”) within and around a vegetation area and a user defined scaling factor of 5



11 Wet deposition

11.1 Masenberg

11.1.1 Dataset description

In Austria exists a monitoring network for wet deposition. Here the focus is on modelling wet deposition of nitrogen for the year 2015 for the station Masenberg, which is situated on a mountain at 1,100 m above sea level. At this station precipitation is registered and stored as half-hourly average values.

11.1.2 Characterisation

In total 4.0 kg/ha nitrogen was observed in 2015 (Pongratz et al., 2016), whereby 2,5 kg/ha nitrogen were found as $\text{NH}_4\text{-N}$, and about 1,5 kg/ha were registered as $\text{NO}_3\text{-N}$. It is assumed that the wet deposition of nitrogen is due to the ambient air concentrations of NH_3 and NH_4NO_3 (ammonium nitrate). Unfortunately, both these chemical compounds are not observed at the station Masenberg, though, within the European PMInter project, ambient air background concentrations were measured at the monitoring station Arnfels (900 m a.s.l.). For ammonium nitrate an average value of $8 \mu\text{g m}^{-3}$ was found in the particle phase in winter time (Kistler et al., 2013). In the warm season ammonium nitrate is practically entirely existent in the gas phase. Therefore, it is assumed that the annual average concentration of ammonium nitrate is equal to $8 \mu\text{g m}^{-3}$.

In 2011 ambient air NH_3 observations were made at the monitoring station Arnfels, which revealed an average concentration of $1.5 \mu\text{g m}^{-3}$ (Öttl et al., 2012).

Figure 108. Observed chemical compounds at various wet-deposition monitoring stations in Styria, Austria, in 2015

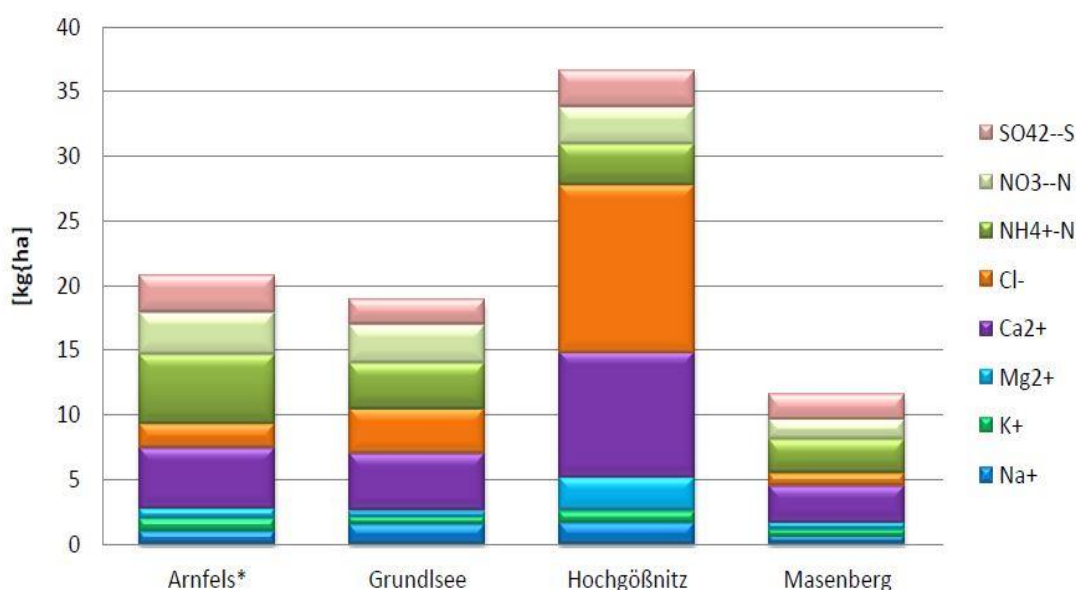
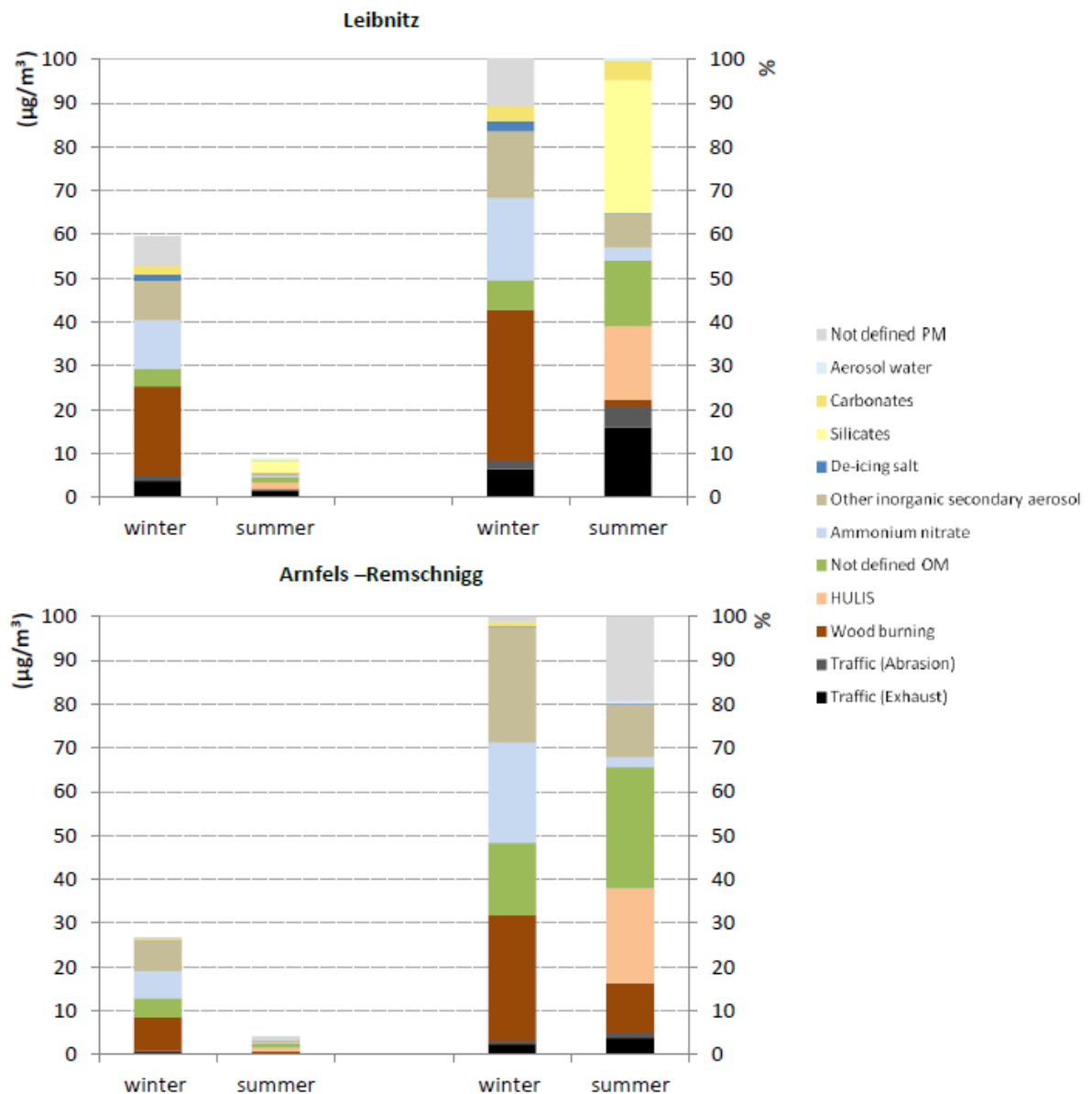


Figure 109. Observed background concentration of ammonium nitrate in the particle phase at Arnfels-Remschnigg in 2011



11.1.3 Model set up

For both ammonium nitrate and ammonia the same empirical parameters for computing wet deposition have been taken:

$$\alpha_w = 0.6$$

$$C_w = 0.00012$$

In order to mimic the background concentrations of NH_3 and NH_4NO_3 a volume source has been defined with a vertical extension of 500 m. Within this source the concentrations have been computed in order to meet the assumed background concentration of each. Above this vertical column concentrations were assumed to be zero.

Wet deposition

GRAL has been operated in transient mode.

Topography GRAMM	none
Topography GRAL	none
Obstacles	None
Concentration grid	50 m horizontal, 500 m vertical extension
Model domain	100 m x 100 m
Number of particles	540,000 per hour
Roughness length	0.2 m

11.1.4 Results

Based on the before mentioned assumptions GRAL suggests the following annual nitrogen deposition:

NH₄-N: 2,4 kg/ha

NO₃-N: 1,4 kg/ha

Both values agree very well with the observations. Due to the many assumptions about the background concentrations, the vertical structure of the ambient air concentrations, and the chemical compounds involved in the wet-deposition process, the simulation results should be interpreted very carefully. It does not necessarily mean that GRAL will perform equal well in other cases. However, it seems as if the physical process of wet deposition has been coded correctly in the model.

12 Odour dispersion

In the following datasets are presented where GRAL model results for the concentration-fluctuation intensity and for odour hour frequencies are compared with field inspections. The concentration-fluctuation intensity is a quantity needed for computing odour hours (see sect. 4.7). As field inspections themselves have a certain range of uncertainty too, these comparisons cannot be seen as pure validation exercises. The uncertainty range for the field inspections has been estimated on the basis of the so-called sampling error, which is computed assuming a binomial distribution. However, this assumption introduces itself some uncertainty, thus, the whole error estimation should just be seen as a rough indicator.

The model simulations in all cases are based on an odour threshold of 1 OU/m³ for the 90th percentile, i.e. in 10 % of the time within one hour higher odour concentrations than 1 OU/m³ occur. Based on many observations one can state that the maximum concentrations are typically 5 times higher than the observed 90th percentile. Thus, one can expect that odour concentrations of about 5 OU/m³ and higher will occur. Such concentrations can be usually well recognized by panellists.

In Austria, odour annoyance is judged on the basis of so called odour hours, whereby an odour hour is given when odour can be perceived for at least 6 minutes (not necessarily continuously). The sum over all odour hours per year, expressed as percentage, is then compared with several thresholds (maximum allowed odour hour frequencies), which depend on odour quality (hedonic). While odour hours can more or less be assessed by field campaigns, modelling odour hours is challenging as dispersion models typically provide average concentrations for 30-60 minutes intervals. In addition, meteorological data is usually stored as average values over these time intervals. In the following simulations, the concentration-variance model as described in 4.7 has been used to estimate the 90th percentile (i.e. 6 minutes) of the odour concentration distribution from the computed hourly mean odour concentration.

12.1 Concentration variance - Uttenweiler

12.1.1 Dataset description

The dataset has already been introduced in sect. 9.17. In addition to mean tracer-gas concentrations, fast-response concentration observations have been carried out, which were used to calculate the concentration variances. In each of the 14 available releases fast-concentration measurements were performed at two sites 1 m above ground level at distances varying between 140 m and 280 m from the stack. Averaging time was 10 minutes and sampling rate was 0,1 Hz.

12.1.2 Characteristics

Mylne and Mason (1991) investigated the effect of the averaging time on the shape of the CDF. In their Fig. 20 a clear dependency on the distance to the source is visible: close to the source (75 m) R_{90} is lower by about 30 % for an averaging time of 10 s compared with R_{90} evaluated using the original data sampled with 10 Hz. At a distance of 100 m the difference is some 20 %, and at a distance of 750 m there is practically no difference visible anymore. Hence, one may expect a slight underestimation of observed R_{90} for the Uttenweiler field experiments due to the low sampling rate.

Observed wind speeds at a nearby installed sonic anemometer ranged between 2.5 m s^{-1} and 7.9 m s^{-1} at a height of 10 m above ground level. Atmospheric stability was neutral in all cases. The terrain around the shed is flat with sparse vegetation (the releases took place in late autumn and winter), thus, the roughness length was estimated to be 0.05 m.

12.1.3 Model set up

Topography	Flat terrain
Obstacles	Microscale prognostic model, mixing-length turbulence closure Horizontal resolution: 2 m Vertical resolution: 1 m Vertical stretching factor: 1.0 Minimum iterations: 100 Maximum iterations: 500 Number of vertical cells: 40
Concentration grid	2 m horizontal, 0.2 m vertical extension, 1.0 m above ground level
Model domain	530 m x 480 m
Number of particles	1,200,000 per hour
Roughness length	0.05 m

12.1.4 Results

The average concentration is significantly underestimated. It might be worth noting that the underestimation of mean concentrations is much less pronounced when including all available sampling points, i.e. including those bag samplers where no fast-response observations were carried out (see chapt. 9.17). In contrast to the mean concentration, concentration-fluctuation intensities are relatively well predicted by the model. The model outperforms clearly the simple assumption of setting $R_{90} = 4$.

Table 89. Comparison of observed and modelled mean concentrations, concentration-fluctuation intensities (CFI), and R_{90} applying the new concentration-variance model and $R_{90} = 4$ using the Uttenweiler experiments (28 data points)

	Obs.	Mod.	Obs.	Mod.	Obs.	Mod.	Mod.
	Mean [ppt]		CFI		$R_{90} (2p \text{ Weibull}^{1.5})$		$R_{90} = 4$
Mean	9.76	6.63	1.03	0.87	2.43	2.81	4.00
FB	-	0.38	-	0.17	-	-0.15	-0.49
NMSE	-	1.06	-	0.40	-	0.13	0.32

12.2 Odour dispersion from a pig-fattening shed

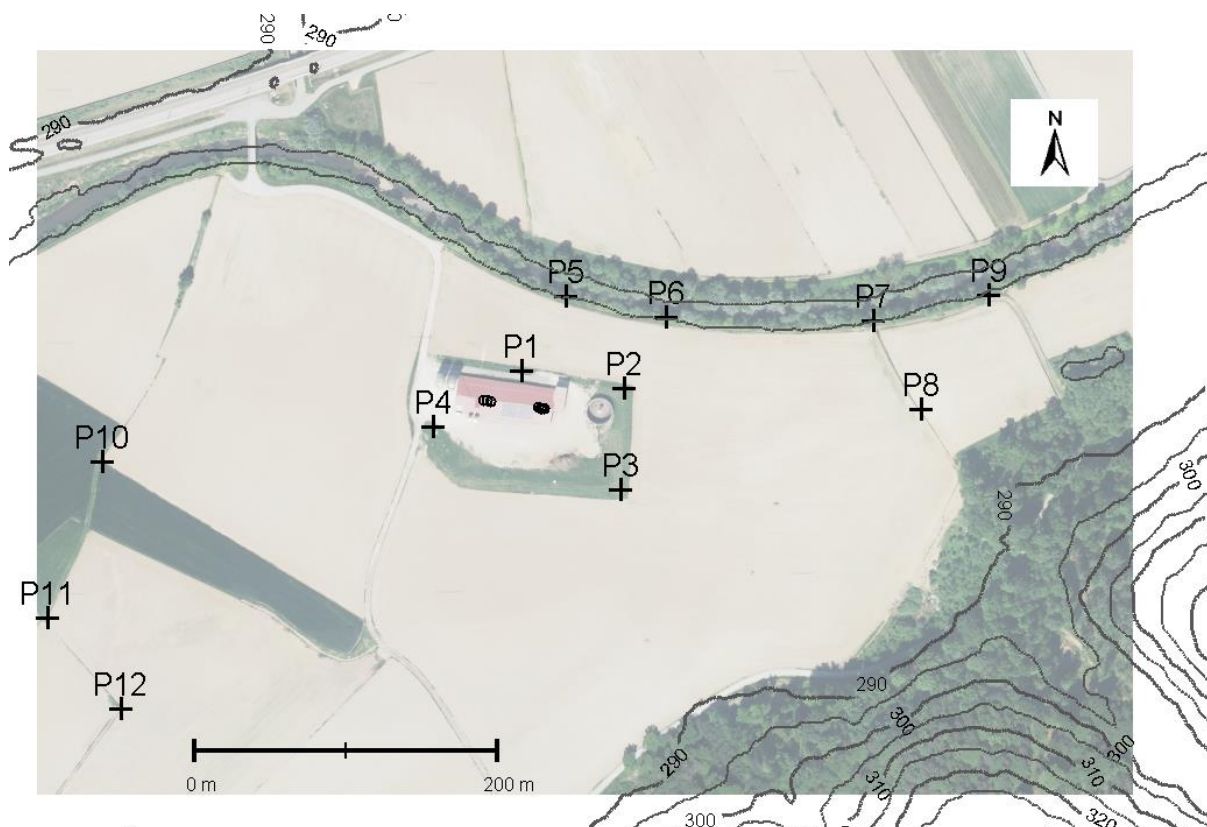
12.2.1 Dataset description

Meteorological data was recorded from February to July 2017, thus not covering a complete year. Field inspections were carried out over the same period. These were made in accordance with the European standard EN 16841-1.

Odour was emitted from a single shed with a total of 6 chimneys, each 8.5 m height. The exit velocity ranged between 1.5 m/s in winter time and about 5.0 m/s in the summer period. The shed itself had a height of 7.0 m. Nearby the shed an open manure storage (205 m²) caused some odour emission, too.

Except to the southeast corner of the modelling area, the terrain was flat with an estimated roughness length of 0.1 m on average (bare soil in winter and maize crops in summer). The odour release rate was 81 MOU/h from the six chimneys and 5.8 MOU/h from the manure storage.

Figure 110. Model domain for dispersion modelling, shed, and position of the inspection points for the panel field study. The meteorological site was positioned close to P3.



12.2.2 Characteristics

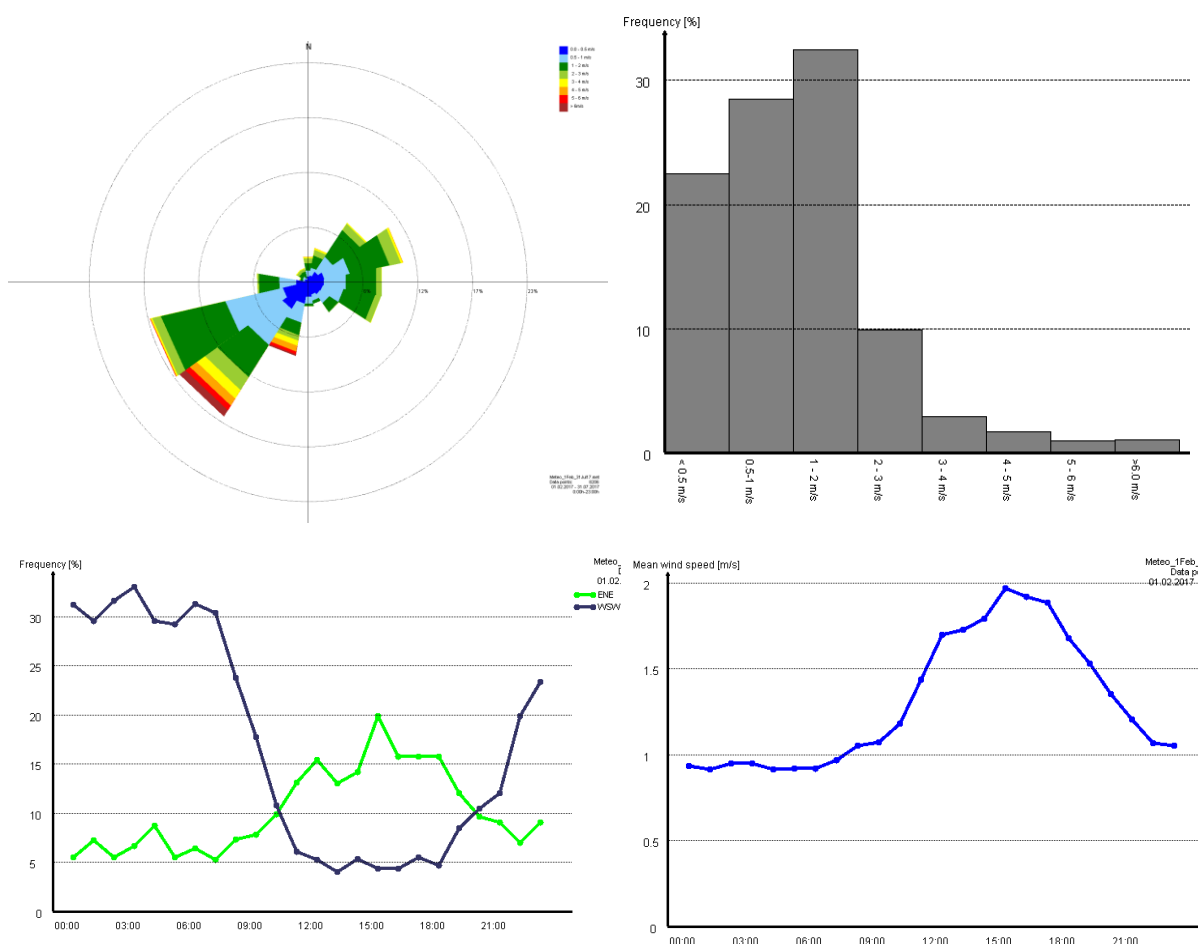
Local wind observations 7 m above ground were taken to run the model. Originally stability classes have been derived according to the recommended method for GRAL (GRAL recommendation guide).

Wind speeds are rather low (annual mean wind speed at 10 m above ground level: 1.4 m/s). Low wind speed conditions ($u < 1.0$ m/s) occur in about 50 % of the time. Stable dispersion conditions prevail in about 45 % of the time. Main wind directions are from southwest and northeast.

Buildings and vegetation have been taken into account in the simulations.

Observed odour-hour frequencies were compared with modelled results using a threshold of 1 OU/m³ in the dispersion model.

Figure 111. Dispersion characteristics



12.2.3 Model set up

Topography	Flat terrain
Obstacles	Microscale prognostic model, mixing-length turbulence closure Horizontal resolution: 2 m

Odour dispersion

	Vertical resolution: 1.0 m Vertical stretching factor: 1.01 Minimum iterations: 100 Maximum iterations: 500 Number of vertical cells: 25
Concentration grid	2 m horizontal, 1 m vertical extension, 1.5 m above ground level
Model domain	820 m x 570 m
Number of particles	720,000 per hour
Roughness length	0.1 m
Adaptive Roughness	1.0 m
Vegetation	considered for GRAL V23.09

12.2.4 Results

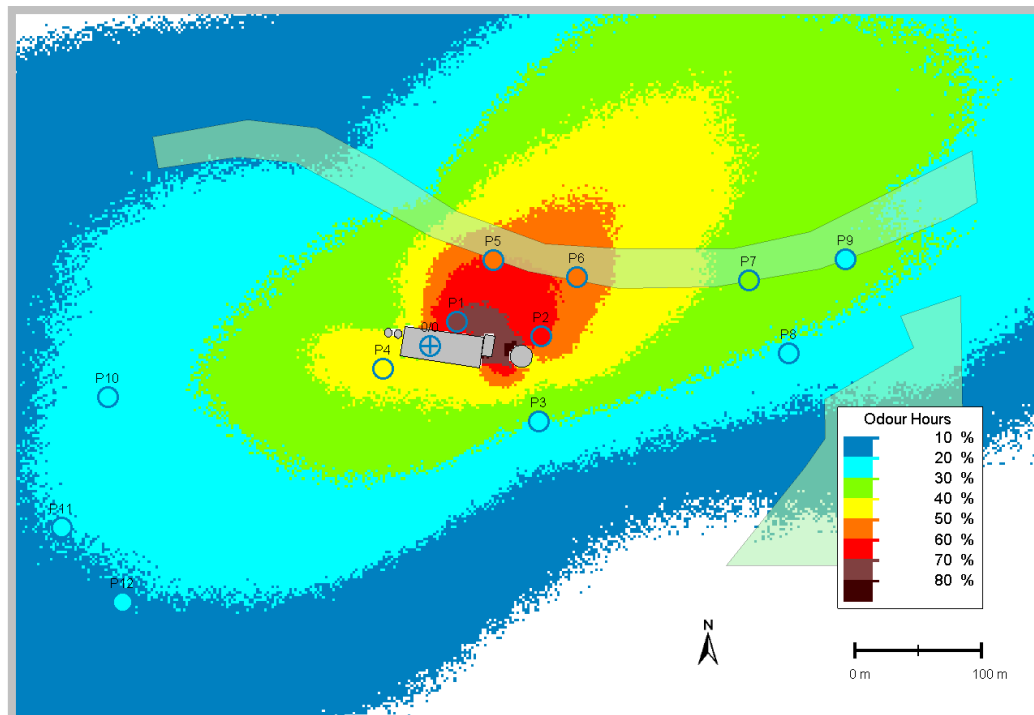
There are two uncertainties related with field studies and the limited number of inspections: (i) a certain lower threshold for the achievable resolution (given in column 2), and (ii) a certain sampling error as the limited number of inspections is taken representative for the entire period over which the field study was run. The sampling error has been numerically computed in this case by arbitrarily seeding “odour hours” within the investigation period and subsequently arbitrarily picking the hours. This procedure has been repeated 500 times for each observed odour-hour frequency. The uncertainty range presented in column 3 of the following table is based on the 95 confidence interval.

GRAL suggests odour-hour frequencies within the range of uncertainty of the field inspections for all points.

Table 90. Observed and modelled odour hours in [%]

Receptor	Obs.	Resolution	Uncertainty range	GRAL	GRAL V21.09	GRAL V23.11
1	70	±1	62 - 79	68	70	71
2	60	±1	51 – 69	59	62	61
3	22	±1	13 – 29	23	27	31
4	38	±1	29 – 47	40	41	44
5	50	±1	41 – 60	56	60	59
6	48	±1	38 – 58	54	56	57
7	28	±1	18 – 37	35	37	38
8	24	±1	14 – 32	26	27	29
9	24	±1	14 – 32	30	31	33
10	22	±1	13 – 30	21	24	21
11	20	±1	12 – 28	20	20	24
12	24	±1	14 - 32	19	20	19

Figure 112. Observed and modelled (low pass filter off) odour hours in [%] (V23.11 incl. adaptive roughness and vegetation)



12.3 Odour dispersion within a village

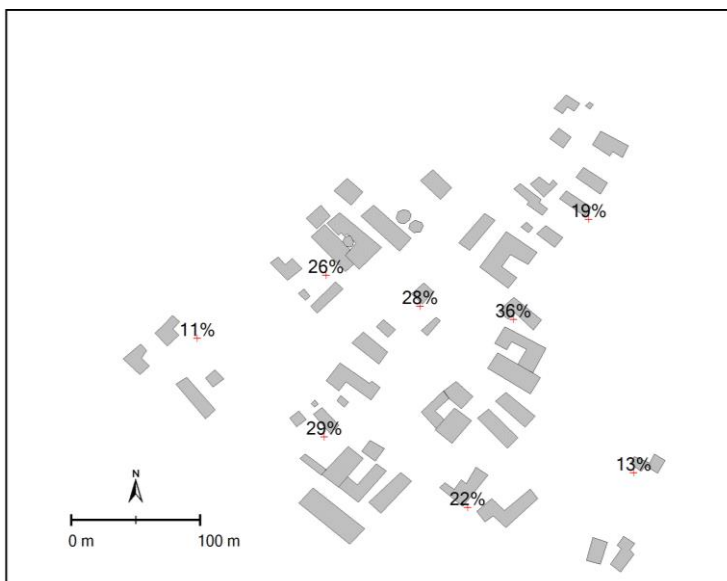
12.3.1 Dataset description

The provision of the data by the Environmental Advocacy Office of the Federal State of Upper Austria is greatly acknowledged.

Meteorological data was recorded from March to October 2005, thus not covering a complete year. Field observations were carried out over the same period. These were made in accordance with the German VDI guideline 3940-1 "Measurement of odour impact by field inspection - Measurement of the impact frequency of recognizable odours - Grid measurement".

Several farms for fattening pigs were situated within a small village. All receptor points of the panel field study were placed within the village.

Figure 113. Model domain for dispersion modelling, buildings, and position of the inspection points for the panel field study. Numbers indicate the observed frequency of odour hours. The meteorological site was slightly outside the domain.



Terrain is quite flat and was therefore not taken into account in the dispersion simulations. All in all 2,000 fattening pigs, some 600 piglets, and about 150 breeding sows were present in the livestock buildings. Some of the stables were ventilated via stacks at roof top level, while others had no ventilation, i.e. air exchange was managed by keeping windows open.

Basically, emission factors provided by VDI 3894-1 (2009) were applied. However, in case of the non-artificially ventilated stables emissions were reduced by 50 %. Jeppsson (2003) found a strong positive correlation of ammonia emission rates in $[\text{kg h}^{-1}]$ on ventilation rates in fattening pig stables. It is assumed that the non-forced ventilated stables owe rather low ventilation rates of about 10 % of those being artificially ventilated. KTBL (2012) provides the following relationship between normalized volume flux V_n and emission factor e :

$$e = e_0 V_n^{c_v} \quad (107)$$

In equation (1) e_0 is the basic emission factor taken from VDI 3894-1 (2009), which is only valid for stables with forced ventilation and not representative for non-ventilated stables. Schauburger et al. (2012) found for the empirical constant c_v a value of 0.32 in case of odour. Inserting these values results in $e/e_0 = 0.5$.

As for dataset A, in total 55 MOU h^{-1} were released from the livestock buildings.

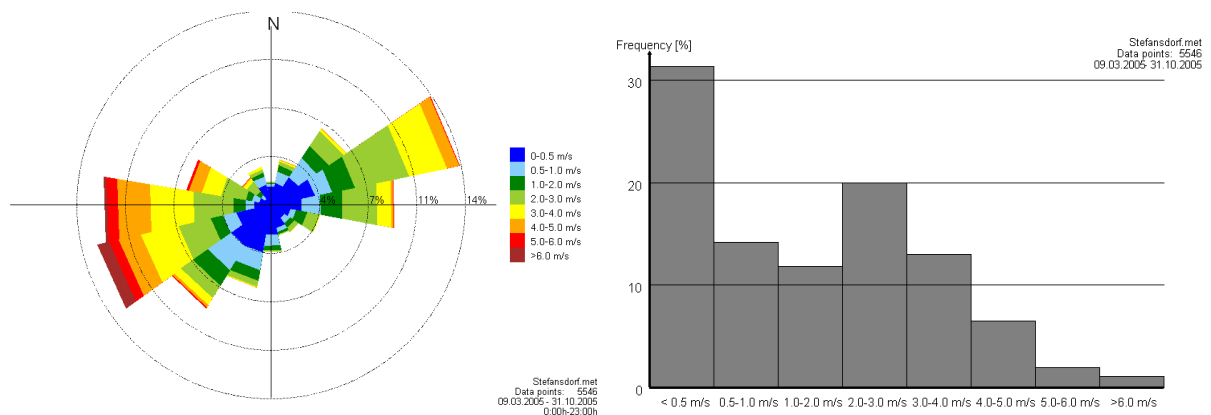
12.3.2 Characteristics

Local wind observations 10 m above ground were taken to run the model. Originally stability classes have been derived according to the Austrian standard method (OENORM M9440), which does provide very unstable conditions (stability class A), introducing bit of uncertainty as the Austrian standard method does not confirm with the GRAL method outlined in this report.

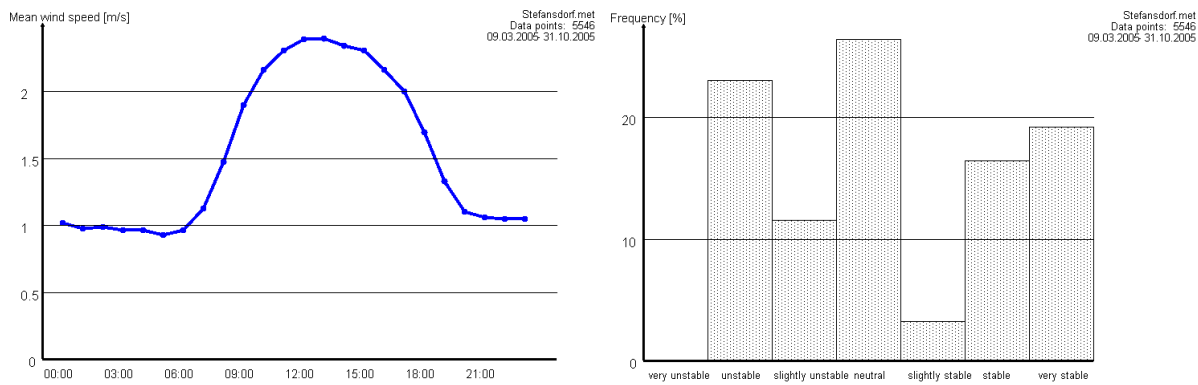
Wind speeds are rather low (annual mean wind speed at 10 m above ground level: 1.6 m/s). Low wind speed conditions ($u < 1.0$ m/s) occur in about 45 % of the time. Stable dispersion conditions occur in about 40 % of the time. Main wind directions are from southwest and northeast.

As outlined in Oettl and Oitzl (2016) the effective odour threshold for evaluating odour hours was set to 1.2 OU/m^3 in order to be able to compare results with data from the field inspections.

Figure 114. Dispersion characteristics



Odour dispersion



12.3.3 Model set up

Topography	Flat terrain
Obstacles	Microscale prognostic model, mixing-length turbulence closure Horizontal resolution: 3 m Vertical resolution: 1.5 m Vertical stretching factor: 1.01 Minimum iterations: 100 Maximum iterations: 500 Number of vertical cells: 25
Concentration grid	3 m horizontal, 1 m vertical extension, 1.6 m above ground level
Model domain	700 m x 450 m
Number of particles	360,000 per hour
Roughness length	0.5 m

12.3.4 Results

There are two uncertainties related with field studies and the limited number of inspections: (i) a certain lower threshold for the achievable resolution (given in column 2), and (ii) a certain sampling error as the limited number of inspections is taken representative for the entire period over which the field study was run. The sampling error has been numerically computed in this case by arbitrarily seeding “odour hours” within the investigation period and subsequently arbitrarily picking the hours. This procedure has been repeated 500 times for each observed odour-hour frequency. The uncertainty range presented in column 3 of the following table is based on the 95 confidence interval. It should be noted that the uncertainty range obtained with this procedure results in smaller values than suggested in the VDI guideline 3940-1.

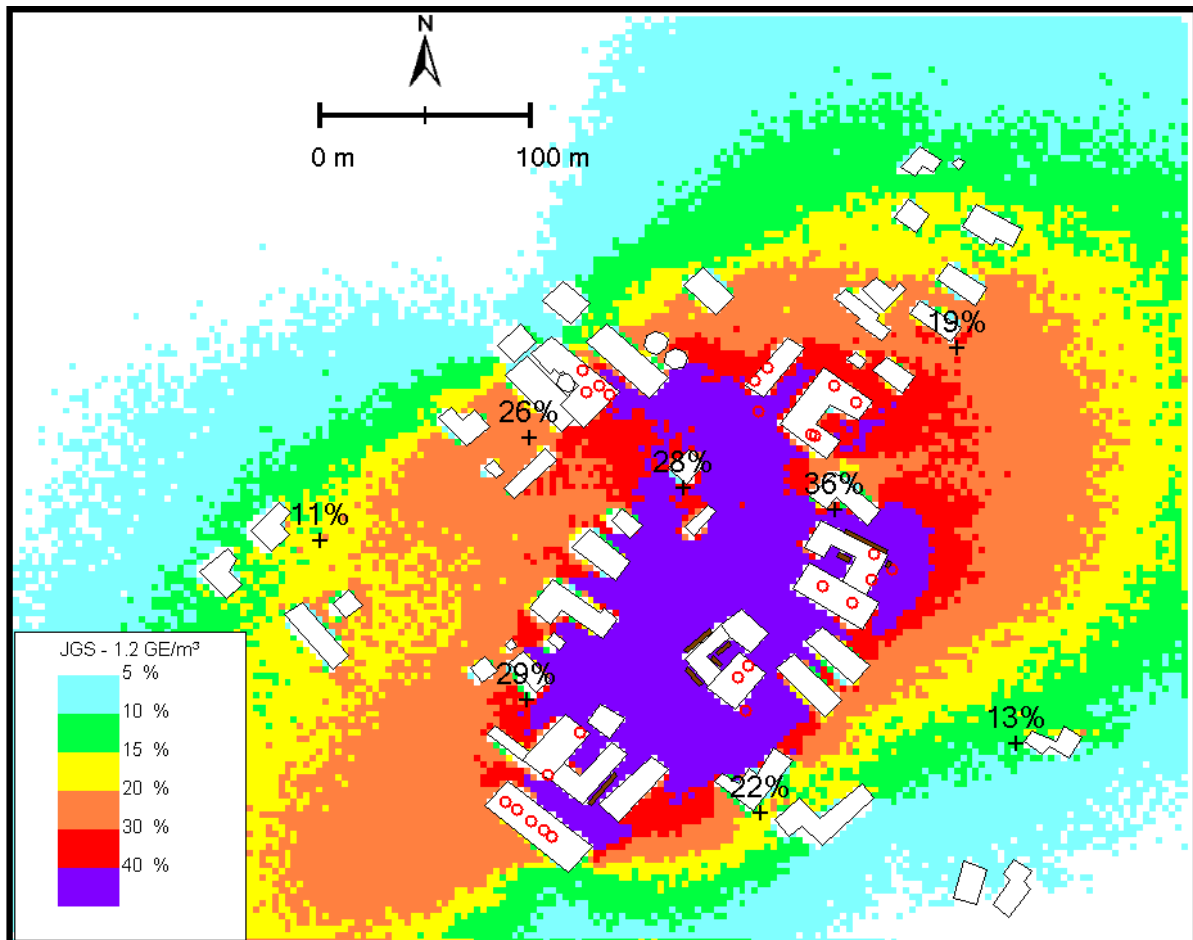
GRAL suggests odour-hour frequencies well within the uncertainty range of the field inspections for all points.

Table 91. Observed and modelled odour hours in [%]

Obs.	Resolution	Uncertainty range	GRAL
13	±1	8 – 21	13
22	±1	14 – 31	20

29	±1	20 – 39	29
11	±1	7 – 18	16
26	±1	18 – 36	24
28	±1	19 – 38	35
36	±1	27 – 46	45
19	±1	12 - 27	25

Figure 115. Observed and modelled odour hours in [%]



12.4 Odour impact from a farm with multiple sheds

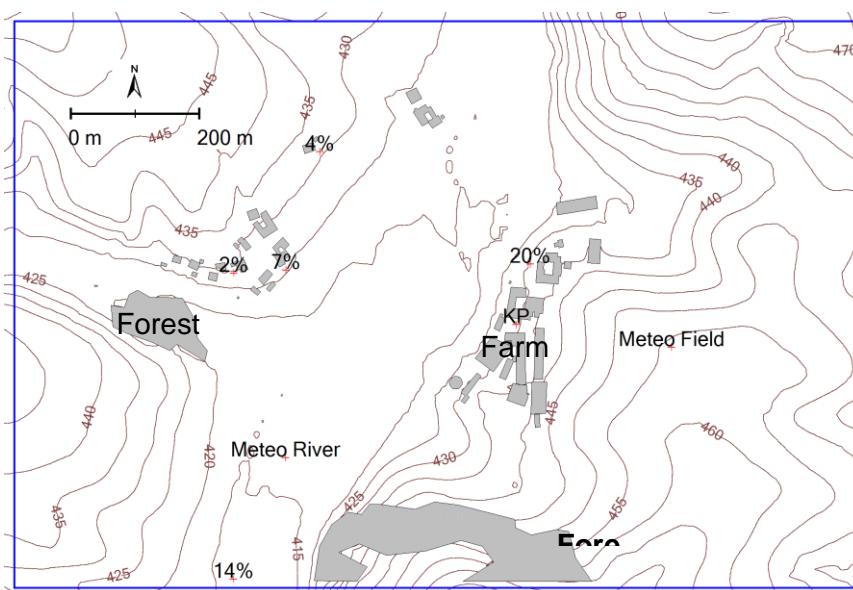
12.4.1 Dataset description

The provision of the data by the Environmental Advocacy Office of the Federal State of Upper Austria is greatly acknowledged.

Meteorological data was recorded from March to September 2007, thus not covering a complete year. Field observations were carried out over the same period. These were made in accordance with the German VDI guideline 3940-1 "Measurement of odour impact by field inspection - Measurement of the impact frequency of recognizable odours - Grid measurement".

Panel field inspections to assess the odour burden were carried out in the vicinity of a farm for 1,600 fattening pigs and 17,000 broilers. Further odour sources at the farm were an open liquid manure storage and a partly open corn silage. As multi-phase feeding for the fattening pigs is applied, odour emissions given by VDI 3894-1 (2009) were cut by 20 %, while for all other sources the emission factors as suggested by VDI 3894-1 (2009) were utilized. In total, 55 MOU h⁻¹ resulted for the site. The pig stable was ventilated via several stacks mounted at the roof, while the broiler stables were ventilated through horizontal openings in the building. With one exception all points for the field inspection were located at distances several hundreds of metres away from the livestock buildings. The area is characterized by softly rolling terrain, small forests, which are treated as obstacles in the dispersion modelling.

Figure 116. Model domain for dispersion modelling, orography, buildings, forests, and position of the meteorological stations as well as the inspection points for the panel field study. Numbers indicate the observed frequency of odour hours.



Odour dispersion

	Number of vertical cells: 30
Concentration grid	3 m horizontal, 2 m vertical extension, 2 m above ground level
Model domain	1.300 m x 900 m
Number of particles	360,000 per hour
Roughness length	0.1 m

12.4.4 Results

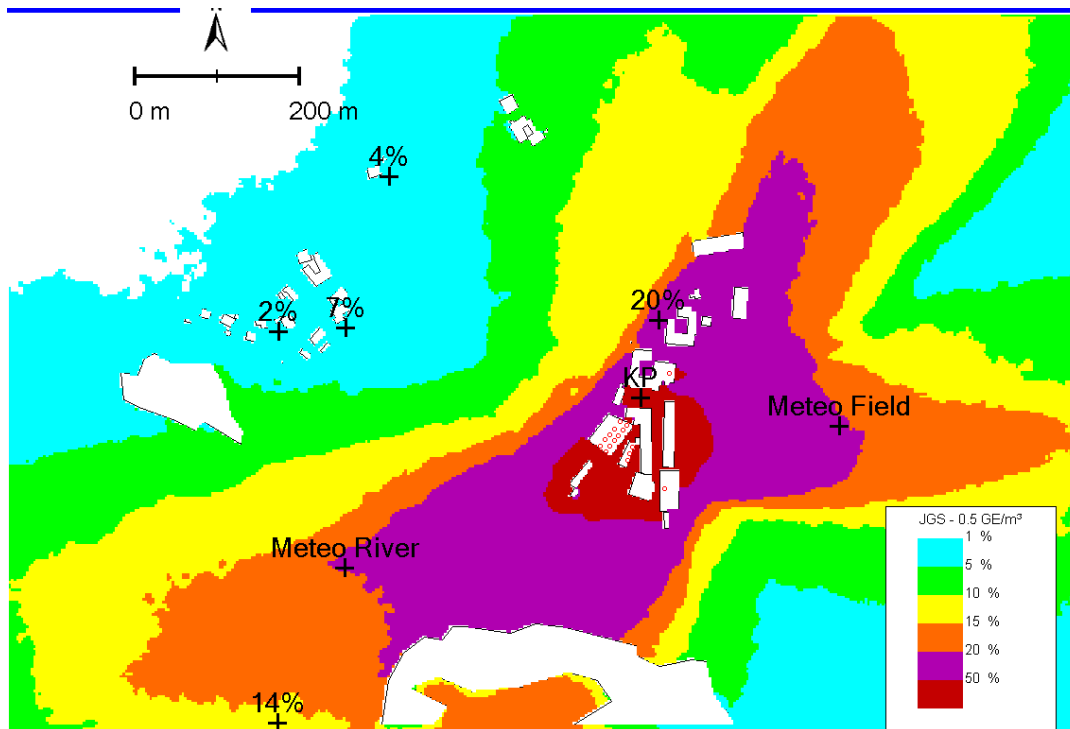
There are two uncertainties related with field studies and the limited number of inspections: (i) a certain lower threshold for the achievable resolution (given in column 2), and (ii) a certain sampling error as the limited number of inspections is taken representative for the entire period over which the field study was run. The sampling error has been numerically computed in this case by arbitrarily seeding “odour hours” within the investigation period and subsequently arbitrarily picking the hours. This procedure has been repeated 500 times for each observed odour-hour frequency. The uncertainty range presented in column 3 of the following table is based on the 95 confidence interval. It should be noted that the uncertainty range obtained with this procedure results in smaller values than suggested in the VDI guideline 3940-1.

GRAL suggests odour-hour frequencies well within the uncertainty range of the field inspections for all points, except one.

Table 92. Observed and modelled odour hours in [%]

Obs.	Resolution	Uncertainty range	GRAL
14	±1	9 – 22	14
2	±1	1 – 5	2
7	±1	4 – 13	3
4	±1	2 – 9	3
20	±1	12 – 28	25

Figure 118. Observed and modelled odour hours in [%]



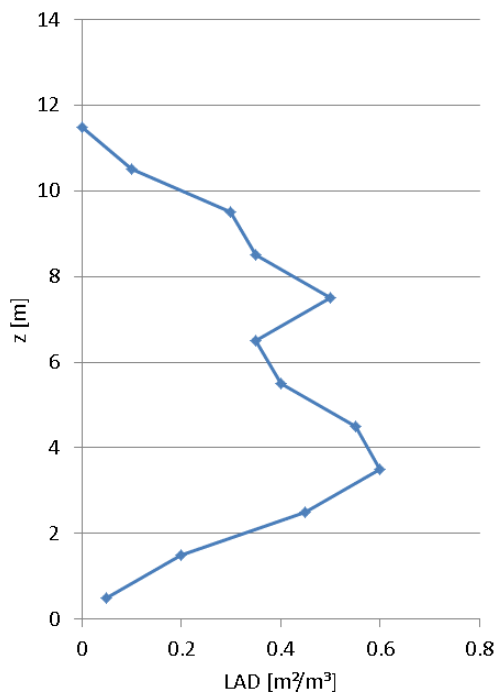
13 Vegetation

13.1 Test Aspen

13.1.1 Dataset description

Amiro (1990) carried out field experiments in a 12 m high aspen forest. Here, the observed wind profile within the Aspen canopy is used for comparison with GRAL. The measured height-dependent leave-area density was used in the simulations. Neutral atmospheric conditions were assumed with a wind speed of 2.3 m s^{-1} at 13 m above ground level. The roughness length was set to 0.5 m in the GRAL simulations.

Figure 119. Leave-area density as observed by Amiro (1990) in an Aspen canopy



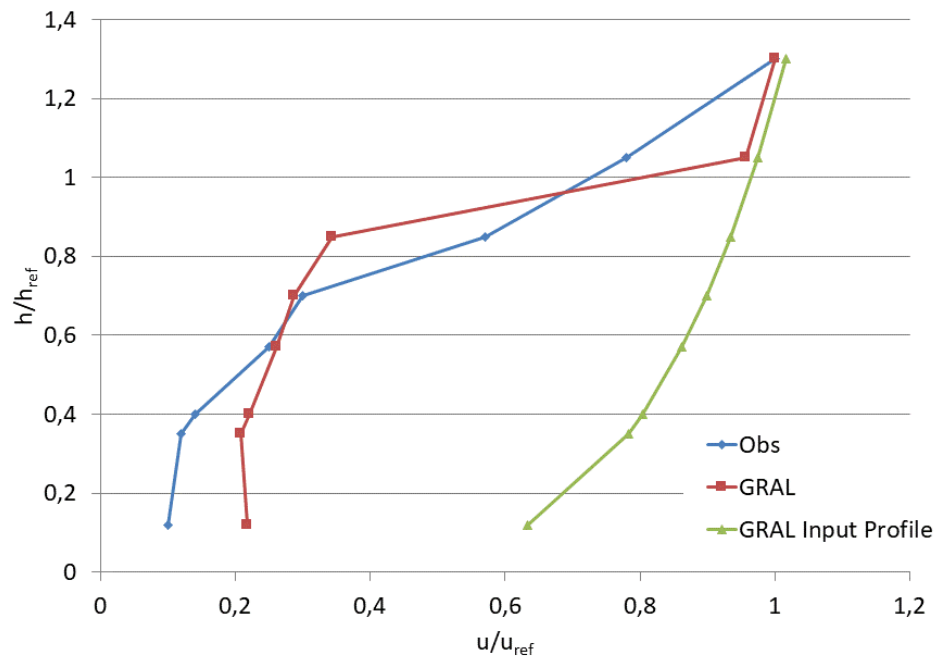
13.1.2 Model set up

Topography	Flat terrain
Obstacles	Microscale prognostic model, mixing-length turbulence closure Horizontal resolution: 2 m Vertical resolution: 0.5 m Vertical stretching factor: 1.01 Minimum iterations: 100 Maximum iterations: 500 Number of vertical cells: 40
Model domain	260 m x 150 m
Roughness length	0.5 m

13.1.3 Results

The agreement between observed and modelled wind profile within the Aspen canopy is not perfect, though, including vegetation in GRAL greatly improves the wind profile compared with the wind profile without vegetation (=input profile).

Figure 120. Comparison of observed and modelled wind profile within the Aspen canopy layer



15 References

- Almbauer, R. A. (1995): A New finite volume discretisation for solving the navier-stokes-equations. Numerical Methods in Laminar and Turbulent Flow 9, Pineridge Press, Swansea, UK., 286-295.
- Almbauer, R.A., Oettl D., Bacher M., and Sturm P.J. (2000a): Simulation of the air quality during a field study for the city of Graz, Atmos. Environ., 34, pp. 4581-4594.
- Almbauer, R.A., Piringer M., Baumann K., Öttl D., and Sturm P.J. (2000c): Analysis of the daily variations of wintertime air pollution concentrations in the city of Graz-Austria, Environmental Monitoring and Assessment, 65 (1/2), 79-87.
- Amiro, B.D. (1990): Comparison of turbulence statistics within three boreal forest canopies. Bound. Layer Meteorol., 51, 99 - 121
- Anfossi D., D. Oettl, G. Degrazia and A. Goulart (2004): An analysis of sonic anemometer observations in low wind speed conditions. Boundary Layer Meteorology, 114, 179-203.
- Anfossi, D., E. Ferrero, G. Brusasca, A. Marzorati, and G. Tinarelli (1993): A simple way of computing buoyant plume rise in Lagrangian stochastic dispersion models. Atmos. Environ., 27A, 1443-1451.
- Anfossi, D., G. Degrazia, E. Ferrero, S.E. Gryning, M.G. Morselli, and S. Trini Castelli (2000): Estimation of the Lagrangian structure function constant C0 from surface layer wind data. Boundary-Layer Meteor., 95, 249-270.
- Anfossi, D., S. Alessandrini, S. Trini Castelli, E. Ferrero, D. Oettl, G. Degrazia (2006): Tracer dispersion simulation in low wind speed conditions with a new 2-D Langevin equation system. Atmos. Environ., 40, 7234-7245.
- Anfossi, D., E. Canepa, H. van Dop (2003): Plume Rise. Chap. 6 of Air Quality and Modeling – Theories, Methodologies, Computational Techniques, and Available Databases and Software. Vol. 1 – Fundamentals (P. Zannetti, Ed.). Published by the EnviroComp Institute (<http://www.envirocomp.org/>) and the Air & Waste Management Association (<http://awma.org/>).

- Anfossi, D., G. Tinarelli, S. Trini Castelli, E. Ferrero, D. Oetl, G. A. Degrazia (2010), L. Mortarini: Well mixed condition verification in windy and low wind speed conditions. *Int. J. Environment and Pollution*, Vol. 40, No. 1/2/3, 49-61
- Anfossi, D., F. Desiato, G. Tinarelli, G. Brusasca, E. Ferrero, D. Sacchetti (1998) "TRANSALP 1989 experimental campaign - Part II: Simulation of a tracer experiment with Lagrangian particle models". *Atmospheric Environment*, 32, 1157-1166.
- ASTM (2000): Standard guide for statistic evaluation of atmospheric dispersion model perfomrance. American Society for Testing and Materials, Destination D 6589-00 ASTM Internatinoal, West Conshohocken, PA (USA), 17pp.
- Barad, M.L. (Editor), (1958): Project Prairie Grass, A field program in diffusion. A Geophysical Research Paper, No. 59, Vol I and II, Report AFCRC-TR-58235, Air Force Cambridge Research Center, 439 pp.
- Bächlin, W., A. Rühling, A. Lohmeyer (2002): Bereitstellung von Validierungsdaten für Geruchsausbreitungsmodelle – Naturmessungen. Forschungsbericht FKA-BWPLUS BWE 2003, 187 pp.
- Baumann-Stanzer, K. (2012): Personnel Communication.
- Benson, P. (1984): CALINE 4 – A dispersion model for predicting air pollutant concentrations near roadways. Office of Transportation Laboratory California Depsaartment of Transporation Sacramento, FHWA/CA/TL-84/15, 247 pp.
- Brusasca G., Tinarelli G. and Anfossi D. (1992): Particle model simulation of diffusion in low windspeed stable conditions. *Atmospheric Environment* 26 A, 707-723
- Carvalho J. C., D. Anfossi, S. Trini Castelli, G. A. Degrazia (2002) "Application of a model system for the study of transport and diffusion in complex terrain to the TRACT experiment". *Atmospheric Environment*, 36, 1147-1161.
- CERC (2013): ADMS 5 Validation Summary. Cambridge Environmental Research Consultants <http://www.cerc.co.uk/environmental-software/model-validation.html>
- Chang, J.C., and S.R. Hanna, 2004: Air quality model performance evaluation. *Meteorology and Atmospheric Physics*, 87, 167-196.

References

- DeBaas, H. van Dop, and F.T.M. Nieuwstadt (1986): An application of the Langevin equation for inhomogenous conditions to dispersion in the convective boundary layer. *Quart. J. Roy. Meteor. Soc.*, 112, 165-180.
- Degrazia, G.A. and Anfossi D. (1998): Estimation of the Kolmogorov constant C_0 from classical statistical diffusion theory. *Atmos. Environ.*, 32, 3611-3614.
- Eichhorn, J., A. Kniffka (2010): The numerical flow model MISKAM: state of development and evaluation of the basic version. *Met. Zeitschrift*, 19, 81-90.
- Eichhorn, J. (2011): MISKAM. Handbuch zu Version 6. pp 60. URL: http://www.lohmeyer.de/de/system/files/content/download/software/HB_MISKAM.pdf
- Ellerman, T., P. Løfstrøm (2002): Spredning af lugt fra svinestalde; SF6-racermålinger ved Roager i 1999 og 2000. (Dispersion of odour from pig houses; SF6 tracer gas measurements). Unpublished report from the National Environmental Research Institute, Denmark. 40 pp.
- Ellis, K., Ch. McHugh, D. Carruthers, and A. Stidworthy (2001): Comparison of ADMS-Roads, CALINE4 and UK DMRB Model Predictions for Roads. 7th Int. Conf. on Harmonisation within Atmospheric Dispersion Modelling for Regulatory Purposes. Belgirate, Italy, 28-31 May 2001.
- EN 16841-1 (2016): Ambient air – Determination of odour in ambient air by using field inspection – Part 1: Grid method. Draft version. 53 pp
- Ferrero, E., L. Mortarini, F. Purghè (2016): A simple parameterization for the concentration variance dissipation in a Lagrangian single-particle model. *Boundary-Layer Meteorol* (in print)
- Finardi S., Brusasca G., Calori G., Nanni A., Tinarelli G., Agnesod G., Pession G., Zublena M. (2002): Integrated air quality assessment of an alpine region: evaluation of the Mont Blanc tunnel re-opening effects. 8th Conference on Harmonization within Atmospheric Dispersion Modeling for Regulatory Purposes. Sofia, 14-17 October, 404-408.
- Finardi, S. and Pellegrini, U., 2004: Systematic analysis of meteorological conditions causing severe urban air pollution episodes in the central Po valley. In: *Proceedings of the Ninth International Conference on Harmonisation within*

- atmospheric dispersion modelling for regulatory purposes. Garmisch-Partenkirchen, Germany, Forschungszentrum Karlsruhe, Vol. 2, pp. 75-79.
- Finn, D., Clawson, K.L., Carter, R.G., Rich, J.D., Eckman, R.M., Perry, S.G., Isakov, V. and Heist, D.K., 2010: Tracer studies to characterize the effects of roadside noise barriers on near-road pollutant dispersion under varying atmospheric stability conditions. *Atmos. Environ.*, 44, 204-214.
- Flassak, Th. (2008): Vergleich von den mit MISKAM und AUSTAL2000 berechneten Konzentrationen mit Naturmessungen in der Göttinger Strasse. 3. WinMISKAM-Benutzertreffen 24. April 2007 Garmisch-Partenkirchen, Ingenieurbüro Lohmeyer, Karlsruhe und Dresden, 13 pp.
- Flassak, Th., and C. Blessing (2007): Vergleich von Windkanalmessungen mit den von MISKAM und AUSTAL2000 berechneten Konzentrationen für U-förmiges Gebäude. 3. WinMISKAM-Benutzertreffen 24. April 2007 Garmisch-Partenkirchen, Ingenieurbüro Lohmeyer, Karlsruhe und Dresden, 30 pp.
- Franzese, P., A.K. Luhar, M.S. Borgas (1999): An efficient Lagrangian stochastic model of vertical dispersion in the convective boundary layer. *Atmos. Environ.*, 33, 2337-2345.
- Frenkiel F.N. (1953): Turbulent diffusion: mean concentration distribution in a flow field of homogeneous turbulence. *Adv. Appl. Mech.*, 3, 61-107.
- Gidhagen, L., Johansson, C., Langner, J., Olivares, G. (2004): Simulation of NO_x and ultrafine particles in a street canyon in Stockholm, Sweden. *Atmos. Environ.*, 38, 2029-2044.
- Golder, D. (1972): Relations among stability parameters in the surface layer. *Boundary-Layer Meteor.*, 3, 47-58.
- Grawe, D., K. H. Schlünzen, F. Pascheke (2013): Comparison of results of an obstacle resolving microscale model with wind tunnel data. *Atmospheric Environment*, 79, 495-509
- Grawe, D., W. Bächlin, H. Brünger, J. Eichhorn, J. Franke, B. Leitzl, W. J. Müller, D. Oettl, M. Salim, K. H. Schlünzen, Ch. Winkler, and M. Zimmer (2014): An updated evaluation guideline for prognostic microscale wind field models. 6th Int. Symposium on Computational Wind Engineering, 8 – 12. June Hamburg.

References

- Green, S.R. (1992): Modeling turbulent air flow in a stand of widely-spaced trees. The PHOENICS Journal of Computational Fluid Dynamics and its Applications 5, 294 – 312, Wimbledon.
- Hanna S.R. (1989): Plume dispersion and concentration fluctuations in the atmosphere, Encyclopaedia of Environmental Control Technology, Volume 2, Air Pollution Control, P.N. Cheremisinoff Editor, Houston, Texas, Gulf Publishing Co.
- Hanna, S. R. (1982): Applications in air pollution modeling. Atmospheric Turbulence and Air Pollution Modeling, F. T. M. Nieuwstadt and Van Dop H., Ed., Chapter 7, Reidel, Dordrecht.
- Hernan, M.A., and J. Jimenez (1982): Computer analysis of a highspeed film of the plane turbulent mixing layer. Journal of Fluid Mechanics, 119, 323-345.
- Hirtl, M., P. Skomorowski, M. Bügelmayer (2009): EVALPORT – Evaluierung von Ausbreitungsmodellen an Tunnelportalen. 1. Modellierworkshop in Leibnitz, 8.10.2009
- Hirtl, M., K. Baumann-Stanzer (2007): Evaluation of two dispersion models (ADMS-Roads and LASAT) applied to street canyons in Stockholm, London and Berlin. Atm. Env. 41, 5959-5971.
- Hsieh, K.J., F.S. Lien, E. Yee (2007): Numerical modeling of passive scalar dispersion in an urban canopy layer. J Wind Eng Ind Aerodyn, 95, 1611-1636
- Hurley, P.J. (2005): The Air Pollution Model (TAPM) Version 3. Part1: Technical Description. CSIRO Atmospheric Research Technical Paper 71, Australia, 57pp, ISBN 0643068910.
- Irwin, J. S., D. Carruthers, J. Paumier, J. Stocker (2002): Application of ASTM D6589 to evaluate dispersion model performance to simulate average centerline concentration values. 8th Int. Conf. on Harmonisation within Atmospheric Dispersion Modelling for Regulatory Purposes. Conference Proceedings (Eds. E. Batchvarova and D. Syrakov), 53-57.
- Janicke (2005): Ausbreitungsmodell LASAT. Arbeitsbuch. Ingenieurbüro Janicke, Gesellschaft für Umweltphysik. 115 pp.

- Janicke, L., und U. Janicke (2003): Some aspects of the definition of meteorological boundary layer profiles and comparisons with measurements. Reports on Environmental Physics, pp 72.
- Janicke, L., und U. Janicke (2011): Entwicklung eines modellgestützten Beurteilungssystems für den anlagenbezogenen Immissionsschutz. Ingenieurbüro Janicke, Dunum, Umweltforschungsplan des Bundesministeriums für Umwelt, Naturschutz und Reaktorsicherheit 20043 256, S126.
- Janicke, L., und U. Janicke (2011): Some aspects of the definition of meteorological boundary layer profiles and comparisons with measurements. Ingenieurbüro Janicke, Hermann-Hoch-Weg 1, 88662 Ueberlingen, Germany, Reports on Environmental Physics, pp72.
- Jeppsson, K.H. (2003): Diurnal variation in ammonia, carbon dioxide and water vapour emissions from a deep litter house for fattening pigs. Int. Symp. on Gaseous and Odour Emissions from Animal Production Facilities, Horsens 1-4 June 2003, 131 – 139
- JOST, D., HUMMEL, H. J. (2005): Die neue TA – Luft. Immissionsschutzrecht für die betriebliche Praxis. Grundwerk einschließlich 101. Aktualisierungs- und Ergänzungslieferung September 2005. WEKA MEDIA GmbH & Co. KG, Kissing
- Kaimal J.C, and Finnigan J.J. (1994): Atmospheric boundary layer flows. Oxford University Press, 289pp.
- Kistler, M., A. Kasper-Giebl, E.C. Cetintas, C. R. Santa-Cruz, E. Schreiner, L.S. Cordeiro-Wagner, S. Szidat, Y. Zhang, and H. Bauer (2013): Analysis of particulate matter in Leibnitz and Arnfels. PMInter project report by Vienna University of Technology, 59 pp
- Klein, P., M. Rau, Z. Wang, E.J. Plate (1994): Ermittlung des Strömungs- und Konzentrationsfeldes im Nahfeld typischer Gebäudekonfigurationen (Experimente), Report No. KfK-PEF 124, Germany.
- Krismer, A. (2010): Personnel Communication. Simulations performed by Andreas Krismer, Government of Tyrol.

References

- Kukkonen, J., J. Härkönen, J. Walden, A. Karppinen, and K. Lusa (2001): Evaluation of the model CAR-FMI against a measurement campaign near a major road. *Atmos. Environ.*, 35, 949-960.
- Lodomez, P. (2010) Entwicklung und Validierung eines Ausbreitungsmodells für Aerosole und Untersuchungen zu deren Koagulation als potentieller Einflussquelle. Ph.D. Rheinische Friedrich-Wilhelms-Universität Bonn, Germany, 141 pp
- Luhar, A. K., and R. E. Britter (1989): A random walk model for dispersion in inhomogeneous turbulence in a convective boundary layer. *Atmos. Environ.*, 23, 1911-1924.
- Manor, A. (2014): A stochastic single particle lagrangian model for the concentration fluctuation in a plume dispersing inside an urban canopy. *Boundary-Layer Meteorol.*, 150, 327-340
- Milliez, M., B. Carissimo (2008): Computational fluid dynamical modeling of concentration fluctuations in an idealized urban area. *Boundary-Layer Meteorol.*, 127, 241-259
- Moussiopoulos, N., E.A Kalognomou, Z. Samaras, G. Mellios, S.E. Larssen, K.I. Gjerstad, F.A.A.M. de Leeuw, K.D. van den Hout, S. Teeuwisse (2004): Street emission ceiling exercise. Phase 1 report. ETC/ACC Technical Paper 2003/11. European Topic Centre on Air and Climate Change, 134 pp (http://air-climate.eionet.europa.eu/docs/ETCACC_TechPaper2003_11_SEC_Phase1Rep.pdf)
- Moussiopoulos, N., E.A Kalognomou, A. Papathanasiou, S. Eleftheriadou, Ph. Barmpas, Ch. Vlachokostats, Z. Samaras, G. Mellios, I. Vouitsis, S.E. Larssen, K.I. Gjerstad, F.A.A.M. de Leeuw, K.D. van den Hout, S. Teeuwisse, R. Van Aalst (2005): ETC/ACC Street emission ceiling (SEC) exercise. Phase 2 report. ETC/ACC Technical Paper 2003/11. European Topic Centre on Air and Climate Change, 134 pp (http://air-climate.eionet.europa.eu/docs/ETCACC_TechPaper_2004_5_SEC_Phase2Rep.pdf)
- Mylne, K. R., and P. J. Mason (1991) Concentration fluctuation measurements in a dispersing plume at a range of up to 1000m. *Q J R Meteorol Soc*, 117, 177-206

- Nanni, A., Brusasca G., Calori G., Finardi S., Silibello C., Tinarelli G., Zublena M., Agnesod G., Pession G., Savoye M. (2002): Integrated assessment of traffic impact in an Alpine region. Seventh Highway & Urban Pollution Symposium, Barcelona, 20-23 May.
- NHMRC (2008): Air Quality in and Around Traffic Tunnels. National Health and Medical Research Council, Australian Government, pp 190 (http://www.nhmrc.gov.au/_files_nhmrc/publications/attachments/eh42.pdf)
- Oenorm M9440 (1996): Dispersion of pollutants in the Atmosphere. Calculation of ambient air concentrations and determination of stack heights. Pp 25.
- Oettl, D. (2000a): Weiterentwicklung, Validierung und Anwendung eines Mesoskaligen Modells. Diss., Institut für Geographie Universität Graz, p. 155.
- Oettl, D., R.A. Almbauer, P.J. Sturm, M. Piringer, and K. Baumann (2000b): Analysing the nocturnal wind field in the city of Graz, Atmos. Environ., 35, pp. 379-387.
- Oettl, D., R.A. Almbauer, and P.J. Sturm (2001a): A new method to estimate diffusion in stable, low wind conditions. J. of Appl. Meteor., 40, 259-268.
- Oettl, D., J. Kukkonen, R.A. Almbauer, P.J. Sturm, M. Pohjola and J. Härkönen (2001b): Evaluation of a Gaussian and a Lagrangian model against a roadside dataset, with focus on low wind speed conditions. Atmos. Environ., 35, 2123-2132.
- Oettl, D., P. J. Sturm, M. Bacher, G. Pretterhofer, R. A. Almbauer (2002): A simple model for the dispersion of pollutants from a road tunnel portal. Atmos. Environ., 36, 2943-2953.
- Oettl, D., P.J. Sturm, G. Pretterhofer, M. Bacher, J. Rodler, R.A. Almbauer (2003a): Lagrangian dispersion modeling of vehicular emissions from a highway in complex terrain. J. of the Air and Waste Management Association, 53, 1233-1240.
- Oettl, D., P.J. Sturm, R. Almbauer, S. Okamoto, K. Horiuchi (2003b): Dispersion from road tunnel portals: Comparison of two different modelling approaches. Atmos. Environ., 37, 5165-5175.

References

- Oettl, D., R. A. Almbauer, P. J. Sturm, and G. Pretterhofer (2003c): Dispersion modelling of air pollution caused by road traffic using a Markov Chain - Monte Carlo model. *Stochastic Environmental Research and Risk Assessment*, 58-75.
- Oettl, D., P.J. Sturm, and R. A. Almbauer (2004): Evaluation of GRAL for the pollutant dispersion from a city street tunnel portal at depressed level. *Environmental Modeling & Software*, 20, 499 – 504.
- Oettl, D., Ch. Kurz, W. Hafner and P. Sturm (2005): PM10 source apportionments within the city of Klagenfurt, Austria. 10th International Conference on Harmonisation within Atmospheric Dispersion Modeling for Regulatory Purposes, October 11 –14, Sissis, Greek, 638-642.
- Oettl, D., S. Hausberger, M. Rexeis, and P.J. Sturm (2006a): Simulation of traffic induced NO_x-concentrations near the A 12 highway in Austria. *Atmos. Environ.*, 40, 6043-6052.
- Oettl, D. (2006b): Evaluierung der Ausbreitungsmodelle AIR.LAG, LASAT und AUSTAL 2000 für die Schadstoffausbreitung von Punktquellen mit thermischer Überhöhung. Unpublished Report Nr. FVT-28/06/Öt V&U 05/05/6300 vom 24.4.2006.
- Oettl, D., R. Onchang, S. Vogelsang, M. Rexeis, P. Sturm, and S. Hausberger (2008): Dispersion modeling in complex terrain with frequent low wind speed conditions. Chapter XX of *Environmental Sciences & Environmental Computing*, Vol. III (Eds. P. Zannetti, et al.). Published by The EnviroComp Institute (<http://www.envirocomp.org/>) and the Air & Waste Management Association (<http://www.awma.org/>).
- Oettl, D., W. Köberl, and Th. Pongratz (2012): NH₃ Passivsammlermessungen im Leibnitzer Feld. Amt d. Stmk. Landesregierung, Referat Luftreinhaltung, LU-02-2012, 20 pp
- Oettl, D. (2014): Evaluation of the Lagrangian Particle Model GRAL against the US-EPA near Roadway Tracer Study 2008. Proceedings of the International Symposium “Transport and Air Pollution”, Sept 18-19, Graz, Austria.

- Oettl, D. (2015a): Quality assurance of the prognostic, microscale wind-field model GRAL 14.8 using wind-tunnel data provided by the German VDI guideline 3783-9. *Journal of Wind Engineering & Industrial Aerodynamics*, 142, 104-110
- Oettl, D. (2015b): A multiscale modelling methodology applicable for regulatory purposes taking into account effects of complex terrain and buildings on the pollutant dispersion: a case study for an inner Alpine basin. *Environmental Science and Pollution Research*, 22 (22), 17860-17875
- Oettl, D. (2015c): Evaluation of the revised Lagrangian particle model GRAL against wind-tunnel and field experiments in the presence of obstacles. *Boundary Layer Meteorol*, 155, 271-287
- Oettl, D., and St. Oitzl (2016): Comparing dispersion modelling and field inspection for odour impact assessment in the vicinity of two animal husbandry farms. 17th International Conference on Harmonisation within Atmospheric Dispersion Modeling for Regulatory Purposes, May 9 – 12, Budapest, Hungary, pp 2-6
- Olesen, H.R. (1995): The model validation exercise at Mol: overview of results. *Int. J. Environment and Pollution*, 5, 761-784
- Olesen H.R. (1997): Description of Indianapolis data, National Environmental Research Institute, http://www2.dmu.dk/AtmosphericEnvironment/harmoni/m_v_kit.htm.
- Olesen, H.R. (1994): Model validation kit for the workshop on operational short-range atmospheric dispersion models for environmental impact assessments in Europe (Mol, Nov 21-24 1994): prepared at the National Environmental Research Institute, Denmark.
- Olesen, H.R. (2005): User's Guide to the Model Validation Kit. National Environmental Research Institute, Denmark, 72pp. – Research Notes from NERI no. 226. <http://research-notes.dmu.dk>
- Onchang, R., P.J. Sturm, D. Öttl (2006): Evaluation of Dispersion Models Performance Using a Standard Procedure ASTM D6589. Thailand national conference - Air Pollution Technology: Community with Better Breath held on 24-25 March 2006, Bangkok Thailand.

References

- Pahlow, M., Parlange, M.B., and Porté-Agel, F. (2001): On Monin-Obukhov similarity in the stable atmospheric boundary layer. *Boundary-Layer Meteorol.* 99, 225-248.
- Panofsky, H.A., and J.A. Dutton (1984): *Atmospheric Turbulence*. 397 pp, Wiley, New York.
- Panofsky, H.A., H. Tennekes, D.H. Lenschow, and J.C. Wyngaard, (1977): The characteristics of turbulent velocity components in the surface layer under convective conditions. *Bound.-Layer Meteor.*, 11, 355-361.
- Patankar, S.V., 1980: *Numerical heat transfer and fluid flow*. *Hemisphere publishing corporation, Washington*.
- Piringer, M., and K. Baumann-Stanzer (2009): Modellvalidierung – Ergebnisse mit zwei Testdatensätzen. Modellierworkshop Leibnitz 8.10.2009.
- Prandtl (1925): Bericht über Untersuchungen zur ausgebildeten Turbulenz. *Z Angew. Math. Mech.*, 5, 136-139.
- Ramsauer and Bachler (2010): *Personnel Communication*. Simulations made by the Graz University of Technology.
- Pongratz, Th. Et al. (2016): Jahresbericht der Luftgütemessungen in der Steiermark. Amt d. Stmk. Landesregierung, Referat Luftreinhalteung, LU-08-2016, 158 pp
- Rexeis, M. and S. Hausberger (2005): Calculation of vehicle emissions in road networks with the model NEMO. *Proceedings of the 14th Int. Conf. on Transport and Air Pollution in Graz*, Ed. Institute for Internal Combustion Engines and Thermodynamics, Graz University of Technology, 118-127.
- Rodean, J.C. (1994): *Stochastic Lagrangian Models of Turbulent Diffusion*. *Met. Monographs*, 48, Vol. 26, American Met. Soc., Boston, 85pp.
- Rodi, W. (1980): *Turbulence Models and Their Application in Hydraulics - A State of the Art Review*. *Iahr Monograph Series*, A. A. Balkema, Delft.
- Romberg, E., R. Bössinger, A. Lohmeyer, R. Ruhnke, E. Röth (1996): NO-NO₂ conversion for predicting the air quality impact of traffic (German). *Gefahrstoffe-Reinhalteung der Luft*, 56, 215-218.

- Sagendorf, J. F., and C. R. Dickson (1974): Diffusion Under Low Windspeed, Inversion Conditions. NOAA Technical Memorandum ERL ARL-52, National Oceanic and Atmospheric Administration.
- Schaedler, G., W. Baechlin, A. Lohmeyer, Tr. Van Wees (1996): Comparison and Judgement of currently available microscale flow and dispersion models (German). Rep. No. FZKA-PEF 138, Forschungszentrum Karlsruhe, pp 201.
- Schauberger, G., T.T. Lim, J.Q. Ni, D.S. Bundy, B.L. Haymore, C.A. Diehl, R.K. Duggirala, A.J. Heber (2012): Empirical model of odor emission from deep-pit swine finishing barns to derive a standardized odor emission factor. *Atmos. Environ.*, 84-90
- Schlunzen K.H. (1997): On the validation of high-resolution atmospheric mesoscale models. *J. Wind Engineering and Industrial Aerodynamics*, 67&68, 479-492.
- Sharan, M., and A. K. Yadav (1998): Simulation of experiments under light wind, stable conditions by a variable K-theory model. *Atm. Env.*, 32, 3481-3492.
- Start, G.E., N.F. Hukari, J.F. Sagendorf, J.H. Cate, and C.R. Dickson (1981): EOCR Building Wake Effects on Atmospheric Diffusion. NUREG/CR-1395, National Oceanic and Atmospheric Administration, Idaho Falls, ID.
- Stocker, J., D. Heist, Ch. Hood, V. Isakov, D. Carruthers, S. Perry, M. Snyder, A. Venkatram, and S. Arunachalam (2013): Road Source Model Intercomparison study using new and existing datasets. 15th Conf. on Harmonisation within Atmospheric Dispersion Modelling for Regulatory Purposes. 6.-9. May 2013, Madrid, pp 10-15
- Stull, R. B., 1989. *An Introduction to Boundary Layer Meteorology*. Kluwer Academic Publishers, Dordrecht – Boston – London, pp 666.
- Sykes, R.I., W.S. Lewellen, S.F. Parker (1984): A turbulent-transport model for concentration fluctuations and fluxes. *J Fluid Mech*, 139, 193-218
- Thunis, P., S. Galmarini, A. Martilli, A. Clappier, S. Andronopoulos, J. Bartzis, M. Vlachogianni, K. deRidder, N. Moussiopoulos, P. Sahm, R. Almbauer, P. Sturm, D. Oettl, S. Dierer, H. Schlunzen (2003): MESOCOM An inter-comparison exercise of mesoscale flow models applied to an ideal case simulation. *Atmos. Environ.*, 37, 363-382.

References

- Tinarelli, G., D.Anfossi, M. Bider, E. Ferrero, S. Trini Castelli (2000) "A new high performance version of the Lagrangian particle dispersion model SPRAY, some case studies". Air Pollution Modelling and its Applications XIII, S.E. Gryning and E. Batchvarova eds., Kluwer Academic / Plenum Press, New York, 499-507.
- Trini Castelli, S., Anfossi D., Ferrero E. (2003) "Evaluation of the environmental impact of two different heating scenarios in urban area". Int. J. Environment and Pollution, 20, 207-217.
- Trini Castelli, S., S. Morelli, D. Anfossi, J. Carvalho, S. Zauli Sajani (2004) "Intercomparison of two models, ETA and RAMS, with TRACT field campaign data". Environmental Fluid Mechanics, 4, 157-196.
- Trini Casteli, S., Falabino, S., Mortarini, L., Ferrero, E., Anfossi, D., Richiardone, R. (2011) "Analysis of urban boundary-layer turbulence on the basis of an experimental campaign in Turin city – UTP project". Proceedings of the 14th Conf. On Harmonisation within Atmospheric Dispersion Modelling for Regulatory Purposes 2-6 Oct. 2011 (Eds. Bartzis et al.), Kos, Greece, 414-417
- Turner, D. B. (1970): Workbook of atmospheric dispersion estimates. Air Resources Field Research Office, Environmental Science Services Administration, U.S. Department of Health, Education, and Welfare, Cincinnati, Ohio, 84pp.
- US-EPA (2000): Meteorological Monitoring Guidance for Regulatory Modeling Applications. EPA-454/R-99-005. Office of Air and Radiation. Office of Air Quality Planning and Standards. Research Triangle Park, NC 27711, p 171
- US-EPA (2003): AERMOD, Latest Features and Evaluation Results. EPA-454/R-03-003.
- Van Dop, H. (1992): Buoyant plume rise in a Lagrangian framework. Atmos. Environ., 26A, 1335-1346.
- VDI 3782-1 (2016): Environmental Meteorology. Atmospheric dispersion models. Gaussian Plume Model for the determination of ambient air characteristics. Germany, Düsseldorf, 36 pp
- VDI 3945-3 (2000): Environmental Meteorology. Atmospheric dispersion models. Particle Model. Germany, Düsseldorf, 60 pp

- VDI 3894-1 (2009): Emissions and immissions from animal husbandry – Housing systems and emissions – Pigs, cattle, poultry, horses. Düsseldorf, 84 pp
- VDI 3940-1 (2006): Measurement of odour impact by field inspection – Measurement of the impact frequency of recognizable odours – Grid measurements. Düsseldorf, 44 pp
- VDI 3783-8 (2012): Environmental meteorology – Turbulence parameters for dispersion models supported by measurement data. Kommission Reinhaltung der Luft im VDI und DIN, Postfach 101139, 40002 Düsseldorf.
- VDI (2016): VDI Guideline 3783 – draft version, Part 9, Environmental meteorology – Prognostic microscale wind field models – Evaluation for flow around buildings and obstacles. Commission of Air Pollution Prevention of VDI and DIN, Düsseldorf, Germany.
- Venkatram, A., and S. Du (1997): An analysis of the asymptotic behavior of cross-wind-integrated ground-level concentrations using Lagrangian Stochastic simulation. *Atmos. Environ.*, 31, 1467-1476.
- Whiteman, D. (1990): Observations of thermally developed wind systems in mountainous terrain. In *Atmospheric Processes over Complex Terrain* (Ed. W. Blumen). Meteorological Monographs, Vol. 43, Nr. 45, American Met. Soc., pp 324.
- Weil, J.C. (1990): A diagnosis of the asymmetry in top-down and bottom-up diffusion using a Lagrangian stochastic model. *J. Atmos. Sci.*, 47, 501-515.
- Wilcox, D.C., (2006): *Turbulence Modelling for CFD*, 3rd edition, DCW Industries. California, 515 pp
- Willis, G. and J. Deardorff (1987) : Buoyant plume dispersion and entrainment in and above a laboratory mixed layer. *Atmos. Environ.*, 21, 1725-1735
- Wilson, J. D., and B. L. Sawford (1996): Review of Lagrangian stochastic models for trajectories in the turbulent atmosphere. *Boundary-Layer Meteor.*, 78, 191-210.
- Zannetti, P. (1990): *Air pollution modelling, Theories, computational methods and available software*. Computational Mechanics Publications, Southampton Boston.

Zannetti, P. and N. Al-Madani (1984): Simulation of transformation, buoyancy and removal processes by Lagrangian particle methods. Proceedings of the 14th International Technical Meeting on Air Pollution Modelling and its Application (edited by de Wispelaere Ch.), pp. 733-744. Plenum Press, New York.

17 Appendix A

17.1 Startup parameter

The following optional startup parameters can be passed to GRAL:

Existing path	Path to the GRAL working directory
LOGLEVEL01	additional logging output
LOGLEVEL02	additional logging output
LOGLEVEL03	additional logging output
show_w	show the GNU warranty paragraph
show_c	show the GNU redistribution paragraph

17.2 Control files

Below, the file formats for the necessary and optional input and output files to operate the GRAL model are described. A graphical user interface (GUI) facilitates generating the input files and provides several features to analyse the output of GRAL. For more details about the GUI the reader is referred to the manual, which is included in the GRAMM/GRAL package that can be downloaded from the website: <https://gral.tugraz.at/>

17.2.1 Input files

17.2.1.1 GRAL.geb (mandatory)

Used by: GRAL.exe, GUI

GRAL.geb gives some basic information about the GRAL grids and the model domain. The exclamation marks are used to separate the numbers used in the GRAL model from the user information.

The first and second lines are the cell-sizes for the microscale flow field model in GRAL.

The third line represents the vertical grid size for the lowest layer followed by the stretching factor for the vertical cell dimension. If pairs of numbers indicating the height above ground and the corresponding stretching factors are added, a height dependend stretching factor is applied.

Lines 4 and 5 are the number of grid cells used for the concentration grid in GRAL, which might be different in size than the one for the flow field model.

In line 6 the number of horizontal slices for the concentration grid(s) is given.

Appendix A

Line 7 lists all source groups separated by a comma to be computed.

Finally, lines 8 – 11 are the lateral boundaries of the GRAL domain. The domain size needs to be a multiple integer of the chosen grid sizes.

```
10      !cell-size for cartesian wind field in GRAL in x-direction
10      !cell-size for cartesian wind field in GRAL in y-direction
2,1.00,20,1.50,1.05,150,1.1,250,1.2      !cell-size for cartesian wind field in GRAL in z-direction, stretching factor for increasing cells heights with height
508      !number of cells for counting grid in GRAL in x-direction
181      !number of cells for counting grid in GRAL in y-direction
1      !Number of horizontal slices
4,      !Source groups to be computed separated by a comma
-2600      !West border of GRAL model domain [m]
2480      !East border of GRAL model domain [m]
-930      !South border of GRAL model domain [m]
880      !North border of GRAL model domain [m]
```

17.2.1.2 Meteopgt.all (default meteo input)

Used by: GRAL.exe, GRAMM.exe, GUI

It is the standard input file for categorized meteorological data. A complete description can be found in the GRAMM documentation.

17.2.1.3 Inputzr.dat (optional)

Used by: GRAL.exe

Another way for providing meteorological input data is using the file inputzr.dat. The first line sets the number of meteorological observations of a vertical profile. The second line are the heights of the observations (e.g. 2, 10, 15) separated by a comma.

From the third and following lines the observations are listed. Each line represents data for a specific point in time. The first column is the hour of the day (not used by the model), the second column is the friction velocity [m s^{-1}], the third is the Obukhov length [m], the fourth the boundary-layer height [m] (if not known use -1). Column 5 – 7 are the standard deviation of the horizontal wind fluctuations (is taken the same for the u- and v-components) in [m s^{-1}], the u-component (west-east) in [m s^{-1}], and the v-component (south-north) [m s^{-1}]. Westerly winds and southerly winds are positive. Columns 8 – 10 are the same as 5 – 7 but for the next monitoring height, and so on.

If the calculation of dispersion from tunnel portals is desired, for each tunnel portal the following data has to be added:

nth column: exit velocity of the tunnel jet stream [m s^{-1}]

n+1th column: temperature difference between tunnel jet stream and ambient air [K]

inputr.dat							
1	1						
2	3						
3	1	0.55	-611	-1	1.37	5.79	0.68
4	2	0.58	-503	-1	1.29	5.76	1.22
5	3	0.55	-183	-1	1.63	5.51	-0.58

17.2.1.4 Sonic.dat (optional)

Used by: GRAL.exe

Yet another way for providing meteorological input data is using the file sonic.dat. In the first line the height of the point observation is set. From the second line onwards the individual meteorological situations are listed using the following input data:

1st column: wind speed [m s^{-1}]

2nd column: wind direction (deg.)

3rd column: friction velocity [m s^{-1}]

4th column: standard deviation of along wind fluctuations [m s^{-1}]

5th column: standard deviation of cross wind fluctuations [m s^{-1}]

6th column: standard deviation of vertical wind fluctuations [m s^{-1}]

7th column: Obukhov length [m]

8th column: ensemble average dissipation rate of turbulent kinetic energy [m^2/s^3] – not used yet

9th column: meandering parameter m (see Anfossi et al., 2005; Oetli et al. 2006)

10th column: meandering parameter T3 (see Anfossi et al., 2005; Oetli et al. 2006)

sonic.dat												
1	1.5											
2	0.311	0.21	0.055	0.327	0.455	0.074	6.4	0.00773	4.6	23	-0.5087	318
3	0.507	353.795	0.05	0.551	0.501	0.087	76.2	0.01996	6.2	9	-0.587	900
4	0.189	96.027	0.082	0.419	0.418	0.042	17.1	0.00193	5.0	23	-0.5223	379

17.2.1.5 in.dat (mandatory)

Used by: GRAL.exe, GUI

It defines the main control parameters to run GRAL.

Line 1: Numbers of released particles per second

Appendix A

- Line 2: Dispersion time in [s]. The shorter the dispersion time the smaller the horizontal standard deviations of wind speed
- Line 3: Flag determining whether simulations are steady-state (1) or transient (0).
- Line 4: Flag determining the meteorological input file.
- Line 5: Flag determining whether receptor points are set or not.
- Line 6: Roughness length in [m]. In case that GRAMM wind fields are used as input, and that the land-use file landuse.asc is available, the roughness length defined here is not used. Define an average roughness length here. When using the option "Adaptive Roughness", the roughness here is the minimum surface roughness.
- Line 7: Latitude in deg.
- Line 8: Plume meandering can be switched on/off using (J/N). N is recommended.
- Line 9: Unused. The pollutant is defined in the file "Pollutant.txt" (see chapter 17.2.1.27)
- Line 10: Height of the horizontal slices in [m] above ground level separated by a comma.
- Line 11: Vertical extension of the concentration grid. Together with horizontal grid size it defines the volume size of the concentration grid.
- Line 12: The number of the weather situation from which onward the simulation starts.
- Line 13: Flag indicating the method to take buildings into account. 0 = no buildings; 1 = diagnostic approach; 2 = prognostic approach; the second number determines the number of cells around obstacles, where the prognostic equations are applied. The default value is 15.
- Line 14: Flag determining the output format of the concentration files (*.con files). This value should be 0 or -2. GRAL writes the file "building_heights.txt" if this flag is set to -2. The value 1 is reserved for a Soundplan output format.
- Line 15: "compressed" indicates that all GRAL output-files are contained within a zipped file with extension .grz; "not compressed" indicates that GRAL output-files are written separately as .con, .odr, .dep files.
"compressed V02" is an optimized output format (smaller and more error proof)
"compressed V03" is a more error proof output format. This mode writes all cells to the output.
- Line 16: "WaitForKeyStroke" indicates that any key stroke by the user is necessary to close the CMD window, where the GRAL simulation was displayed.

Line 17: “ASCIIResults 0” determines that no additional ASCII files are generated by GRAL. Setting “ASCIIResults 1” causes GRAL to generate both binary (used by the GUI) and ASCII concentration files (very large sometimes).

```

1 300      !Particlenumber
2 3600     !Dispersion time
3 1        !steady state=1,single case=0
4 4        !Meteorology: inputzr.dat=0,meteo.all=1,elimaeaki.prn=2,SONIC.dat=3,meteopgt.all=4
5 1        !Receptor points: Yes=1
6 0.2      !Surface Roughness in [m]
7 47       !Latitude
8 N        !Meandering Effect Off=J/On=N
9 NOX      !Pollutant: NOx,CO,PM,HC
10 1.5,     !Horizontal slices [m] separated by a comma (number of slices has to be defined in GRAL.gsh!)
11 1        !vertical grid spacing in [m]
12 1        !start calculation with weather number...
13 2,15     !How to take buildings into account? 1=simple mass conservation, 2=mass conservation with Poisson equation + advection, Factor for prognostic sub domains
14 -2       !Stream Output for SOUNDPLAN 1=activated -2=write buildings height
15 compressed ! write compressed output files
16 WaitForKeyStroke ! wait for keystroke when exiting GRAL
17 ASCIIResults 0 ! no additional ASCII result files

```

Line 18: Adaptive surface roughness - max value [m]. If this value is 0, the adaptive surface roughness is not used. Otherwise this value defines the maximum surface roughness allowed within the GRAL domain.

Line 19: Radius surrounding source in [m]. If buildings are present, prognostic calculations are performed within this radius. Beyond this radius, the wind fields are always calculated diagnostically

Line 20: Flag determining whether the GRAL online functions are used (1) or not used (0)

Line 21: Flag determining whether the AVX512 vector extension should be used (1) or not (0); the AVX512 Vector extensions are faster on some processors and slower on others compared to AVX256

Line 22: This flag determines whether the reproducible mode is activated (1) or not (0). If the reproducible mode is activated, GRAL delivers exactly the same results for the same projects for every weather situation in a reproducible manner. For this purpose, the flow field calculation must be performed sequentially and is therefore slower and the internal pseudo-random generators are generated with reproducible start values. Progress notification is not sent to the GUI in this mode

17.2.1.6 point.dat (optional – defines point sources)

Used by: GRAL.exe

Includes all point sources for the simulation. From line 3 onwards each line represents one point source:

1st and 2nd lines: header files not used by the model.

3rd and following lines:

Appendix A

- 1st column: x-coordinate of the area source
2nd column: y- coordinate of the area source
3rd column: z- coordinate of the area source above ground level
4th column: Emission of any pollutant in [kg/h]
5th column: not used anymore
6th column: not used anymore
7th column: not used anymore
8th column: exit-velocity in [m/s]
9th column: stack-diameter in [m]
10th column: exit-temperature in [K]
11th column: source group (Note: each source group is stored separately in the resulting concentration files).
12th column: Share of PM_{2.5} emissions in [%]
13th column: Share of PM₁₀ emissions in [%]
14th column: Particle diameter of PM₃₀ emissions in [μm]
15th column: Particle density in [kg/m^3]
16th column: Dry deposition velocity for PM_{2.5} [m/s]
17th column: Dry deposition velocity for PM₁₀ [m/s]
18th column: Dry deposition velocity for PM₃₀ [m/s]
19th column: Mode -> "1" indicates that the given emission rate applies for PM_{2.5};
 "2" indicates that the given emission rate applies for PM_{2.5} + PM₁₀
Temp@_+ Reference name of an exit temperature time series
Vel@_+ Reference name of an exit velocity time series

```
1 Generated:
2 x,y,z,poll[kg/h],--,--,--,exit vel.[m/s],diameter[m],Temp.[K],Source group
3 563799.1,5182467.7,11,1,0,0,0,6,0.8,293,1,40,90,30,2000,0.001,0.01,0.05,2
```

17.2.1.7 Cadastre.dat (optional – defines area sources)

Used by: GRAL.exe

Includes all area sources for the simulation. From line 2 onwards each line represents one area source:

1st line: header file not read by the model.

2nd and following lines:

- 1st column: x-coordinate of the area source
 2nd column: y- coordinate of the area source
 3rd column: z- coordinate of the area source above ground level (mean height)
 4th column: extension in x-direction in [m]
 5th column: extension in y-direction in [m]
 6th column: extension in z-direction in [m]
 7th column: Emission rate of any pollutant in [kg/h]
 8th column: not used anymore
 9th column: not used anymore
 10th column: not used anymore
 11th column: source group (Note: each source group is stored separately in the resulting concentration files).
 12th column: Share of PM_{2.5} emissions in [%]

Page 225 of 244

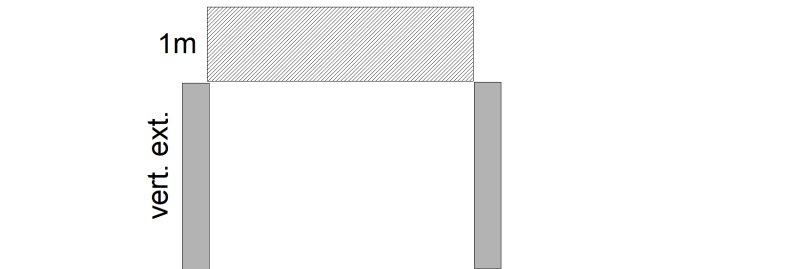
Appendix A

- 21th column: Particle diameter of PM₃₀ emissions in [μm]
- 22th column: Particle density in [kg/m³]
- 23th column: Dry deposition velocity for PM_{2.5} [m/s]
- 24th column: Dry deposition velocity for PM₁₀ [m/s]
- 25th column: Dry deposition velocity for PM₃₀ [m/s]
- 26th column: Mode -> “1” indicates that the given emission rate applies for PM_{2.5};
“2” indicates that the given emission rate applies for PM_{2.5} + PM₁₀

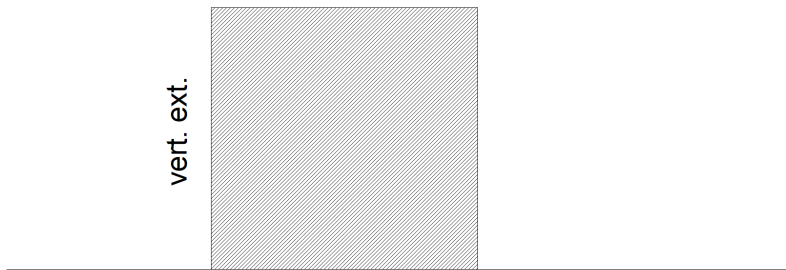
```
1 Generated:
2 Generated:
3 Generated:
4 Generated:
5 StrName,Section,Sourcegroup,x1,y1,z1,x2,y2,z2,width,noiseabatementwall,Length[km],--,pollutant[kg/(km*
6 Test,1,1,563907.9,5182575.7,0,564010.8,5182597.9,0,7,0,0,0,1,0,0,0,0,0,4,30,30,1800,0.001,0.01,0.05,1
```

Figure 121. The meaning of value „vert. ext.” (column 11) in the file line.dat

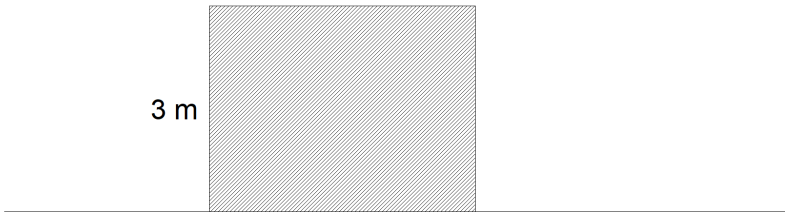
vert. ext. > 0:



vert. ext. <= 0:

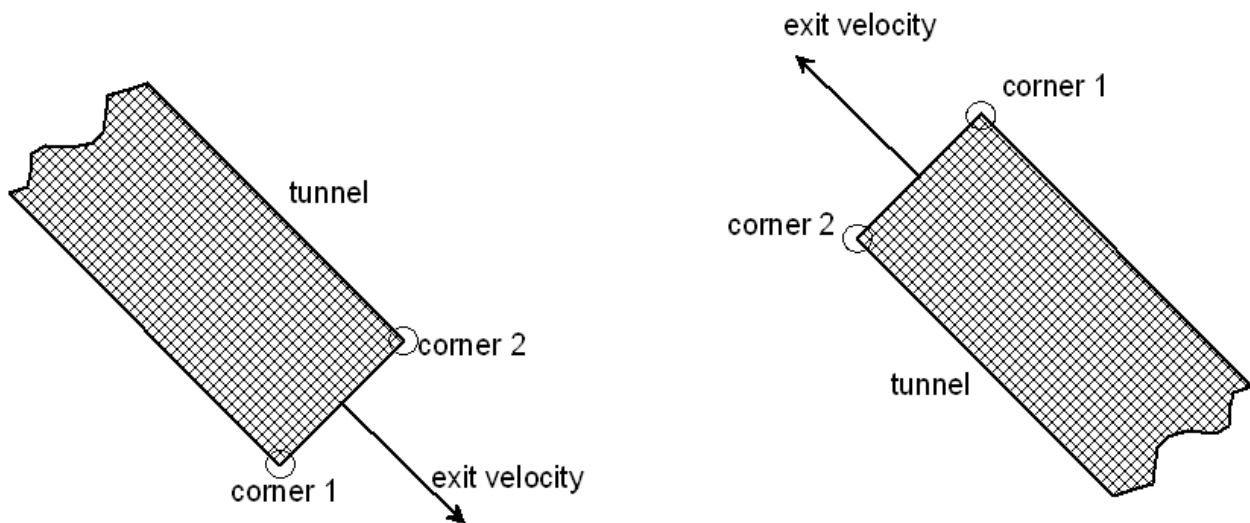


vert. ext. = 0:



Appendix A

Figure 122. How to set the corners of a tunnel portal.



17.2.1.10 Buildings.dat (optional – defines buildings)

Used by: GRAL.exe

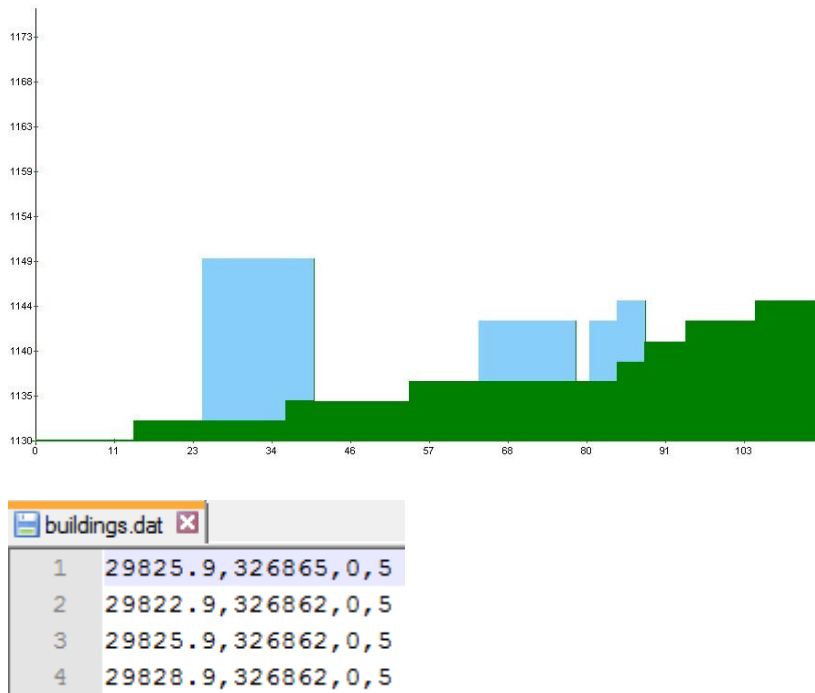
It is used to define grid cells in the microscale model of GRAL, which are blocked. Each grid cell containing one (or more) of the listed coordinates in building.dat is blocked and treated as obstacle. The structure of the file is as follows:

1st column: x-coordinate in [m]

2nd column: y-coordinate in [m]

3rd column: lower z-coordinate in [m] (currently not used; buildings reach always the ground, therefore, structures such as bridges cannot be modelled)

4th column: height in [m] of a building. All grid cells up to this height are blocked. The height of the grid-cell centre determines whether a grid cell is blocked or not. If the height listed in buildings.dat is equal or higher than the grid-cell centre, then, the cell is blocked. In case of negative values the building heights are interpreted as absolute values, while positive values are taken as relative heights above ground level. In complex terrain relative building heights may lead to roofs, which are following the terrain (see right building in the following figure), while absolute building heights ensure flat roofs (see left building in the following figure).



17.2.1.11 BuildingsRaster.dat (optional – defines buildings)

As an alternative to the file Buildings.dat it is possible to define buildings using an ESRI ASCII raster file. This file must match the flow field raster (cell number, cell size) and may only contain positive values (relative building height above terrain).

17.2.1.12 Vegetation.dat (optional – defines vegetation areas)

Used by: GRAL.exe

It is used to define grid cells in the microscale model of GRAL, which are identified as vegetation. Each grid cell containing one (or more) of the listed coordinates in vegetation.dat is treated as vegetation. The structure of the file is as follows:

Lines starting with “D”:

1st column: “D”

2nd column: total vegetation height in [m]

3rd column: trunk height in percentage of the total height [m]

4th column: leave-area density within the trunk zone [m²/m³]

5th column: leave-area density within the crown zone [m²/m³]

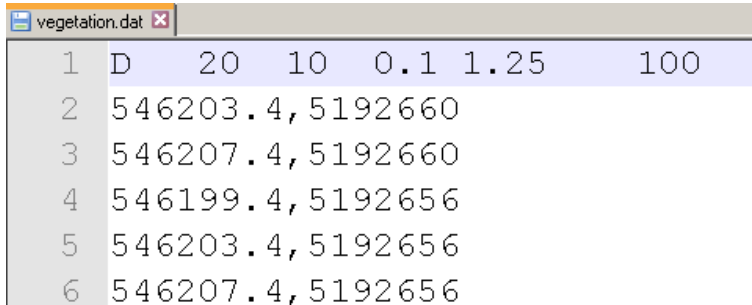
6th column: vegetation coverage in percentage

Appendix A

All other following lines:

1st column: x-coordinate in [m]

2nd column: y-coordinate in [m]



1	D	20	10	0.1	1.25	100
2	546203.4,	5192660				
3	546207.4,	5192660				
4	546199.4,	5192656				
5	546203.4,	5192656				
6	546207.4,	5192656				

17.2.1.13 Ggeom.asc (mandatory, when GRAL is coupled with GRAMM)

The file ggeom.asc contains much of the GRAMM-grid information as well as about topography as used for the GRAMM model. For a detailed description of this file the reader is referred to the GRAMM documentation. The file is only needed in case that orographic effects should be taken into account.

If the GRAMM wind fields are not stored in the recent project folder, this file is a simple and small text file. The 1st line points to the windows path of the GRAMM wind fields. If you use the LINUX version of GRAL, the 2nd line is used for the UNIX path. From version 20.09 the 1st line is also checked in UNIX systems. If this check fails, the 2nd line is used.

17.2.1.14 Landuse.asc (mandatory, when GRAL is coupled with GRAMM)

Used by: GRAL.exe, GRAMM.exe, GUI

The file landuse.asc contains much of the GRAMM-grid information. For a detailed description of this file the reader is referred to the GRAMM documentation. The file is only needed in case that orographic and land-use effects should be taken into account.

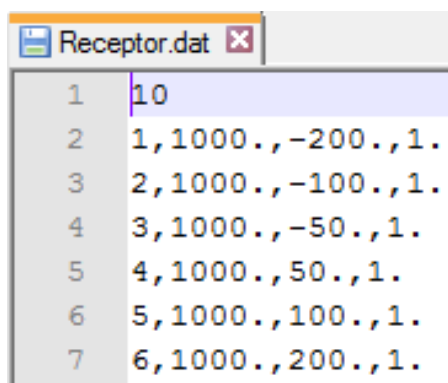
17.2.1.15 Receptor.dat (optional – defines receptor points)

Used by: GRAL.exe, GUI

It defines the location of receptor points for which GRAL generates an additional file zeitreihe.dat containing the concentrations at each receptor separated for each defined source group.

The first line sets the total number of receptor points. From the second line onwards the file is structured as follows:

- 1st column: Number of receptors in ascending order
- 2nd column: x-coordinate of a receptor point in [m]
- 3rd column: y-coordinate of a receptor point in [m]
- 4th column: z-coordinate of a receptor point in [m] above ground level
- 5th column: optional: name of the receptor point
- 6th column: optional: user defined receptor point value for the GUI

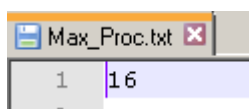


17.2.1.16 Max_Proc.txt (optional - recommended)

Used by: GRAMM.exe, GRAL.exe

Sets the maximum number of processor cores to be used for parallel computing. The number can be larger than the actual number of processors available on the computer (in this case simply all available processors are used). The file contains only one line with the corresponding figure.

If this file does not define the maximum number of processor cores, GRAL takes all available cores automatically.

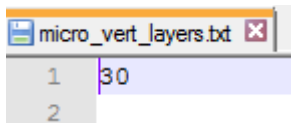


17.2.1.17 Micro_vert_layers.txt (mandatory)

Used by: GRAL.exe, GUI

Appendix A

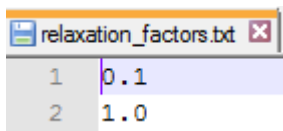
Defines the number of vertical layers used in the prognostic microscale flow field model of GRAL. Note that above this height still wind fields are computed by utilizing a diagnostic approach.



17.2.1.18 Relaxation_factors.txt (optional)

Used by: GRAL.exe, GUI

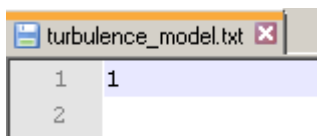
This is an optional file used to set the relaxation factors in the prognostic microscale flow field model of GRAL. The default values are 0.1 for velocity and 1.0 for non-hydrostatic pressure.



17.2.1.19 Turbulence_model.txt (optional)

This is an optional file used to select the desired turbulence model. Note that the default turbulence model is the mixing-length model. The various turbulence models are invoked by the following numbers:

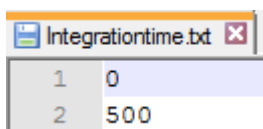
- 0: no diffusion
- 1: mixing-length model (invoked when the file "turbulence_model.txt" is not existent).
- 2: standard k- ϵ model



17.2.1.20 Integrationtime.txt (optional - recommended)

Used by: GRAL.exe, GUI

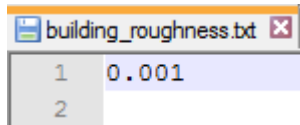
This is an optional file used to set the minimum and maximum number of iterations for the solution algorithm in the prognostic microscale flow field model of GRAL. The default values are 100 for the minimum and 500 for the maximum number of iterations.



17.2.1.21 Building_roughness.txt (optional - recommended)

Used by: GRAL.exe, GUI

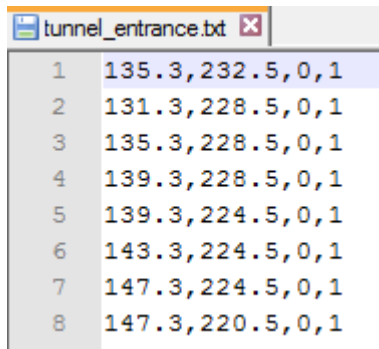
This is an optional file used to set the surface roughness for obstacles used in the prognostic microscale flow field model of GRAL. The default value is 0.001.



17.2.1.22 Tunnel_entrance.txt (optional)

Used by: GRAL.exe

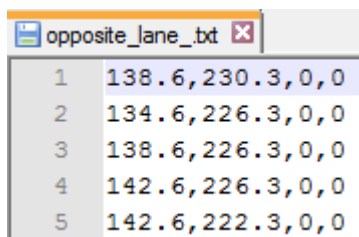
The file contains x- and y-coordinates for all grid cells, where particles are removed from the dispersion process. In this way the effect of tunnel portals, where air is sucked in, is modelled in a simple way. Note that columns 3 and 4 are not used currently.



17.2.1.23 Opposite_lane.txt (optional)

Used by: GRAL.exe

The file contains x- and y-coordinates for all grid cells, where particles pass from the a dispersion process governed by a tunnel jet stream into the standard dispersion process without any influence of the jet stream. In this way the effect of traffic on the opposite lane on a motorway, where the tunnel jet is destroyed, is modelled in a simple way. Note that columns 3 and 4 are not used currently.



17.2.1.24 Trans_conc_threshold.txt (optional – recommended in the GRAL transient mode)

Used by: GRAL.exe

The file contains a single value, which sets the lower concentration limit in transient simulations above which concentrations from the previous weather situation are neglected. The higher the limit the less accurate are the simulations, but the simulation can be speed up enormously.

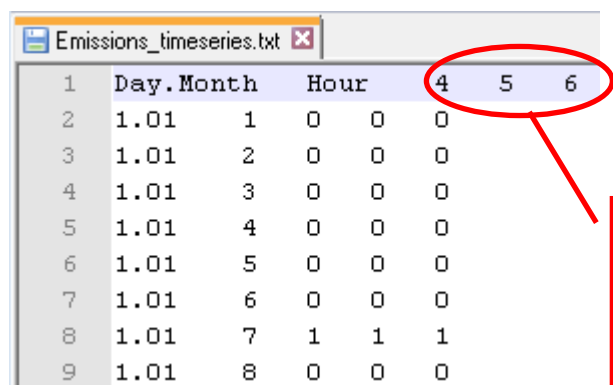
17.2.1.25 Emissions_timeseries.txt (optional – recommended in the GRAL transient mode)

Used by: GUI, GRAL.exe (in transient mode only)

It is imperative to use the date and time information as stored in the file “mettimeseries.dat”, which can be found in the sub-directory “Computation” of the current project. It is recommended to copy the file in an application such as Excel. In a next step all columns, except the first two ones containing the date and time information, must be deleted.

It is important to define a correct header line for the file „emissions_timeseries.txt“:

The first column is the date, the second the hour, followed by the numbers of **each used** source group. It is not important in which order the source groups are aligned.



1	Day.Month	Hour	4	5	6
2	1.01	1	0	0	0
3	1.01	2	0	0	0
4	1.01	3	0	0	0
5	1.01	4	0	0	0
6	1.01	5	0	0	0
7	1.01	6	0	0	0
8	1.01	7	1	1	1
9	1.01	8	0	0	0

Source group numbers indicating the columns containing the emission modulation factors for each hour of the

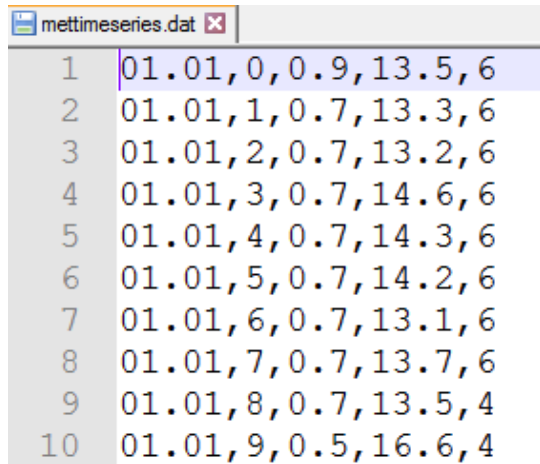
Tabulator, semi-colon, hyphen, blank or colon characters are accepted column separators

17.2.1.26 mettimeseries.dat (mandatory)

This file contains the time series of meteorological data. When using GRAL in the transient mode, the entire time series of dispersion situations (as defined in the file mettimeseries.dat) has to be computed one after each other.

Accepted row delimiter characters are the blank, comma, tabulator or semi-colon characters, allowed decimal separator is the dot.

The date and time format must use the colon, hyphen or dot character to separate day, month and year or hour and minute.



```
mettimeseries.dat
1 01.01,0,0.9,13.5,6
2 01.01,1,0.7,13.3,6
3 01.01,2,0.7,13.2,6
4 01.01,3,0.7,14.6,6
5 01.01,4,0.7,14.3,6
6 01.01,5,0.7,14.2,6
7 01.01,6,0.7,13.1,6
8 01.01,7,0.7,13.7,6
9 01.01,8,0.7,13.5,4
10 01.01,9,0.5,16.6,4
```

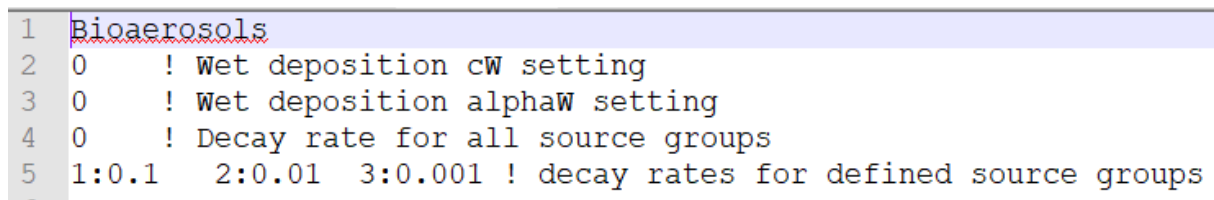
17.2.1.27 Pollutant.txt (mandatory)

The file contains the name of the pollutant. The pollutant name “odour” forces GRAL to compute and write the concentration-fluctuation intensity.

The additional entries are the washout parameters for the computation of the wet deposition. These values are 0 by default.

The wet deposition is computed solely if these values are not 0, the number of entries in the file “Precipitation.txt” matches the number of entries in the file “mettimeseries.dat”, the precipitation rate is greater than zero and the transient GRAL mode is used.

Further, a decay rate can be defined for each source group, which directly acts on the particle mass during the dispersion process (see chapt. 4.10).



```
1 Bioaerosols
2 0 ! Wet deposition cW setting
3 0 ! Wet deposition alphaW setting
4 0 ! Decay rate for all source groups
5 1:0.1 2:0.01 3:0.001 ! decay rates for defined source groups
```

17.2.1.28 Precipitation.txt (optional)

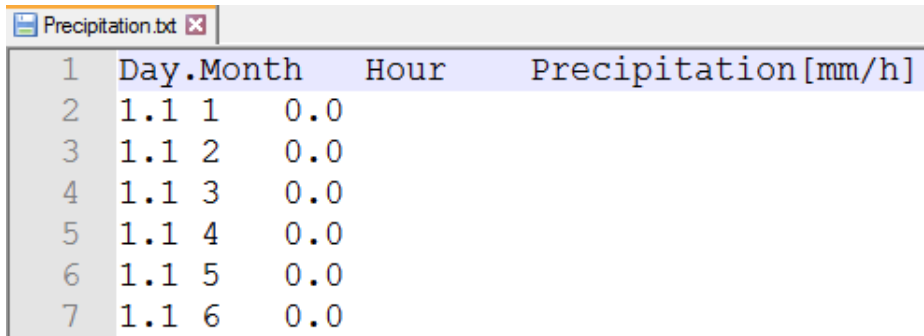
This file contains the time series of precipitation data. When using GRAL in the transient mode, this information is used to compute the wet deposition.

Appendix A

The accepted row delimiter character is the tabulator and the allowed decimal separator is the dot.

The date and time format has to use the colon, hyphen or dot character to separate day, month, or hour and minute.

The number of entries in that file must match the number of entries of the file mettimeseries.dat.



1	Day	Month	Hour	Precipitation [mm/h]
2	1.1	1	0.0	
3	1.1	2	0.0	
4	1.1	3	0.0	
5	1.1	4	0.0	
6	1.1	5	0.0	
7	1.1	6	0.0	

17.2.1.29 GRAL_topofile.txt (optional, needed when GRAL is coupled with GRAMM and high resolution GRAL terrain should be used)

This file contains topographical data with a horizontal resolution as applied in the GRAL simulation for the flow field. The horizontal extend of the file must be the very same as the GRAL domain. The format is ESRI ASCII.

17.2.1.30 TimeSeriesPointSourceVel.txt (optional)

This file contains data about the exit velocities [m/s] for stacks. This file is used for transient simulations with GRAL and time dependent exit velocities.

The first line is a header, whereby the names of the exit velocity presets is given there (in the example below the name of the preset is "Stack"). The presets (reference names) are used to be identified by each source as used in the file "point.dat" (see chapter 17.2.1.6), such that the corresponding exit velocities can be attributed accordingly.

The accepted row delimiter character is the tabulator or the comma and the allowed decimal separator is the dot. The date and time format must use the colon, hyphen or dot character to separate day, month and year, or hour and minute. The number of entries (line numbers) in that file must match the number of entries of the file mettimeseries.dat.

1	Day.Month	Hour	Stack
2	09.10	10	8
3	09.10	11	8
4	09.10	12	8

17.2.1.31 TimeSeriesPointSourceTemp.txt (optional)

This file contains data about the exit excess temperatures (=temperature difference between stack and ambient air) in [°C or K] for stacks. The format and usage are the same as for the file TimeSeriesPointSourceVel.txt.

17.2.1.32 TimeSeriesPortalSourceVel.txt (optional)

This file contains data about the exit velocities for tunnel portals. The format and usage are the same as for the file TimeSeriesPointSourceVel.txt.

17.2.1.33 TimeSeriesPortalSourceTemp.txt (optional)

This file contains data about the exit excess temperatures (=temperature difference between tunnel jet stream and ambient air) in [K] for tunnel portals. The format and usage are the same as for the file TimeSeriesPointSourceVel.txt.

17.2.1.34 KeepAndReadTransientTempFiles.dat (optional)

If this file is stored in the GRAL computation directory, the temporary concentration files generated by GRAL in transient mode are not deleted if GRAL has been finished and are used for the restart, regardless the number of the recent dispersion situation. The file itself contains a single integer number defining the interval (number of dispersion situations) for storing temporary concentration files. This setting should be used carefully by experienced users only.

17.2.1.35 GFF_FilePath.txt (optional)

This file contains a string, which defines the full path (folder and directory), where the *.gff files (containing the wind field data of the microscale flow field simulations for each dispersion situation) are stored and read.

The 1st line is reserved for WindowsOS.

The 2nd line is used to set the UNIX (LINUX) path.

17.2.1.36 GRAL_FlowFields.txt (optional)

If this file exists, the micro-scale flow field files are written. The number defined in the file specifies the write mode (0 to 2, see chapter 17.2.2.4).

17.2.1.37 RoughnessLengthsGral.dat (optional)

This file overrules the adaptive surface roughness algorithm and defines the spatially varying surface roughness based on the values defined in this file. This file must be an ESRI ASCII raster file and the file must match the flow field raster (cell number, cell size).

17.2.1.38 windfeld.txt (optional)

This optional file contains a path to the GRAMM windfield data. The 1st line is used for Windows, the 2nd line for LINUX.

From version 20.09 the 1st line is also checked in UNIX systems. If this check fails, the 2nd line is used. GRAL tries to read the wind data from the project path if there is no valid path.

17.2.1.39 GFF_FilePath.txt (optional)

This optional file contains a path to store or read the GRAL windfield data. The 1st line is used for Windows, the 2nd line for LINUX.

From version 20.09 the 1st line is also checked in UNIX systems. If this check fails, the 2nd line is used. GRAL tries to read the wind data from the project path if there is no valid path.

17.2.1.40 “VegetationDepoFactor.txt” (optional)

The first line specifies the scaling factor for gases, PM2.5 and PM10, the second line the scaling factor for PM30 and larger. The specified deposition velocity for each source is subsequently increased by the scaling factor * coverage within vegetation zones. Factors below one are set to at least one.

If GRAL can read the user settings, you will find the imported values in the terminal output and in the file "Logfile_GRALCore.txt".

17.2.2 Output files

17.2.2.1 *.con files

Used by: GUI

Calculated two-dimensional concentration fields are stored in binary files with the file extension „con“. If the files are to be used for post-processing with the GUI, they need to have one header line first (negative integer value in the last line of the input file in.dat). The filename itself contains the weather situation utilizing 5 digits (e.g. 00001-101.con corresponds to the flow field of the first weather situation) followed by 3 digits indicating the number of the horizontal slice (1-9) and the number of the source group (01-99) The header is an integer*4 value equal to -1.

Optionally, the files can be stored in a zipped container with the extension *.grz.

17.2.2.2 *.odr files

Used by: GUI

In order to run the concentration variance module for computing odour hours (see chapt. 4.7) several quantities are needed by the GUI. These are stored as binary files with the file extension „odr“. The filename itself contains the weather situation utilizing 5 digits (e.g. 00001-101.odr corresponds to the flow field of the first weather situation) followed by 3 digits indicating the number of the horizontal slice (1-9) and the number of the source group (01-99).

Optionally, the files can be stored in a zipped container with the extension *.grz..

17.2.2.3 *.dep files

Used by: GUI

Computed deposition values are stored as binary files with the file extension „dep“. The filename itself contains the weather situation utilizing 5 digits (e.g. 00001-101.odr corresponds to the flow field of the first weather situation) followed by 2 digits indicating the number of the source group (01-99)

Optionally, the files can be stored in a zipped container with the extension *.grz.

17.2.2.4 *.gff files

Used by: GRAL, GUI

Appendix A

Computed three-dimensional flow fields are stored in binary files with the file extension „gff“. Note that these files are stored in as zipped files to save storage capacities. The filename itself contains the weather situation utilizing 5 digits (e.g. 00001.gff corresponds to the flow field of the first weather situation). There are 3 formats how the flow field files are compressed.

Mode 0: old default mode

Mode 1: best compression, slow

Mode 2: fast, compression rate depends on the number of buildings and the presence of terrain

17.2.2.5 GRAL_geometries.txt

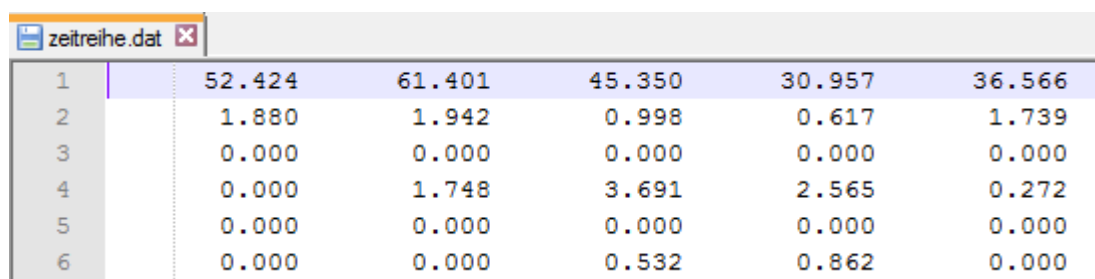
Used by: GRAL, GUI

The file contains information about topography and buildings in order to assign the flow fields stored in *.gff files correctly.

17.2.2.6 Zeitreihe.dat (up to version 20.01)

Used by: GUI

Contains the simulated concentrations at each receptor point separated for source groups. Each line contains concentrations for one weather situation. The order is as follows: in a first loop the concentrations for the first source group for every receptor is written to the file, followed by the second and so on.



1	52.424	61.401	45.350	30.957	36.566
2	1.880	1.942	0.998	0.617	1.739
3	0.000	0.000	0.000	0.000	0.000
4	0.000	1.748	3.691	2.565	0.272
5	0.000	0.000	0.000	0.000	0.000
6	0.000	0.000	0.532	0.862	0.000

17.2.2.7 ReceptorTimeseries.dat (from version 20.09)

Used by: GUI

Contains the simulated concentrations at each receptor point separated for source groups for each classified dispersion situation, this file is tab separated and written in invariant culture.

The header contains 5 lines:

- receptor name
- source group number
- X coordinate
- Y coordinate
- Z coordinate

Each line contains concentrations for one weather situation, corresponding to the situations in the file meteopgt.all.

1	ReceptorA	ReceptorB	ReceptorC
2	5	5	5
3	23.3	35.3	59.4
4	13.3	25.5	29.2
5	20	4	4
6	---	---	---
7	40.69924555665918	121.24714929734513	204.482396
8	32.088251799753756	140.2622663010304	171.360342
9	47.50360661863616	124.28020753795295	227.810452
10	40.46452584395496	142.15560249177386	125.628969
11	46.03198856687035	129.35334295036847	160.370804
12	21.647380751193683	174.8075238320114	156.114873

17.2.2.8 GRAL_Meteozeitreihe.dat

Used by: GUI

Up to version 19.01 (outdated)

For each defined receptor point the computed u- and v-component are written to this file. Each line lists results for all receptors for one specific weather situation.

1	0.08,	-0.47,	-0.13,	-0.33,	-0.01,	-0.33,
2	2.08,	0.36,	2.19,	0.49,	0.95,	0.63,
3	1.35,	0.75,	1.47,	0.66,	0.78,	0.69,
4	-2.32,	-1.64,	-1.69,	-1.36,	-2.25,	-2.13,

From version 20.06

The file got a header, containing the first line with the stored parameters, U and V wind vector components, stability class (SC) and boundary layer height (BLH).

The following header lines contains:

- receptor name
- X coordinate

Appendix A

- Y coordinate
- Z coordintate

This file is tab separated and written in invariant culture.

1	U,V,SC,BLH+				
2	ReceptorA				ReceptorB
3	23.3				35.3
4	13.3				25.5
5	22				4
6	U	V	SC	BLH	U
7	-0.03	-0.38	7	37	0.01
8	-0.09	-0.37	7	37	0.00
9	-0.16	-0.35	7	37	-0.02
10	-0.22	-0.32	7	37	-0.04
11	-0.27	-0.27	7	37	-0.06
12	-0.31	-0.22	7	37	-0.08
13	-0.34	-0.16	7	37	-0.09

17.2.2.9 Receptor_Timeseries_Transient.txt

This file contains the simulated concentrations at each receptor point separated for source groups. Each line contains the concentrations for this weather situation.

This file is written in transient mode only.

The file is tabulator separated, the decimal separator from the OS language settings is used.

A statistical error of the concentration is estimated for each receptor point at the end of a calculation (if the last weather situation in mettimeseries.dat has been calculated).

1	Rec/SourceGroup	Rec.1/SG: 2	Rec.1/SG: 1
2	X	17,2	17,2
3	Y	25,1	25,1
4	Z	1	1
5	Date/time	[µg/m³]	[µg/m³]
6	01.01.2020 01:00:00	2,8023e+003	3,4970e+003
7	01.01.2020 02:00:00	1,9764e+003	2,5054e+003
8	01.01.2020 03:00:00	1,5817e+003	2,1824e+003
9	01.01.2020 04:00:00	1,3365e+003	1,5238e+003
10	01.01.2020 05:00:00	1,4997e+003	1,9246e+003
11	01.01.2020 06:00:00	1,5970e+003	2,0256e+003
12			
13	Est.statistical error[%]	0,3%	0,3%

17.2.2.10 Building_heights.txt

Used by: GUI

GRAL writes this file if the absolute value of the flag in line 14 of the file "in.dat" is larger than 1. The file format is standard ESRI ASCII and contains the exact heights of the buildings as used in the simulations. These heights are in most cases different to the heights specified in the input file buildings.dat, because of the dimensions of the GRAL grid for the microscale flow field model.

1	<code>ncols</code>	187
2	<code>nrows</code>	160
3	<code>xllcorner</code>	-190
4	<code>yllcorner</code>	-154
5	<code>cellsize</code>	2.00000000
6	<code>NODATA_va</code>	-9999
7	0.	0.
8	0.	0.
9	0.	0.
10	0.	0.
11	0.	0.

17.2.2.11 GRAL_topography.txt

Used by: GUI

This file is generated by GRAL in case that an empty file “GRAL_topography.txt” is stored in the working directory. It contains the exact orographic data as used in GRAL.

1	<code>ncols</code>	438
2	<code>nrows</code>	293
3	<code>xllcorner</code>	29424
4	<code>yllcorner</code>	326391
5	<code>cellsize</code>	3.00000000
6	<code>NODATA_va</code>	-9999
7	459.1	459.1
8	459.1	459.1
9	459.1	459.1

17.2.2.12 Vertical_Concentrations.txt

This file contains concentration layers for the GRAL internal used concentration grid in transient mode. This file is written if the computation is finished. This is a simple text file and can be analysed in several applications.

17.2.2.13 „Vertical_Concentrations.tmp“, “Transient_Concentrations.tmp“

These are a temporarily files, written in the GRAL transient mode. These files contain the recent status of the transient concentration for all cells. If the computation is interrupted, these files are loaded at the restart to continue the dispersion with an already valid transient status and the corresponding dispersion situation. These files are written each 24 dispersion situations.

17.2.2.14 RoughnessLengthsGral.txt

This file contains the results of the adaptive surface roughness algorithm for the spatially varying surface roughness. This file is an ESRI ASCII raster file. This file is created if the option "Write building_heights.txt" and the option "Adaptive roughness" are activated (see 17.2.2.10 and options in the file "in.dat" in chapter 17.2.1.5).

17.2.2.15 PrognosticSubDomainAreas.txt

This file shows regions where prognostic (1) or diagnostic (0) calculations are performed. This file is written if GRAL is calculated prognostically and an absolute value larger than 1 is set in the file "in.dat" (see 17.2.1.5) in line 14